5th CNS International Steam Generator Conference
Toronto, Ontario, Canada
November 26 - 29, 2006

Serious Concerns and Actions for Mitigating Future Degradation in Modern Steam Generators

R. W. Staehle, Consultant, Staehle Consulting

Abstract

This review discusses both corrosion-related degradation that can occur in the future in modern steam generators and what actions should be taken to predict and minimize such degradation. This review considers the full set of tubing materials now being used: Alloys 600MA, 600TT, 690TT, 800NG, and Type 321 stainless steels. It appears that the Alloys 690TT and 800 give the best performance in vertical SGs and that the Type 321SS gives adequate lifetimes for the horizontal steam generators. Predicting future modes of degradation for long life plants is emphasized with respect to the expected longer lives of SGs, higher performance, and less inspection. A method for predicting degradation after long times is described. Special attention is given to the effects of lead- and sulfur-related SCC together with the tendencies of such species to accumulate in the deposits of heat transfer crevices. A set of damage scenarios is given, and high priority tasks that should be considered are identified.

1.0 Introduction

As an overture to this discussion, the concept underlying the hoped for reliable performance of materials over time is recognizing that all materials are chemicals. The surprise is never that they fail; but, rather, the surprise is that they work. Components are fabricated from materials that are not only fragile chemically and mechanically but even more fragile in the presence of many combined chemical and mechanical environments.

A second underlying feature of this overture is the fact that materials have no inherent strength such as given in handbooks. Materials only have the strength that exists in the environment in which they must perform, the environments being mainly those related to stress and chemistry. Handbook values are those determined in dry air, which is rarely the environment of service. Thus, the strength that is available for materials is a "situation dependent strength" as described by Staehle.[1]

The purpose of this discussion is to identify modes of degradation and failure (Sections 3.0 and 4.0) that are reasonably possible in the future operation of modern steam generators and to recommend work (Section 5.0) that should be undertaken to predict the occurrence and severity of such modes together with identifying approaches to mitigation. Such considerations are necessary at this time for the following reasons:

- Modern steam generators are expected to last longer than those in the past, and there is little if any reliable experience for predicting performance for such longer times in high temperature water. Further, these SGs can be expected to be subjected to more intense stressors as higher outputs are imposed including higher temperatures and higher flow rates.
- There are many in the LWR industry who assume that there are now no more problems after the past experiences with Alloy 600MA tubes and drilled hole tube supports. While it would seem that there has been progress in decreasing the occurrence of degradation, one only needs to look at recent times to see that serious degradation continues to occur in SGs as well as other components and in BWRs as well as PWRs: Mihama, Davis Besse, non-sensitized stainless

steels, welds in main coolant piping, welds in pressurizer piping, pump shafts, accelerated SCC from cold work, increasing failures of fuel and more. Further, it should be noted that it was experienced engineers in the past who chose 600MA, sensitized and non-sensitized stainless steels, oxidizing water chemistries, and superheat in OTSGs.

- With the increased pressures for economy together with the assumption that the main problems are behind us, the extent of inspections will be reduced. A general trend in the world nuclear fleet is to add capacity by obtaining more time at power and to increase the thermal output. These imply higher flows, higher temperatures, and fewer inspections. While the implied changes may seem unimportant, the synergy of multiple "small changes" could produce large changes in patterns of degradation. Therefore, inspection should not be reduced but possibly increased.
- Historically, even the very best people have done badly in predicting performance and providing assurances of reliable behavior with respect to degradation processes. Unfortunately, the thinking and analyses about reliability continue to be near term; and, contrary to claims, there is no proactive work anywhere that considers the guidance that is available in fundamental but obvious considerations from thermodynamics, electrochemistry, physical metallurgy, interactions of systems, as well as past degradations.
- Today, most of the common knowledge has left the nuclear industry with the retirement of those who built nuclear power. There is now a lack of institutional memory. Young engineers, who are no doubt bright, lack the appreciation of inevitable degradations that result from combined mechanical-metallurgical-chemical-system-design influences.
- There is an unfortunate view in the industry that all the problems have been solved with new designs, new materials, and better water chemistry. Such hoped for benefits are not clear and have yet to be subjected to critical analyses. In fact, arguments are presented here that some of these improvements may lead to increased degradation over time. Further, the pressure for increasingly pure water may not lead to further benefits but may lead to increased degradation; higher purity of materials, in general, has often led to worse rather than better performance in the nuclear industry.
- Already in the laboratory, potential degradation of engineering materials presently in use has been recognized. The occurrence of such degradation processes in operating SGs is not a matter of "whether" but more a matter of "when."
- In the present time, organizations claim that they are now conducting "pro-active" research aimed at searching out failure processes especially that may be important at longer times. So far as I am aware, this commitment is just words, and there is no substantive commitment by any organization to consider such "pro-active" research. In fact, some organizations have actively resisted such approaches.

While the design and reliability of SGs seem to have been improved, the capacity to achieve reliable performance over the long times is neither obvious nor is it assured.

This discussion is directed primarily toward modern vertical steam generators in pressurized water reactors including CANDU plants. By the term, "modern," is meant present and future designs that are intended for extended performance and utilize improved tubing materials, improved designs, and improved water chemistries. The SGs considered here are those of the recirculating

(RSG) and once through (OTSG) types, which utilize tubing of Alloy 600TT, 690TT, and 800NG. Horizontal SGs with stainless steel tubing, mainly used in VVWRs, are nominally included in this discussion although little is said here of these. In view of the broad use of these SGs, more should be said.

These modern SGs, in general, will have to endure fewer inspections, longer fuel cycles, higher flows, and higher primary temperatures. Further, these SGs will be required to perform satisfactorily for longer lives than past SGs of older designs.

This discussion is also directed toward modes of degradation that should be expected to occur much farther into the future and toward corresponding approaches to predicting their occurrences and mitigating their possible damage.

There is some literature on evaluations of SGs and recommendations for the future. One source of these are articles by Staehle and Gorman and their co-workers.[2,3,4,5,6,7,8,9,10,11,12,13,14] Further, two major meetings have been organized to consider the properties of heat transfer crevices.[4,15] Staehle and Gorman have published an extensive review of corrosion in SGs.[5] Several reviews and meetings have been published concerning the special topic of PbSCC.[16,17] Also, workshops on special problems in SGs have been organized by EPRI in the late 1980s and 1990s.[18,19,20,21,22,23,24,25,26,27,28,29,30,31,32,33,34,35,36,37] Two important handbooks on the performance of SGs have been published by EPRI.[38,39] Also, the SCC of SG vessels has been assessed by Fleming et al.[40]

Two comprehensive assessments of present and future degradations in the nuclear island have been prepared by the EPRI[41] and the NRC.[42] When read together, these two extensive works provide an authoritative assessment of the present status of degradation and what degradation should be considered in the near future. Neither of these documents considers the longer term where failures might occur in the future but have not occurred in the past.

While some Alloy 600MA is still in service, it is not useful here to consider this material. It has been substantively dealt with in the Staehle and Gorman review,[5] as well as with other reviews by Staehle[43] and Scott.[44] However, while better materials are now used and seem to have provided good service, e.g. Alloy 800NG, Alloy 690TT, and possibly Type 321 stainless steel, with some consideration of Alloy 600TT, it is already clear, from laboratory testing, that these materials are prone to degradation over long times. While Alloy 690TT is widely regarded as satisfactory, it is an inherently reactive material and its inherent fragilities should be more cautiously considered and investigated as described in this discussion.

In addition to considering tubing in SGs, this review considers possible degradation in other components as well as ancillary components of SGs such as the SG vessel, thick sections in the lower plenum, FAC in the inlet and outlet secondary piping, transport of low valence sulfur to turbines, and welds of attached piping.

An important point of view for predicting failures after long times is introduced here based on the work of Staehle.[45,46] This approach is discussed in Section 2.3 and involves the consideration of precursor events which must occur before SCC damage can develop. Such precursors might require tens of years before SCC commences. Examples of such past and shorter term precursors include denting and SCC of tubing at TSP crevices where the initial steps involve the accumulation of corrosive chemicals due to local superheat.

In this discussion, an overview including background and approach for prediction are considered in Section 2.0. Thereafter, Section 3.0 considers various possible future modes of degradation of tubing. Section 4.0 considers the same future possible degradation of non-tubing components. In Section 5.0, specific tasks that should be undertaken toward predicting and mitigating future

degradation are identified. Such actions are aimed at taking simple and minimally expensive steps until a way forward is clear.

2.0 Overview

2.1 Scope

Figure 1 shows the two main types of steam generators (RSG and OTSG) now used although with various changes and improvements. The VVWR SGs are not shown nor are their issues discussed although their relatively large number and generally good performance merits more consideration is a review such as this.

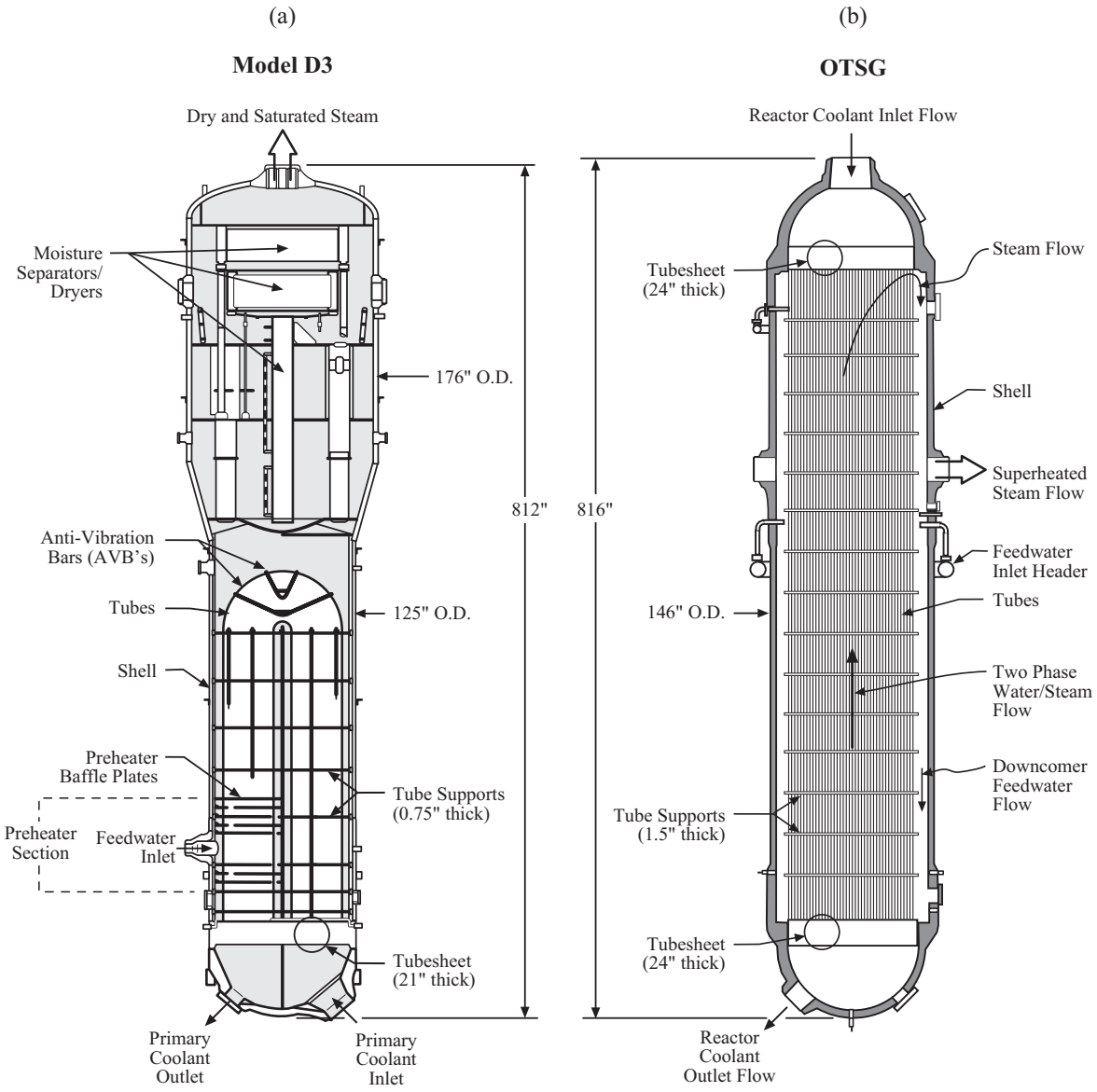

Figure 1 Schematic view of (a) RSG (Westinghouse Model D3) and (b) OTSG showing typical features. The RSG design is typical of that of Westinghouse, its licensees, CE, and Siemens. The OTSG design is typical of the B&W SGs. From Staehle and Gorman.[5]

Figure 2 shows the array of modes of possible degradations throughout SGs. The failure modes include those associated with tubing, the vessel, heavy sections, ancillary piping, flow, and carryover to turbines and are as follows:

Tubing

- Antivibration bar wear.
- Freespan cold work.
- Impurities entering with the feedwater.
- Vibration and wear at TSP.
- Scaling due to locally concentrated Pb environments.
- Deposit accumulation at TSP, TTS, and freespan (fouling) and subsequent accumulation of impurities on hot surfaces.
- Denting and SCC in tubes at the top of the tubesheet.
- SCC on primary (LPSCC) and secondary sides including especially SCC due to Pb, reduced sulfur, and sulfate impurities, PbSCC, S^{y-}SCC, and AcSCC(SO_4^{2-})respectively, on the secondary side. The reduced sulfur is produced by the reaction between sulfate impurities and hydrazine on the secondary side.

Heavy sections

- SCC in divider plates especially associated with Alloy 182/82 welds.

Vessel

- SCC of vessels at girth welds.

Ancillary piping

- Welds and SCC.
- Carryover of low valence sulfur to turbines.
- FAC in steam and feedwater lines.

2.2 Elements of the Approach

Approaching and predicting modes of degradation in SGs should rely on contributions from the following:

1. Over long times materials tend toward their thermodynamically stable states. For example, Cr will tend to dissolve from Alloy 690TT with even moderate alkaline pHs in ammoniacal solutions resulting from advanced amines. N_2H_4 will reduce SO_4^{2-}.
2. SCC, especially, may require preceding processes, e.g. deposits, before the local conditions will promote such degradation. This follows from the concept of "precursors" as described by Staehle[45,46] and discussed in this Section 2.3.
3. Recognition that "good performance" observed today does not imply that the "good performance"

will last. Already with Alloy 600MA and older designs many aspects of the serious degradations did not occur early: SCC in the OTSG upper bundle, LPSCC, thick sections of Alloy 600, FAC.

4. Accumulation of deposits with time at TTS, TSP, free surface; accumulation of impurities in these deposits.
5. Consideration of both initiation and propagation segments that occur in SCC.

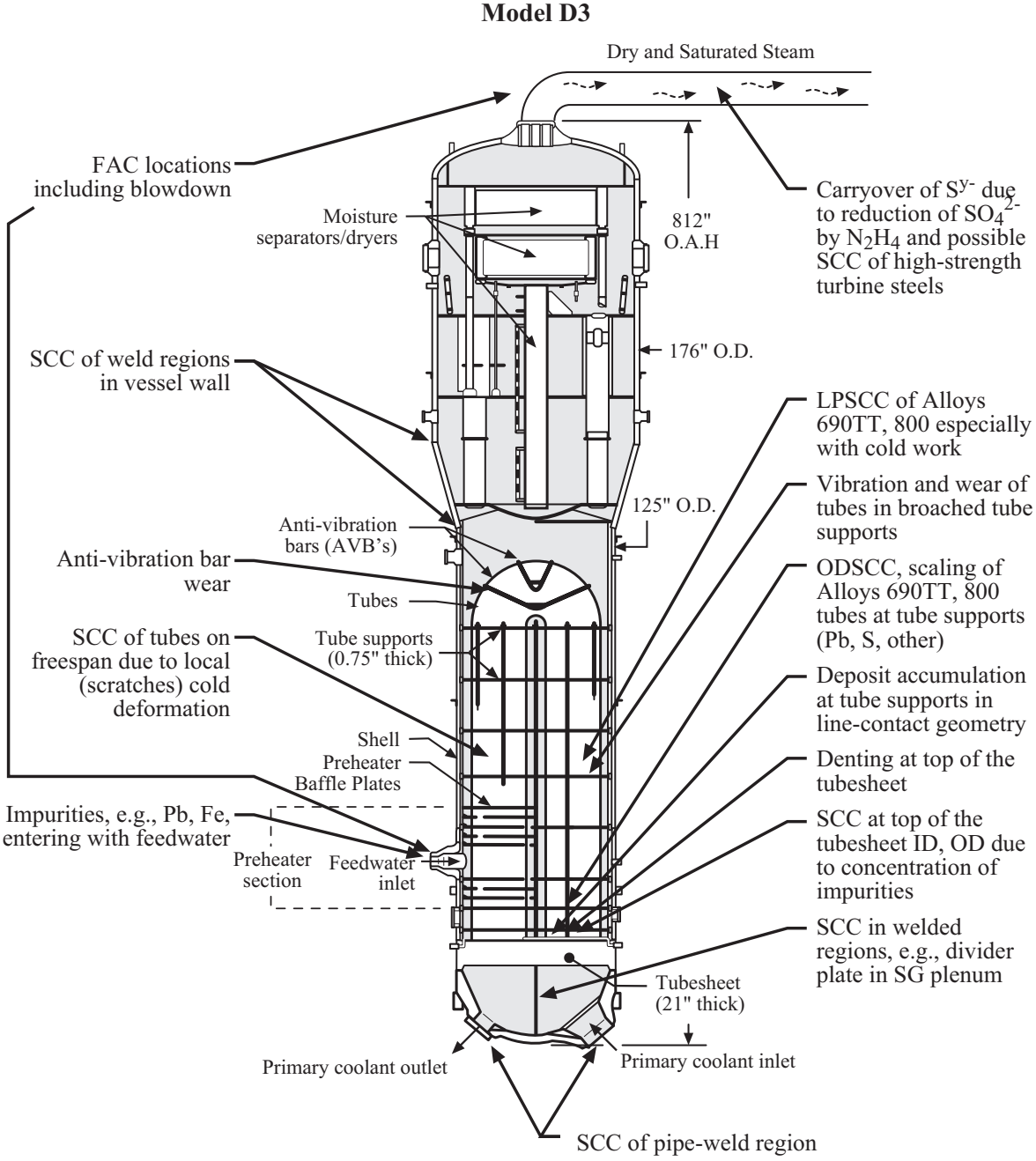

Figure 2 RSG with locations of possible modes of degradation identified for the SG and ancillary connections. From Staehle et al.[2]

6. Metallurgical changes at grain boundaries, in second phases, and in movement of dislocations as they interact with barriers associated with grain boundaries and second phases.
7. Presence of cold work both in bulk and preferentially at surfaces.
8. Changes in passive films as they react with B, Zn, reduced valence sulfur, Pb, and other species, e.g. Al and Si, that accumulate over time.
9. Changes in water chemistry: higher purity; loss of species that immobilize Pb; raised pH, which is good for lowering iron concentration but accelerates the loss of Cr from high Cr alloys; hydrogen change on the primary side but negligible hydrogen on secondary side giving higher electrochemical potentials; shutdown and startup.
10. Homogeneous chemical reactions among hydrazine, dispersants, iron, advanced amines, boron.
11. Detailed examination of pulled tubes to give boundary conditions and insights.
12. Ancillary equipment: steam lines, feedwater lines, feedwater heaters, condenser, turbine.
13. Inevitability of SCC occurring in thick sections fabricated from materials as in tubes, e.g. Alloy 600, just longer times; if SCC occurs in a tubing alloy, it should also occur in thicker sections of the same alloy.
14. Flow effects: FAC (including hydrogen produced), flow induced vibration, relative velocities in line contact crevices.

2.3 Predicting Failures That Have Not Yet Occurred

The purpose of this section is to show how predictions can be developed for SCC at long times. The approach involves mainly the idea of identifying precursor events that provide conditions, which are necessary for later SCC to develop.

The emphasis in this discussion is not on predicting degradation that can occur in short times. Such degradation is already occurring including crack propagation in thick sections of Alloy 600 and its welding analog, Alloys 182/82.

The emphasis here is upon predicting mainly SCC that is expected to occur at relatively long times. Other relatively rapid degradations such as FAC and wear/fretting are also important in this long term context, but the emphasis here is mainly on SCC.

To start, a conventional approach to describing a continuous generally monotonic development of SCC is shown in Figure 3. Here, the depth of SCC is plotted schematically vs. time with the slopes of the segments indicating the relative rates. The segments in Figure 3 are generally understood as follows:

- The first segment involves no or negligible penetration and this is called an “incubation” segment. Nothing is visible in cross sectional metallography.
- The second segment is called “initiation,” and the rate of growth of such SCC is slow. These SCC events may be only a grain or so deep and are often present as colonies. These small SCC events gradually aggregate and coalesce as shown in Figure 4.
- At some point the coalescence of the small cracks acquires sufficient stress intensity that the growth rate increases; this is the segment of propagation as shown in Figure 3. Typically, the rate of penetration of the propagation is about ten times that of initiation.

- The evolution of SCC, which is described in Figure 3, is understood to be part of the same overall and monotonic process that evolves through segments that depend on the same chemistry, applied stresses, and metallurgy. This process is also understood to initiate at zero time.

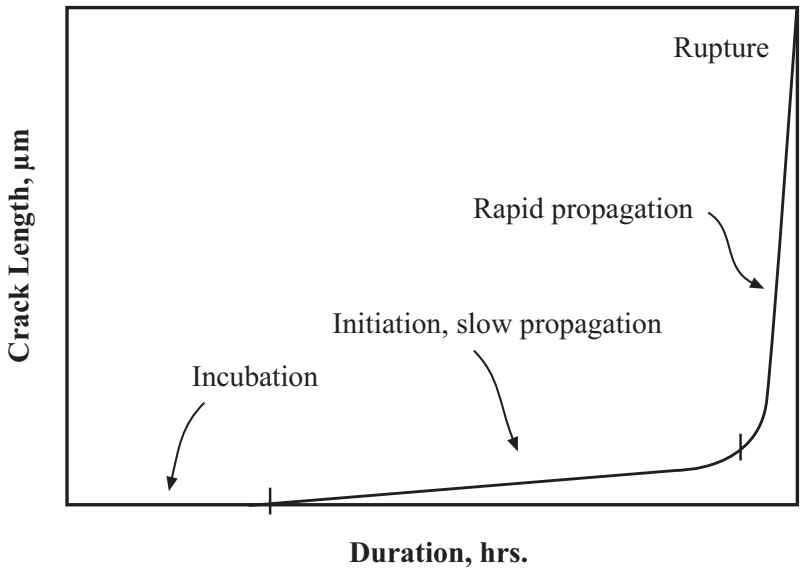

Figure 3 Schematic illustration of crack length vs. time for typical SCC. Stages of incubation, slow propagation, and rapid propagation shown. From Le Hong et al.[47]

Figure 3 provides a useful concept for characterizing SCC itself but does not deal with long times. It is not likely that any monotonic SCC process would take more than a few years and not more than about ten.

In order to develop a method of predicting degradation after very long times, I developed the "Microprocess Sequence Approach (MPSA)" that provides the framework for developing reasonable predictions for long times. This approach is described in detail in two references.[45,46] The essential idea here is that long term SCC degradation is not monotonic but requires some prerequisite conditions to prepare the surface for the occurrence of SCC. This idea is illustrated in Figure 5.

The essence of the MPSA approach is that some preliminary process must occur first before conditions are sufficient for SCC to start. This preliminary process is called the "precursor." Once the precursor produces conditions necessary for SCC, then the initiation and propagation processes, which are shown in Figure 3, for the monotonic SCC, begin.

The technical challenge is to predict the precursor. This process of formulating a reasonable precursor is described by Staehle.[45,46] A framework for identifying possible precursors is shown in Figure 6; this identifies the six domains from which likely precursors can be identified. After such precursors are identified, they can be characterized experimentally or by analysis. In some cases multiple precursors, "microprocesses," might be required; such multiple steps are discussed in connection with Figures 11-15. The process of selecting scenarios for these precursors is described in detail in the papers by Staehle.[45,46]

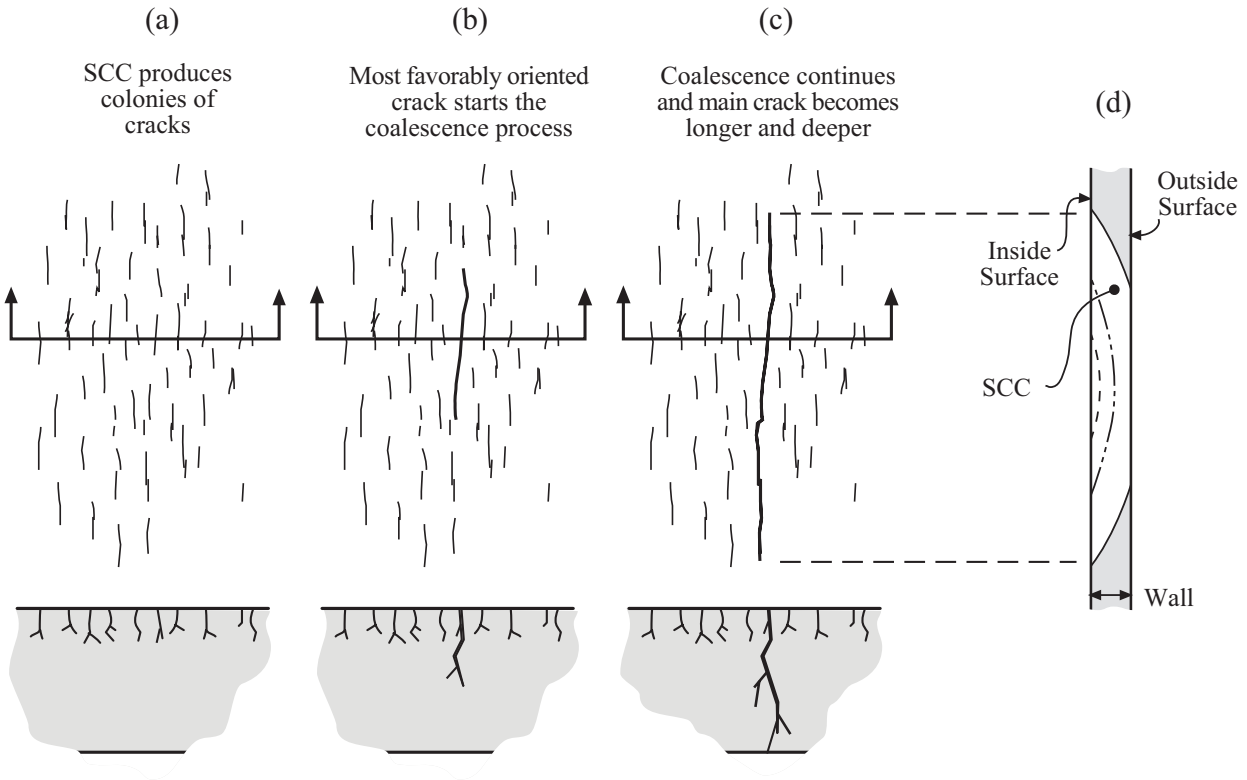

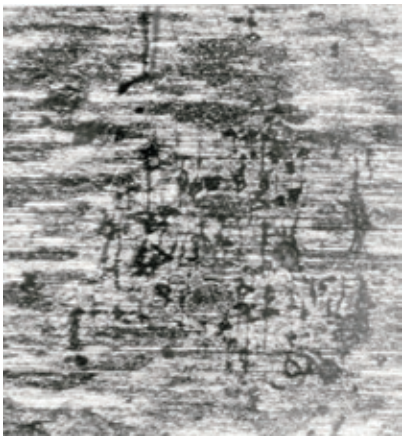

(e)

Colony of SCC on T304 SS at 204°C in dilute NaCl solution

Figure 4 (a)-(c) Evolution of initiation and propagation from a plan view and cross sections. (d) Side view of depth of SCC. (e) Macrograph of SCC of stainless steel exposed at 200°C in an oxygenated chloride solution.

In Figure 5, three cases are shown for predicting SCC or any other corrosion process over time. These are described as follows:

Case I - No Precursor

Case I monotonic degradation begins generally at the start of operation and is the same as the pattern in Figure 3; no special precursor process is required as shown in Figure 3. The Mihama FAC

failure, as shown in Figure 7, is a good example here since FAC begins when the high velocities of water begin to flow. Case I is also shown in Figure 8(a), (b) for Alloy 600MA in primary water as it sustains LPSCC; and in Figure 8(c), (d) for sensitized stainless steel in BWR water. Case I applies to the case for LPSCC due to residual stresses in primary water as shown in Figure 9. Case I also applies to the SCC in the piping in the V.C. Summer case of Figure 10.

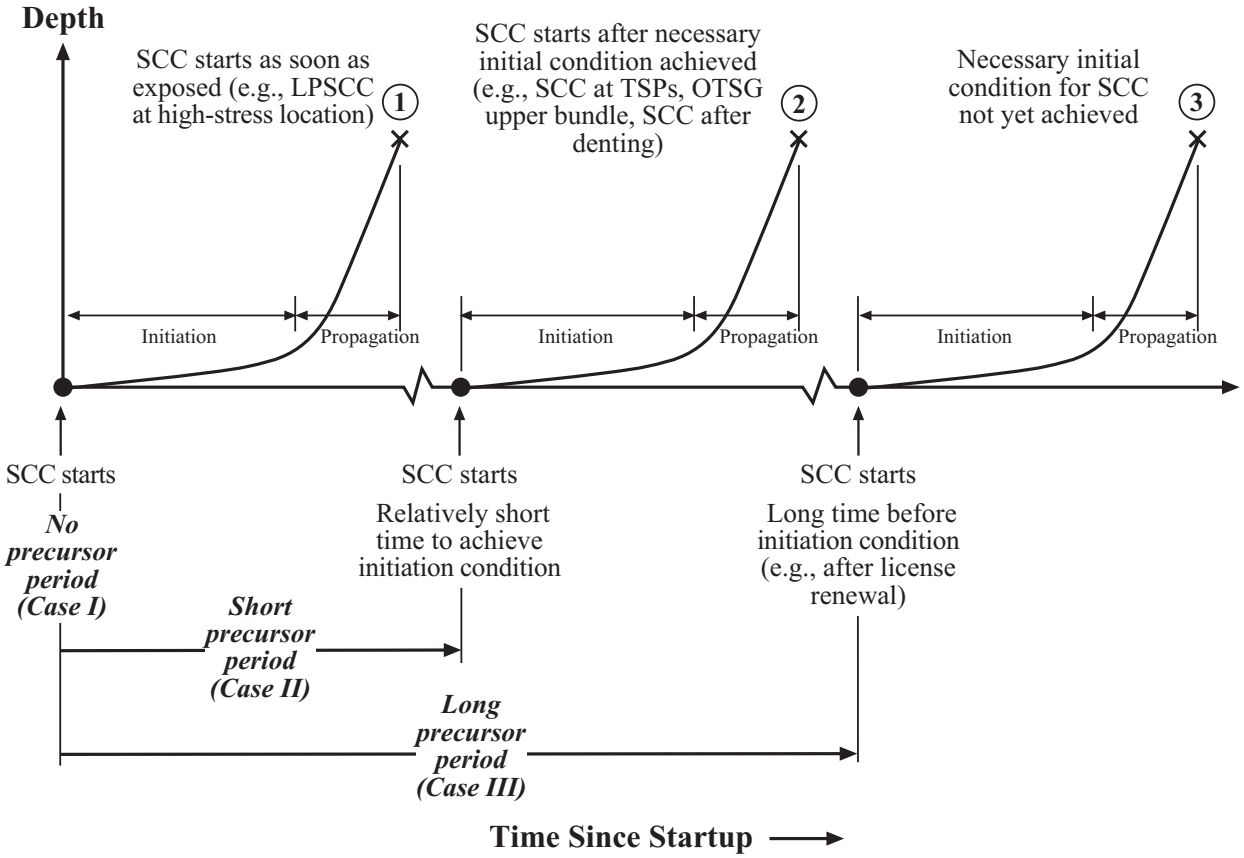

Figure 5 Three cases for progress of SCC vs. time depending on the time required for precursors. (a) No precursor. (b) Relatively short precursor. (c) Relatively long precursor. From Staehle.[45,46]

Thus, there are numerous examples of Case I where degradation damage begins with the start of equipment, and no special condition must accumulate prior to the monotonic SCC as shown in Figures 3 and 5. While these cases may proceed slowly, as for FAC and V. C. Summer, they still belong in the category of Case I.

In this description of Case I, Figure 3 is implicitly applied. For example, before SCC is visible some diffusion at grain boundaries may be required. However, such preliminary steps are part of the incubation indicated in Figure 3.

Case II - Relatively Short Precursor

In Case II, as shown in Figure 5, some precursor process is required before the requisite

conditions are present for SCC. Such short term precursors are usually in the range of half to 20 years. ODSCC of SG tubes is a good illustration as shown in Figure 11. Here, chemicals must accumulate in the superheated crevices before SCC occurs. The time required for such accumulations was relatively short and ODSCC occurred typically within a few years, sometimes less, from startup. Refer to the Staehle and Gorman paper[5] for background.

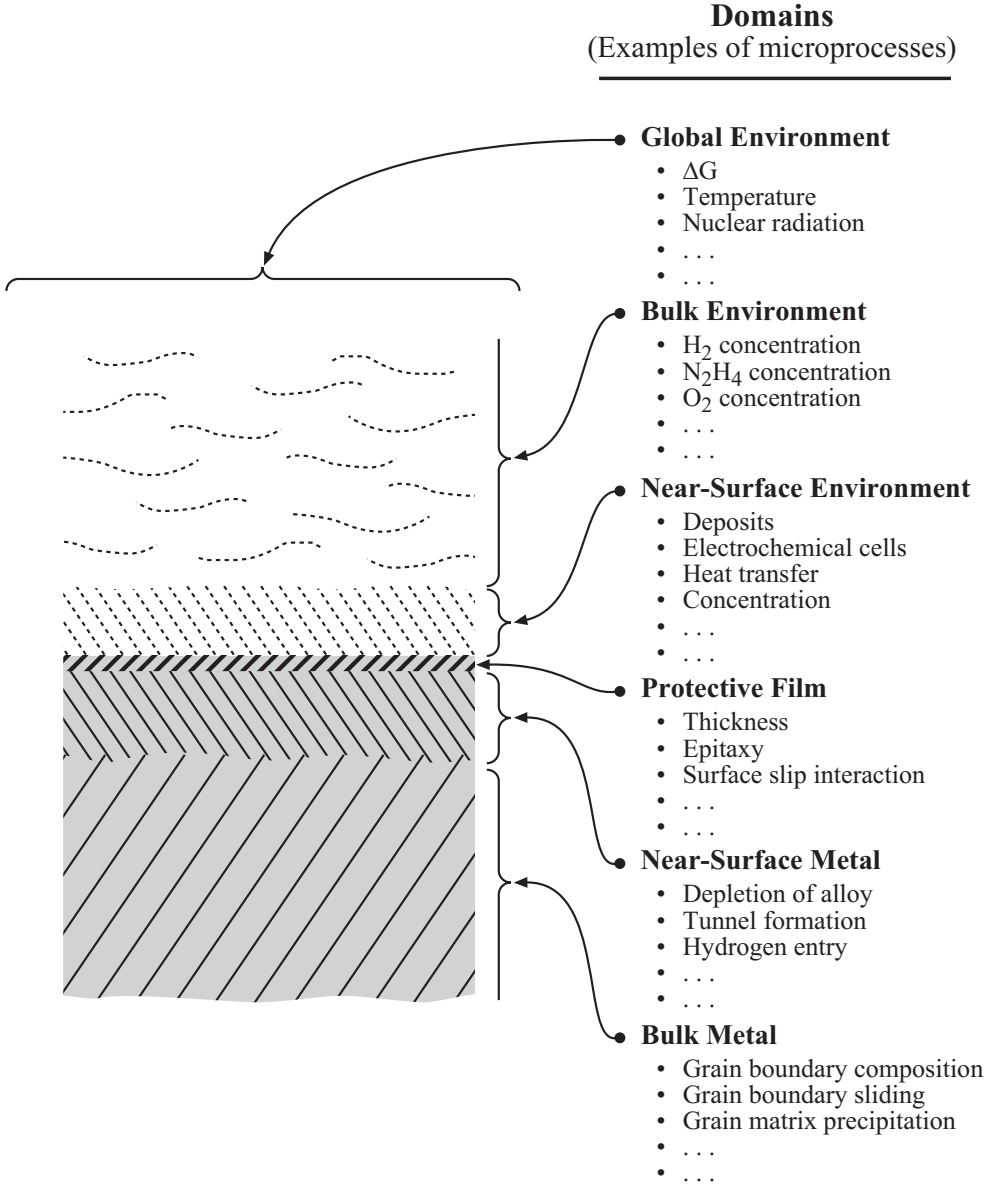

Figure 6 Domains in which single and multiple precursors can be identified. Within each domain are "microprocesses," which can become part of a precursor scenario. These domains are: global environment, bulk environment, near-surface environment, protective film, near-surface metal, and bulk metal. These domains are only illustrative. From Staehle.[45,46]

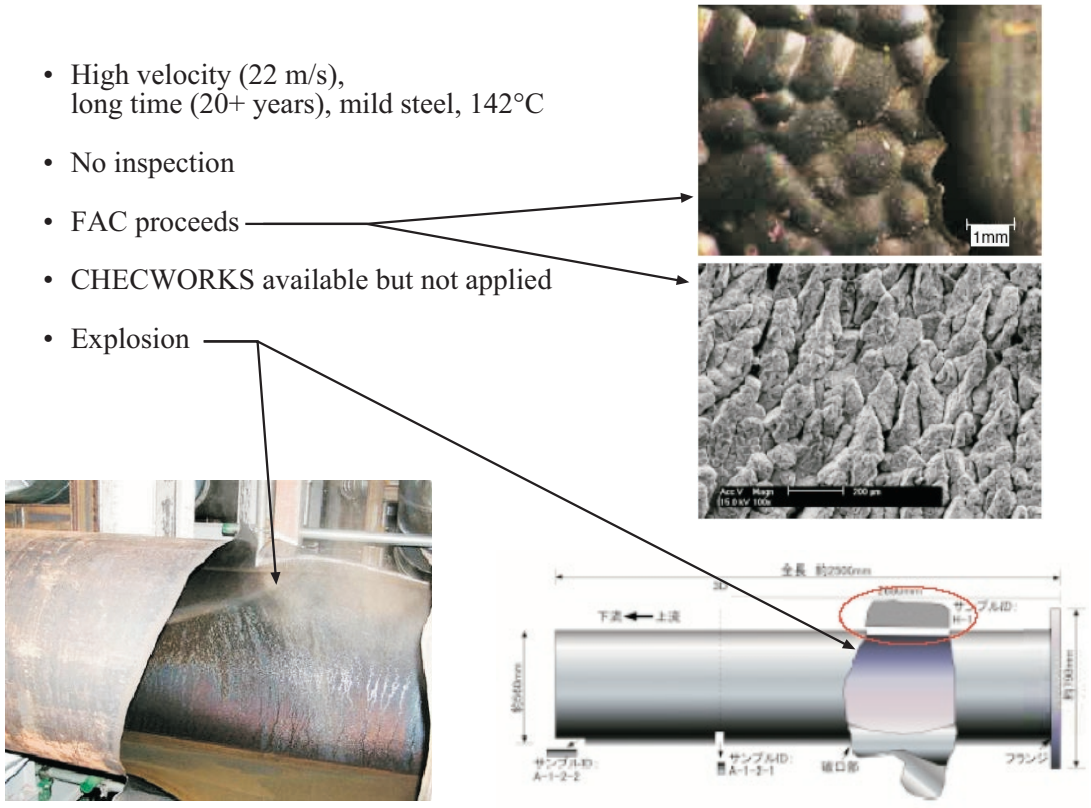

Figure 7 Sequence of events for FAC failure at Mihama. The FAC was a Case I type failure with no precursors required.

Also, a relatively short time is required for the perforation of fuel element cladding when the local power is too high, and deposits are also forming as in Figure 12. Here, deposits develop more rapidly at locally high power. These deposits produce a thermal resistance that increases the temperature on the surface of the zirconium alloy cladding. The zirconium alloy corrodes more rapidly, and the resulting zirconium oxide product produces more thermal resistance and a still higher surface temperature. This synergistic increasing thickness of surface deposits and zirconium oxide leads eventually to perforation within several years. Here, the precursor consists of two different physical processes as in the deposition of deposit materials and the oxidation of the cladding. This accelerated perforation results from excessive local power densities.

The occurrence of denting, shown in Figure 13, on SG tubes is a good example of a Case II precursor. The term, "denting," refers to the narrowing of the diameter of the tube as a result of expanding corrosion products produced by accelerated corrosion at the tube support. Thus, when a probe is inserted into the tube for inspection, it encounters "dents" in the diameter. Here, as with Figure 11, the first precursor is the accumulation of iron oxide; the second is the accumulation of corrosive chemicals from the evaporation of chemicals due to superheat. For the case of denting, the tube support material corrodes and produces oxide of a volume about three times that of the corrode metal. Such an increase in volume of oxides relative to the original metal is based on the work of Pilling and Bedworth[55] in 1923. The progressive corrosion and resulting strain on the tube produces ODSCC and IDSCC both of which can perforate the tube wall.

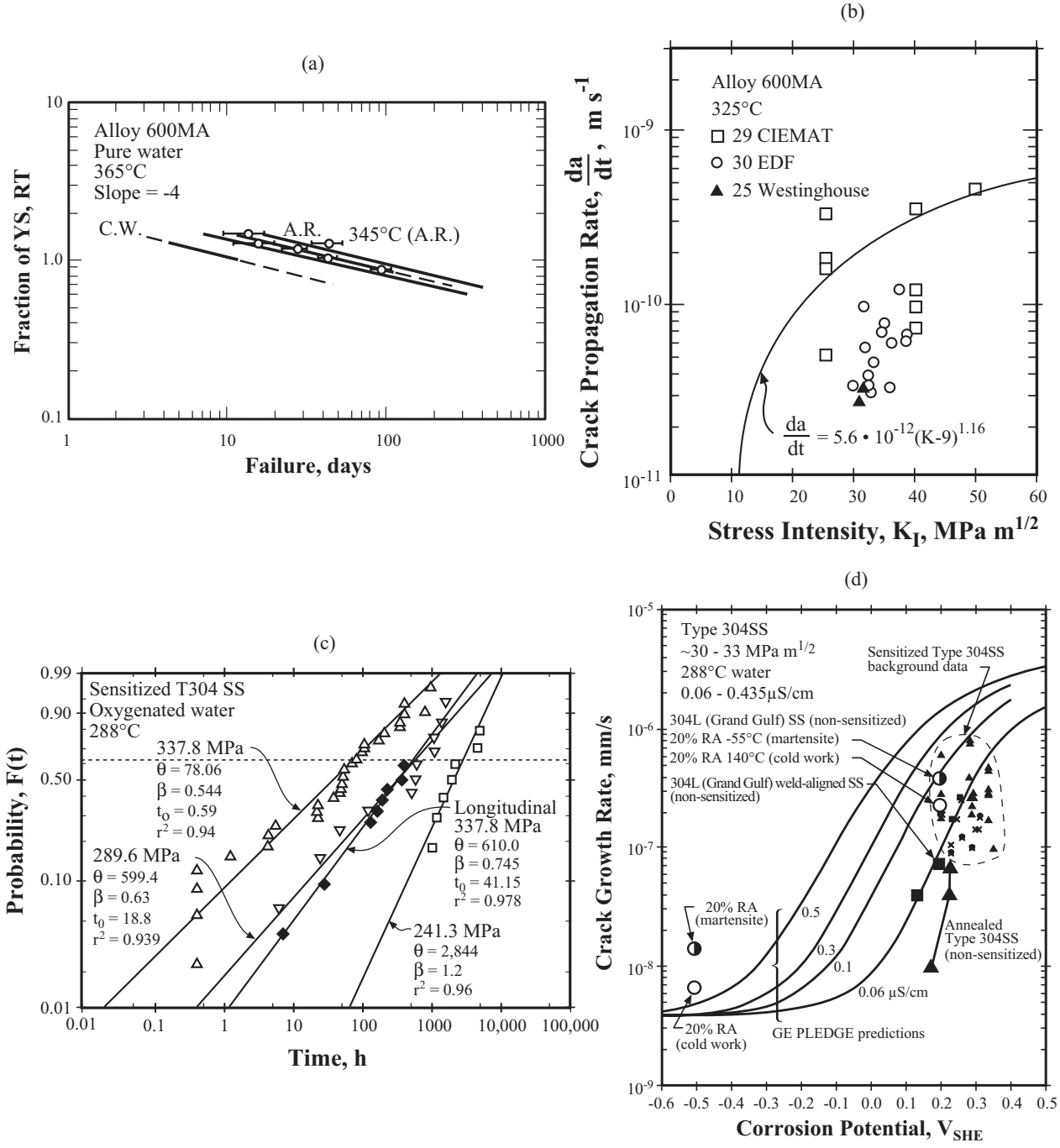

Figure 8 (a) Alloy 600MA in pure water at 365°C; fraction of yield stress vs. failure time for as rolled and cold worked. From Bandy and van Rooyen.[48] (b) Crack propagation rate vs. stress intensity for Alloy 600MA at 325°C. From Scott.[49] (c) Probablity vs. time-for-initiation controlled-failure of sensitized Type 304SS exposed to 288°C pure oxygenated water. From Clarke and Gordon.[50] (d) Crack growth rate vs. corrosion potential for Type 304 in conditions of sensitized, non-sensitized, and cold worked, exposed in 288°C BWR water. From Angeliu et al.[51]

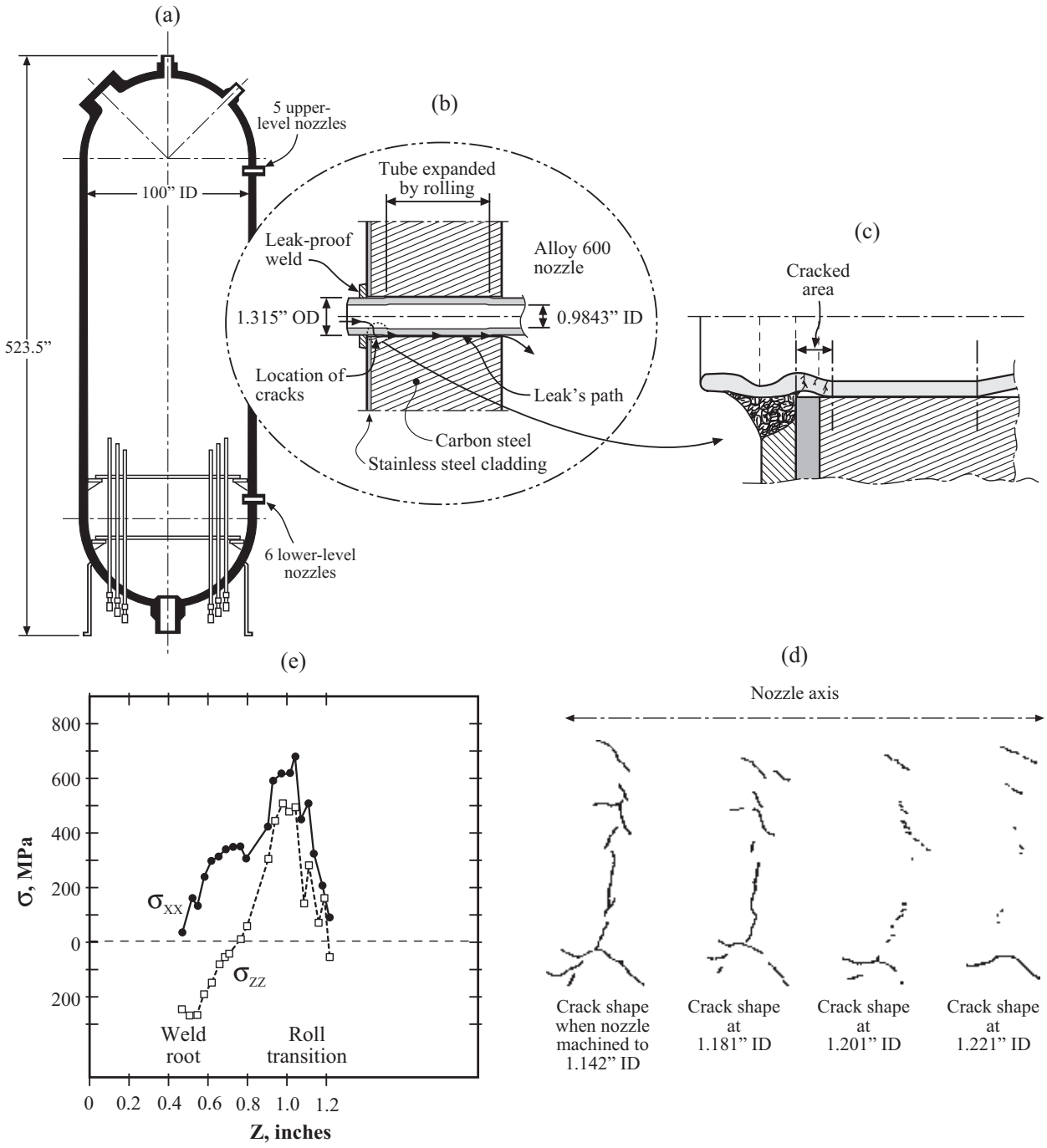

Figure 9 (a) Overall view of pressurizer from 1300 MW plant showing locations of instrument nozzles. (b) Overview of nozzle showing locations of weld and leaks. (c) Detailed view of nozzle showing effect of welding on the roll transition zone and location of cracks. (d) Detailed view of SCC with dimensions given in terms of ID and successive machining to reveal shape of SCC. Destructive examination of one nozzle from Flamanville-2. (e) X-ray diffraction measurements of the inner surface residual stresses. From Alter, et al.[52]

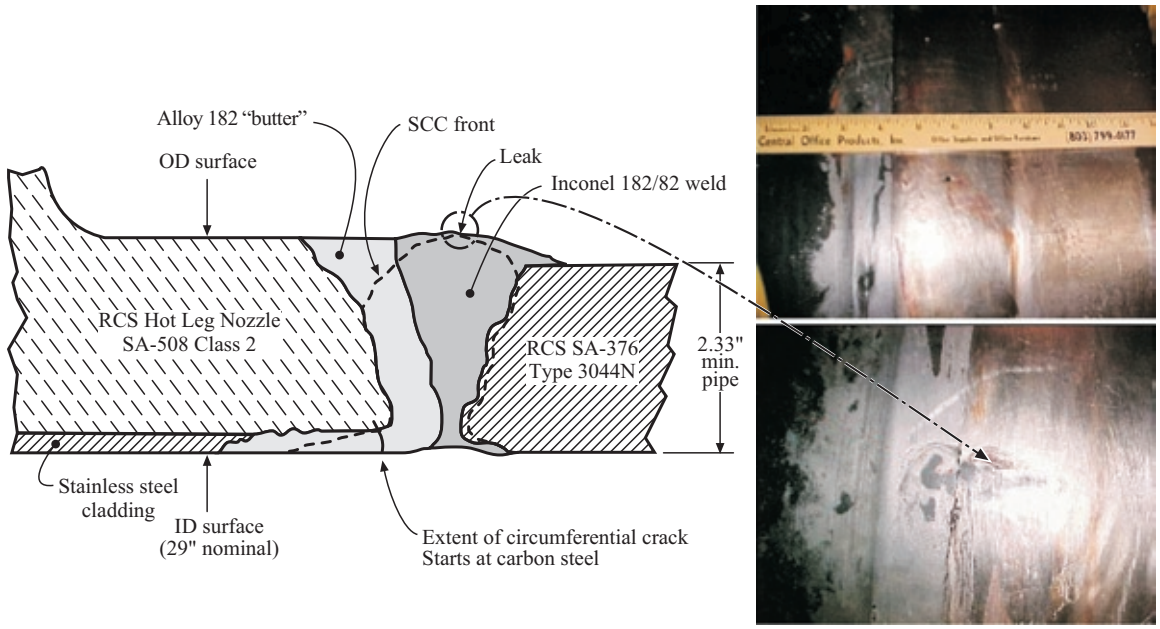

Figure 10 SCC in hot leg nozzle to pipe weld with Alloy 182 and 82. Crack discovered in Fall 2000 at the V.C. Summer plant. From EPRI.[53]

A longer time for accumulation of deposits occurred in OTSGs in the upper bundle as illustrated in Figure 14. Here, about 10 years were required (shown in Figure 14(c)) before significant SCC occurred; and then it occurred initially at pre-existing scratches. This initial time was required before the concentration of impurities (Figure 14(b)) on the superheated surfaces of the upper bundle had accumulated sufficiently.

The near catastrophe at Davis Besse is shown in Figure 15. Here, the first step was the residual stresses at the weld. Second, LPSCC was incited. Third, the leak and expansion of the steam through the LPSCC concentrated the boric acid and lithium that produced a corrosive solution. The ultimate corrosion rate was on the order of several inches per year. Such a high rate of corrosion in steel at low pH had been established in the work of Pourbaix[56] many years ago in similarly mild acidic solutions.

Each of the Case II examples shown in Figures 11-15 followed a different sequence involving different physical processes as follows, generally in order of increasing length of precursor time:

Figure 11 ODSCC in RSG tube supports

- Deposits of mainly iron oxide.
- Chemicals concentrate in tight crevice.
- SCC develops in OD of tube.
- Earliest OD SCC probably 1-2 years.

Figure 12 Fuel perforates

- Deposits accumulate on fuel.
- Surface temperature of zirconium alloy increases due to thermal resistance of deposit and

corrodes increasingly rapidly.

- Increased thickness of zirconium oxide further increases the thermal resistance and the surface temperature of the remaining metal.
- Perforation occurs.
- Requires 2-3 years.

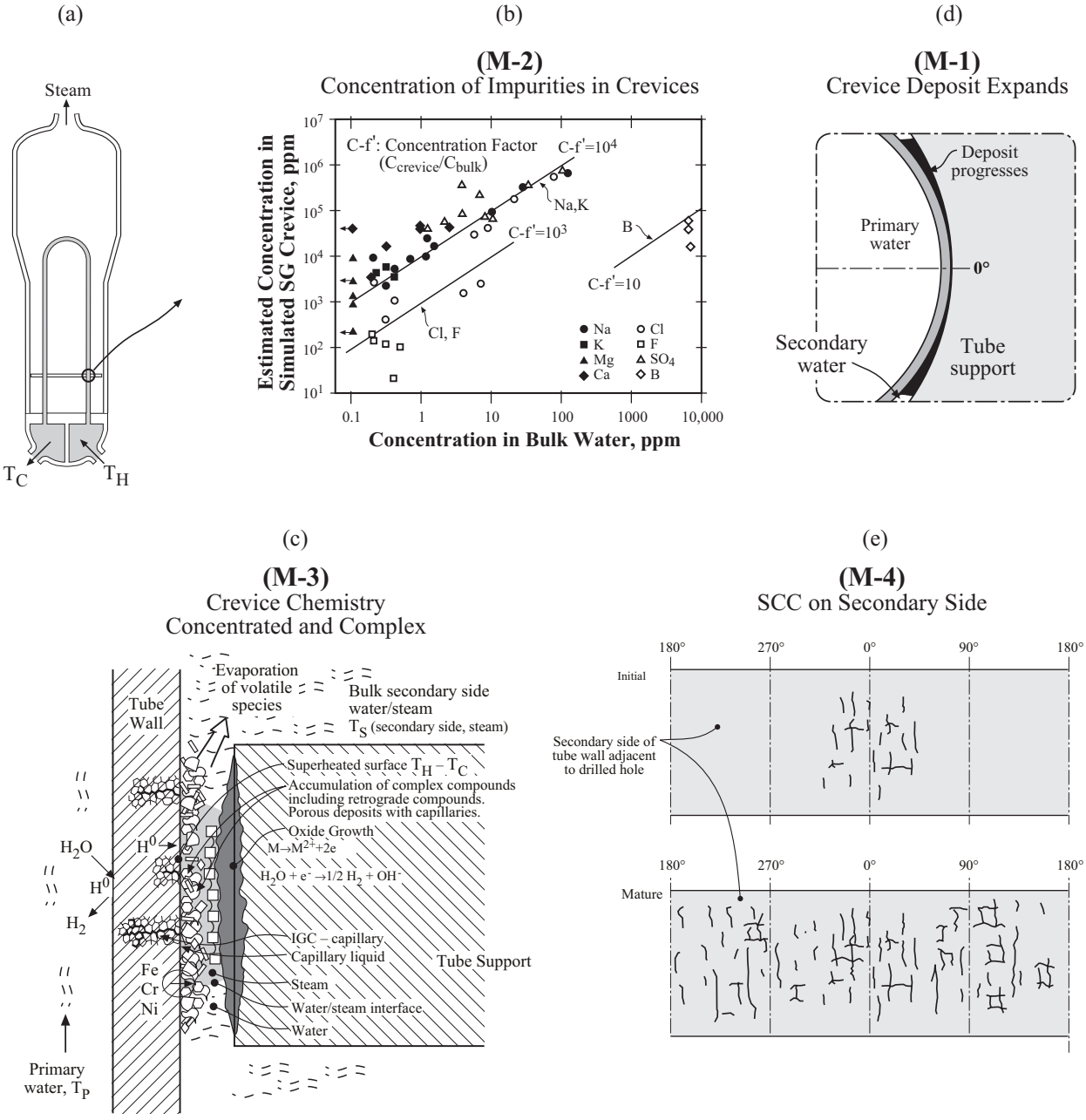

Figure 11 Sequence of events for ODSCC in RSGs. (a) (M-1) Iron oxide accumulates. (b) (M-2) Concentration of dilute environmental species in superheated crevice. From Staehle and Gorman.[5] (c) (M-3) Schematic view of conditions in a heat transfer crevice. (d) (M-4) Evolution of SCC.

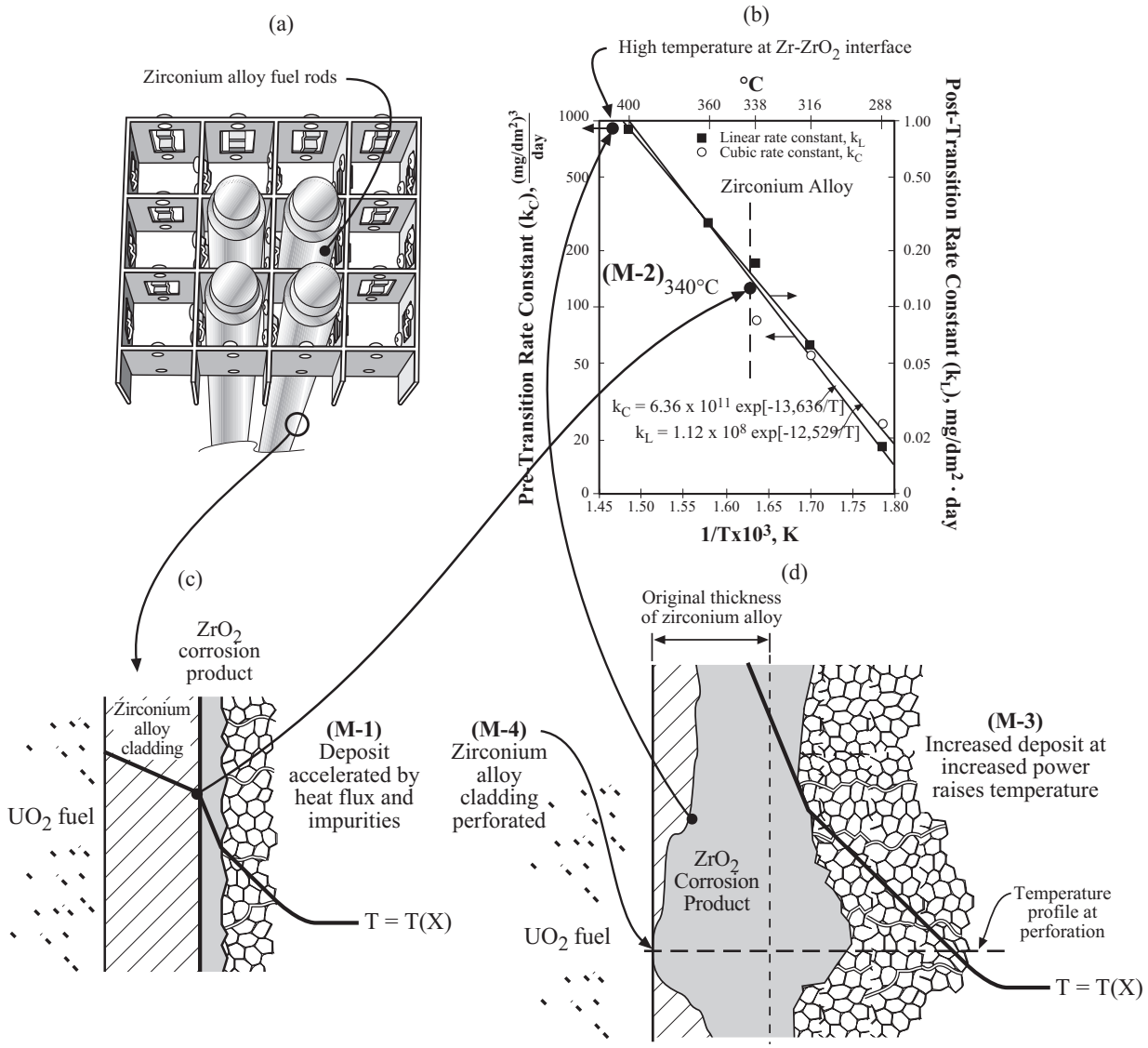

Figure 12 (a) Zirconium alloy fuel rods with hot surfaces (M-1). (b) Rate constants vs. 1/T for pre and post transition oxidation of zirconium alloy (M-2). From Hillner.[54] (c) Schematic view of deposit formed on surface of zirconium alloy cladding with think oxide of zirconium. (d) Thicker deposit (M-3) and thicker ZrO_2 producing perforation (M-4).

Figure 13 Denting at RSG tube supports

- Deposits of mainly iron oxide.
- Chemicals concentrate.
- Corrosion product oxide thickens.
- Tube strains reducing diameter from the exterior force of the expanding oxide and produce stress at transition from original tube diameter to constricted diameter.
- Earliest evidence about 4-5 years.

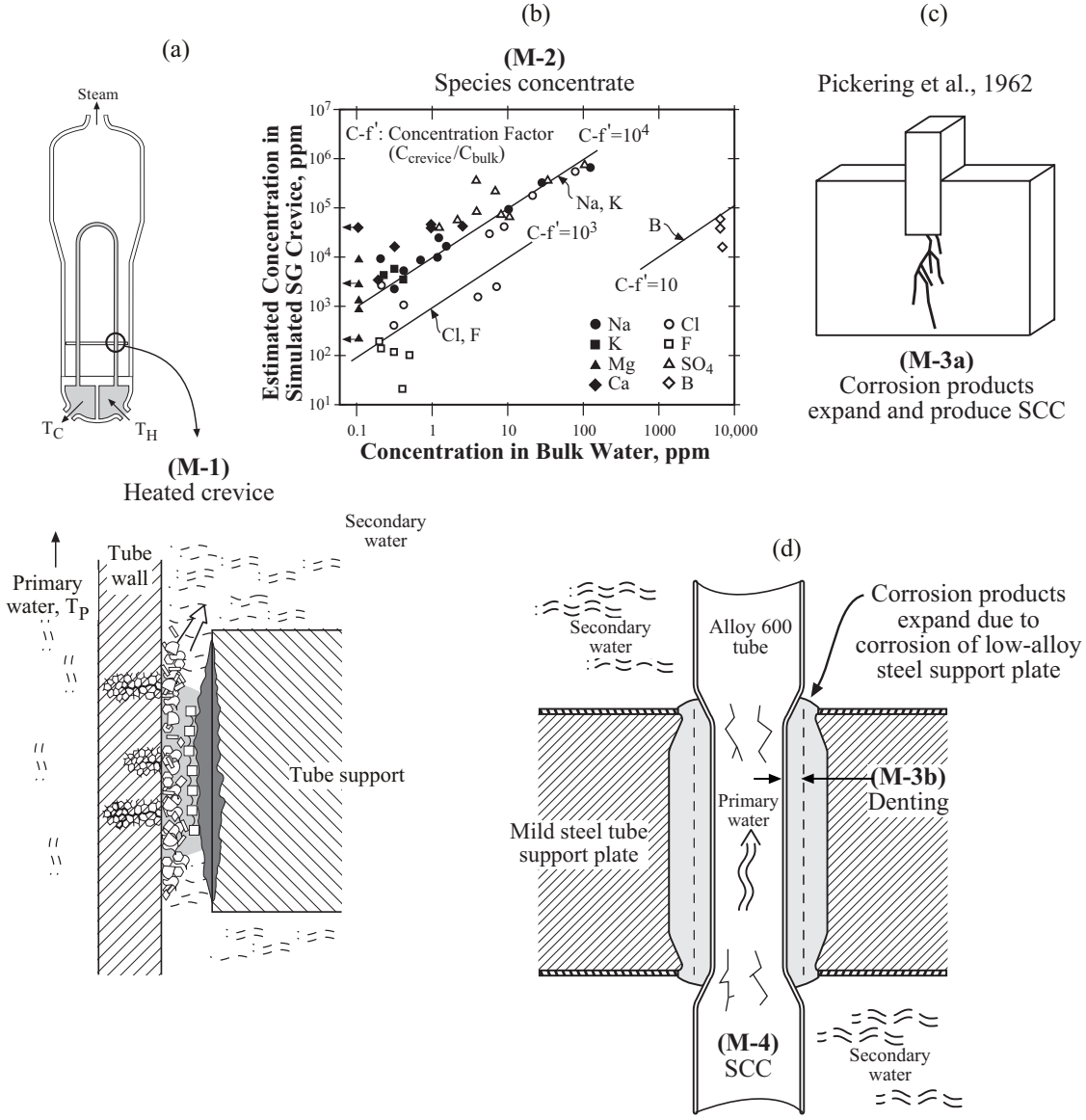

Figure 13 (M-1) Heated crevices concentrate mostly iron oxide and chemical species. (M-2) Chemical species concentrate in superheated crevice. (M-3a) Vignette shows Pickering et al.[143] experiment that elucidated denting 12 years before it occurred. (M-3b) Volume of corrosion products increases. (M-4) SCC on ID and OD develop at the locations of highest strain.

Figure 14 OTSG upper bundle

- Upper bundle surfaces are superheated.
- Scratches present.
- Chemicals concentrate on superheated surfaces.
- SCC initiates at scratches but extends to non-scratched region.
- About 10 years required for significant SCC.

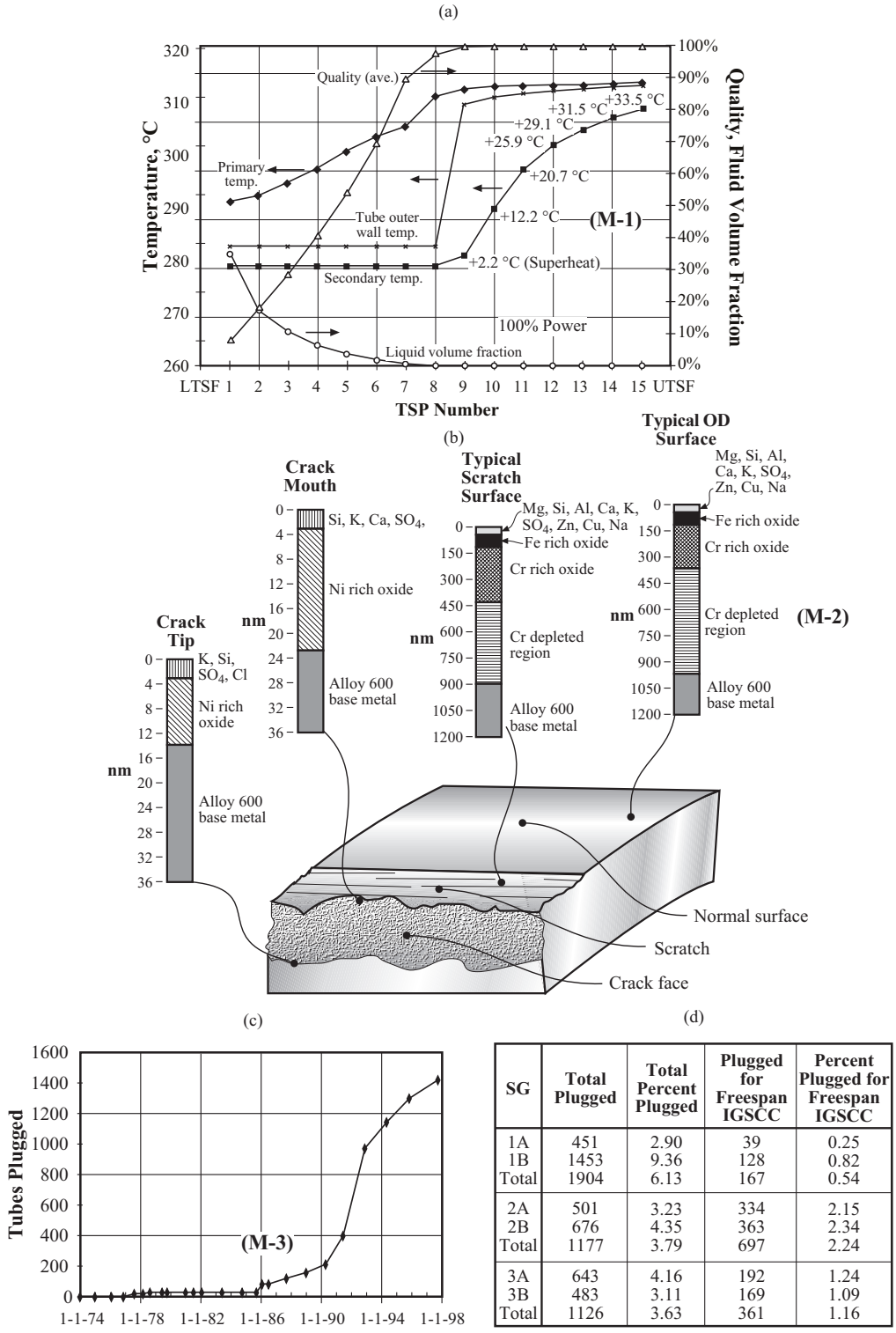

SG	Total Plugged	Total Percent Plugged	Plugged for Freespan IGSCC	Percent Plugged for Freespan IGSCC
1A	451	2.90	39	0.25
1B	1453	9.36	128	0.82
Total	1904	6.13	167	0.54
2A	501	3.23	334	2.15
2B	676	4.35	363	2.34
Total	1177	3.79	697	2.24
3A	643	4.16	192	1.24
3B	483	3.11	169	1.09
Total	1126	3.63	361	1.16

Figure 14 Occurrence of SCC in upper bundle of OTSG. (a) Temperature and physical conditions of SG (M-1). Courtesy of D. Rochester.[57] (b) Surface chemistry on surface and in scratches and SCC (M-2). From Rochester.[58] (c) Tubes plugged vs. time (M-3). From Rochester and Eaker.[59] (d) Details of tube plugging.

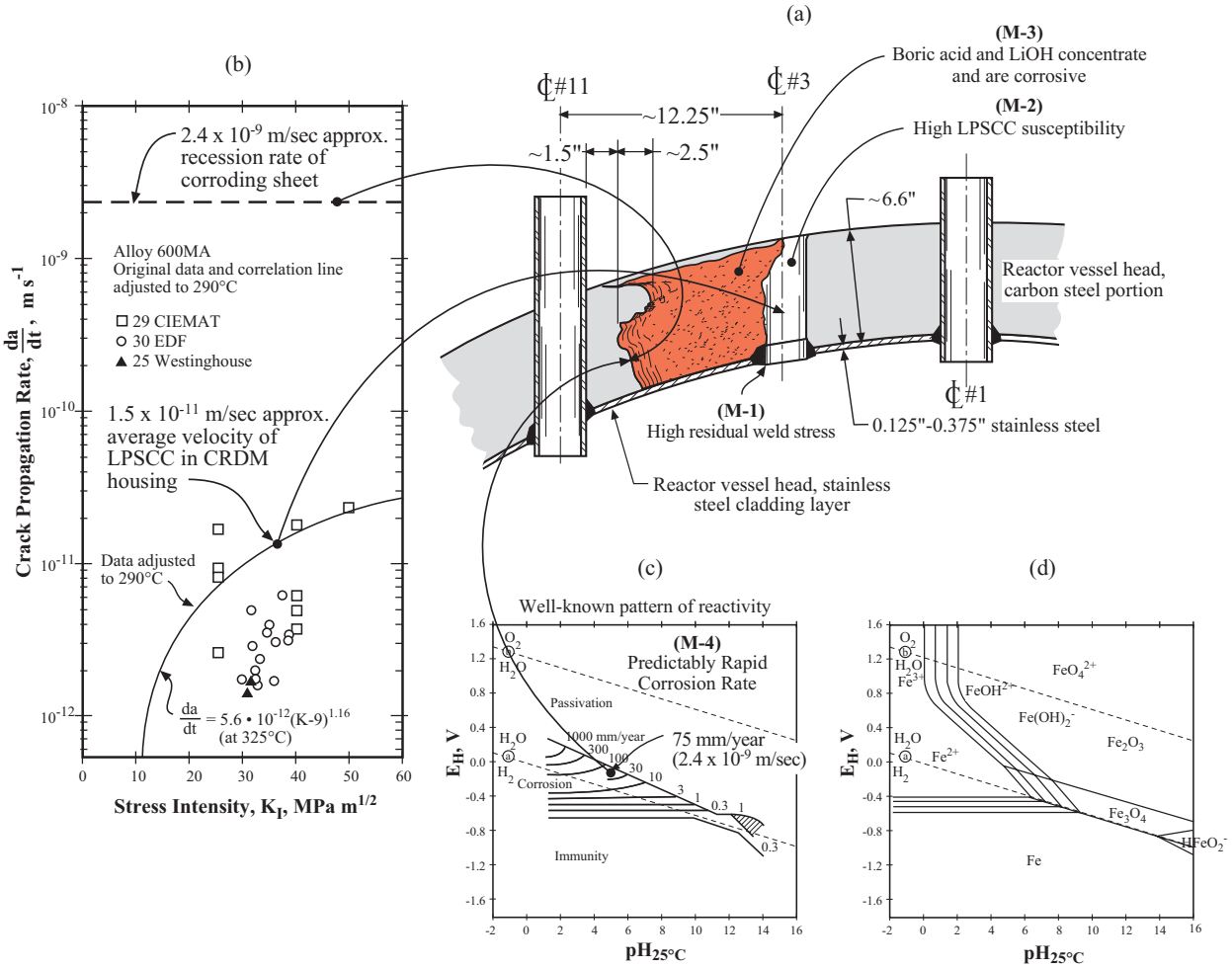

Figure 15 Failure at Davis Besse plant. (M-1) High residual weld stresses. (M-2) High susceptibility to LPSCC in Alloy 600MA. (M-3) Exiting steam deposits boric acid and lithium hydroxide. (M-4) High corrosion rate. From Pourbaix.[56]

Figure 15 Davis Besse corrosion of reactor vessel head

- Residual stresses from weld of CRDM housing.
- LPSCC perforates wall of CRDM.
- Water exits through LPSCC.
- Boric acid and lithium hydroxide concentrate.
- Vessel head corrodes.
- About 16-20 years required for serious corrosion.

The sequence of events described in the different examples of Figures 11-15 shows that precursors lasting up to 20 years are credible in terms of even present observations from plants that have less than thirty years of life.

Case III - Long Time Precursors

In Case III the precursor process is much longer than for Case II as shown schematically in Figure 5; Case III precursors might easily require 20-30 years or more, especially with the more pure water, improved alloys, and line contact crevices.

Thus, predicting degradation in the long term will require more attention to the precursor events than to the SCC, which may be already well defined. However, after these long times, the conditions that produce SCC may be different and such possibilities should be investigated according to the methodology of MPSA.[45,46]

As shown by Staehle[45,46] there may be several scenarios that lead to conditions that can produce SCC, just as there are several scenarios that are identified in Figures 11-15. In most cases, these scenarios can be calculated or at least evaluated semi-quantitatively; thereafter, experiments can be conducted to evaluate the calculations.

2.4 Materials

The purpose of this section is to characterize generally the alloys of interest in steam generators.

Materials of SGs are shown in Figure 16. These vary from the medium to high nickel alloys, as well as stainless steels for the VVWR reactors, for SG tubing, to the lower nickel alloys, e.g. 410 stainless steel for support plate materials, and to the low alloy and carbon steels for tubesheets, secondary piping, and vessels. Alloys 690, 600, 800, and Type 321 stainless steel are used in various steam generators for tubing although the use of Alloy 600 is now decreasing owing to its proneness to SCC on the secondary and primary sides.

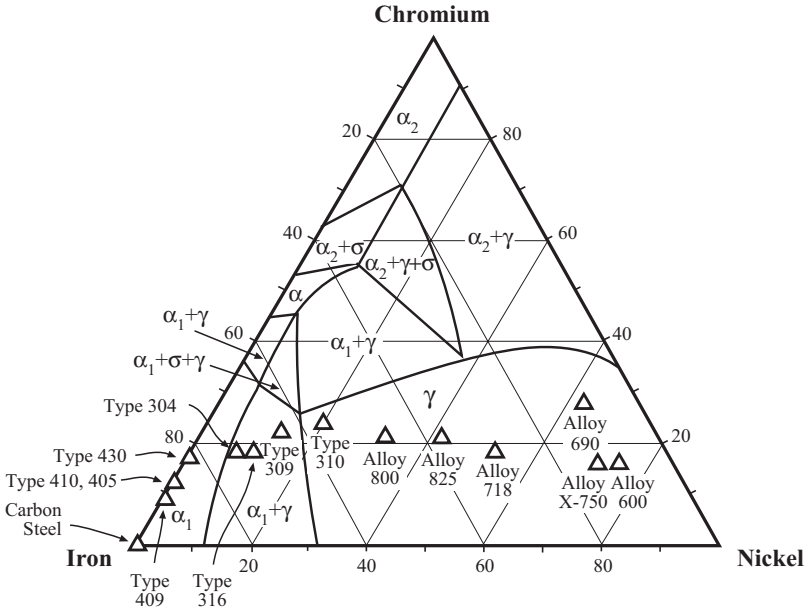

Figure 16 Compositions of important SG alloys superimposed on ternary phase diagram of Fe-Ni-Cr alloys at 400°C. From Pugh and Nisbet.[60]

The most well known trend in the performance of Fe-Cr-Ni alloys is shown in Figure 17(a) from the work of Copson and Cheng.[61,62] Here, the times-to-failure for alloys in boiling $MgCl_2$

are plotted vs. Ni concentration for base alloys having 20% Cr. These data show that the Ni concentration above which SCC does not occur is about 40%. These data ultimately became the bases for choosing high nickel alloys for applications such as SG tubing. Figure 17(b) from Berge and Donati[63] shows the SCC of Alloy 600MA exposed to a boric acid/chloride solution where transgranular SCC also occurred as with the alloys in Figure 17(a); this figure also indicates that the conclusions reached on the basis of Figure 17(a) were specific only to a specific chloride electrolyte, $MgCl_2$.

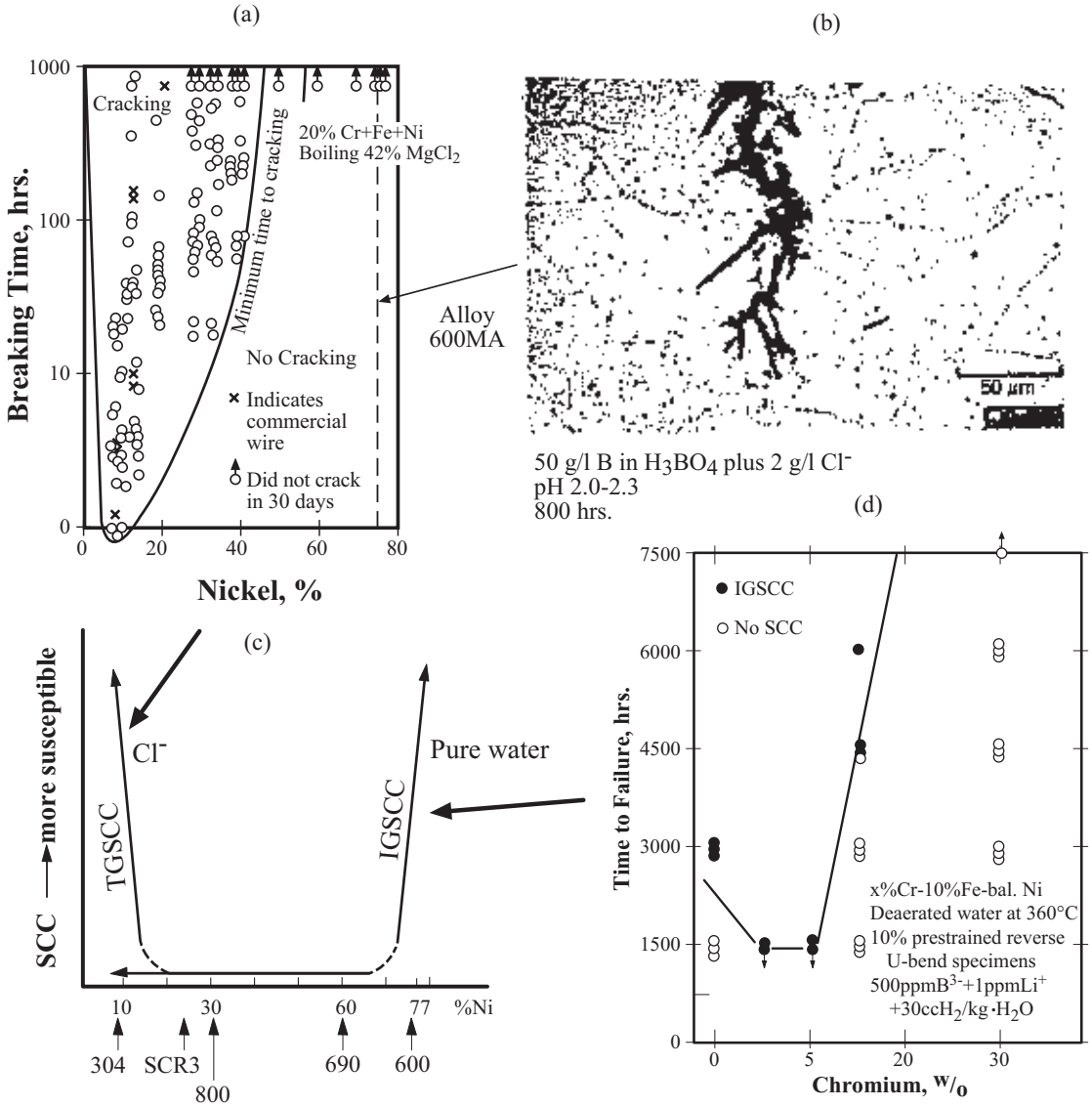

Figure 17 (a) Breaking time vs. Ni for Fe-Cr-Ni alloys exposd to boiling $MgCl_2$ solutions. From Copson and Cheng.[61,62] (b) Transgranular SCC of Alloy 600 exposed to a 100°C solution of boric acid and chloride. From Berge and Donati.[63] The composition of Alloy 600 is noted on (a). (c) Schematic view of susceptibility of Fe-Cr-Ni alloys to SCC in chloride solutions and in pure water. From Coriou et al.[64] (d) Time-to-failure as concentration of Cr for Fe-Cr-Ni alloys with 10w/o Fe. From Nagano and Kajimura.[66]

Figure 17(c) shows the well known schematic plot from Coriou and co-workers[64] suggesting the general patterns for the alloy dependence of SCC in pure water as compared with the SCC, as in Figure 17(a), for chloride solutions. This plot and associated data became the basis for recognizing that the Alloy 600 was not suitable either for SG tubing or for heavy sections and for weld metals. Figure 17(c) also provided the basis for the use of both Alloy 800 and Type 321 stainless steel in SG tubing—the assumption being that concentrated solutions known to produce SCC in these materials would not be present. Both alloys have given good performance for about 30 years.

Figure 17(d) shows the basis for developing Alloy 690 based on work of Nagano and Kajimura.[66] Here, the LPSCC is shown to be negligible above about 20% Ni. Actually, the first such data were published by Copson et al.,[65] and reviewed by Sarver,[161] but Figure 17(d) illustrates the effect of Cr better.

In modern SGs, the tube support materials are in the range of Cr of 12% such as a 410 stainless steel. This prevents the gross corrosion products that produce denting as shown in Figure 13 and minimizes the development of iron oxide in these crevices.

While carbon steel has been used in steam and feedwater piping in the secondary side, its proneness to FAC has lead some vendors to consider alloys of a slightly high Cr concentration based on the data shown in Figure 18.

While Alloy 600TT sustains some SCC, it seems somewhat improved over Alloy 600MA, and the data of Cattant et al.[68] show that Alloy 600TT is superior to Alloy 600MA over long operating times. These data are shown in Figure 19(a). Figure 19(b) shows the relative performance of Alloys 600MA, 600TT, 690MA and TT and 800L SP as a function of pre-strain vs. time exposed in deaerated water at 360°C. Here, the 690 and 800 alloys are substantially superior over the range of cold work to a 20% prestrain.

With time, as shown in Figure 20, the modern SGs in the United States have tended to use Alloy 690TT in their SGs; however, both Alloy 800NG and Type 321SS are used with the Alloys 690TT and 800NG exhibiting the best performance and Type 321 stainless steel in VVWR plants being adequate, exhibiting some but not excessive failures.

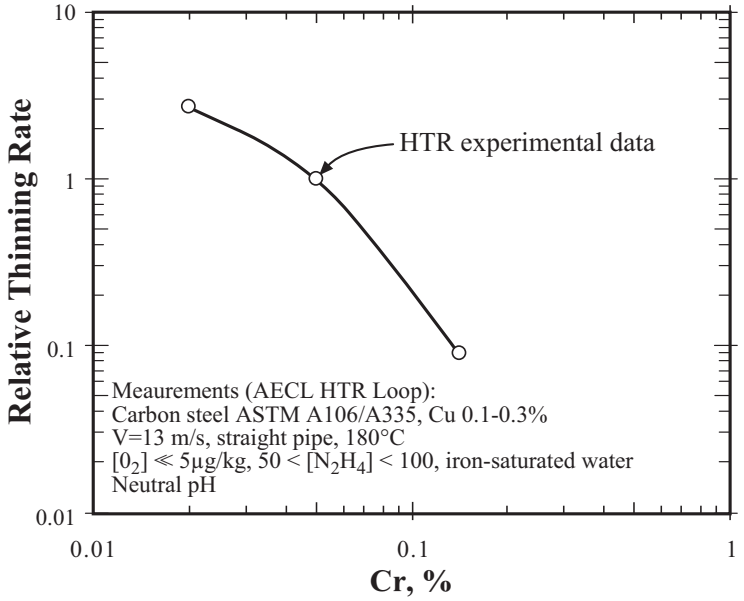

Figure 18 Relative thinning rate vs. concentration of Cr at 180°C. From Tapping.[67]

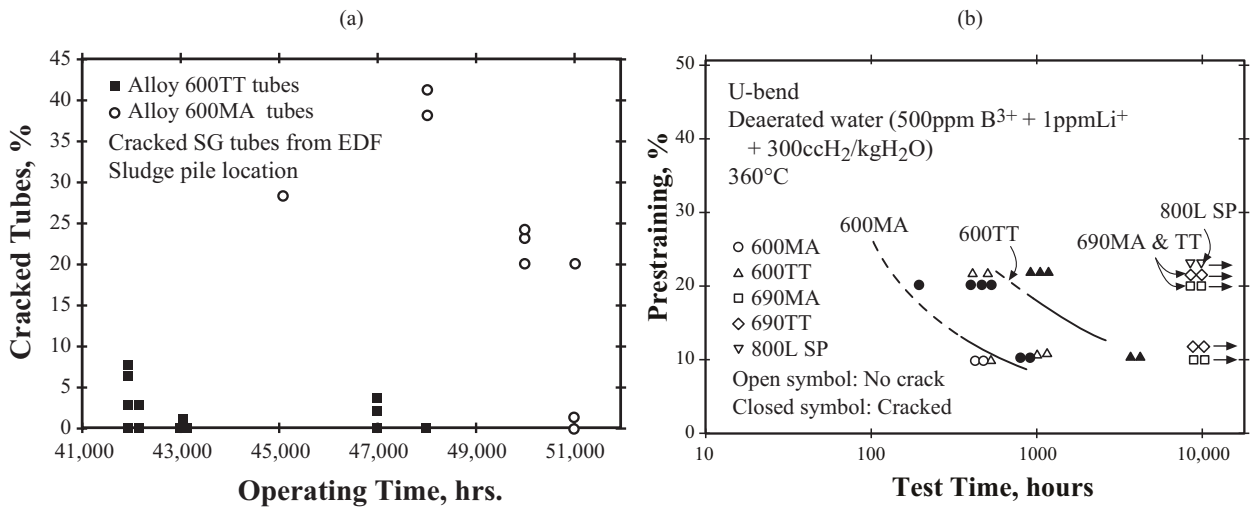

Figure 19 (a) Percent cracked tubes vs. operating time for Alloys 600TT and 600MA. From Cattant et al.[68] (b) Prestrain vs. test time for cracked specimens of Alloys 600MA, 600TT, 690MA, 690TT, 800L SP, exposed to deaerated water as U-bends at 360°C. From Nagano et al.[69]

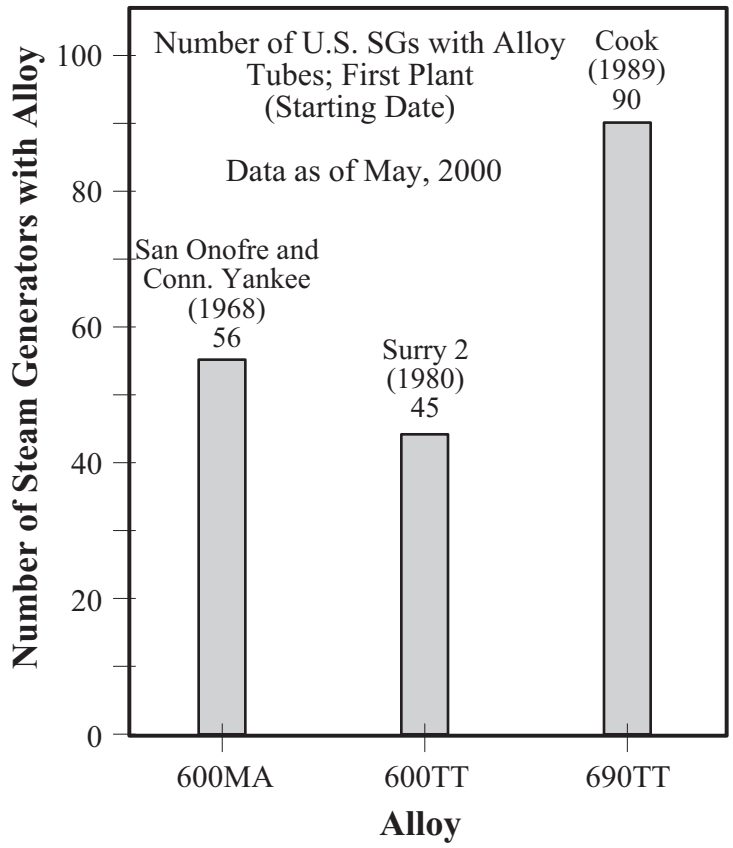

Figure 20 Usage of high Ni alloys in US SGs as of May 2000. First plant to use alloy and date shown at tops of bars. Courtesy of A. McIlree.[70]

In general, trends in the use of tubing alloys seem to be the following based on performance in operating plants:

- Alloy 800 continues to provide good performance since about 1975.
- Alloy 690TT has provided good performance since 1989.
- Type 321 continues to provide adequate performance with low but acceptable rates of failure.
- Alloy 600TT exhibits performance that is improved, but not significantly, over Alloy 600MA considering both primary and secondary environments.
- Alloy 600MA can perform adequately for reduced times. This alloy is now sustaining SCC in thick sections.

2.5 Aqueous Thermodynamics

The purpose of this section is to identify the important role of aqueous thermodynamics as it is relevant to corrosion and water chemistry. This section provides background for subsequent sections in Section 2.0.

Aqueous thermodynamics provides the primary framework for understanding corrosion and water treatment as well as the bases some of the precursors as identified in Figure 5. Much of this understanding comes from the potential-pH diagrams in Figure 21 as shown for important alloying elements taken at 300°C. Figure 22 shows the solubilities of Fe, Cr. and Ni at 300°C, which correspond to the respective diagrams in Figure 21. From Figures 21 and 22 the following are important:

- Cr is more stable in the acidic region than Fe.
- Fe is more stable than Cr in the alkaline region. Cr is unstable in the alkaline region.
- The maximum insolubility of Fe is at about $pH_{300°C}$ 7. This is the basis for most of secondary water chemistry: i.e. minimize the solubility of iron by keeping the pH in the high temperature range of 7.
- Ti is broadly stable in PWR primary and secondary systems owing to the broad insolubility of TiO_2. This is the basis for using Ti tubes in condensers and for using TiO_2 or an inhibitor.
- The Cu^+ and Cu^{2+} are not soluble in deaerated systems and their equilibrium potentials with copper are oxidizing.
- The solution potentials for Pb and Ni are similar.

An overall view of equilibrium potentials for metals and compounds relevant to corrosion in SGs is shown in Figure 23. Here, the potential on the standard hydrogen scale is shown for the hydrogen electrode, hydrazine, iron, chromium, mixed oxides, nickel, lead and copper. Features that are evident from Figure 23 are the following:

- The open circuit potential in an SG, not considering hydrazine, readily oxidizes Fe.
- The very low hydrogen concentration on the secondary side gives a relatively high equilibrium potential.
- The mixed oxides, which contain Ni, are significantly more stable than NiO.
- The solution potential of Pb is about the same as for Ni.

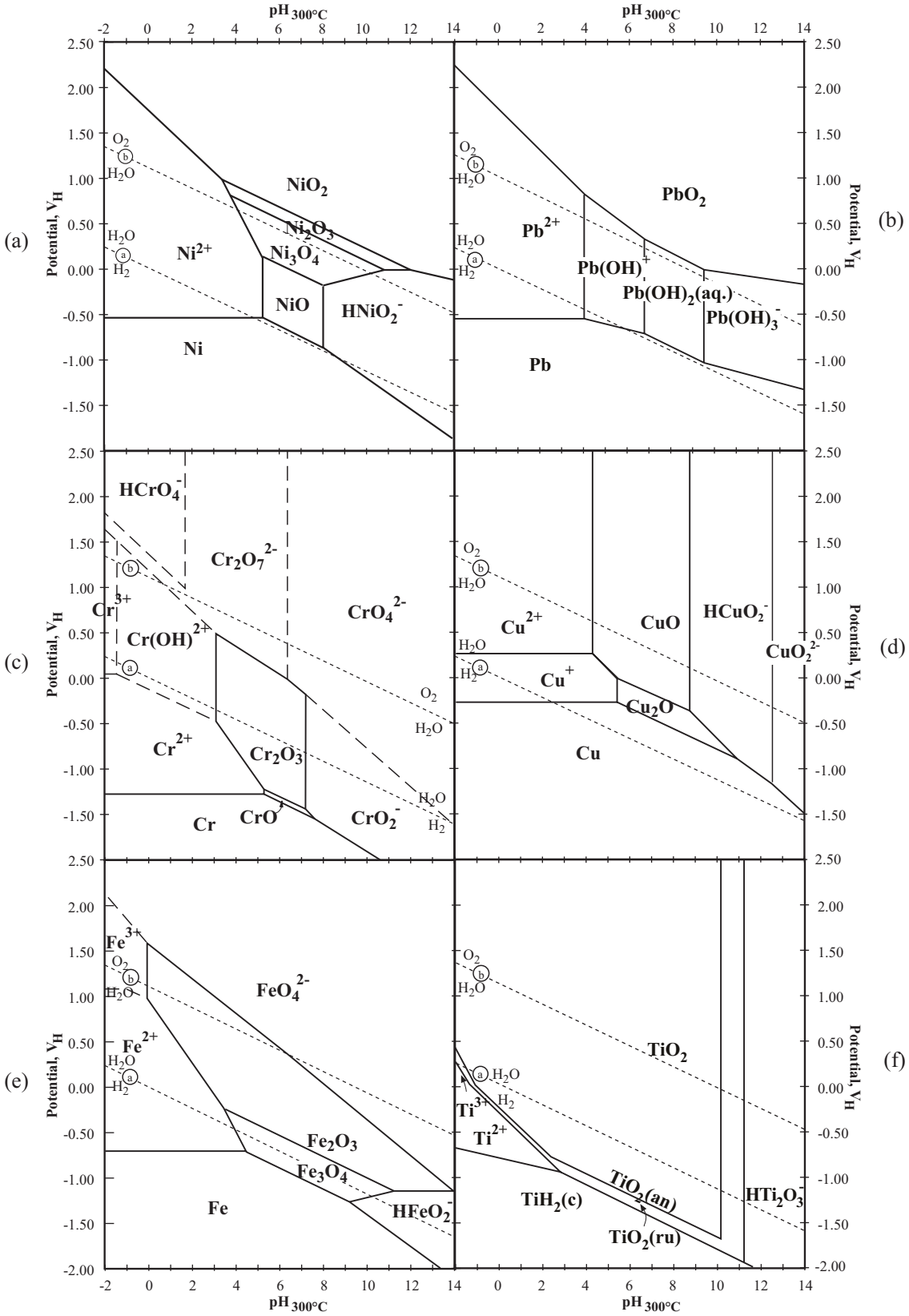

Figure 21 Potential vs. pH for Ni, Cr, Fe, Cu, Ti, Pb at 300°C. From Staehle and Gorman[5] and from Chen et al.[71] and Miglin.[72]

- Copper should not be oxidized in an SG but if present as ions should be oxidizing.
- While hydrazine exhibits a low equilibrium potential, its slight effect on the overall open circuit potential suggest that its reducing effect is sluggish.
- Increasing the pH, e.g. to advanced amines, will increase the solubility of Cr.

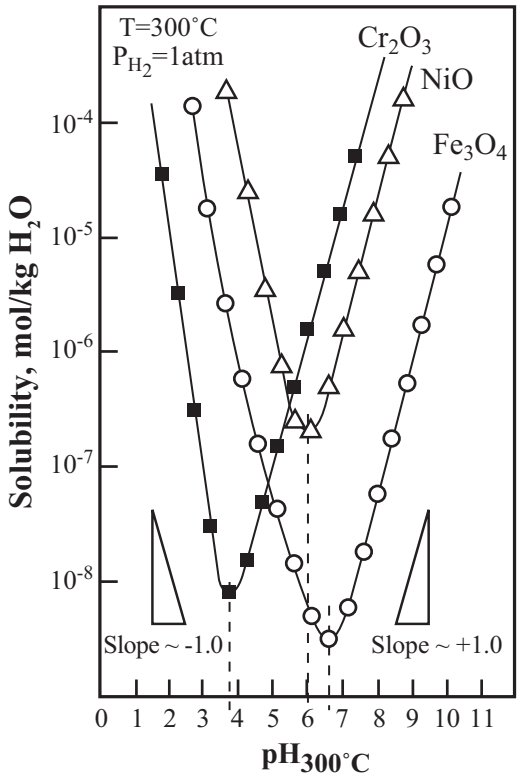

Figure 22 Solubility in pure water vs. $pH_{300°C}$ for Fe, Ni, Cr. From Arioka.[73]

Figure 24 shows, schematically, the effects of hydrogen on the equilibrium potential. Important here are the increased potential owing to the low hydrogen on the secondary side, the lower potential on the primary side owing to the intentionally added hydrogen, which is about 2 ppm, the effect of accumulated hydrogen in a static autoclave on the potential, and the basis for low hydrogen on the secondary side. An important implication of Figure 24 is that corrosion studies conducted in static autoclaves are probably useless for application to the secondary side unless the corrosion-produced hydrogen is controlled to the range of about 1 ppb.

Finally, important to the occurrence of PbSCC and S^{y-}SCC, which are discussed in Sections 3.2, 3.3, and 3.4, is Figure 25 which compares the E-pH diagrams of Pb and sulfur at 300°C. Whereas, the Pb tends to become less soluble in the neutral range and to change sign from minus to plus with decreasing pH, the -2 sulfur tends to become more soluble as it forms HS^- and then H_2S with decreasing pH in contrast to the lower solubility of the S^{2-} alkaline species. This trend suggests that the low valence sulfur species may be more aggressive for S^{y-}SCC of Alloy 690TT in the neutral region than PbSCC in the same range. However, as discussed in Section 3.4, S^{y-}SCC, like PbSCC, is minimum in the neutral AVT range.

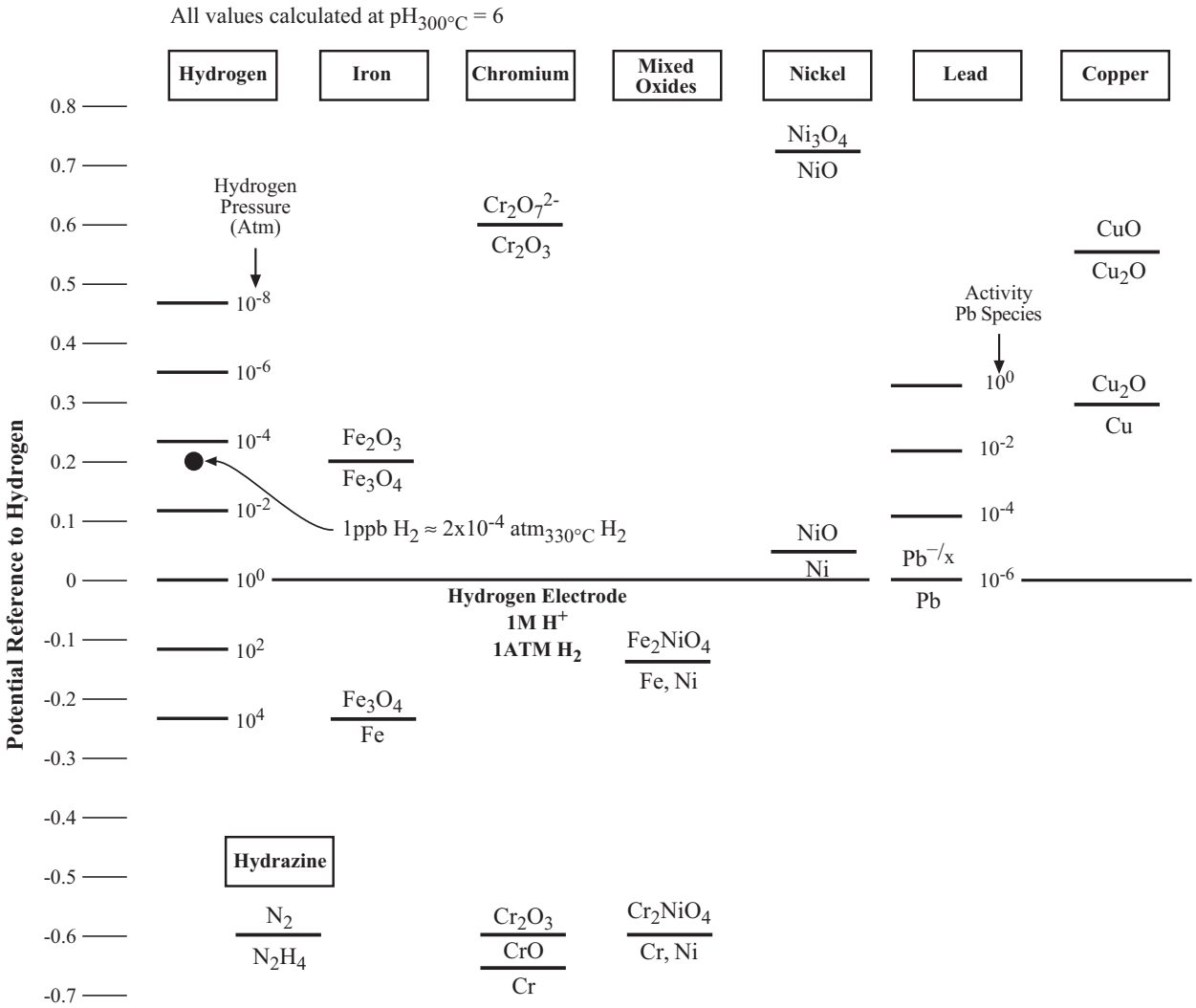

Figure 23 Standard electrochemical potentials vs. material at $pH_{300°C}$6 with respect to the standard hydrogen electrode.

The thermodynamically based aqueous electrochemistry in Section 2.5 together with the metallurgy of Section 2.4 provides the major bases for interaction among materials and aqueous environments.

2.6 Submodes

The purpose of this section is to describe the dependence of different submodes of SCC, mainly of Alloy 600, on potential and pH.

With the evolution of ODSCC starting in the early 1970s especially, as well as IDSCC, the possible SCC of Alloy 600MA was studied in various environments that were considered likely to model the chemistry in crevices. These environments included mainly alkaline and acidic environments although variations in these environments were considered including ones containing chloride or alumino silicates. Also, more complex environments having complex chemistries, which might model crevice chemistries were also studied. Early, these studies were focused on

Alloy 600MA, but later these studies were extended to Alloy 600TT. Still later, Alloy 690TT received more attention, based on reasonable expectations of chemistries that might accrue in the superheated crevices.

At the same time, deoxygenated and oxygenated environments of mainly pure water or primary water were extensively studied.

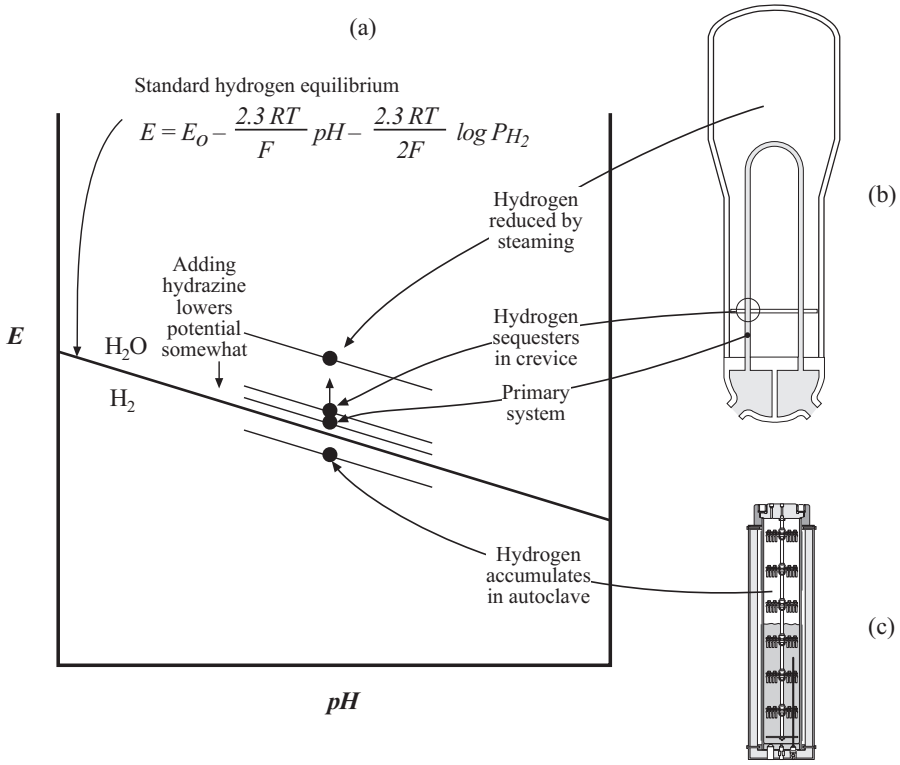

Figure 24 (a) Schematic potential vs. pH diagram for the hydrogen electrode as applied to various cases on primary side (b), secondary side (b), static autoclaves (c), and in crevices. The Nernst equation in (a) is the basis for estimating these effects.

By the end of the 1980s, it was possible to group these possible environments, in which SCC occurred, as shown in Figure 26. These data could be easily grouped since they exhibited explicitly different dependencies on the seven primary variables: pH, potential, species, alloy composition, alloy structure, stress, and temperature. These groups were identified as "submodes" of SCC since they were already in the mode of SCC, but they exhibited these explicitly different dependencies. These submodes could be correlated in the framework of pH and potential. These submodes were first published by Staehle and Gorman[74] in 1989 and by Combrade[75] in 1988.

Figure 26 shows the array of submodes of Alloy 600MA in the framework of potential and pH for the Ni-H_2O and Fe-H_2O diagrams of potential and $pH_{300°C}$ for the general range of 300-350°C. This approach to plotting SCC data on E-pH diagrams was first introduced by Parkins.[76] The various submodes are shown in two diagrams of Figures 26(a) and 26(b) for convenience. I call these, respectively, major and minor submodes. The dependencies of these submodes on the seven primary variables are described in detail by Staehle and Gorman.[5] While the E-pH diagrams are, strictly speaking, thermodyamic references, they define regions where SCC tends to occur

for some submodes, e.g. AcSCC, AkSCC, LPSCC and HPSCC. Other submodes, e.g. PbSCC and S^{y-}SCC, seem not so dependent on these thermodynamic features relating to properties of the materials, but rather follow patterns related to the stability of water.

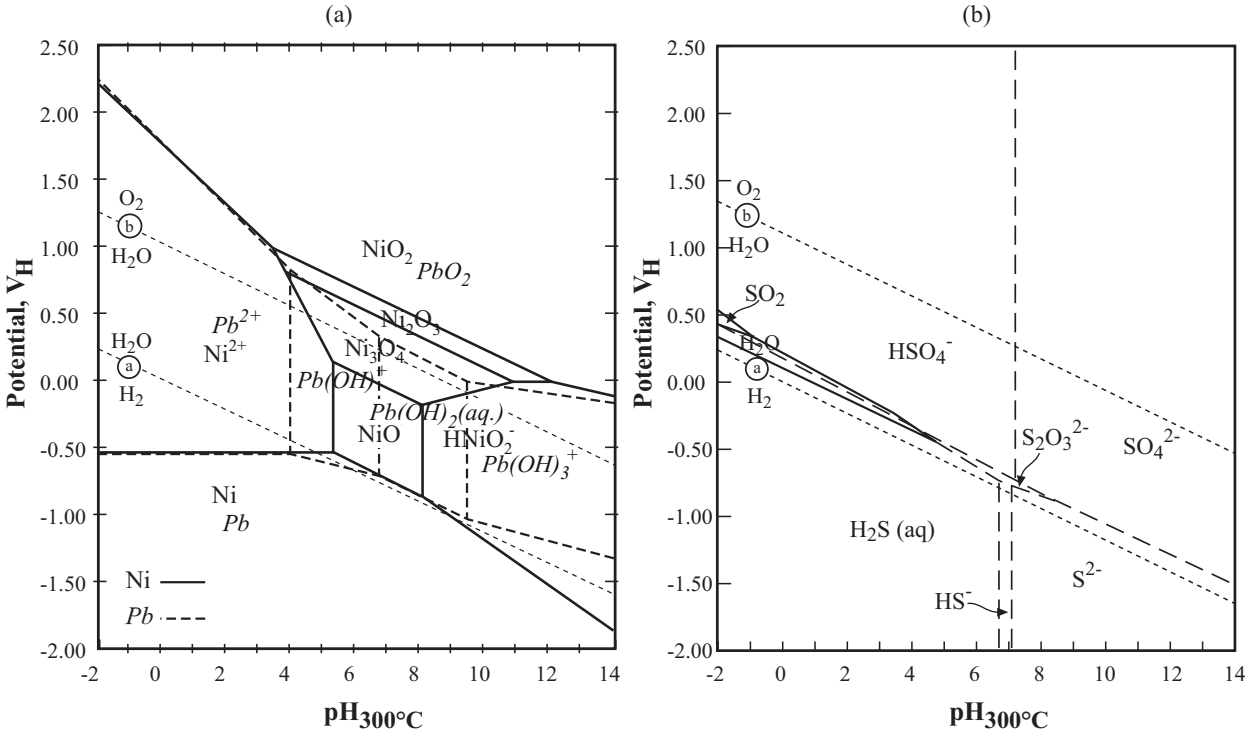

Figure 25 Potenial vs. $pH_{300°C}$ in water for (a) Pb and (b) sulfur. From Chen et al.[71]

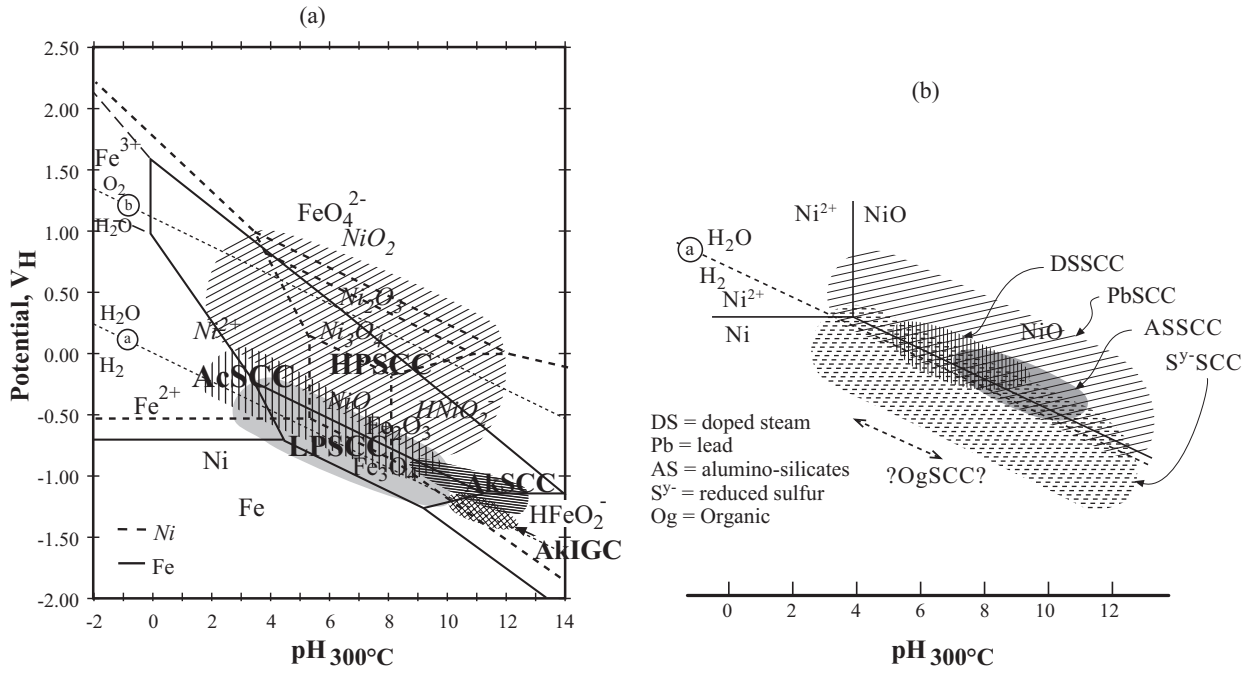

Figure 26 Potential vs. $pH_{300°C}$ for Ni-H_2O and Fe-H_2O with submodes of SCC superimposed. (a) Four major submodes. (b) Minor submodes.

Such a mode diagram, as in Figure 26, for Alloy 690 and Alloy 800, has not been developed although sufficient data are now available to suggest some important patterns. Some effort to develop such a diagram based on experimental work was published by Ohsaki, et al.[77] and Tsujikawa and Yashima,[78] and is shown in Figure 27. This diagram includes Alloys 600TT and 690TT as well as 600MA but is incomplete even for Alloy 600MA. Figure 27 does not include other important submodes such as in Figure 26(b). Figure 27 does not include either Alloy 800 or Type 321 stainless steel.

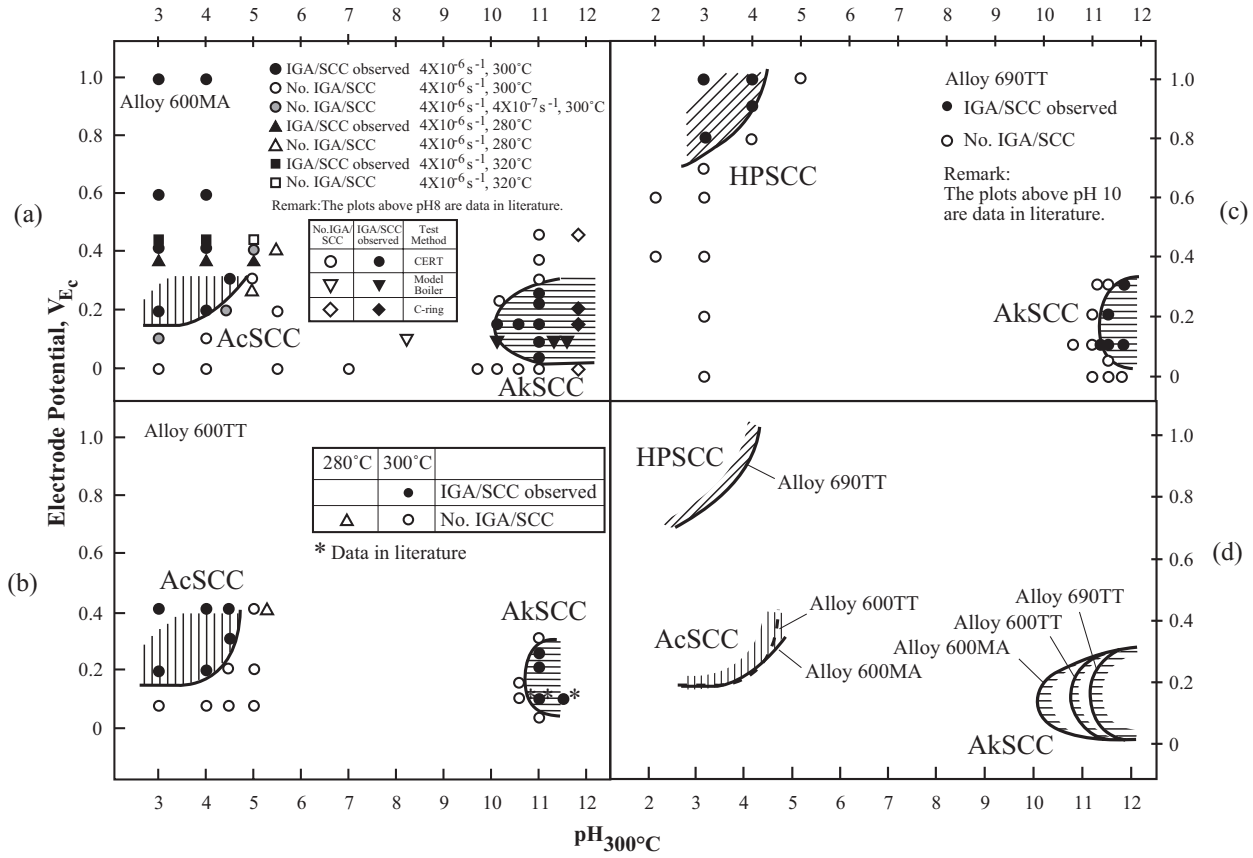

Figure 27 IGC/SCC tests results in the range of 180°C to 320°C range as a function of electrode potential and pH taken at 300°C for (a) Alloy 600MA, (b) Alloy 600TT, (c) Alloy 690TT. From Ohsaki, et al.[77] (d) Comparison of IGA susceptibility among Alloy 600MA, Alloy 600TT, and Alloy 690TT in the range of 280°C to 320°C as a function of electrode potential and pH taken at 300°C. From Tsujikawa and Yashima.[78]

2.7 Initiation and Propagation

The purpose of this section is to identify the segments of initiation and propagation, as shown in Figure 3, together with the early incubation, and demonstrate how these interact generally with environmental and metallurgical chemistry and how they apply to thin sections such as tubing and thick sections such as divider plates.

The ideas of incubation, initiation and propagation as the main segments in the evolution of SCC are well known although variously defined by different workers. Following the schematic view of SCC evolution in Figure 3, the total time to failure is:

$$t_f = t_b + t_i + t_p$$

where:

t_f = total time to failure
t_b = time for incubation
t_i = time for initiation
t_p = time for propagation

It appears that the roles of environmental and metallurgical chemistry vary both with respect to their effects on initiation and propagation and with respect to the bulk chemistry. For purposes of this discussion, initiation is important mainly for SG tubing and propagation is important mainly for thick sections such as welds. Unfortunately, there have been no rigorous studies of the transitions from initiation to propagation with respect to the effects of alloy and environmental chemistry; and the present understanding must be assembled from rather more miscellaneous information. In general, for steam generators, the thick sections occur in the pure water domain, so that propagation of such SCC needs only to be considered in pure water. The thin sections of tubing occur in both the superheated and concentrated domain as well as the pure water domain.

In steam generators, there are essentially two general kinds of environments in which SCC occurs:

- One is the pure water environment, which is characteristic of the primary side and most of the freespan of the secondary side tubes. Also, the steam line and feedwater are essentially pure water.
- The second environment is that on the superheated surfaces where concentrated chemistries accumulate. These include tube supports where the deposits build up at line contacts, the top of the tube sheet crevice, surfaces beneath deposits on freespans may qualify for this category, and the superheated tubing in the upper bundle of OTSGs.

It appears that the relationship between environmental effects in the pure water differ from superheated surface domains; the broad outlines of these two domains seem to be the following:

1. “Pure” water

The “pure water” environment seems to include all the environments except those in superheated conditions. Further, for a broader consideration these pure water environments include those in BWR “primary” systems. Andresen has presented evidence[79,80,81,82] that the propagation processes of SCC in BWR and PWR environments for stainless steels and Alloy 600 are the same and possibly part of a single continuum. There is also good evidence that at least the dependence of the initiation and propagation of both materials on the applied potential is the same.[5]

The argument for the similarity of materials and initiation and propagation is based on the observations of crack tip chemistries by Andresen[81] and Shoji et al.[83,84,85,86] who find similarities

between crack tip chemistries in the BWR and PWR environments. This argument is also based on the fact that the crack tip should operate at the deaerated open circuit potential, which is probably true regardless of the outside environment. However, as the crack tip operates at the deaerated open circuit potential, this does not prescribe the details of chemistry. This, as Andresen points out, for the pure water class of crack tips, the main dependence of SCC is on local chemistry.

The arguments for the similarities of PWR and BWR as well as initiation and propagation apply in the SG only to the thick sections in pure water such as the vessel and the divider plates.

2. Superheated chemistries

The superheated chemistries seem to exhibit different patterns of dependence of initiation and propagation on surface chemistry. The mode diagrams of Figures 26 and 27 are based directly on results from experimental studies. Thus, there is no question that there are discrete differences in dependencies at least of initiation.

One option for describing initiation and propagation is shown in Figure 28. Here, the figure suggests that the initiation depends on discrete chemistries as shown in Figure 26; whereas, the propagation for all the submodes would behave about the same and would depend on the deaerated open circuit potential with less dependence on the crack tip chemistry. Such a possibility could be supported by the analysis of Figure 29 by Wright and Mirzai.[89]

Figure 29(a) comes from the work of Wright and Mirzai[89] based on the work of several authors on the propagation of PbSCC over the range of concentrations at 320°C for Alloy 600MA. Here, depth of PbSCC is plotted vs. time. These data show that the slope of the depth vs. time plots from 1 to 2000 ppm Pb are about the same, being about 6.0×10^{-11} m/s, thereby suggesting that the propagation does not depend significantly on bulk concentration. The data of Figure 29(a) suggest that it is the intercept at zero SCC depth that depends on Pb; and this intercept is plotted in Figure 29(b), which gives essentially the initiation time vs. Pb. Figure 29(b) suggests that the main effect of Pb is on initiation. Thus, the implication of Figure 29 is that chemistry is most important for initiation and less so for propagation, and this fits the suggestion from Figure 28.

A plot similar to Figure 29 is shown in Figure 30 where the penetration vs. time for SCC in stainless steels is shown from the work of Eckel.[94] Here, as with Figure 29 the rates of SCC, i.e. depth vs. time are about the same, but the intercepts depend more on alloy chemistry. Again, this supports to some extent the argument in Figure 28.

A contrary view of the effects of bulk composition on propagation of SCC is shown in Figure 31 from the work of Berge and Donati.[95] Here, the effect of concentration of the NaOH is reflected in the propagation of SCC similarly to the well known effect of concentration of NaOH on initiation as described in the Staehle and Gorman review.[5] The results of Figure 31 suggest that much of the trends shown in the mode diagrams of Figures 26 and 27 apply to propagation as well as to initiation.

A reasonable overall view of the chemical dependencies of initiation and propagation as shown by available data is the following:

1. For environments that are essentially pure water, such as the SG pressure vessel, piping attachment welds, and divider plates, which involve thick sections, there is little difference between the chemical conditions of initiation and propagation. The conditions of the deaerated mixed potential apply both on the surfaces and near the tips of propagating SCC. These circumstances may also involve freespans of tubing. In the BWR case for pure water, the deaerated nature of the crack tip seems the same as that for PWRs.

2. For environments that are concentrated in superheated conditions, such as TSP, TTS, within the tube sheet, and upper bundle surfaces in OTSGs, the chemistry of both initiation and propagation are most likely similar based on the trends of Figure 31. However, the trend in Figure 31 does not apply uniformly as shown by the pattern for Pb as in Figure 29. This category applies to the thin walls of SG tubes.

The available data does not distinguish usefully between the chemistries of initiation and propagation. More definitive work is needed here.

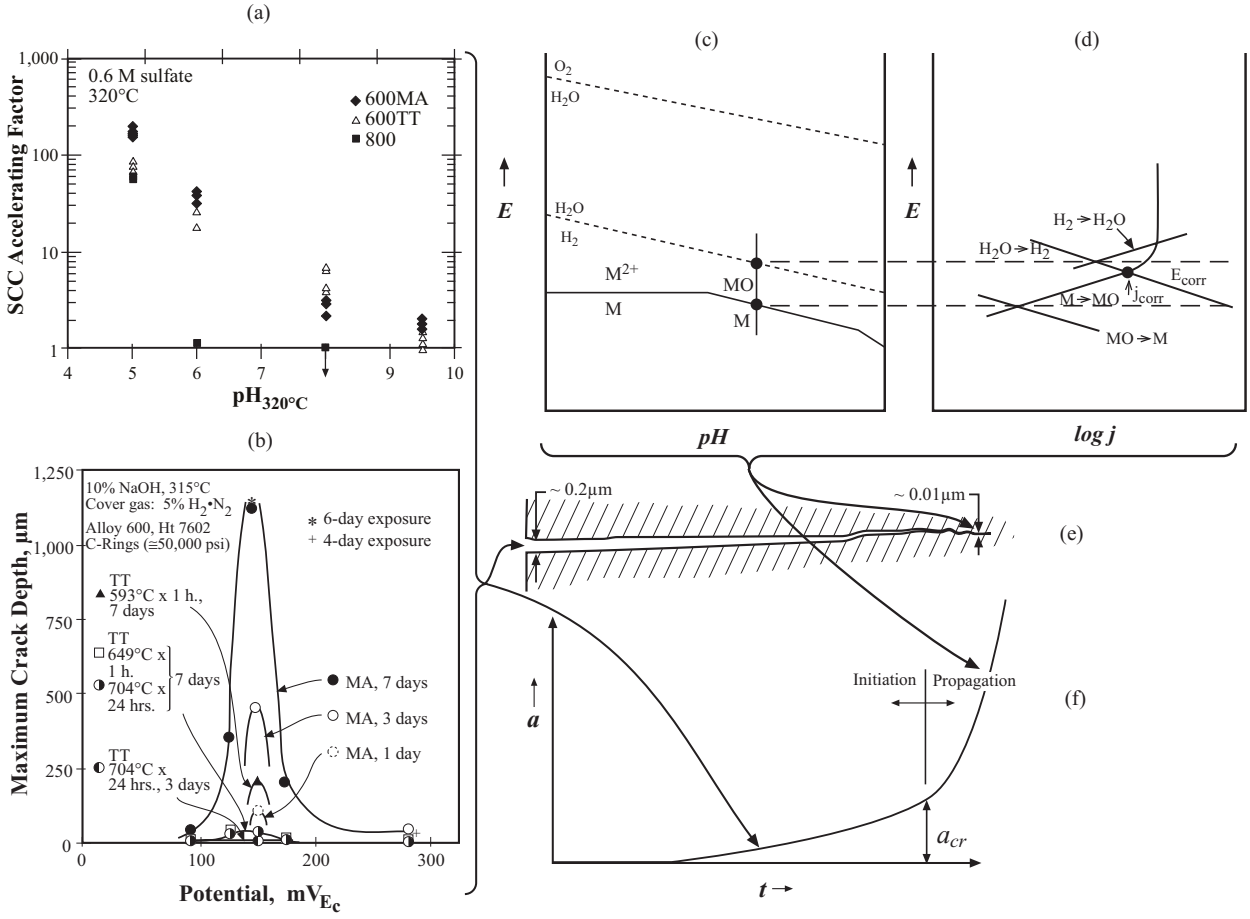

Figure 28 Schematic view of possible chemical dependencies for initiation and propagation. (a) Example of SCC dependence of Alloy 600MA, 600TT, 800 on pH in sulfate acidic solutions at 320°C. From deBouvier et al.[87] (b) Example of SCC dependence of Alloy 600 on applied potential in concentrated NaOH solutions at 315°C. From Pessall.[88] Both (a) and (b) use specimens with smooth surfaces and therefore relate mainly to initiation. (c) and (d) Schematic view of E-pH and E vs. log j as applied to crack tip. (e) and (f) Locations where initiation and propagation processes apply.

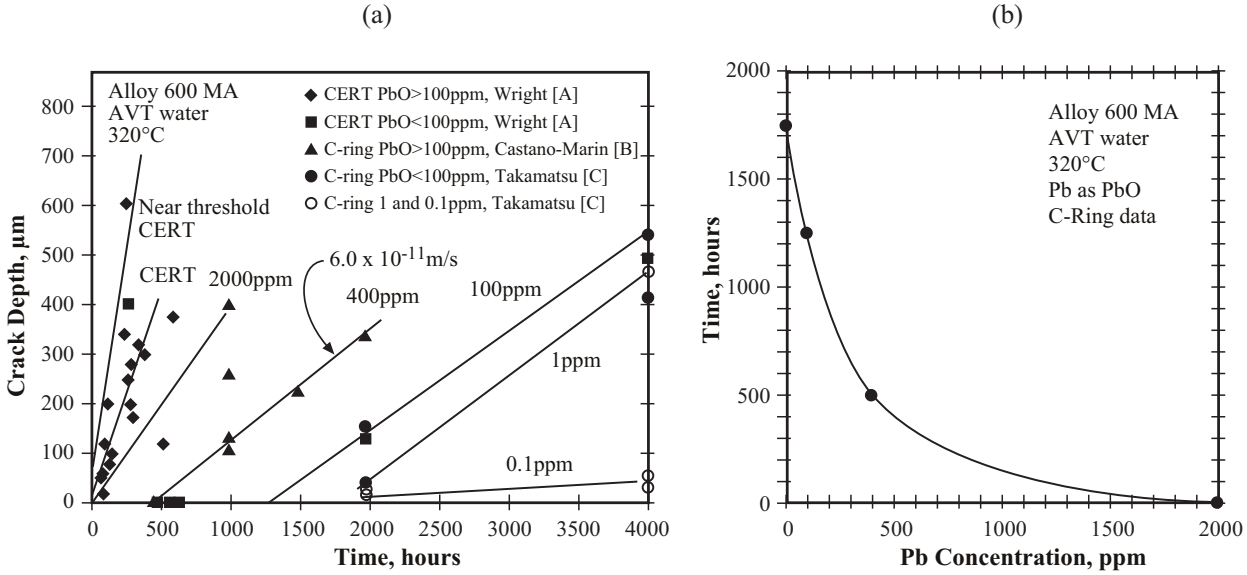

Figure 29 (a) Crack depth vs. time data for Alloy 600MA in AVT water at 320°C with various concentrations of PbO. Wright and Mirzai,[89] with data from [A] Wright,[90] [B] Castano-Marin, et al.,[91] [C] and Takamatsu, et al.[92] (b) Initiation time vs. concentration of lead. Initiation time determined from (a) where depth vs. time plots intersect zero depth. From Staehle.[93]

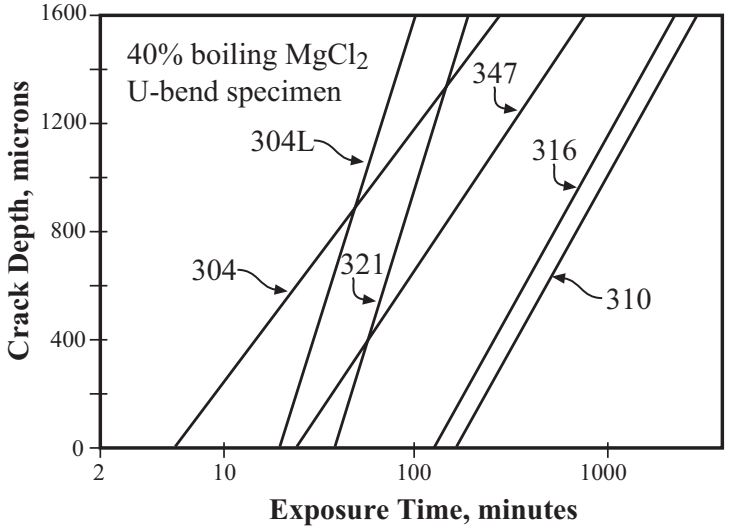

Figure 30 Depth vs. time for the SCC of stainless steels exposed to boiling $MgCl_2$ solutions. From Eckel.[94]

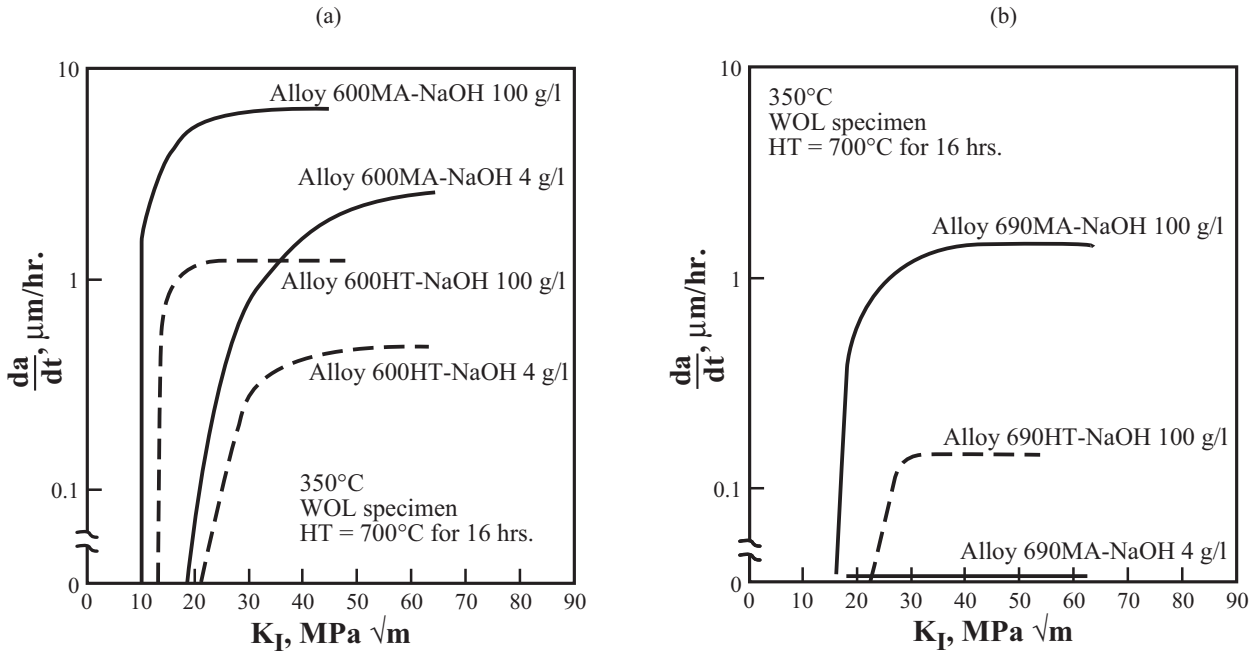

Figure 31 (a) and (b) da/dt vs. K for Alloys 600 and 690 exposed to various concentrations of NaOH at 350°C with a WOL type specimen. HT corresponds to 700°C for 16 h. From Berge and Donati.[95]

2.8 Water Chemistry: Primary, Secondary

The chemistry of the water, including intentional additives and impurities, dominates the corrosive degradation that can occur on free and occluded surfaces. With no water, there is no corrosion. It appears that most utilities have the water chemistry under generally good control with respect to conventional guidelines and have programs of improvement, e.g. zinc injection, advanced amines, and dispersants, well underway and showing good results.

An overall view of the bulk water environments and general conditions is shown in Figure 32. Here, the steam generator is shown as part of the primary and secondary systems. Approximate conditions are shown but these vary among PWR systems. The steam generator is a central component and must be compatible with both primary and secondary systems.

In an overall sense, the design and operation of the steam generator must integrate the materials in the primary and secondary systems. A schematic view of this array of materials is shown in Figure 33. Again, as with Figure 32, these materials vary somewhat among plants, and some of these details are considered elsewhere in this discussion. Regardless, in addition to being the nexus of primary and secondary water chemistry circuits, the steam generator is the nexus of many materials. The overall design must consider possible influences of these other materials on the operation of the SG, e.g. the release of species as contaminants, such as Fe, or as potentially radioactive sources.

The historical development of initiatives in water treatment on primary and secondary sides has been discussed by Fruzzetti and Wood,[96] and the chronological developments are shown in Figure 34(a,b) for primary and secondary chemistries. The implications of these initiatives are discussed in this section where degradation processes are discussed.

Primary Water Chemistry

Role	Species	Concentration
Burnable poison	H_3BO_3	1500 ppm to zero
pH adjust	LiOH	Adjust to meet 7.1-7.4 pH_T
Minimize radiolytic oxygen	H_2	25-50 STP cc/kg
Oxygen	O_2	< 5 ppb
Corrosion product	Fe	No spec.
	Ni, Co	
Contaminant	Cl, SO_4, F	Each < 0.15 ppb

Secondary Water Chemistry

Role	Species	Conc., ppb
pH control	NH_3	≈ X
O_2 decrease	N_2H_2	≤ 8xO_2
Leaks	O_2	< 10
Boil off remnant	H_2	≈ 1
Corrosion product	Cu	< 1
	Fe	< 5
Contaminant	Na	< 5
	Cl_2	< 10
	SO_4	< 10

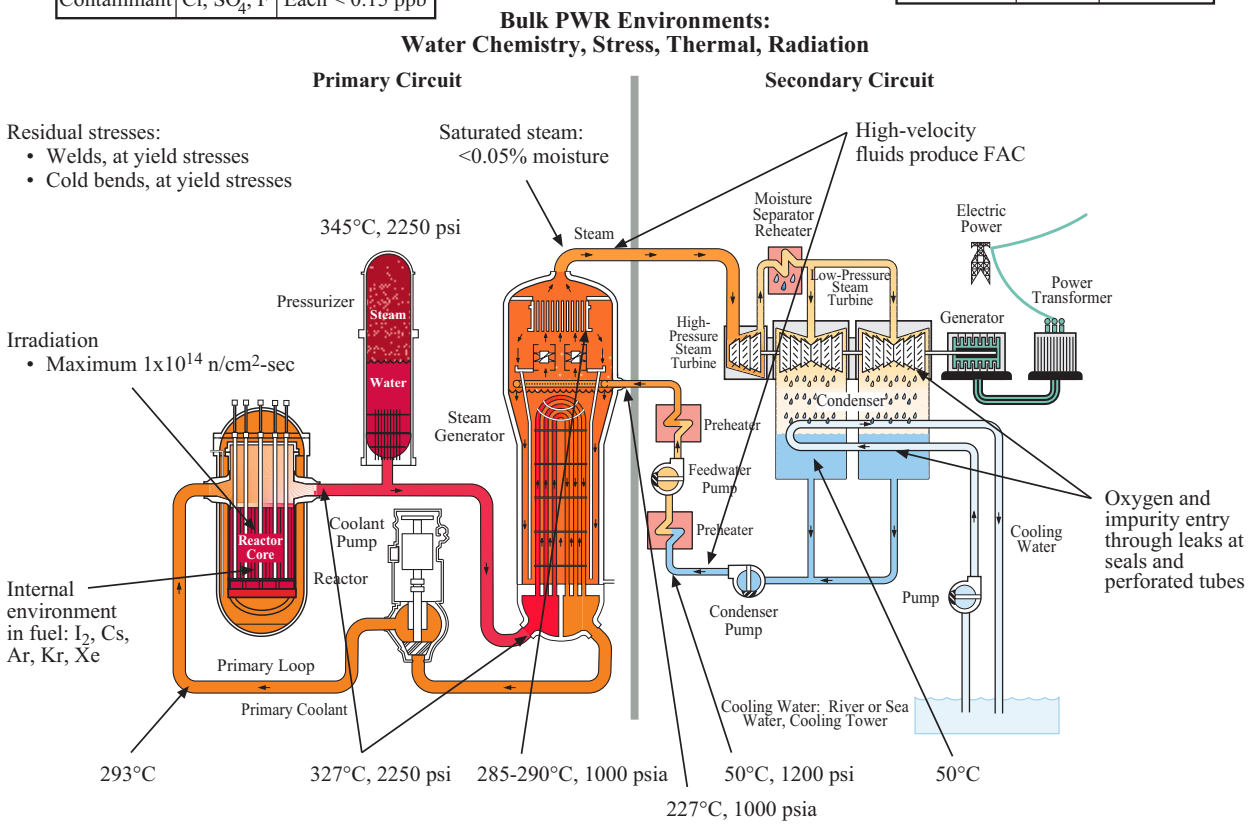

Figure 32 Schematic view of primary and secondary environmental systems in which the steam generator resides. Values of conditions are approximate and vary among specific plants.

However, the present water chemistry activities are not considering a number of potential problems and approaches toward understanding and resolving concerns for degradation. These are discussed in this section.

1. Superheat configurations

The superheat configurations are important because they promote the concentrations of corrosive impurities, and these then can lead to degradation on the secondary side as shown schematically in Figure 35. Figure 35 also illustrates the contributions of residual stresses on primary and secondary sides. Whereas residual stresses react with the bulk environment on the primary side, they react mainly with the superheat crevices on the secondary side.

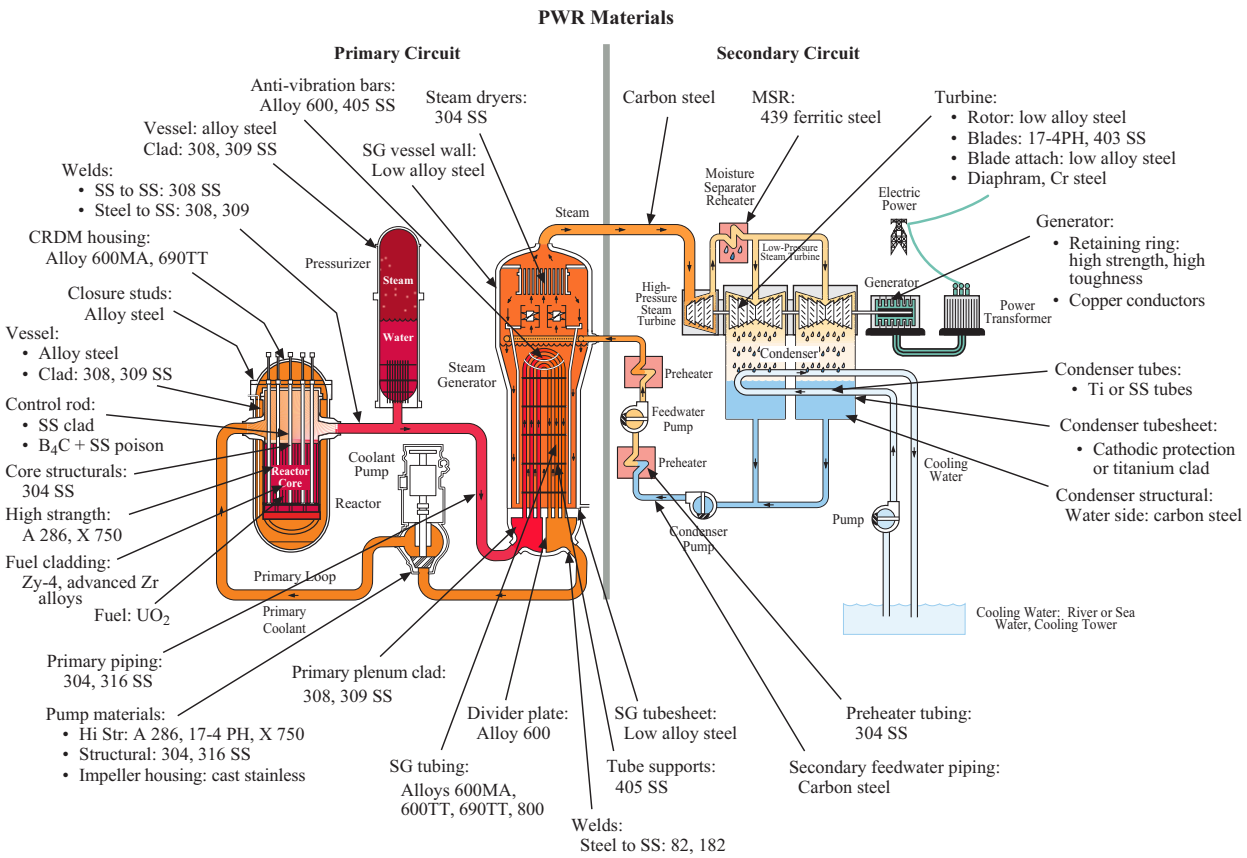

Figure 33 Schematic view of important materials in primary and secondary systems.

In modern SGs there are five types of superheated surfaces, and these are discussed in subsequent sections:

- Line contact TSPs.
- TTS crevices.
- Deep TS crevices, burrowing.
- Fouled free spans.
- OTSG upper bundles.

a. Line contact TSPs

Cross sectional views of tube support configurations are shown in Figure 36. The earliest designs were mainly drilled hole with flow holes, as shown in Figure 36(a). As the degradation with this type of geometry increased, designs were changed to line contact geometries, as shown in Figures 36(b,c,d). It should be noted that some manufacturers started early with line contact TSPs. Details of the historical evolution of these designs are discussed by Staehle and Gorman.[5] The lattice bar or egg crate configuration is shown in Figure 36(b). Broached hole designs are shown in Figures 36(c,d). The latter three are "line contact" crevices where the intention is to minimize the contact area and the accumulation of deposits. The flow holes of Figure 36(a) are replaced by

flow directly adjacent to the tubes in the line contact geometries of Figures 36(b,c,d).

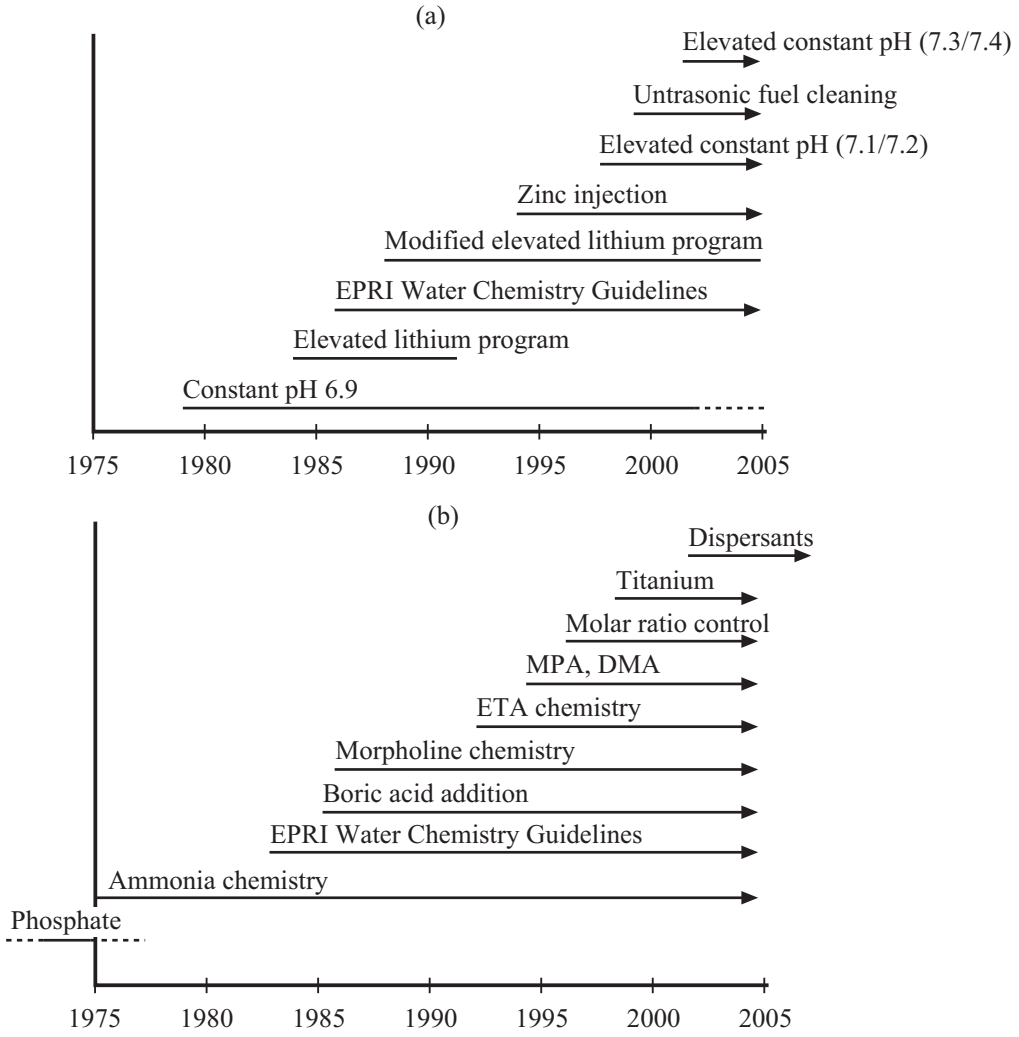

Figure 34 (a) Historical trends in PWR primary water chemistry. (b) Historical trends in PWR secondary water chemistry. From Fruzzetti and Wood.[96]

As it became clear that the drilled hole and Alloy 600MA design sustained excessive degradation, designs, water chemistries, and materials were changed. While some designs started with Alloy 600MA and drilled holes, others did not and used broached holes and lattice bars as well as Alloy 800 and stainless steel from the beginning. This history is described in detail by Staehle and Gorman.[5] Figure 37 shows main features of these changes.

Until the changes noted in Figure 37 were gradually implemented, the chemical-degradation situation that existed in the drilled hole designs where Alloy 600MA was used are illustrated in Figure 38. Here, chemicals accumulated at the superheated crevices in essentially saturated concentrations and produced both corrosion of the tube support and SCC/IGC degradation of the tubes as shown in Figure 38(a). Despite the generally good control of water chemistry, a broad array of impurities concentrated as noted in Figures 38(b,c).

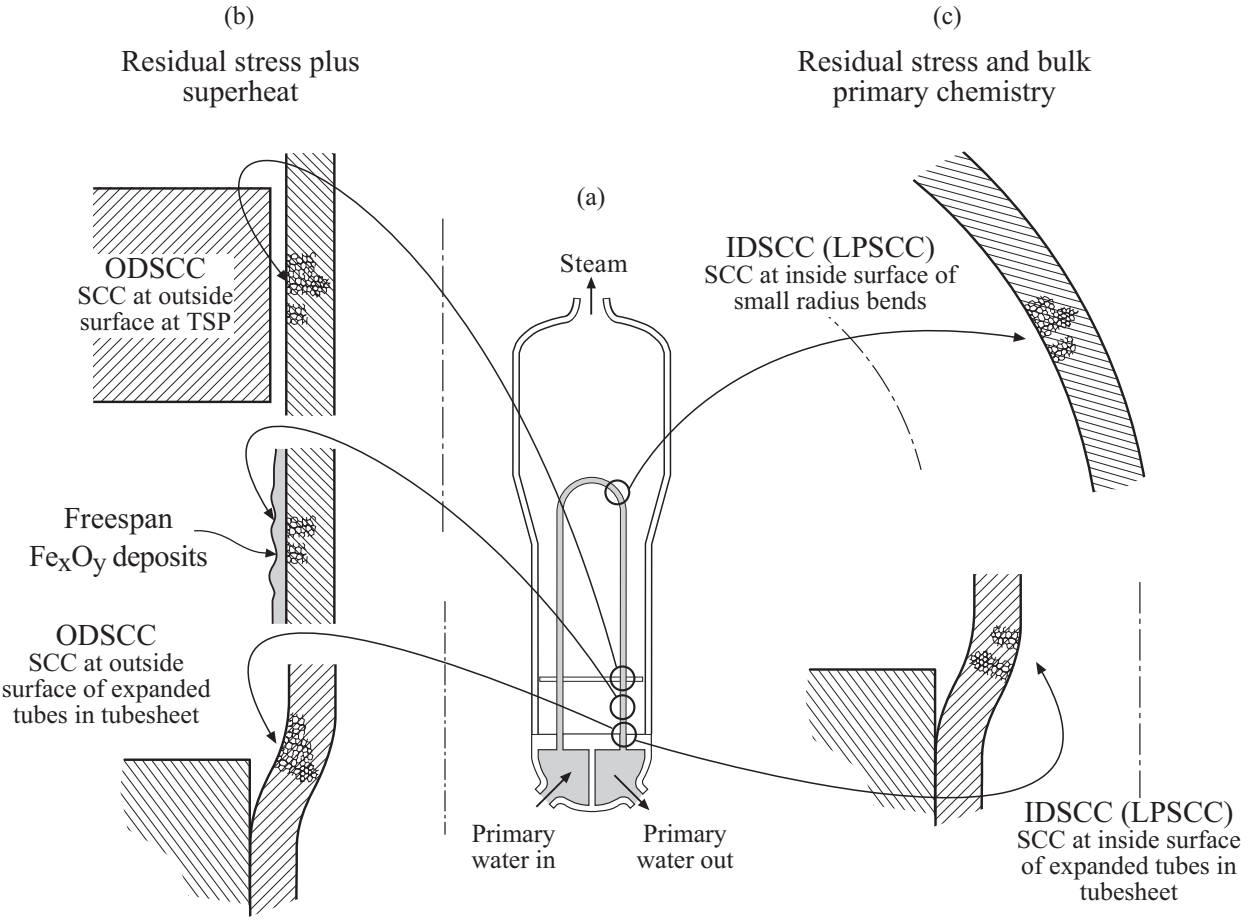

Figure 35 Schematic illustration of distribution and primary influences on degradation: superheated crevices and residual stresses on the secondary side and bulk chemistry and residual stresses on the primary side.

For the reasons that are obvious in Figure 38 the PWR industry shifted, if it had not already done so as noted in Figure 37, to the "line contract" geometries of Figures 36(b,c,d).

Despite the intention of the "line contact" crevice design, deposits continue to accumulate as shown in Figure 39(a,b). The deposits form at the contact points and then spread as shown in Figure 39(b). These geometries then approach the same conditions for superheat as shown in Figure 38. The lattice bar design is shown in Figure 39 but similar processes can occur in broached hole designs.

The configuration shown in Figure 39 results in conditions which are likely to produce SCC in the long term even with advanced alloys. It is quite likely that these configurations will produce PbSCC, S^{y-}SCC, and AcSCC(SO_4^{2-}) as discussed in Sections 3.2, 3.3, 3.4, and 3.5. The schematic views in Figure 39 shows that the following conditions occur in line contact crevices:

- Deposits accumulate at the locations of contact, as suggested in Figure 39(b).
- As shown in Figure 39(d) there is a large gradient in water velocity on the surface of the tubes that varies from about 1 m/s at (A) to about zero at (B). This gradient is capable of providing a

streaming potential effect that will affect the growth rate and properties of deposits.

- There is a large thermal gradient in the tubes. At the location of contact (B), the temperature of the tube surface is close to the primary temperature and the tube surface at (A) is close to the secondary water temperature. It is likely that this gradient would be relatively sharp and capable of producing significant thermal stresses at the edge of the deposit on the secondary side.
- At (B) the concentration of impurities is not well defined, since no useful experimental studies of such concentrations are available, but it would be significant.

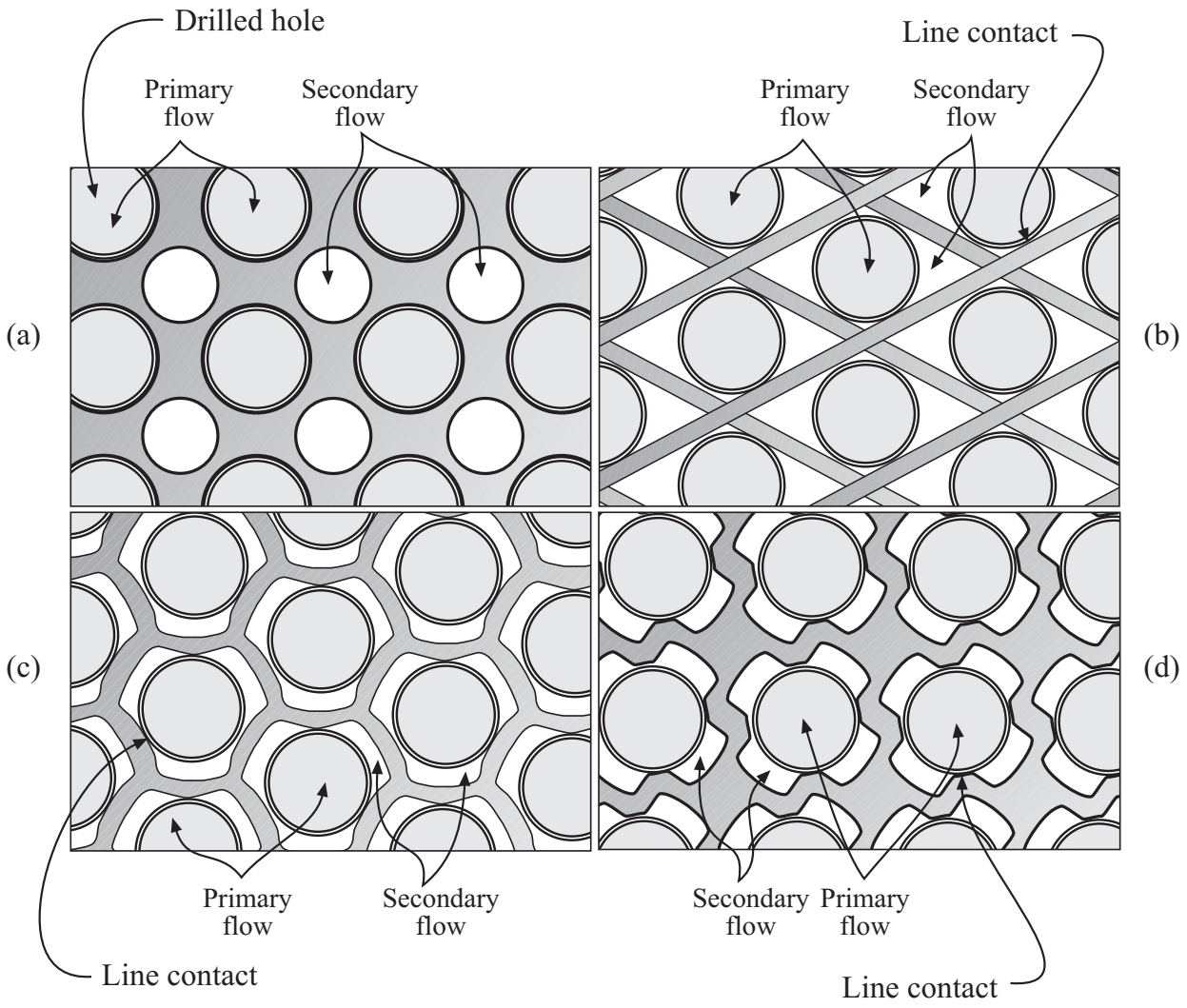

Figure 36 Cross sections of tube support and tubing configurations. Locations of primary and secondary flow noted. Locations of line contacts are also identified. (a) Drilled hole geometry with flow holes. (b) Lattice bar or "egg crate" geometry. (c) and (d) trefoil and quatrafoil geometries, respectively, for broached hole designs.

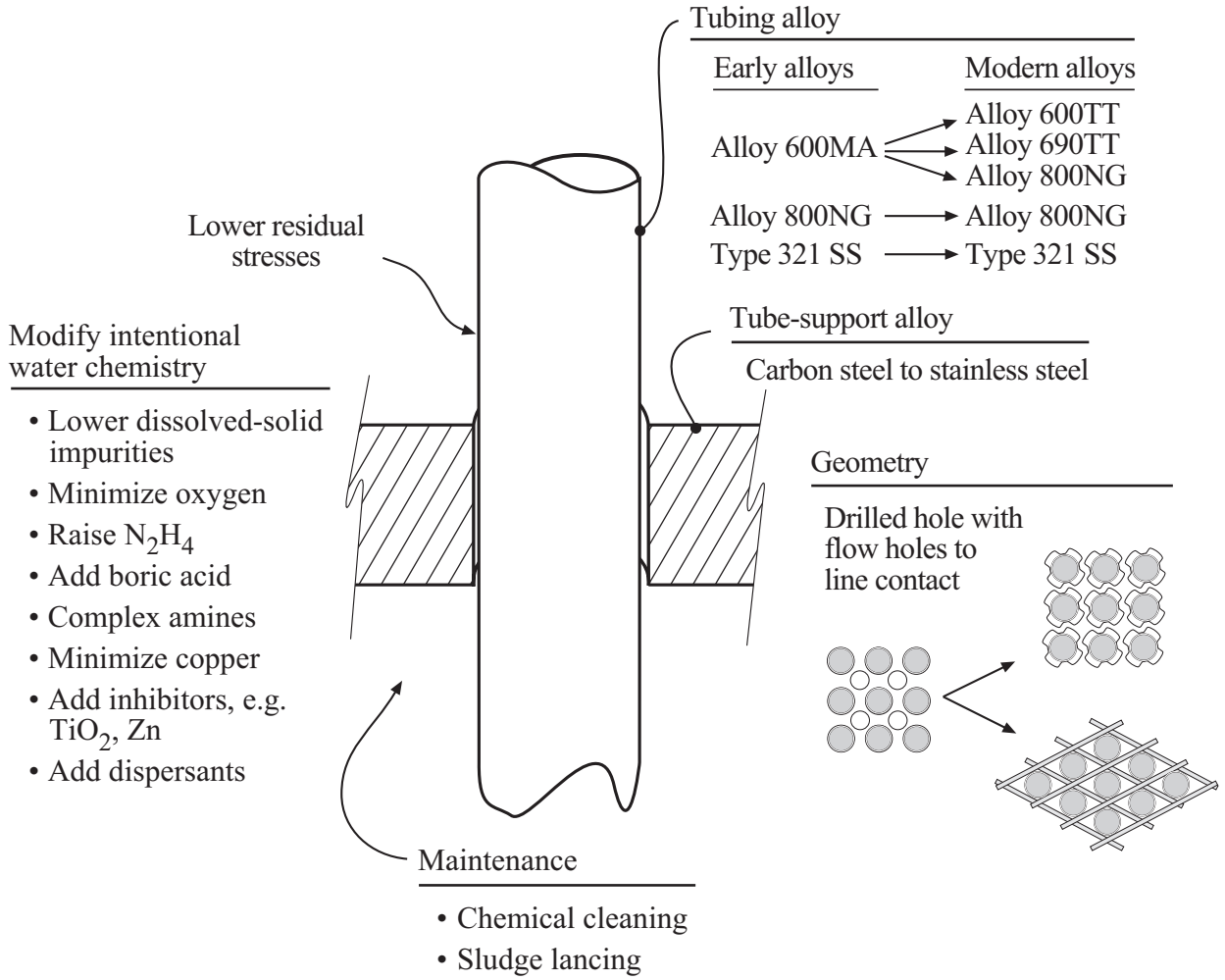

Figure 37 General view of historical changes in materials, design, and water chemistry in tube supports.

The significance of the line contact crevice being a site of accumulation and corrosion was confirmed by Thomas and Bruemmer[99] as shown in Figure 40 from studies of SCC at line contact crevices at the Seabrook plant. Here, a concave broached hole design with nominal Alloy 600TT had been used although there seemed to be some question about the heat treatment of the alloy based on the analysis of the microstructure. Nonetheless, 15 tubes had indications of axial cracks at the first support plate at the locations of contact. The average depth was 30% penetration with the deepest being 99.5%. The SCC was the full length of the line contact. In total, there were 42 indications at both hot and cold legs. Subsequent ATEM examination showed that the SCC contained Pb. Courtesy of A. McIlree.[98]

While it is not surprising that the Alloy 600TT tubing, whether it was properly heat treated or not, sustained PbSCC. What is important, is that there was sufficient Pb in the line contact crevice at Seabrook that the PbSCC could occur.

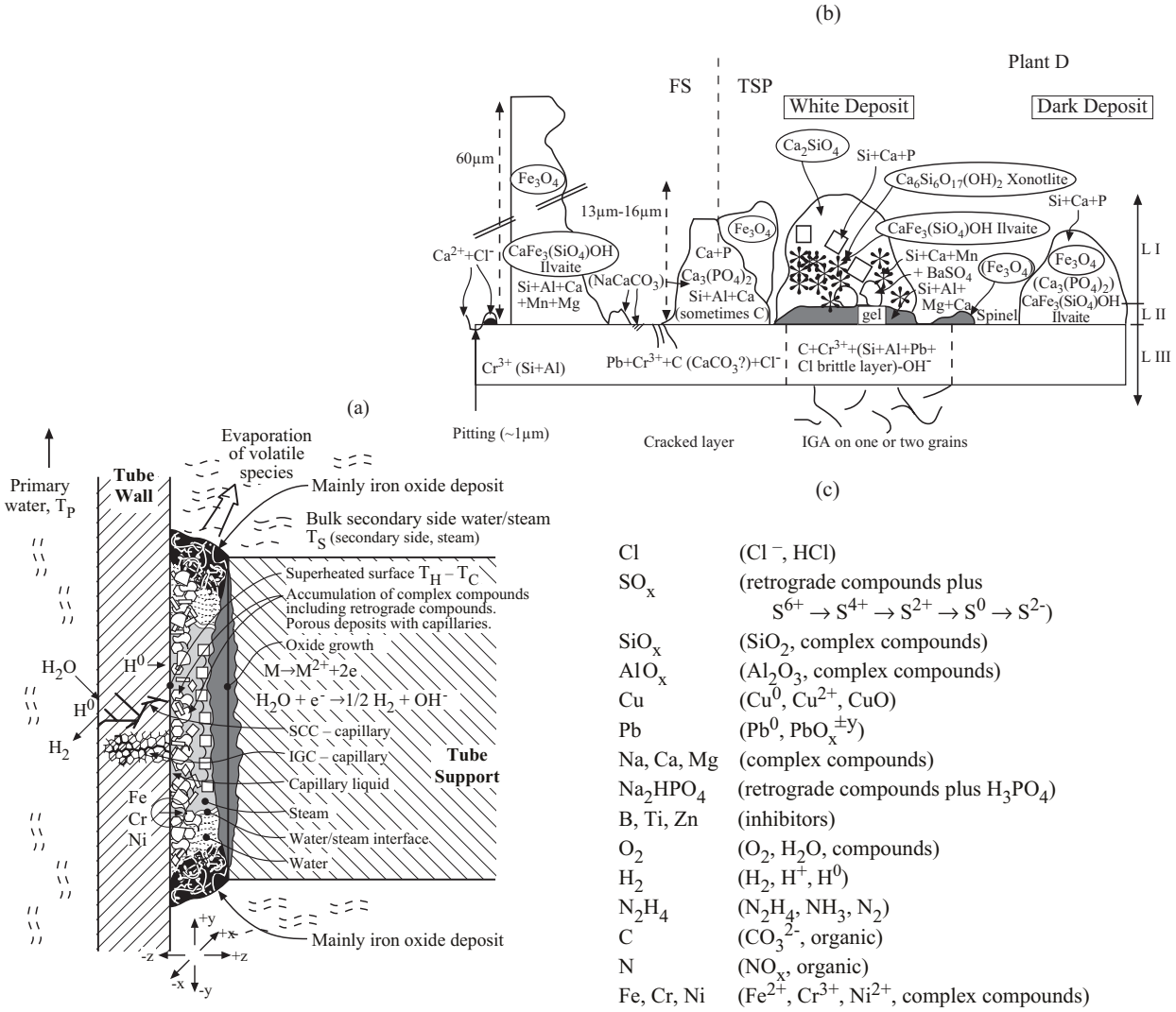

Figure 38 (a) Schematic view of accumulation of chemicals and SCC/IGC degradation of tube walls. Saturated solutions, solids, and two phases (water and steam) are shown at the interface between the tube support and tube wall. (b) Accumulation of chemicals on free span and tube support crevices. Here, condenser used Ti tubes and water conditioning was NH_3. Tube was examined after 81,900 hours. From work by Cattant et al.[97] (c) Identity of chemicals accumulated at typical crevices.

In addition to the evidence from Seabrook, Figure 41 compares the hideout returns from drilled hole and broached hole plants from the work of Ollar and Viricel-Honorez.[100] This figure shows clearly that essentially the same impurities that were nominally in the crevices for drilled holes are present for the line contact (broached hole) design.

In view of the data from the Seabrook experience and from Figure 41, it seems that line contact crevices accumulate the same impurities as the drilled holes; further, considering the relative peripheral lengths of the contacts, the line contact crevices accumulate chemicals more efficiently per peripheral measure than the drilled holes. There do not seem to be such data for the lattice bar geometry.

It seems that there is sufficient residual stress in the tubes for the SCC to initiate and propagate despite the TT heat treatment. Such stresses could result from straightening and/or final surface treatments.

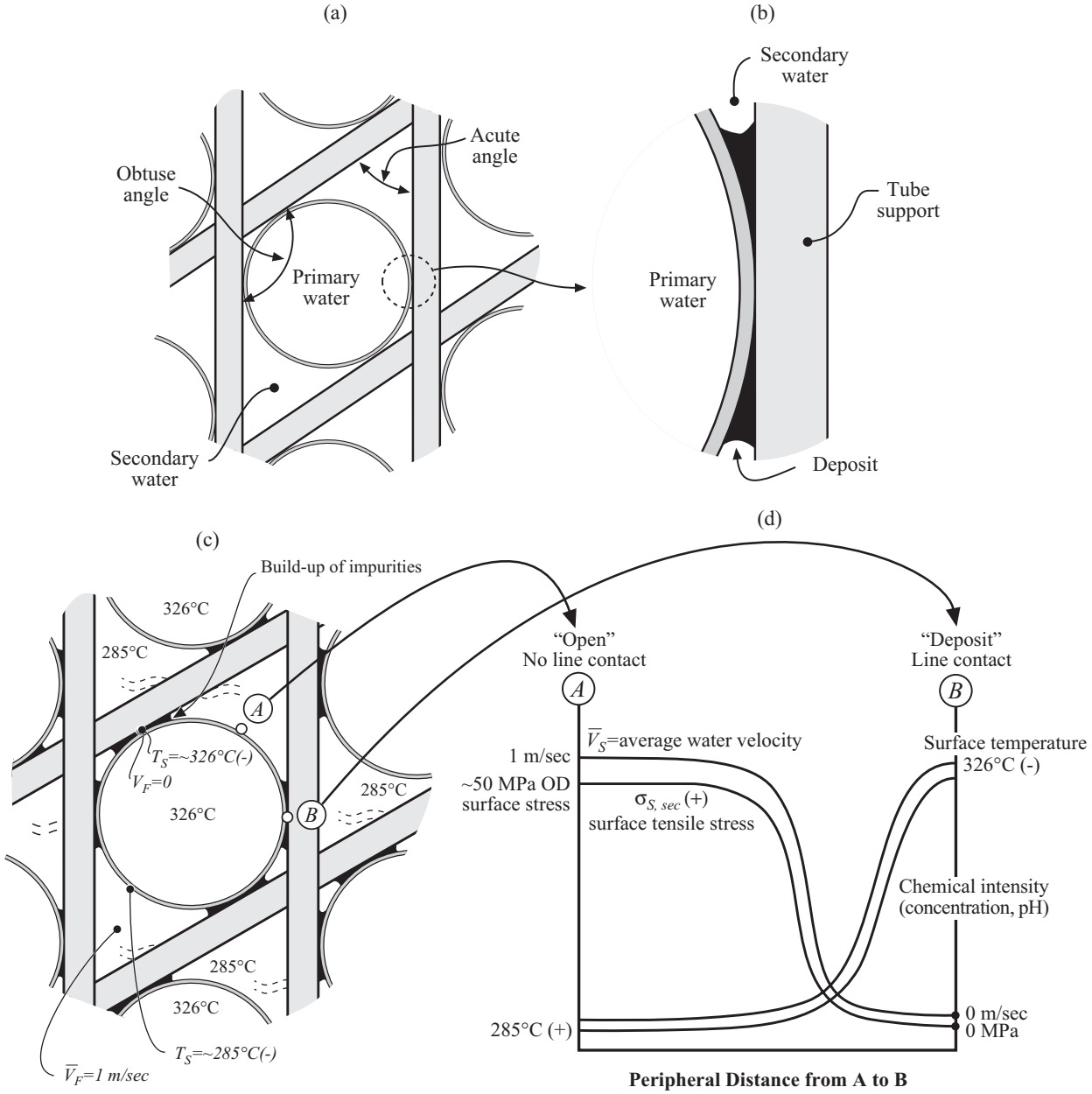

Figure 39 Accumulation and effects of deposits at lattice bar geometries. (a) Geometry of lattice bar arrangement. (b) Development of deposits. (c) Nominal conditions of temperature and flow in lattice bar geometry with deposits. (d) Schematic distribution of flow, surface stress, surface temperature, and concentration of accumulated chemical species.

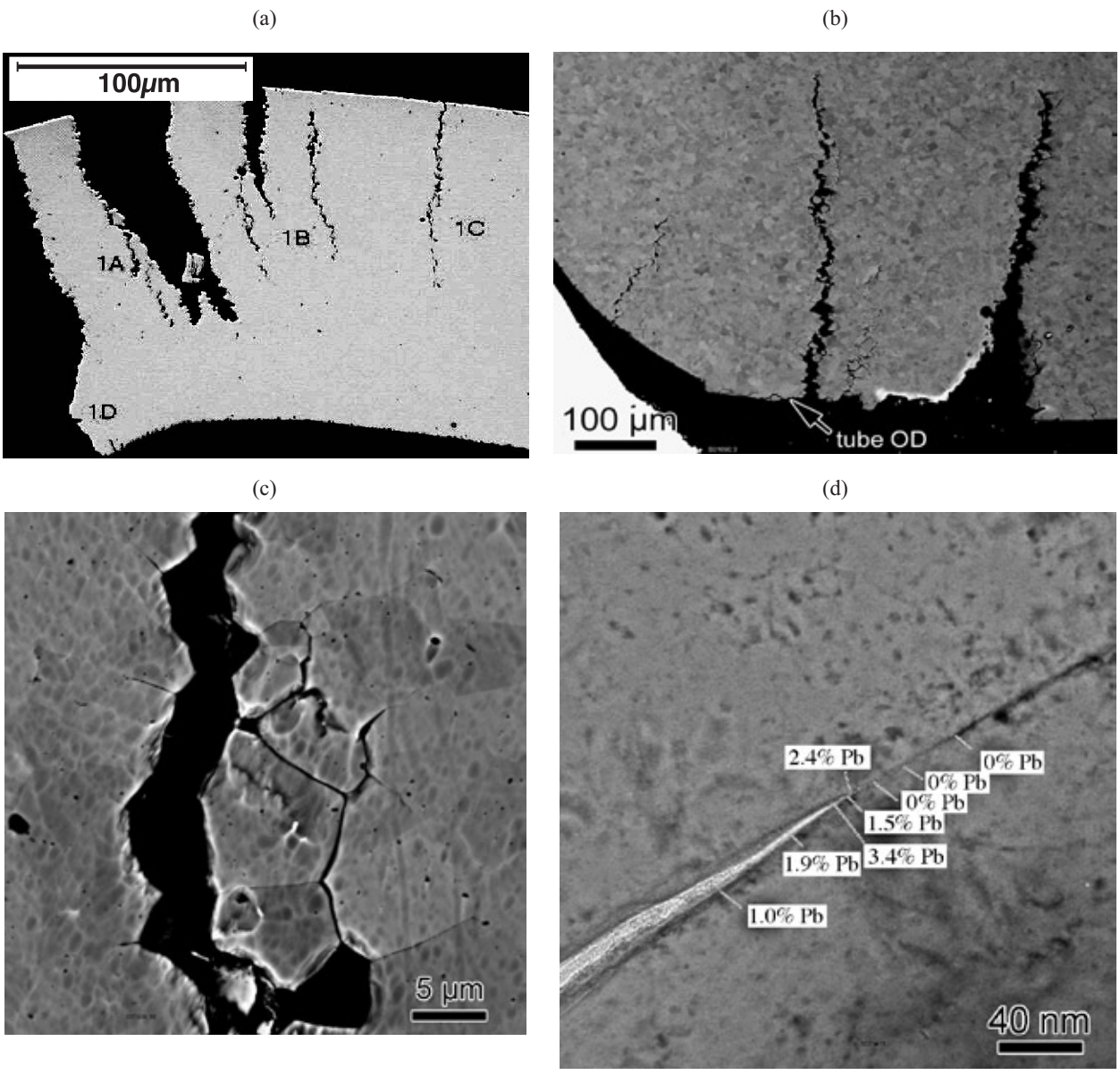

Figure 40 (a) Optical photomicrograph from Seabrook-1 RSG tube R5-C62 after burst test. Specimen removed after 9.7 EFPY. Grain size 10-11. XRD and EDS showed evidence of Cu and Pb in deposits and at tube surfaces. As polished. (b) Micrograph of partically ion-milled TEM disc sample. (c) Detailed view of secondary cracks. (d) Crack tip along grain boundary with weight fraction of Pb noted at respective locations. From Thomas and Bruemmer.[99] Permission from Electric Power Research Institute.

From the Seabrook experience, it seems that the SCC is mostly axial at line contact TSPs. This morphology seems to follow from the axial geometry of line contacts. Such geometries may be of less concern than the circumferential geometry at the TTS.

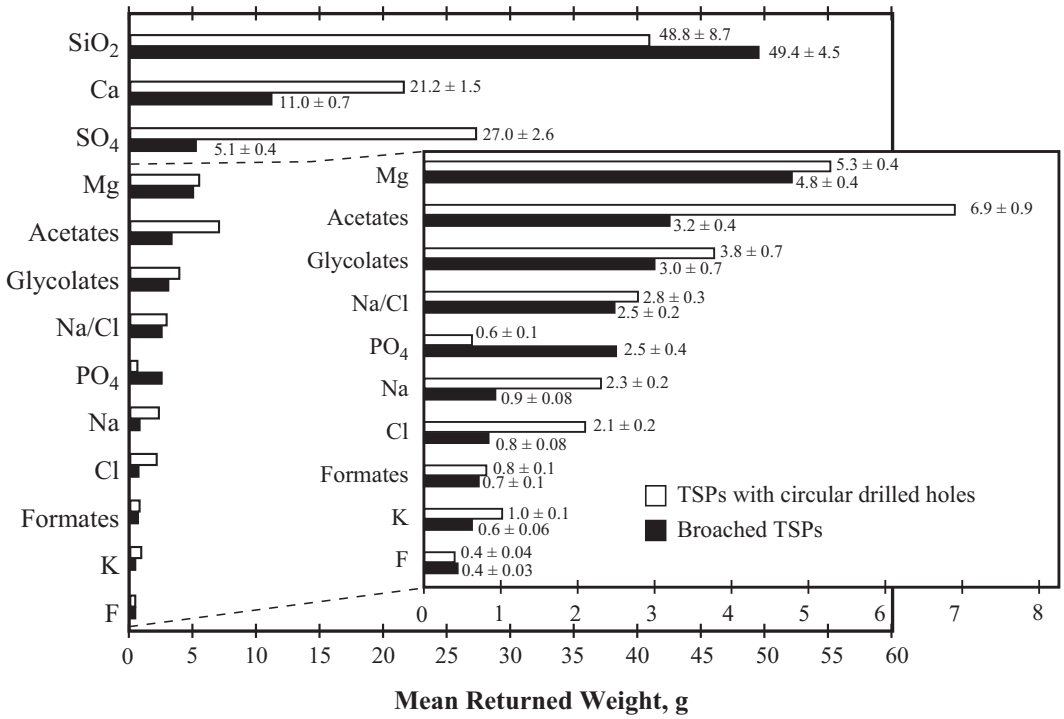

Figure 41 Species analyzed vs. mean weight per steam generator equipped with either circular drilled holes or broached holes. Data from 150 hideout returns from 20 units. From Ollar and Viricel-Honorez.[100]

b. TTS crevices

At the top of the tubesheet there is a short but significant crevice, the design of which has not changed significantly from the designs of the original SGs, in which TTS short crevices were used. The evolution of these geometries is shown in Figure 42. While the deep crevice approach was used early, it was not as attractive as the simple short crevice shown in Figure 42(b). Not surprisingly, the long crevice, shown in Figure 42(b), was more prone to corrosion owing to the greater length of the superheated region. The kiss-roll seemed to offer no advantage. Associated with the TTS crevice, as well as being at the bottom of the SG, are the following as illustrated in Figures 42 and 43:

- An important difference between the TSP and the TTS is the circumferential nature of the deposits, the crevice, and the tube expansion. These crevices together with the deposits at the bottom of the SG, as shown in Figure 43, produce the same kinds of crevices as in the past; and this fully circumferential geometry provides a higher risk of serious damage, i.e. a double ended break.
- Deposits at the bottom accumulate generally with time, as shown in Figure 43, although the amounts of deposits are less than in past years owing to the cleaner water chemistry. These deposits can produce by themselves a superheating crevice at the surface of a tube.
- The growth of corrosion products, as described in Figure 44, from the steel tubesheet can produce a type of denting and associated increasing stress on the tube. Further, this gradual increase in stress produces a “slow strain rate” effect, which is well known to accelerate SCC. Note that the specific volume of the corrosion products is about 3 times that of the metal based

on the Pilling Bedworth work of 1923.[55]

- The growth of corrosion products also produces forces that will cause the crevice in Figure 44 to deepen with time thereby making the crevice deeper and a more aggressive superheated region. This is a "burrowing" effect and is illustrated in Figure 45. As this process continues, species such as sulfate, sulfide and Pb can accumulate and further accelerate SCC.
- As the tubesheet is pressurized from the primary side, it deforms and causes tubes to bend slightly in response to the curvature of the tubesheet; this produces a bending stress in the tube at the top of the tubesheet.
- Finally, the hot side tubesheet crevice is the hottest location in the SG tubes, and more rapid corrosion processes can be expected.

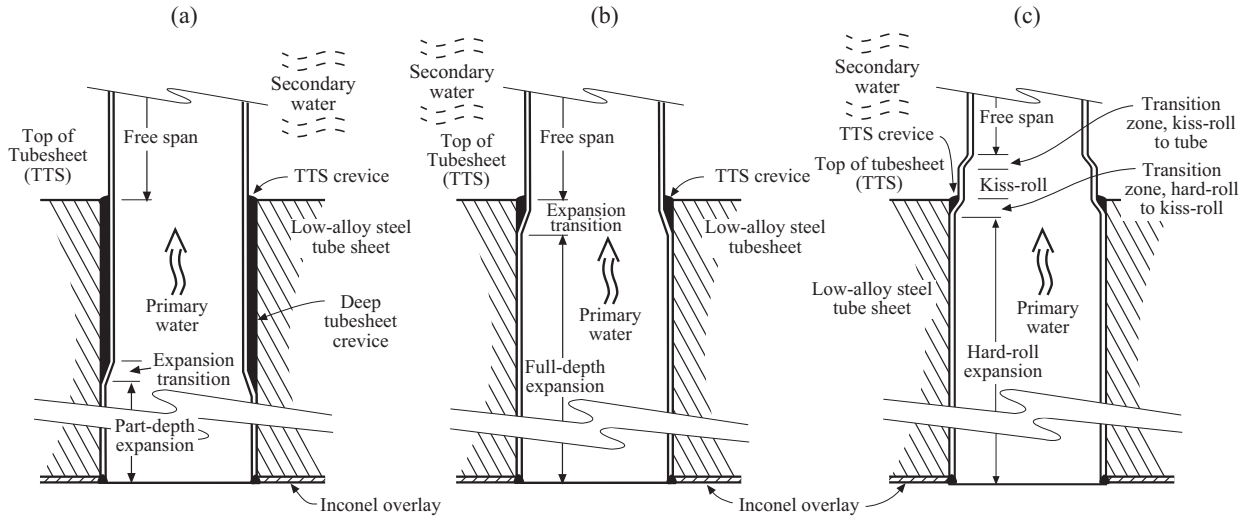

Figure 42 Tubesheet geometries. (a) Partially expanded. (b) Fully expanded. (c) Fully expanded with top "kiss" roll. From Staehle and Gorman.[5]

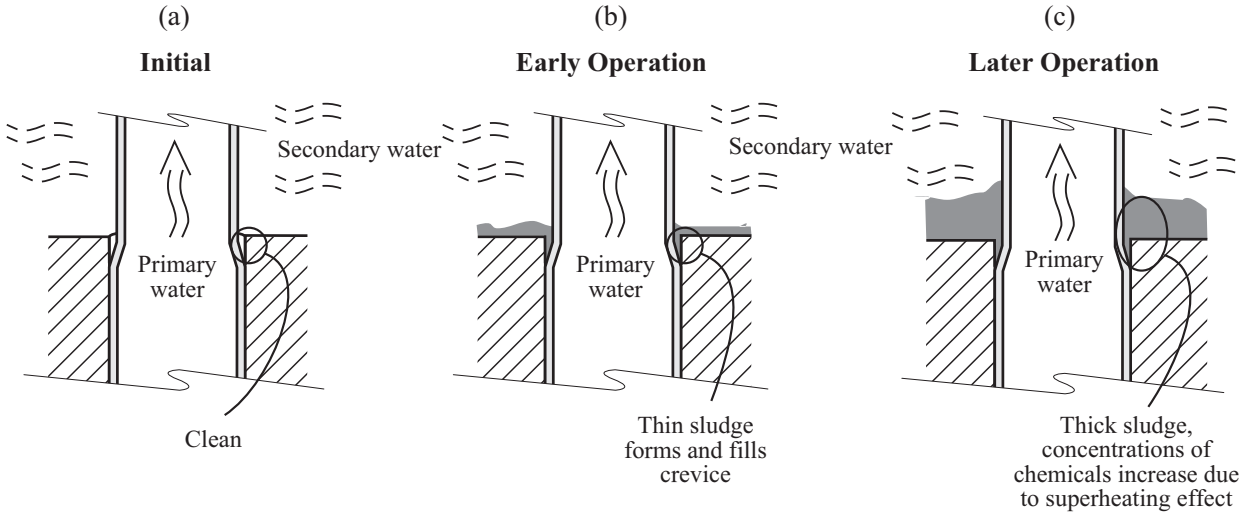

Figure 43 Accumulation of deposits on top of the tubesheet with time. From Staehle and Gorman.[5]

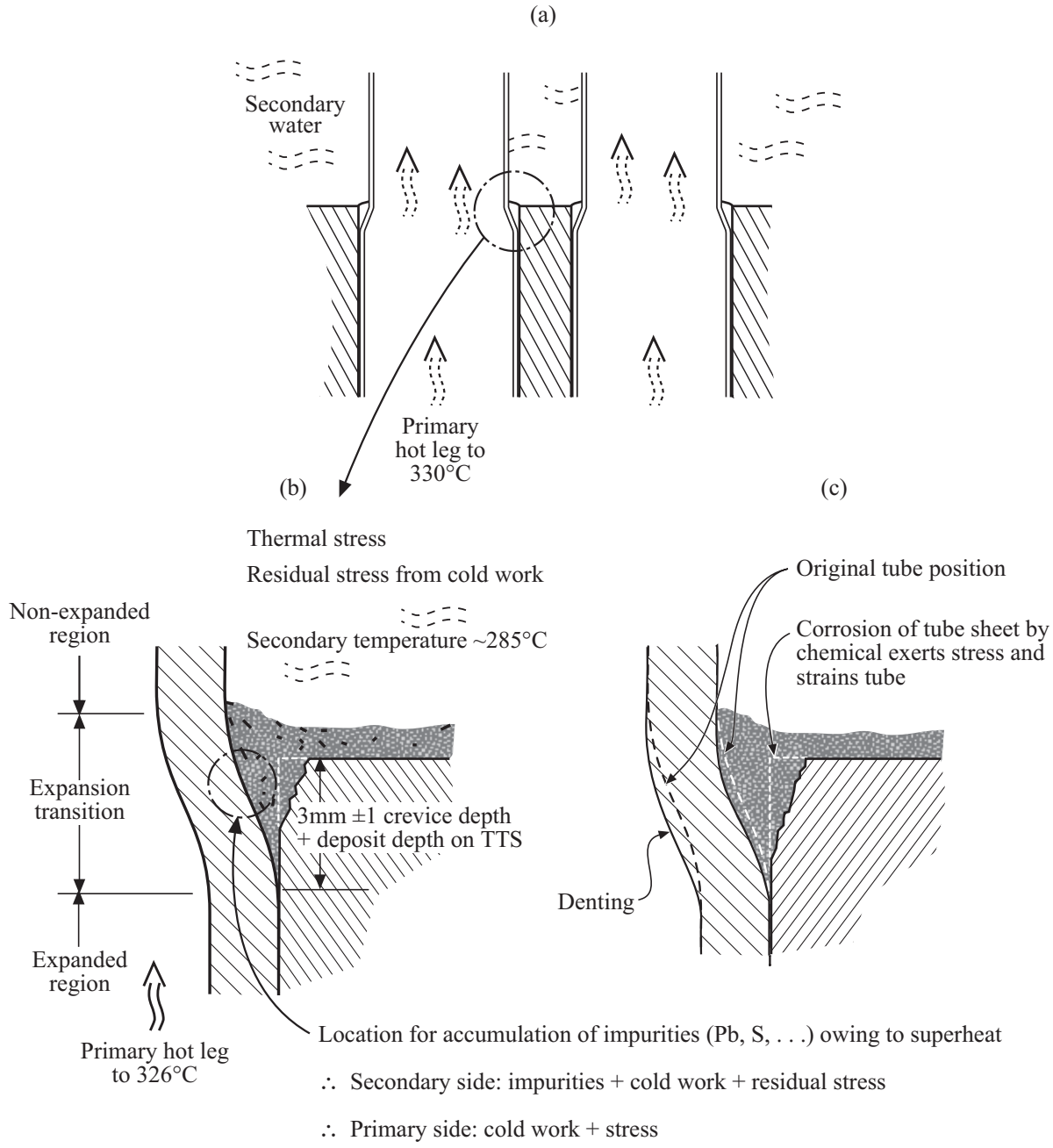

Figure 44 (a) Location of TTS crevices. (b) Initial growth of oxides produced by corrosion of TS steel fills the crevice. (c) Further growth of corrosion products resulting from the corrosion of tubesheet steel by superheated crevice solutions can produce sufficient oxides to deform and strain the tube.

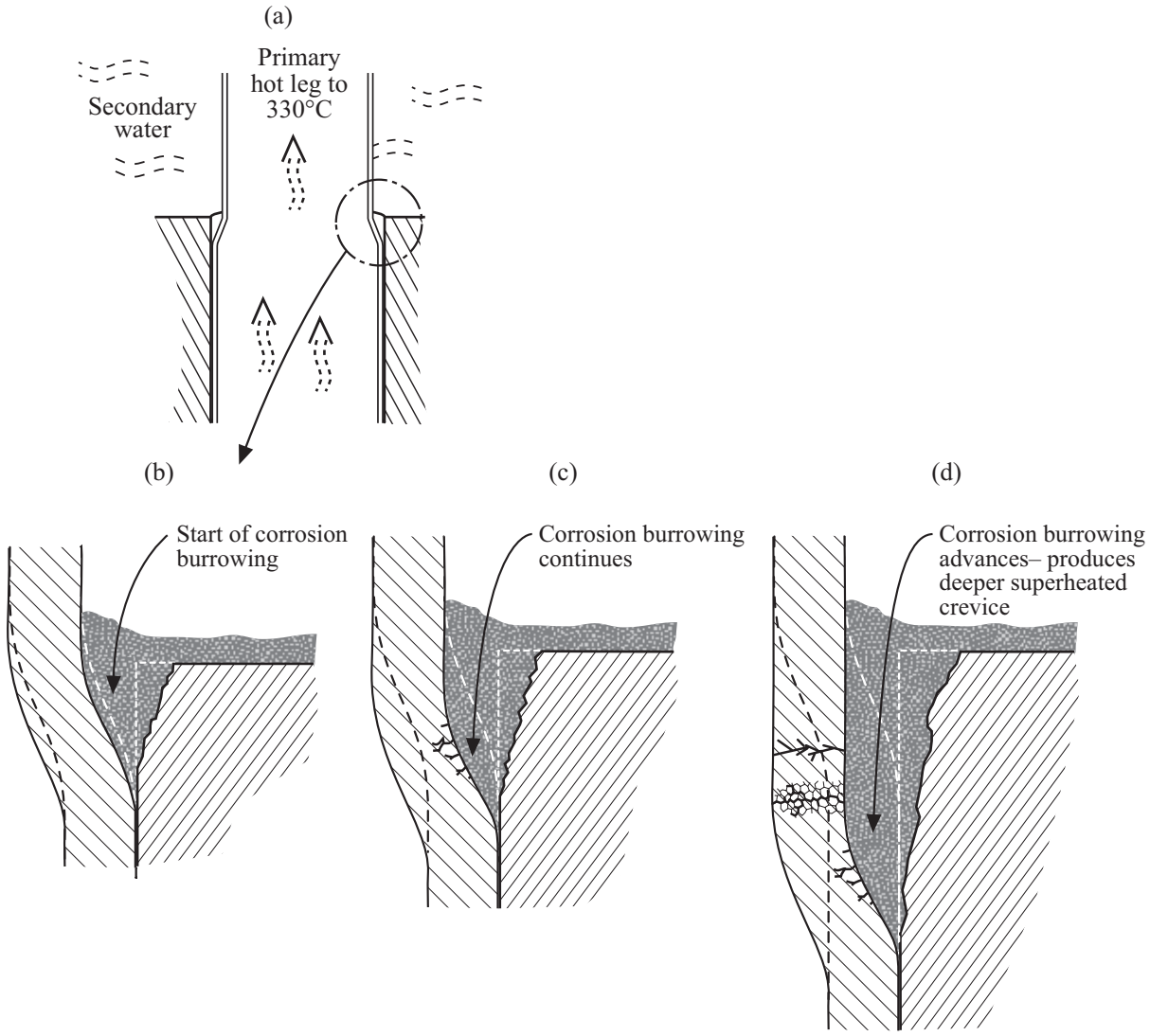

Figure 45 (a) Location of TTS crevice. (b) Short expansion of existing crevice as in Figure 44. (c) through (d) and beyond is "burrowing." (e) Corrosion damage occurs owing to the slow strain rate and the variety of concentrated chemicals, which can accumulate.

Figure 46 shows the full set of influences that produce degradation of tubes at the TTS in tubes. These include:

- Hottest location in tube.
- Insoluble deposits accumulate at the TTS.
- Tube expansion gives residual stresses and cold work around the periphery.
- Corrosion of steel of the TTS fills the crevice and stimulates a superheat crevice around the periphery.
- Once the corrosion products expand in the crevice, this leads to a slow straining that deforms the

initial crevice; this is followed by burrowing that produces a still deeper and more aggressive crevice.

- Bending stresses at the TTS due to the upward deformation of the tubesheet increase applied stresses still further.

This array of influences suggests that degradation at the TTS in the long term should be monitored carefully.

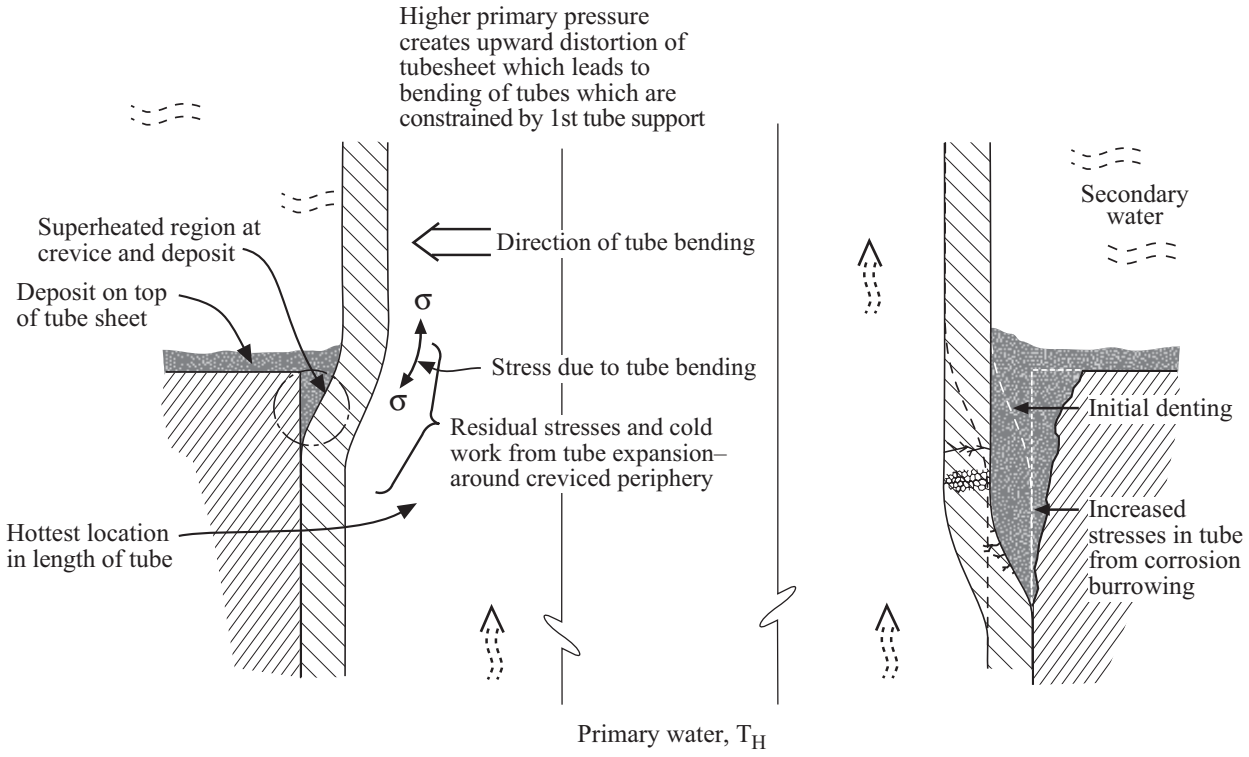

Figure 46 Influences that affect degradation of tubes near the TTS.

c. Deep TTS crevices, "Burrowing"

The deep crevices as shown in Figure 42(a) are no longer used; but the fact that failures due to concentration in the deep crevices occurred provides a bounding case for deepening crevices (such as in burrowing), which are described in Figure 45. Species such as Pb, reduced sulfur, as well as the sulfate shown in Figure 28(a), can produce SCC from the accumulated chemistries in superheated long crevices. It is likely that burrowing would increase its rate with time since the leverage of the expanding corrosion products would increase as the crevice deepens and as the capacity to concentrate species increases.

d. Fouled surfaces

Freespan surfaces on the secondary side are fouled as described in the report by Varrin[101] and shown in Figure 47. Depending on the extent and properties of fouling on surfaces, SCC can occur on the free surfaces as noted by Staehle and Gorman[5] in their Table 2. Fouled surfaces produce two undesirable effects. One is the increase of the pressure drop and the second is the

capacity to produce superheat on free surfaces as deposits accumulate. This superheat then leads to accumulations of impurities at the interface between the deposit and OD surface. In the past, fouling as a source of degradation of tubing has not seemed to be a significant concern. However, with longer times, fewer outages, possibly less cleaning, and higher heat-fluxes, fouled surfaces could become a more important source of degradation.

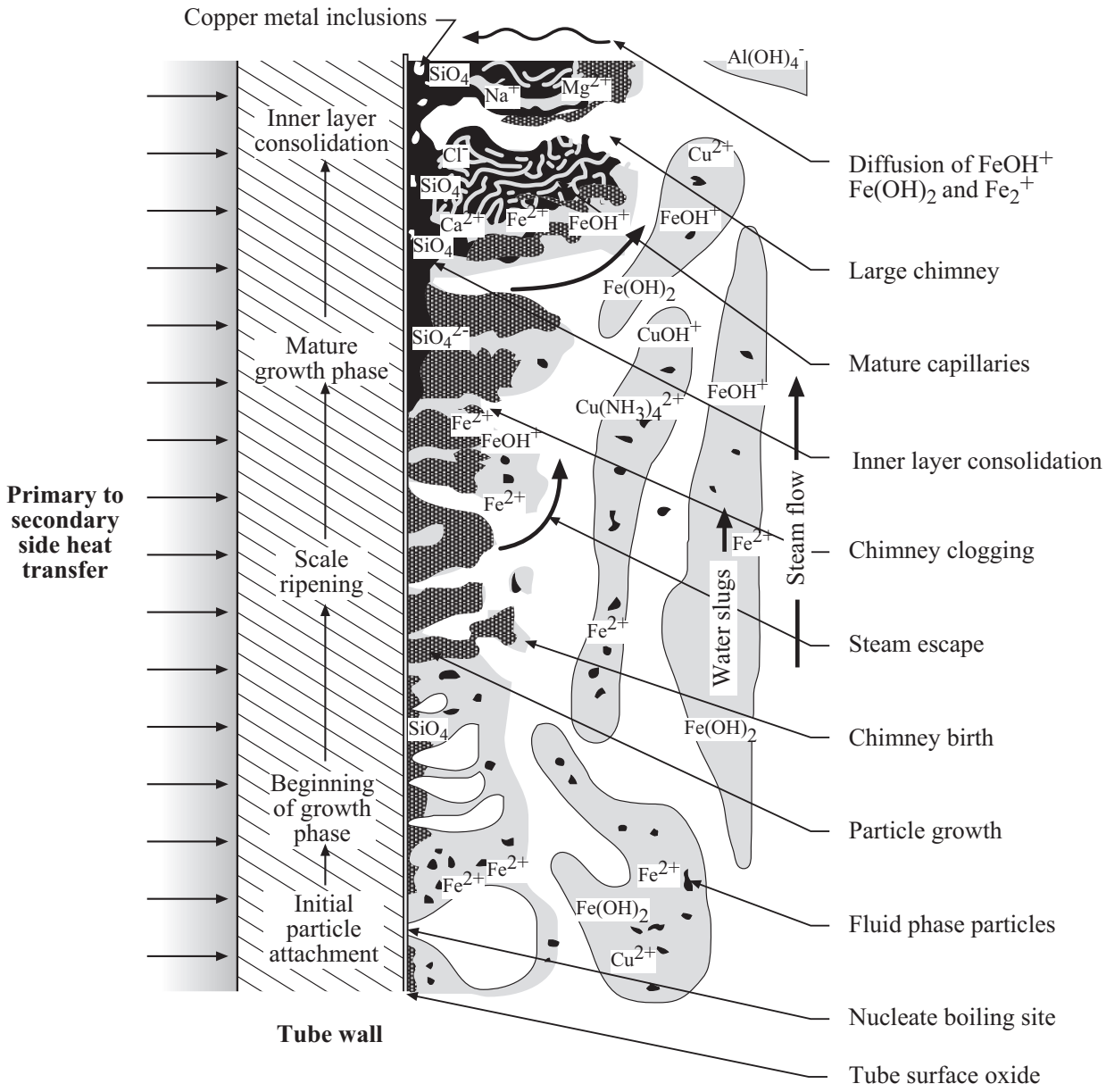

Figure 47 Model for growth of tube deposits on free surfaces including evolutionary steps and morphologies. From Varrin.[101]

The number of reported perforations or indications on free spans has been small. However, some have occurred;[5] this pattern could easily increase with long times. Lead has been shown to accumulate on fouled surfaces. There is little information on the nature of accumulation of impurities on fouled surfaces.

e. OTSG upper bundles

Figure 14 shows that the upper bundle of OTSGs accumulates impurities that eventually produce SCC. This figure also shows that such accumulations require about ten years to produce significant SCC in Alloy 600SR (stress relieved). Superheated surfaces in the upper bundle of SGs seem to be little different from other superheated surfaces with respect to concentrating impurities.

2. Startup and shutdown chemistries

Startup, shutdown, and layup procedures have improved greatly with respect to minimizing pitting and SCC that result from admitting oxidizing conditions. However, this source of impurities still remains as a potential problem in case of inadvertent mishaps; the conservative procedures now in place should not be degraded.

The most frequent contaminant is oxygen from the air. This oxygen often leads to pitting that in turn leads to SCC. Such a sequence seems to have been responsible for the SCC in SG vessel girth welds, which are discussed in Section 4.2.[102,103]

3. Pb impurities

The overall problem of degradation due to the presence of Pb is discussed in Sections 3.2 and 3.3. With respect to the chemistry of water, Pb is a minor impurity in the feedwater being in the range of 1-100 ppt. While Pb was once thought to occur only in connection with "Pb accidents," its minor ubiquity is now widely recognized and accepted. While the first measurements of these low concentrations in secondary water were performed by Takamatsu[104] as shown in Figure 48, these trends have been repeated now by many utilities as described in the PbS workshop of 2005.[105]

4. Low valence sulfur

Sulfate (sulfur at +6 valence as SO_4^{2-}) is permitted in concentrations on the secondary side at about <5ppb as shown in Figure 32. This sulfate can react with hydrazine that is deliberately added to the secondary side for the purpose of lowering the concentration of oxygen; and this reaction between sulfate and hydrazine produces lower valence sulfur in the range of -2 to +2 or +2.5 (H_2S, HS^-, S^{2-}) to $S_2O_3^{2-}$ or $S_3O_4^{2-}$ (hydrogen sulfide, bisulfide, sulfide, thiosulfate, tetrathionate, respectively). Such lower valence sulfur produces SCC, e.g. S^{y-}SCC, in Alloy 690TT as well as in Alloys 800NG, 600TT, and 600MA as discussed in Section 3.4.

In addition, sulfur can be carried to the turbine (discussed in Section 4.8) in the steam to produce possible SCC in the high strength steels—a problem well known in the petroleum industry. This process is shown in Figure 106. Low valence sulfur in the turbine is a special concern owing to the high strength of the turbine alloys and their propensity to SCC in the presence of low valence sulfur. The possibility of carrying S^{y-} in the steam phase has been confirmed by Daret et al.[106]

The fact that hydrazine reacts with sulfate to produce low valence sulfur has been reported in four papers including the work of Sala et al.,[107] Daret et al.,[106] de Bouvier[108,109] and their co-workers.

Figure 49 summarizes results from Daret et al.[106] who investigated the reduction of sulfates by hydrazine in model boiler experiments. These experiments used sulfate from resin contamination and sludge from an operating reactor, Paluel. The experiments were conducted between 290-295°C using boilers with a continuous makeup rate and both blowdown and steam bleed. Hydrazine was in the range of 10 to 50 $mg.kg^{-1}$ and the pH_{RT} was between 9.3 and 9.6. The water used ammonia to achieve the pH.

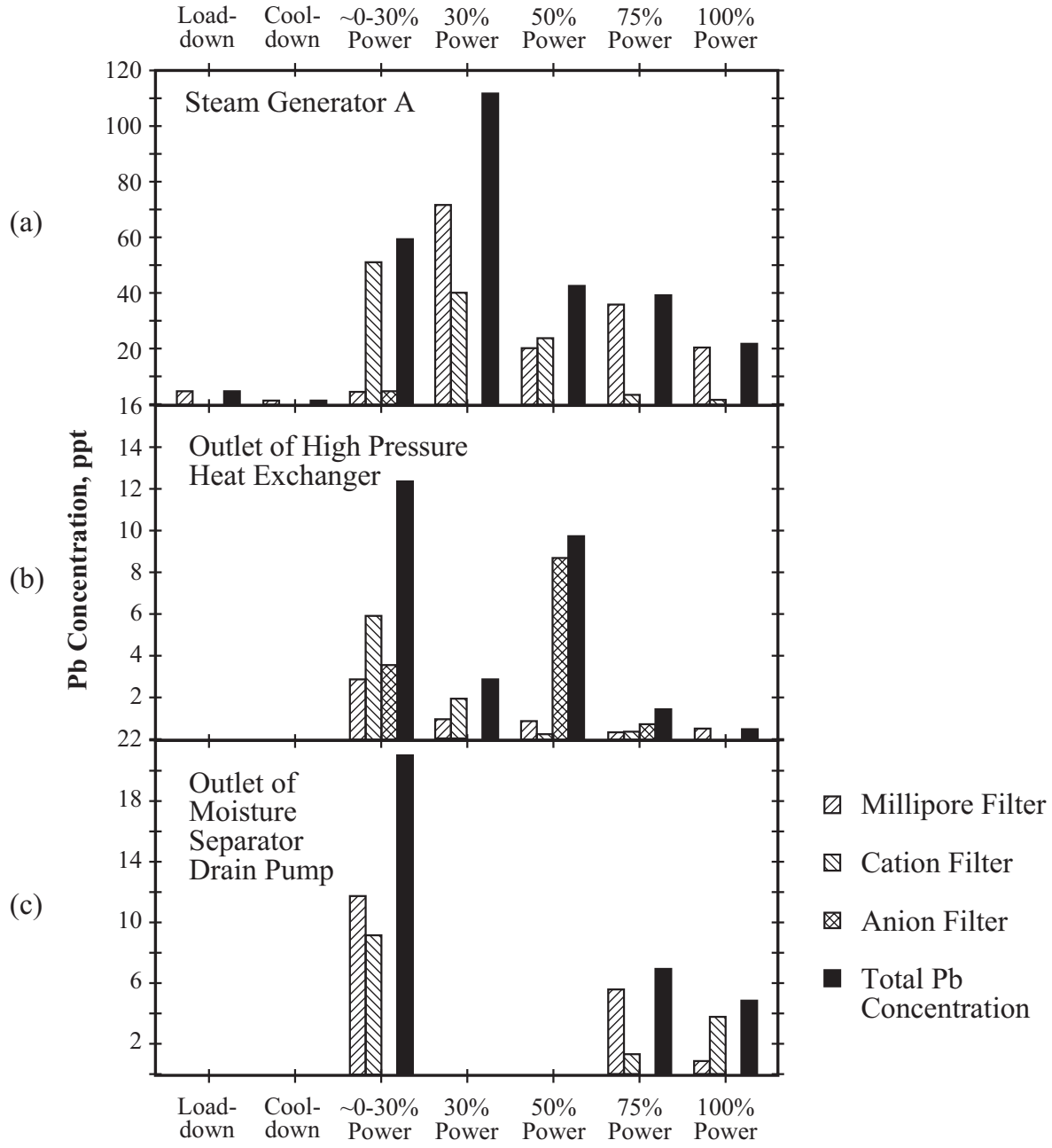

Figure 48 Concentration of Pb vs. power for three locations in Ohi-1 taken in 1993. (a) Steam Generator A. (b) Outlet of high pressure heat exchanger. (c) Outlet of moisture separator drain pump. From Takamatsu.[104]

Of particular note are the results for the reduction of sulfate and the preferential separation to the steam phase. The experiments also measured the difference between sulfide and "reduced sulfur." The meaning of "reduced" sulfur is not so clear, but it could include thiosulfate, tetrathionate, sulfite or one of the S^{2-} species, e.g. H_2S, HS^-, or S^-. These results, as well as experiments using Na_2SO_4, which confirmed the results with sludge, showed the following important patterns:

- The reduced sulfur and sulfide separated preferentially and substantially to the steam phase in the three experiments as shown in Figures 49 (a,b,c). Also, the sulfide and the reduced sulfur separated differently between water and steam. This suggests that the species in the steam might have been H_2S or one of the ionic species that is soluble in water droplets.
- Sulfide could be separated from reduced sulfate. However, it is not clear whether this sulfide also included the other -2 species; it appears that the analyses for sulfide was only for the S^{2-} and not the HS^- or H_2S.
- As the solution became more oxidizing, i.e. test 1 to test 3, the ratio of sulfide in the steam phase relative to the liquid blowdown decreased. However, this more oxidizing condition is not realistic for normal steam generators, except as the low hydrogen raises the potential but not to the extent of the CuO noted for testing in Figure 49(b,c).
- The concentration of hydrazine in the range studied does not seem to affect the amount of sulfates, which are reduced as shown in Figure 49(d). This suggests that the concentration of hydrazine does not enter significantly into the rate process in the range studied.

While PbSCC seems to be a minimum at intermediate pH, e.g. secondary reactor operating pH, S^{y-}SCC might increase monotonically with lowering pH following the suggestion of the juxtaposition of Figures 25(a,b). The point here is that sulfur should become more soluble as the pH is reduced rather than going through a minimum as for Pb, since Figure 25 shows that, while Pb tends toward lowering the solubility in the mid-range of pH, S becomes more soluble with decreasing pH. However, despite this reasonably possible tendency, as discussed in Section 3.4, the S^{y-}SCC is almost 100x less severe in AVT environments than in concentrated alkaline environments.

5. Decreasing iron in secondary water

Minimizing iron in secondary water lowers: fouling on free span surfaces, buildup of deposits on the TTS, and buildup of deposits at the TSPs. Thus, minimizing such iron (iron oxide) deposits decreases pressure drop and decreases corrosive degradation.

Current work to reduce the concentration of iron follows from Figure 50 from Neder et al.[110] and Choi and Libby[111], which shows the solubility of iron vs. high temperature pH and that changing the pH_{RT} from about 9.3 to 10.0 lowers the iron concentration about a factor of 10. The aim of such water treatments is to keep the iron at its minimum solubility. Keeping iron at such minimum solubility is accomplished by adding amines that are more stable than ammonia and that raise the pH or by adding higher concentrations of ammonia.

While raising the pH is beneficial to lowering iron, as shown in Figure 50, such a direction may also alter other processes such as the capacity of fouling deposits to sequester impurities, the rate of dissolution of more active species from alloys, e.g. Cr in Alloy 690TT, or the immobilization of Pb.

6. Boron additions in primary and secondary water

Boron is added to primary water for purposes of controlling the nuclear reactivity and is added to the secondary side in some reactors nominally to minimize corrosion in superheated crevices. The addition of boron initially assumed that the ODSCC was alkaline and that the acidification

provided by boric acid would mitigate the SCC. While it is now clear that the ODSCC is not related to alkaline environments in superheated crevices, it appears that the addition of boric acid is still beneficial as shown in Figure 51. Such a beneficial effect may be related to the capacity of boron to form insoluble compounds following the work of Seo et al.[112] Here, the boron was distributed in a thin layer of the passive film, as is the bonaccordite, on primary fuel surfaces as shown in Figure 52.

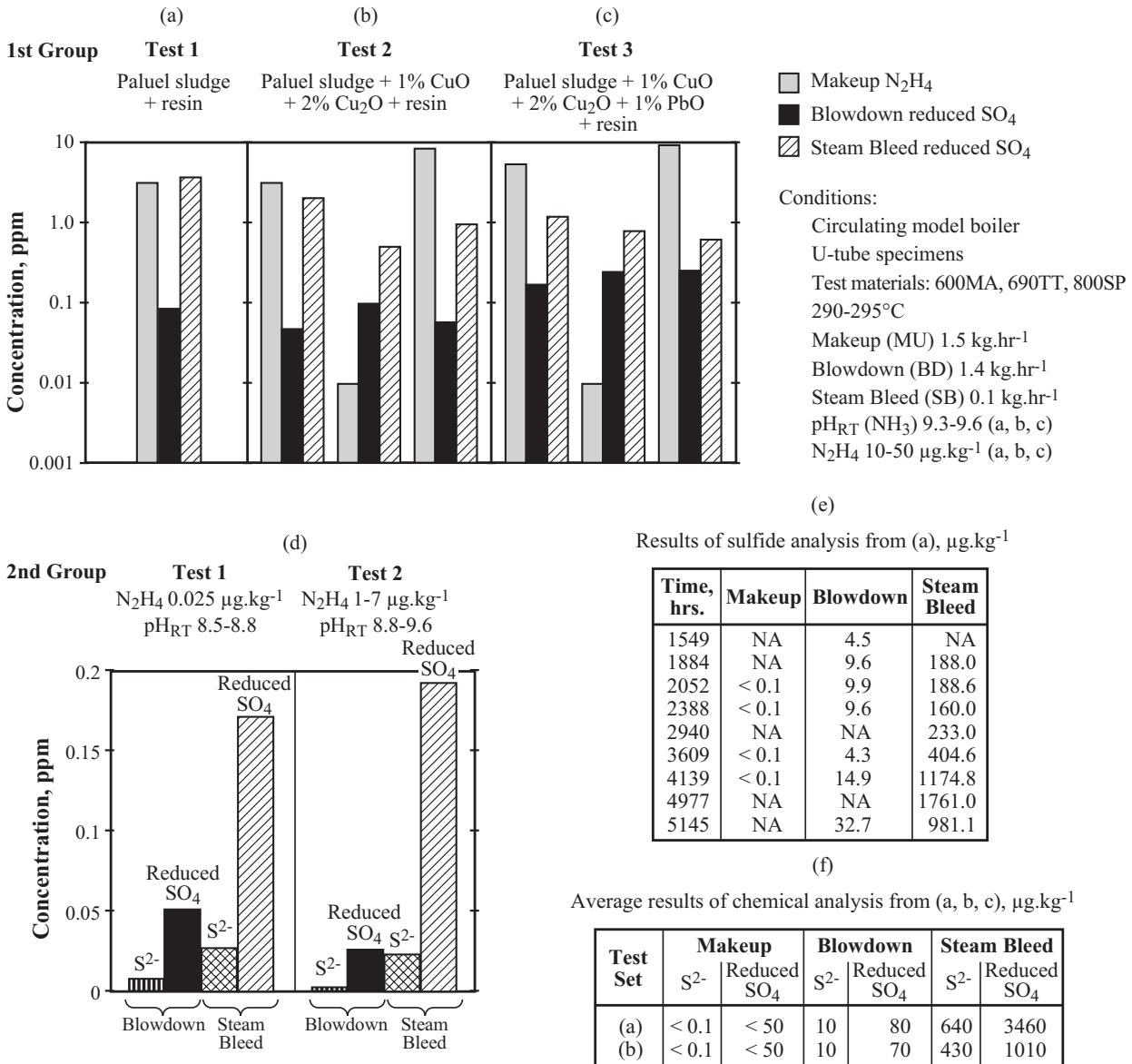

Results of sulfide analysis from (a), µg.kg^{-1}

Time, hrs.	Makeup	Blowdown	Steam Bleed
1549	NA	4.5	NA
1884	NA	9.6	188.0
2052	< 0.1	9.9	188.6
2388	< 0.1	9.6	160.0
2940	NA	NA	233.0
3609	< 0.1	4.3	404.6
4139	< 0.1	14.9	1174.8
4977	NA	NA	1761.0
5145	NA	32.7	981.1

Average results of chemical analysis from (a, b, c), µg.kg^{-1}

Test Set	Makeup		Blowdown		Steam Bleed	
	S^{2-}	Reduced SO_4	S^{2-}	Reduced SO_4	S^{2-}	Reduced SO_4
(a)	< 0.1	< 50	10	80	640	3460
(b)	< 0.1	< 50	10	70	430	1010
(c)	< 0.1	< 50	40	240	200	900

Figure 49 (a) Average results from Test 1. (b) Average results from Test 2. (c) Average results from Test 3. (d) Mean data from Tests 1 and 2 from tests with Na_2SO_4 (e) Results from sulfide analyses for Test 1. (f) Average results from three tests. From Daret et al.[106]

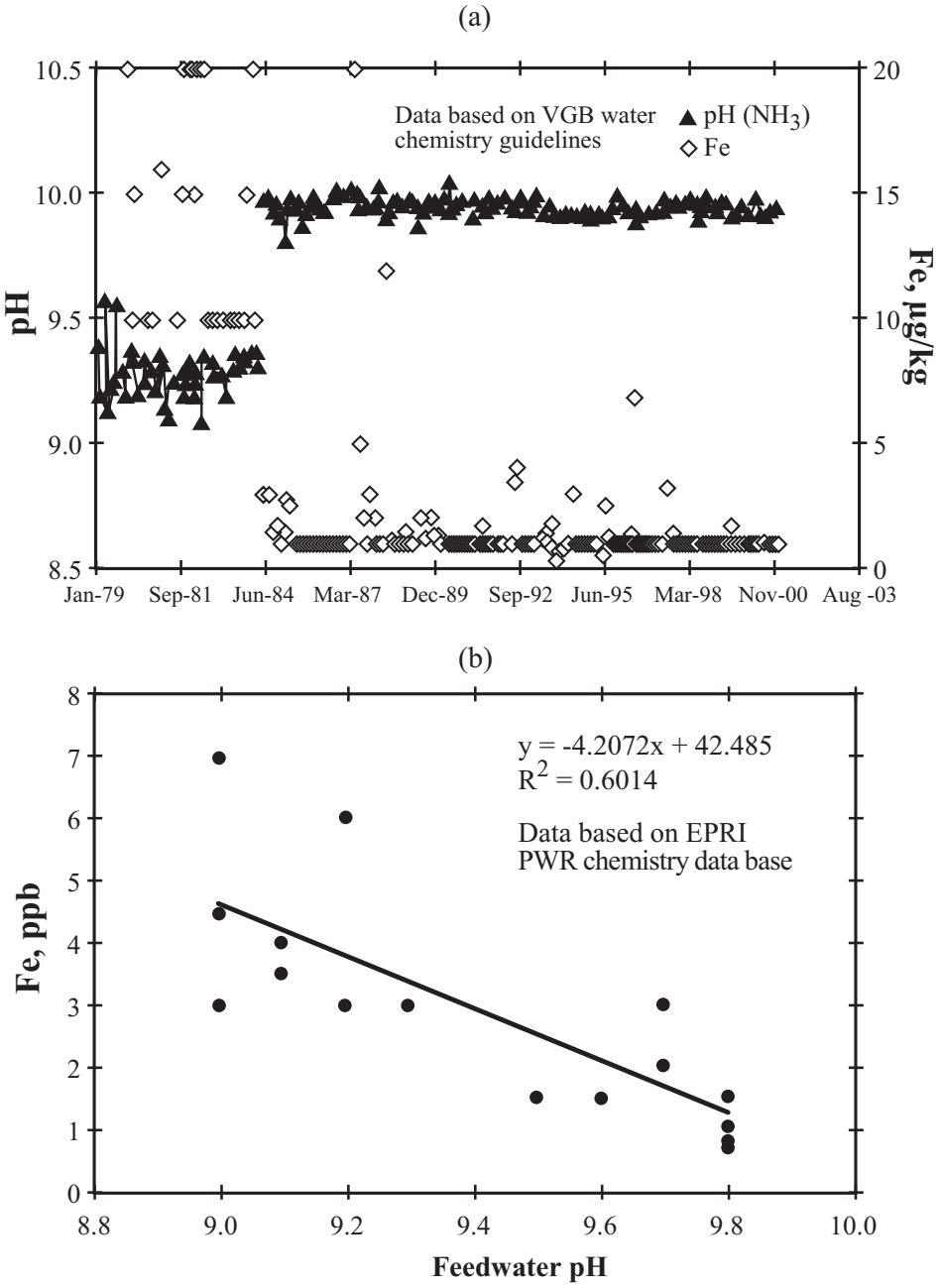

Figure 50 (a) pH_{RT} and iron vs. time. pH achieved by using high AVT chemistry. From Neder et al.[110] (b) Iron concentration vs. pH_{RT} in the secondary system based on EPRI PWR chemistry database. From Choi and Libby.[111]

With respect to the primary side, boron forms compounds that are insoluble and that accumulate on the surfaces of fuel cladding, as shown by Byers et al.[113] Here, boron forms a mineral, bonaccordite (N_2FeBO_5). When the boron is so sequestered, it lowers the local nuclear reactivity of the adjacent fuel. This produces uncertainties in the performance of the core. This is not really a corrosion problem but rather a nuclear problem but the formation of this compound may be analogous to

the inhibitive compounds on the secondary side. This change in power along the length of fuel tubes is called "Axial Offset Anomaly (AOA)." Figure 52 from Byers et al.[113] shows schematically the distribution of reaction produces on the surface of a fuel tube. The bonaccordite is shown to occupy a relatively thin layer close to the surface of the fuel tube and this same compound may be important to the use of boric acid as an inhibitor on the secondary side.

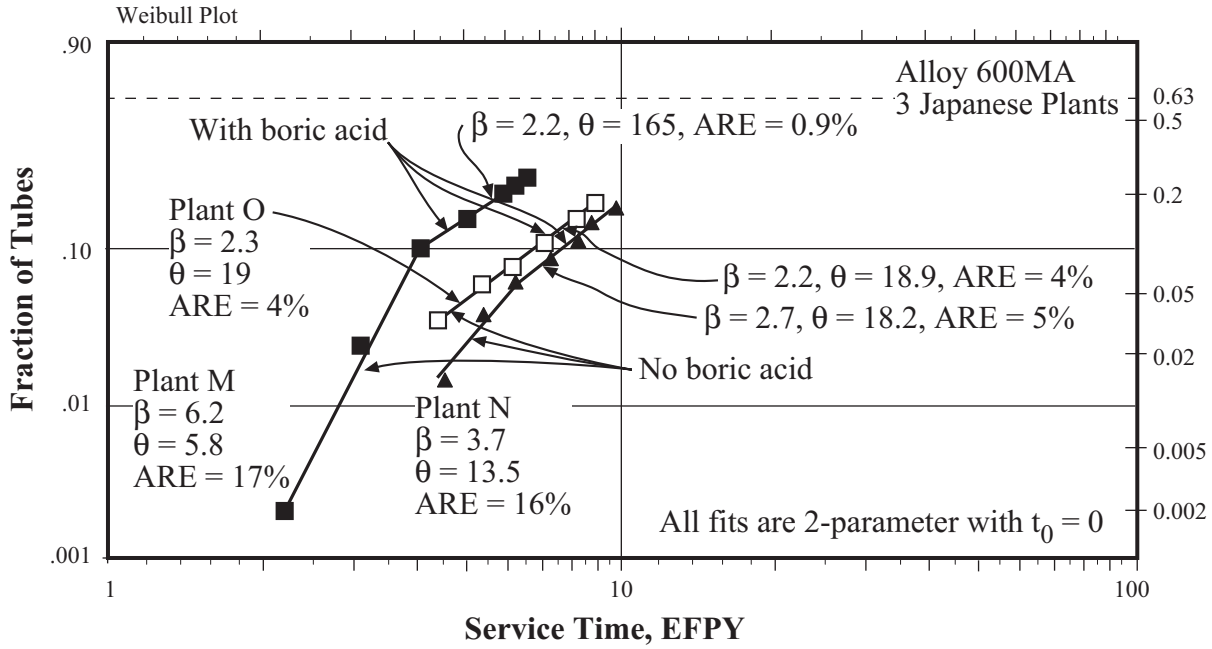

Figure 51 Probability vs. service time for the failure of Alloy 600 tubes in three Japanese plants where boric acid has been added. From Staehle, et al.[7]

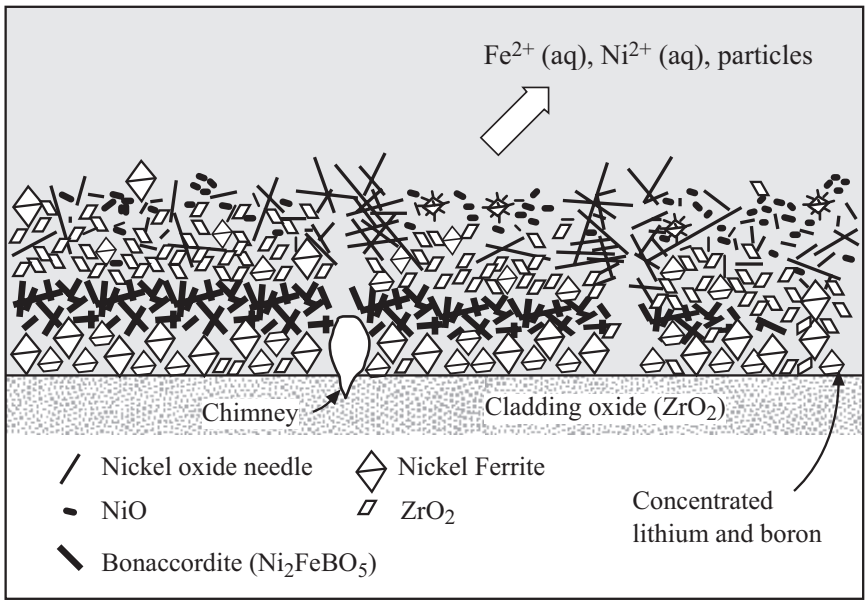

Figure 52 Structure of deposit formed in fuel cladding after Cycle 10 in the Callaway plant. From Byers et al.[113]

7. Zinc additions

Zinc is being developed as a corrosion inhibitor mainly for the primary side as it reduces the release of corrosion products that can become activated. Zn injection started in 1994 with injection at the Farley 2 plant in 1994, and the application of Zn has increased.[114,115,116] Zn also seems to inhibit LPSCC.[117] However, LPSCC may be less important in the future as improved alloys are being used that seem to minimize or prevent LPSCC. Whether LPSCC will become important in the long term for minimizing possible future degradation in Alloys 800NG and 690TT is not clear, as it may depend on the dissolution of Cr with time as discussed in Section 3.13.

Zn seems to enter into the protective film on the Fe-Cr-Ni alloys by stabilizing the spinel protective film as suggested by the data in Figure 53 from Lin.[118,119,120]

Oxide Formula	Free Energy of Formation K/cal/mol (560K)	Cation Distribution
Fe_3O_4	-290	Fe^{3+} [$Fe^{2+}Fe^{3+}$]
$NiFe_2O_4$	-280	Fe^{3+} [$Ni^{2+}Fe^{3+}$]
$CoFe_2O_4$	-283	Fe^{3+} [$Co^{2+}Fe^{3+}$]
$ZnFe_2O_4$	-303	Zn^{2+} [$Fe^{3+}Fe^{3+}$]
$NiCr_2O_4$	-348	Ni^{2+} [$Cr^{3+}Cr^{3+}$]
$FeCr_2O_4$	-360	Fe^{2+} [$Cr^{3+}Cr^{3+}$]
$CoCr_2O_4$	-361	Co^{2+} [$Cr^{3+}Cr^{3+}$]
$ZnCr_2O_4$	-380	Zn^{2+} [$Cr^{3+}Cr^{3+}$]

Figure 53 Data for the distribution of species in spinel compounds including Zn. From Lin.[118,119,120]

Adding Zn to the primary coolant in the amount of about 5-15 ppb is generally accumulated as shown in Figure 54(a) from Rich.[121] Figure 54(b) shows how the addition of Zn first increases the concentration of Fe in the primary environment but then reduces it substantially to its original concentration. Studies, in general, have shown that the use of Zn substantially reduces the radioactivity in the primary system as shown in Figure 54(c) from the work of Wolter et al.[114,115,116]

LPSCC is somewhat, not totally, reduced by the presence of Zn as shown in Figure 54(d). While the importance of Zn in mitigating LPSCC may be moot for the long term, lowering the iron concentration and minimizing the corresponding hot spots of radioactivity is a substantial benefit.

Zn, as an inhibitor, is being considered increasingly. However, its long term effect on the composition of passive films and metal substrates should be monitored in view of the tendency of the active Cr to dissolve preferentially as discussed in Section 3.13.

8. TiO_2 additions

TiO_2 has been developed as an inhibitor for SCC on the secondary side by Lumsden et al.[122] Their work to survey a range of inhibitors is summarized in Table 1.

TiO_2 derives its application from Figure 21(f), which is the E-pH diagram for Ti in water. TiO_2 exhibits a broad range of stability in water. Its development as an inhibitor is based on the premise that this broad range of stability would also provide improved inhibition.

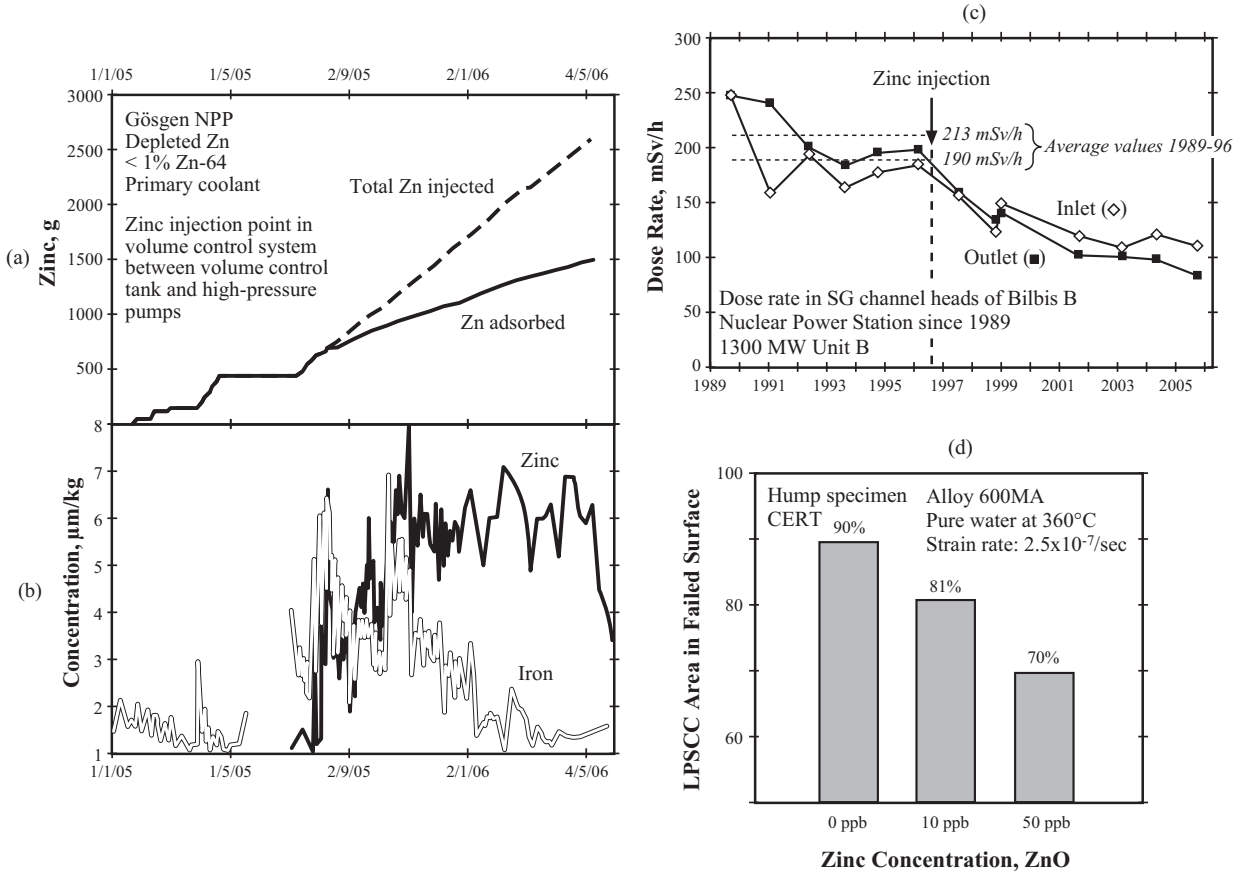

Figure 54 (a) Zn injected and absorbed in primary coolant vs. time. From Rich et al.[121] (b) Simultaneous concentrations of injected Zn and iron from the primary system. From Rich et al.[121] (c) Dose rate vs. time in the steam generator channel heads of Biblis B since 1989. From Wolter et al.[114,115,116] (d) LPSCC area on fracture surface vs. concentration of Zn added to pure water at 360°C tested in CERT. From Maeng et al.[117]

9. Dispersants

While one approach to minimizing iron in secondary water is to reduce its solubility, another is to solubilize the iron so that it can be easily removed in the blowdown. Such a technology for solubilizing iron deposits involves using dispersants, and this method has been used widely in the fossil industry. Such a dispersant, which is now appropriate to use in the nuclear plants, is polyacrylic acid (PAA); PAA is normally used in the range of about 2 ppb. This approach is being studied by Duke Power as well as many other utilities, and results from recent experimental studies are shown in Figure 55 from Rochester et al.[123] Figure 55 shows that adding the PAA dispersant does in fact solubilize the iron and that it is carried away in blowdown. However, this technology is still in early stages.

A potential problem with the use of dispersants relates to the immobilization of Pb as discussed in Section 3.2. If dispersants are efficient at breaking bonds and solubilizing the iron oxides, it is possible that dispersants could exert the same effects on the lead compounds or adsorbed bonding that seem to be immobilizing Pb. Thus, the iron would be reduced to low concentrations and the lead would be released to exert damage. Such effects might also relate to S^{y}-SCC.

Table 1
Effect of Inhibitors on SCC of Alloy 600MA in Alkaline Solutions.
From Lumsden et al.[122]

Potential, mV_{E_C}*	0	100	150	200
Reference (50% NaOH) - 2 days	N**	N	Y	Y
Reference + 5% H_3BO_3 - 2 days	N	N	Y	Y
Reference + 15% H_3BO_y - 2 days	N	N	Y	Y
Reference + 0.1% $Ca(OH)_2$ - 1 week	N	Y	Y	Y
Reference + 2% Na_2ZrO_3 - 1 week	N	Y	Y	Y
Reference + 2% ZnO - 1 week	N	N	N	Y
Reference + 2% $Zn(PO_4)_2$ - 1 week	N	N	N	Y
Reference + SAT H_2TiO_3 - 1 week	N	N	N	Y
Reference + 0.5% SiO_2TiO_2 - 1 week	N	N	N	Y
Reference + 1% TiO_2 (TiLAC) - 1 week	N	N	N	N
Reference + 0.8% TiO_2 (TiLAC) - 1 week	N	N	N	N
Reference + 0.5% TiO_2 (TiLAC) - 1 week	N	N	N	N
Reference + 0.1% TiO_2 (TiLAC) - 1 week	N	N	N	Y
Reference + 1.0% TiO_2 (TiOE) - 1 week	N	N	N	N
Reference + 1% Anatase - 1 week	N	N	N	Y
Reference + 1.0% TiB_2 - 1 week	N	N	N	N
Reference + Amorph TiO_2 - 1 week	N	N	N	N
Reference + Rutile - 1 week	N	N	Y	Y
Reference + $ZnTiO_3$ - 1 week	N	N	Y	Y
Reference + 2% $Ce(Ac)_3$ - 1 week	N	N	N	Y
Reference + 2% $Ce(Cl)_3$ - 1 week	N	N	N	Y
Reference + 2% $Ce(NO_3)_3$ - 1 week	N	N	N	N

* Potentials taken relative to deaerated open circuit potential
** N = No SCC, Y = SCC occurred

Note: SCC occurs in 50% caustic solutions. The reference environment is 50% NaOH + 1% Na_2CO_3. Exposure times were 2 days in the reference solutions and with boric acid; all others 1 week.

10. Hydrogen concentration on the primary side of SG

LPSCC as noted in the mode diagram of Figure 26 appears to be maximum mainly around the NiO/Ni equilibrium, and Figure 56 shows the dependence of both smooth surface and pre-cracked specimens on the hydrogen or electrochemical potential with the positive direction noted for both plots. This pattern has led to interest in lowering the hydrogen concentration from the point of view of reducing LPSCC of Alloy 600.

It is not clear that changing the hydrogen concentration is prudent for the following reasons:

a. This correlation with potential is based on the NiO/Ni equilibrium when the dominant passive oxide is a mixed oxide of Ni and Cr with a standard potential much lower as shown in Figure 23.

b. This correlation is relevant only to Alloy 600MA and possibly Alloy 600TT; however, in the future, neither of these alloys is relevant to the primary side.

c. The data that support the potential dependence of the LPSCC has not been analyzed for multiple heats.

d. Further, it is not clear how Alloys 800NG and 690TT, as well as Type 321 stainless steel, fit into this correlation with NiO/Ni.

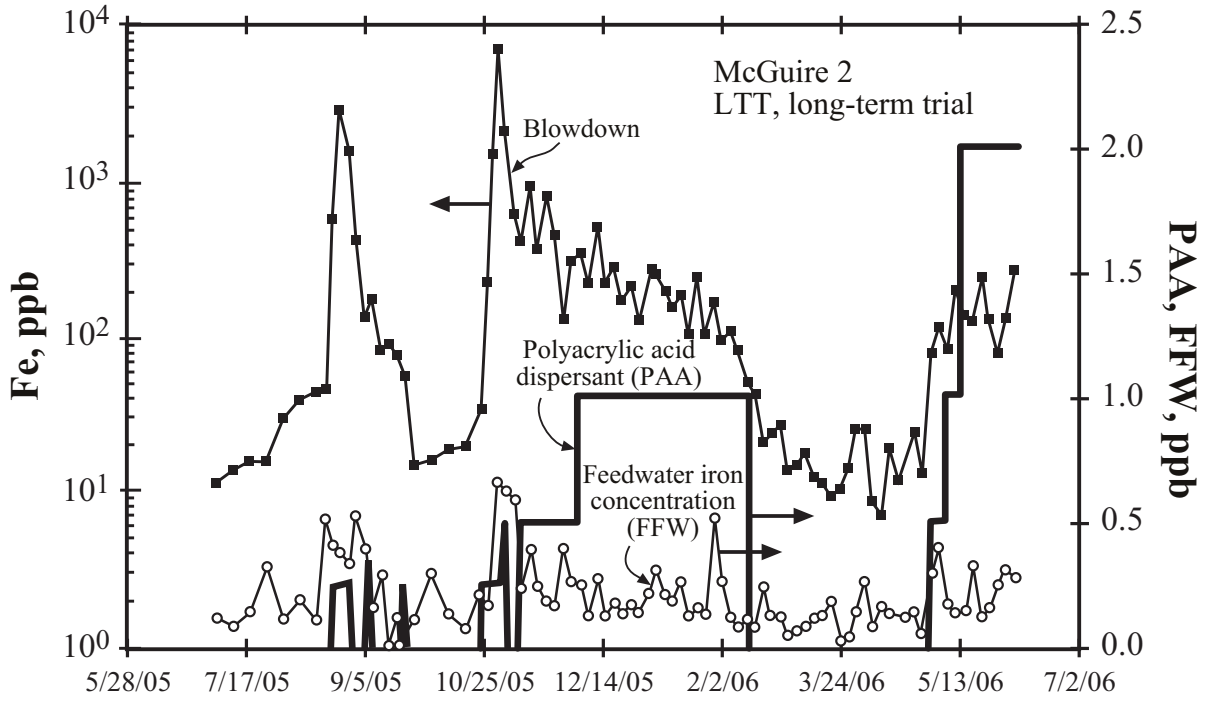

Figure 55 Results from dispersant study at McGuire-2 long term trial. Blowdown iron on the left ordinate and PAA and FFW iron on right ordinate vs. time. From Rochester et al.[123]

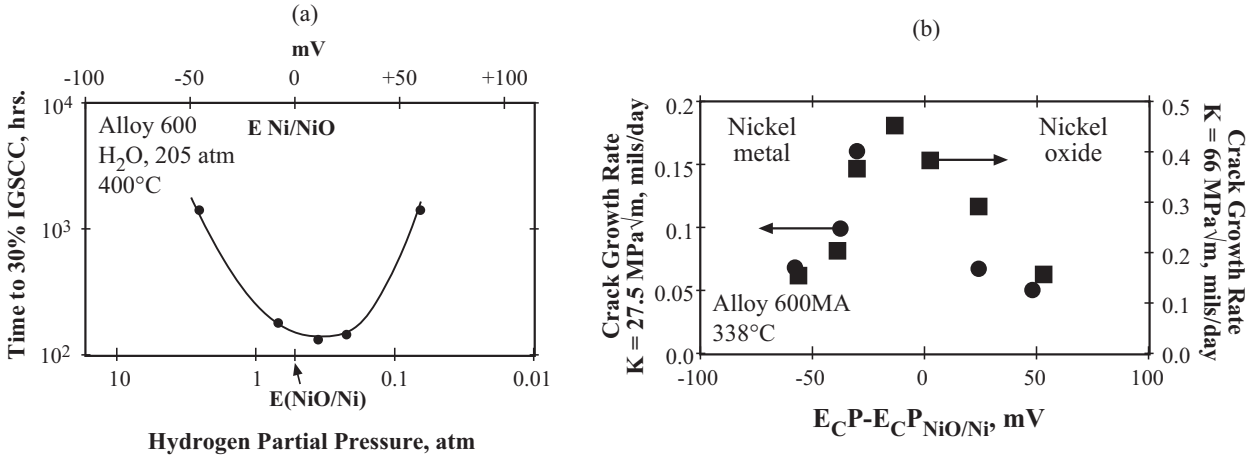

Figure 56 (a) Time to 30% IGSCC vs. hydrogen pressure and potential reference to NiO/Ni equilibrium. Experiments at 400°C and 205 atm pressure of steam. Original data from Economy et al.[124] Data recalculated by Scott and Combrade.[125] (b) Crack growth rate at two stress intensities vs. potential (EcP=electrochemical potential) relative to the NiO/Ni equilibrium potential for Alloy 600MA at 338°C. From Morton et al.[126]

Therefore, a change in the present hydrogen concentration does not seem appropriate. Further, from the point of view of the present discussion, a more important consideration is the very long time performance of the SG alloys such as Alloys 800NG, 690TT, and Type 321 stainless steel related, for example, to questions of changes in the passive film and the metal substrate as noted in Figure 101.

11. Chemical cleaning

Chemical cleaning has been utilized traditionally to remove deposits from TSP crevices and the TTS as well as to reduce the pressure drop due to accumulation of deposits on tube surfaces. An example of the beneficial effect of chemical cleaning for reducing the fouling is shown in Figure 57.

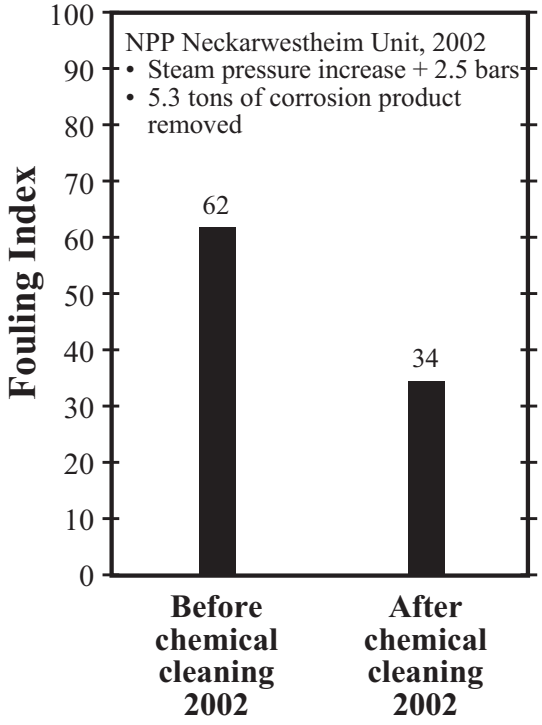

Figure 57 Improvement in fouling index of the SGs at the NPP Neckarwestheim Unit 1 as performed in 2002. The steam pressure was also increased by +2.5 bar and 5.3 tons of corrosion product deposits were removed. From Odar et al.[127]

Chemical cleaning, in general, seems beneficial but there are some concerns:

- Does chemical cleaning remove Pb? So far, there seems to have been no clear effort to assess whether the Pb is removed.
- Would chemical cleaning preferentially remove the species that immobilize Pb? There are neither data nor conceptual bases to answer this question.
- Would chemical cleaning produce pitting in the vessel of the type that possibly initiated SCC at girth welds, as described in Section 4.2?[102,103]

While chemical cleaning has been generally investigated from the point of view of "collateral corrosion damage," it is not clear that it has been viewed from more subtle damages of the type relevant to long term integrity. The questions do not seem to have been asked.

12. "Pure is not necessarily good"

There are persistent efforts to make the chemistry of primary and secondary water more pure. It is not clear that such a direction is desirable:

a. There is no information on what impurities are actually accumulated in line contact and TTS crevices.
b. PbSCC may depend on the absence or presence of some impurities with respect to immobilization and release.
c. Certain impurities may affect the capacity of deposits to absorb further.
d. Historically, purification has not always been desirable either for materials or environments, in the nuclear field.

It seems generally, that the assumption "pure is better" needs to be examined more closely.

2.9 Mechanical Acceleration

The purpose of this section is to identify important mechanically-related influences that generally accelerate degradation of metals and, in particular can produce eventual damage in the future. Further, these mechanical influences, when combined with environmental influences, e.g. those in Section 2.8, act synergistically sometimes to increase degradation substantially.

1. Slow straining (CERT)

For many years, the CERT (Constant Extension Rate Test, also called SSRT for Slow Strain Rate Test) has been used to accelerate SCC in order to obtain results in a short time.[128] In general, increasingly slower rates of strain accelerate SCC; the slower the rate of strain, the greater the loss of strength and ductility when the specimens are exposed simultaneously to the testing environment. This method of testing was first introduced by Parkins and his colleagues[129,130,131,132,133,134] based in turn on some earlier work by Coleman et al.[135] From time to time, SCC failures in service are clearly accelerated by such slowly straining conditions of stressed components, as they are simultaneously exposed to environments.

Figure 58 shows the effect of strain rate on reduction in area for steels. For materials that are considered to sustain SCC by what is called an "anodic process," the failure parameter, e.g. reduction in area, passes through a minimum vs. strain rate as shown in Figures 58(a,c). Materials that seem to fail by hydrogen-related processes often do not exhibit such a minimum and the failure parameter decreases with very low strain rates as shown schematically in Figure 58(d).

While the CERT has been used for testing, this mode of straining is also relevant to engineering applications where such slow strain rates can occur or may occur only periodically. For example, in denting, as shown in Figure 13, it appears that the occurrence of ODSCC as well as IDSCC were accelerated by the slow straining produced by the slowly expanding oxides. Such processes may be applicable to the straining of fuel rods and to denting at the TTS, as shown in Figures 35 and 44,

as well as bending resulting from the pressure-induced bending of the TS, at the TTS of the SG; such possibilities should be considered.

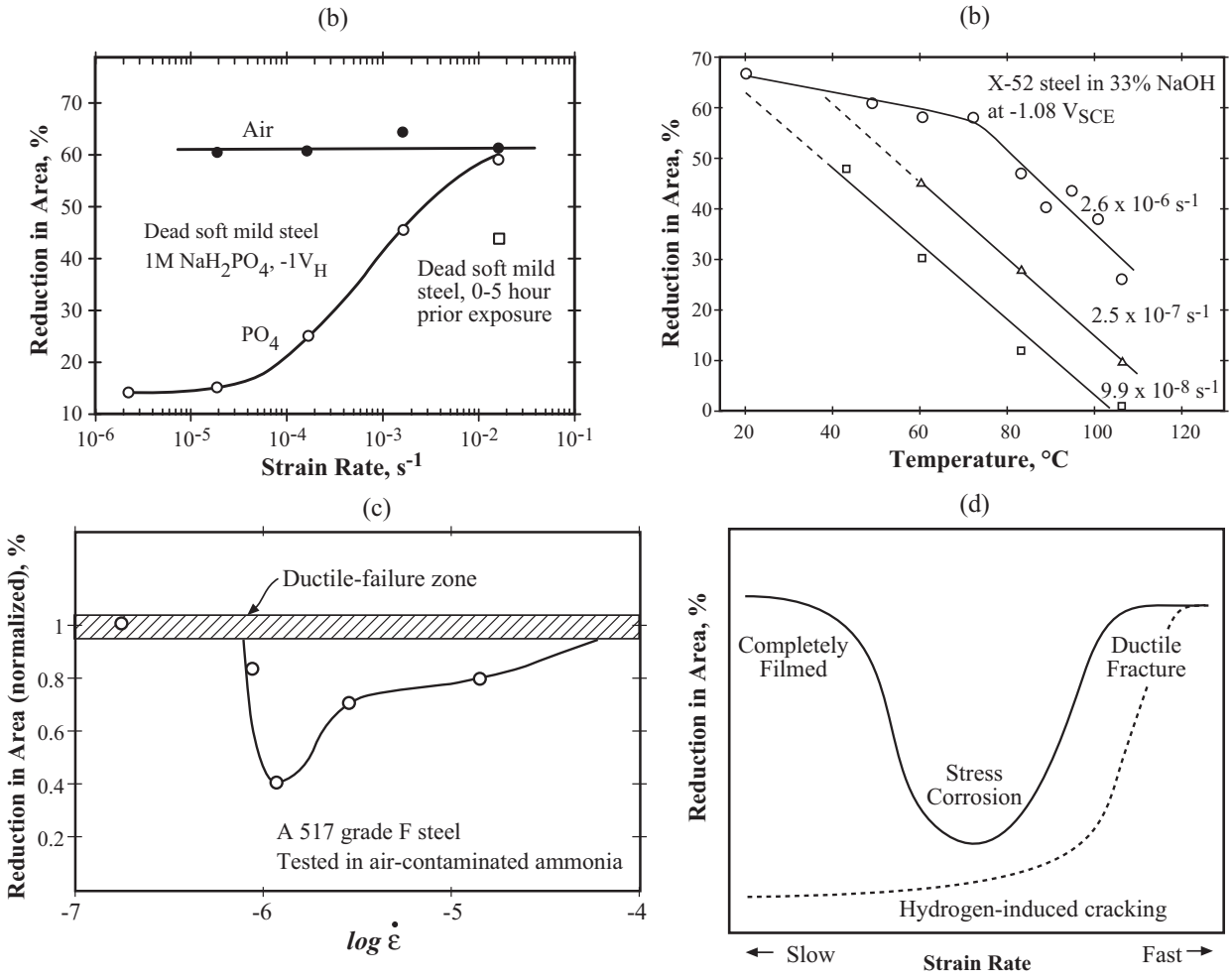

Figure 58 (a) Reduction in area vs. strain rate for dead soft mild steel exposed in 1M NaH_2PO_4 at $-1V_H$. From Parkins.[136] (b) Reduction in area vs. temperature for three strain rates for X-52 steel in 33% NaOH at $-1.08V_{SCE}$. From Payer et al.[137] (c) Reduction in area vs. strain rate for an A 517 Grade F steel tested in air-contaminated ammonia. From the work of Kim and Wilde.[138] (d) Schematic illustration of reduction in area vs. strain rate for two different mechanisms of SCC. From Kim and Wilde.[138]

2. Low frequency corrosion fatigue

In general, the fatigue crack growth rate, da/dn, increases as the cyclic frequency is reduced. This transition starts at about 1-5 Hz below which the da/dn increases 1-3 orders of magnitude to about 0.01Hz. Thus, fatigue studies at cyclic frequencies above 1-5 Hz would "under-predict" substantially the damage, which occurs at lower cyclic frequency. Figure 59 shows the effect of cyclic frequency on da/dn for steels.

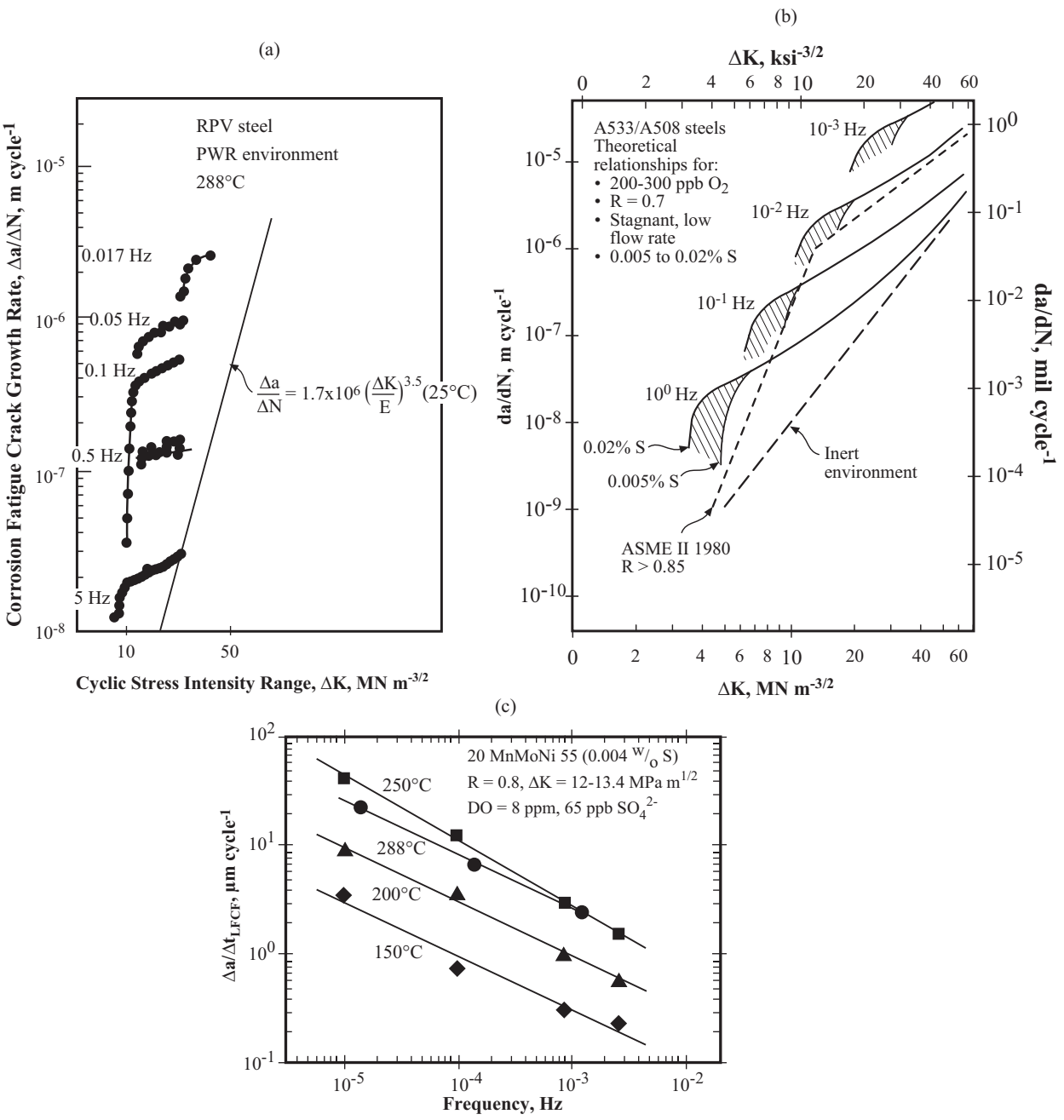

Figure 59 (a) Crack growth rate vs. ΔK as a function of frequency for a pressure vessel steel in a PWR environment at 288°C. (b) Calculated crack growth rate vs. ΔK as a function of frequency in BWR type environments at 200-300 ppb O_2 for low and high sulfur concentration in two pressure vessel steels. From Ford and Andresen.[139] (c) Crack growth rate vs. frequency for a pressure vessel steel as a function of temperature in a 8 ppm oxygen plus 65 ppb SO_4^{2-} environment. From Ritter and Seifert.[140]

Using high cyclic frequencies for studying corrosion fatigue is a common and sometimes disastrous error owing to the lack of appreciation of such effects by engineers. Especially for long times, this effect of decreasing frequency while exposed to environments, as it increases da/dn, is important to extrapolations, e.g. such mistakes have been disastrous in designing propellers for ships.

3. Ripple loading

Ripple loading is a special case of both corrosion fatigue and SCC and involves the superposition of a relatively small stress cycle on a constant mean stress. The damaging effects of ripple loading on SCC have often not been recognized owing to the small amplitude of the ripple that can produce such significant effects. "Ripple loading" usually involves a few percent of stress cycle superimposed on a mean stress. The ripple loading accelerates both the initiation and the propagation as the cyclic frequency of the stress ripple decreases. Examples of ripple loading for initially smooth and pre-cracked specimens are shown in Figure 60. The superposition of the stress (or stress intensity) ripple is increasingly significant with lower cyclic frequencies.

In Figures 60(b,c) the notation of "intergranular" and "mixed" morphologies indicate environmental effects. The "transgranular" morphology indicates the absence of environmental effects, i.e. the results would be the same in dry air. As cyclic frequency of the ripple is decreased, the location of K_{Iscc} is substantially decreased.

Since superimposed cyclic frequencies are common in nuclear applications, Figure 60 implies that the thresholds and crack growth rates must account for the diminution due to the interaction of mean stresses with small magnitudes of ripple loading where the ripple is not in the domain of corrosion fatigue. The ripple effect would contribute to precursors over long times.

4. Expanding oxide or reaction compounds

The denting discussed in Section 2.3 in connection with Figure 13 noted how expanding reaction products could produce stresses that would "strangle" a tube and produce high local stresses that could lead to perforating SCC.

The fact that expanding corrosion products would produce stresses sufficient to break enclosing materials has been studied since at least 1906, where such stresses were measured in connection with reinforced concrete when the oxide expansion from corroding reinforcing steel caused the surrounding concrete to crack. The fact that corrosion products have specific volumes greater than the initial metal was first quantified by Pilling and Bedworth in 1923.[55]

While denting, first observed in 1974-75, was a major event in the corrosion history of steam generators, it was not the first event in recent times. The work by Pickering et al.,[143] which was published in 1962, both measured the stresses involved in the expansion of corrosion products and conducted an important elucidating experiment as shown in Figure 61. This paper was well known in the corrosion community before denting occurred.

The experiment shown in Figure 61 demonstrates two important ideas. Here, a stainless steel block (2) in Figure 61(a) was prepared with a slot (1). A stainless steel insert was prepared to just fit into the slot. The first idea to be demonstrated was whether the corrosion products that were produced in the tight crevice space between the block and insert, Figure 61(b), could produce sufficient force to initiate and propagate SCC at the base of the slot, Figure 61(c). This experiment was carried out by placing the block and insert in an autoclave, which contained a chloride plus

nitric acid solution at 204°C for a time <200 hr. When the specimen was removed from the autoclave, SCC was observed at the base of the slot. The second idea was to remove the insert and determine whether the corrosion products inside the now advancing SCC would further expand to increase the stress at the tip of the SCC to propagate further. Such propagation continued. The phenomenon is referred to as "wedging."

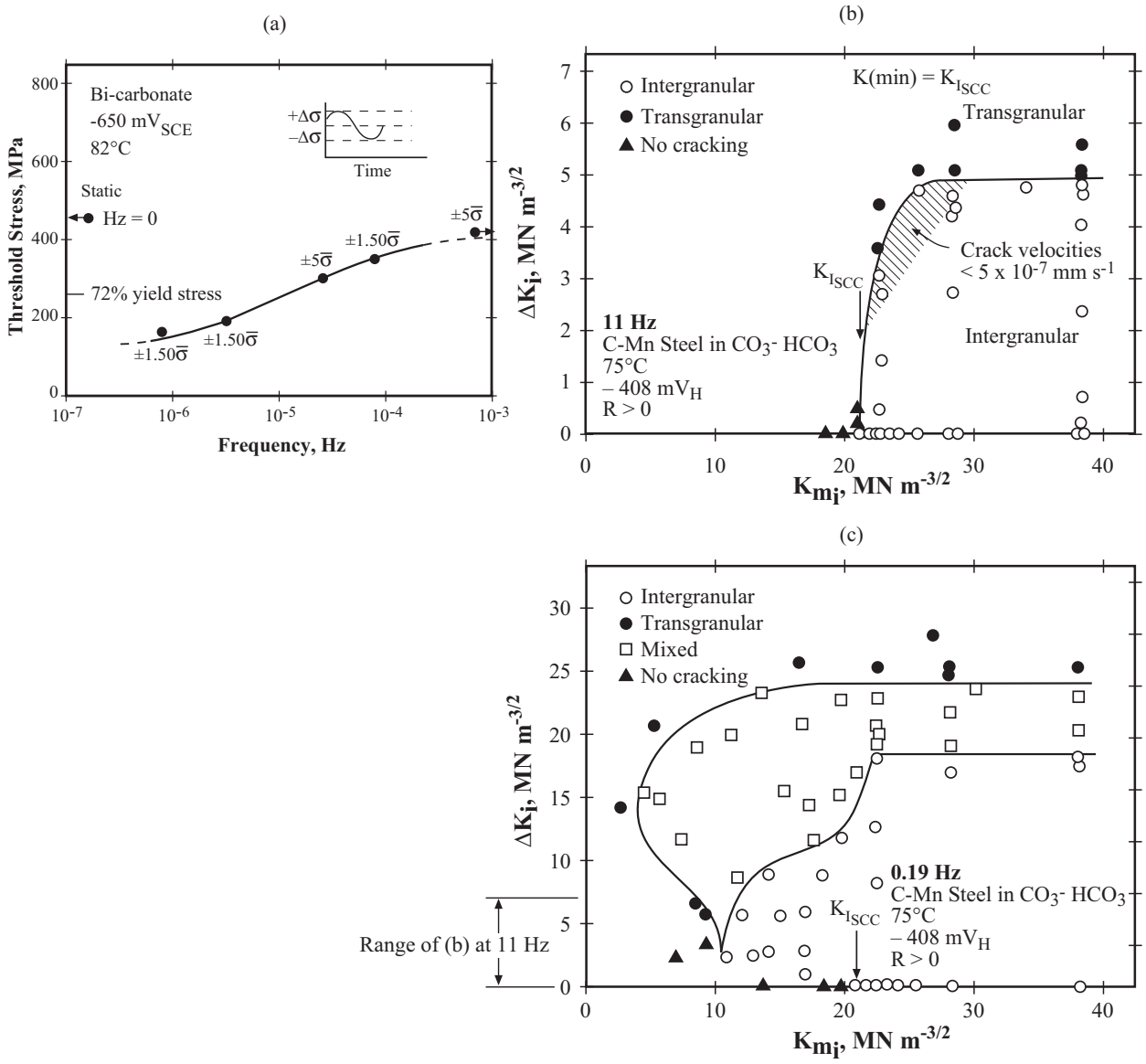

Figure 60 (a) Threshold stress vs. frequency for low fluctuations of stress for a C-Mn steel in a carbonate-bicarbonate solution at -650 mV_{SCE} and 82°C. From Parkins.[141] (b) ΔK_i vs. K_{mi} for a C-Mn steel immersed in a carbonate-bicarbonate solution at 75°C and -408 mV_H for R>0. 11Hz. Location of $K_{I_{SCC}}$ shown. (c) Same as (b) at 0.19Hz. From Parkins and Greenwell.[142]

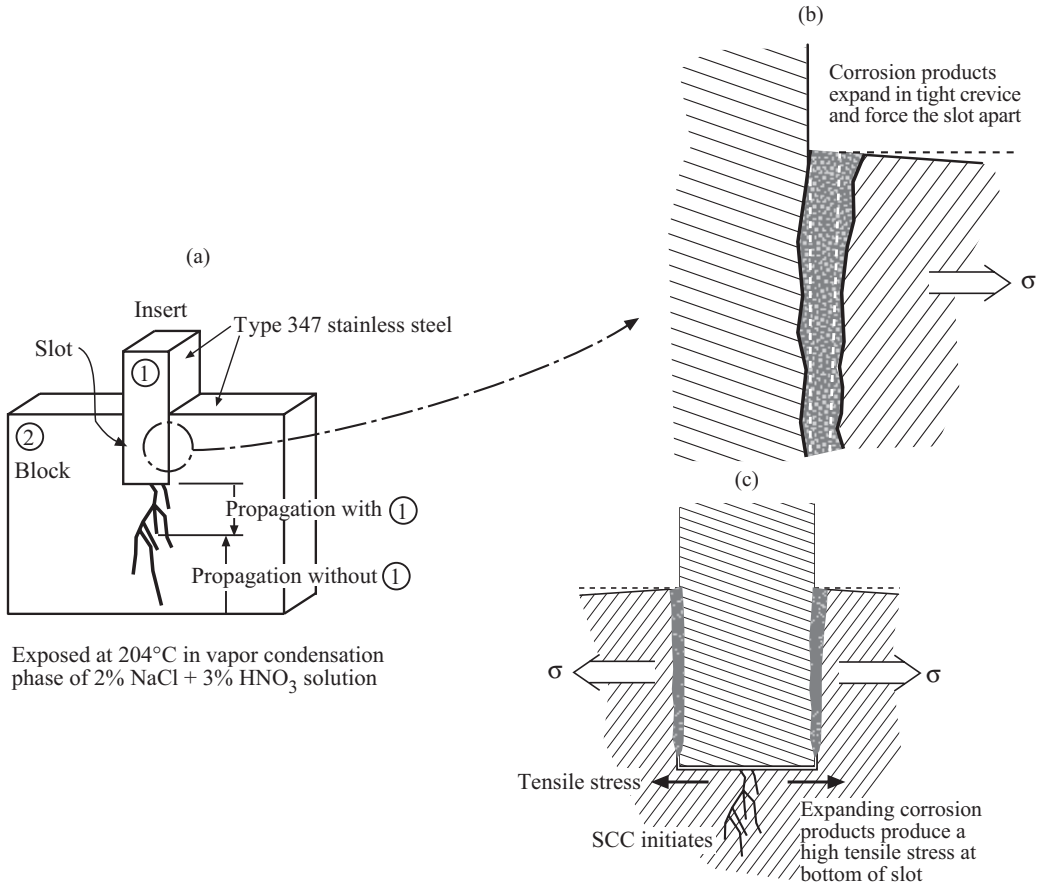

Figure 61 (a) Block of stainless steel with slot and insert. Exposed at 204°C in vapor condensation phase of 2% NaCl + 3% HNO_3 solution for <200 hr. (b) Corrosion in crevice between insert and slot surface expands. (c) Expanding corrosion products exert bending moment at tip of slot and produce tensile stresses that result in SCC. Based on work from Pickering et al.[143]

The "wedging" experiment in Figure 61 was exactly what happened during denting of SG tubes fifteen years later. The possibility of such effects in the future should be expected. These are the kinds of processes that might take relatively long times as precursors before sufficient stress was accumulated to initiate SCC. Such processes can occur in the TTS crevice as shown in Figures 44, 45, and 46.

Further, as corrosion products expand on oxidizing surfaces, they exert lateral forces that break the protective layer or produce stresses that initiate subsurface cracks. This phenomenon is similar to the "breakaway" oxidation of zirconium alloys used for nuclear fuel.

5. Residual stresses

Residual stresses in bulk metals or on surfaces usually result from fabrication practices such as bending, extruding, threading, cold expansion, welding, grinding, machining, straightening, and surface scratching. As the temperatures at which these processes are increased, the magnitude of residual stresses decreases but such diminutions should be evaluated by experiments.

The meaning of "residual stresses" does not need to be explained here. However, the fact that residual stresses are ubiquitous and that they approach or exceed annealed yield stresses does. Virtually all SCC that occurs is related to the presence of residual stresses, and designs generally are out of the range of thresholds for SCC; the presence of residual stresses places the real stresses in the material significantly above the design stresses.

From a practical point of view, the causative stresses in SCC are almost always the residual ones. A particularly good example is the SCC at TSPs where the only calculable stresses are due to pressure and temperature and where these results, by themselves, would not produce SCC. Thus, for the many years of SCC at TSPs, it should be realized that this SCC was primarily related to residual and not applied stresses.

Accounting for the usual stresses from pressure, thermal gradients, flow, bending, tension, and similarly calculable sources is usually the province of mechanical engineers or other engineers who deal with such calculations. However, hardly any engineers who calculate stresses account for residual stresses. Accounting for such residual stresses is important since they add directly to calculated stresses and since they produce such stresses that almost always exceed threshold stresses for SCC.

Figure 9 shows the effect of residual stresses on SCC in a pressurizer instrument tube. Here, welding stresses at this connection produced SCC in the tube adjacent to the weld. Such failures are common for welded joints in nuclear plants and occur frequently. An example of SCC degradation with only nominal applied stresses is shown also in Figure 40 of Section 2.8-1a in the discussion on SCC at line contact crevices at TSPs. Here, again, the stresses that produce SCC are mainly residual.

Residual stresses on surfaces, e.g. from surface grinding or machining, are of particular concern since they can initiate SCC which will then propagate owing to the increasing stress intensity with depth where the need for high stresses is less. A similar effect results from the wedging action after cracks are initiated as discussed in Section 2.9-4.

Residual stresses are important to steam generator tubes, since they are expanded at the TTS and provide stresses to both primary and secondary sides. SG tubes also contain residual surface stresses that result from surface grinding and polishing.

6. Cold work

The presence of cold work, in addition to producing residual stresses, also increases the yield stress and increases the propensity to SCC. These effects are important both for bulk cold work and for relatively thin cold work at surfaces such as from polishing, surface grinding, and surface machining.

Effects of bulk cold work in Alloy 600 are shown in Figure 62 from the work of Speidel and Magdowski.[144]

Cold work on surfaces in the form of scratches has produced significant SCC both in RSGs and OTSGs. Figure 14 shows that SCC nucleated at scratches in the upper bundle of an OTSC. Environmental species associated with these surfaces are also identified. Later studies by Thomas and Bruemmer[146] using the ATEM showed that these SCC contained Pb at the tips, and the significant environmental contribution to these SCCs is generally thought to be Pb. However, as shown in Section 3.13 Figure 102, sulfides were also found to be present and cannot be ignored.

Figure 63 shows the SCC at scratches on the free surface on the cold leg of the secondary side.

Here, tens of SCC sites are observed in the base of the scratch and many of these perforated the tube as shown.

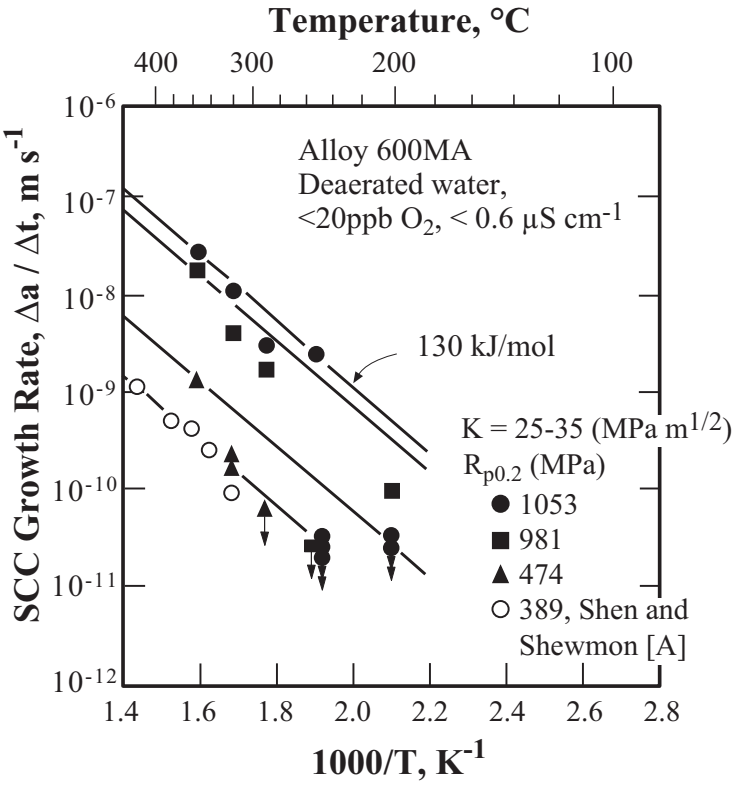

Figure 62 Crack growth rate vs. 1000/T for Alloy 600MA with various yield strengths. From Speidel and Magdowski[144] with data from [A] Shen and Shewmon.[145]

The identity of the critical environmental contribution for the SCC in Figure 63 is not clear. It is possible that the SCC is really LPSCC on the secondary side and is accelerated by the cold work as could be rationalized by well known effects of cold work on LPSCC of Alloy 600. The environment may also be related to the concentration of species on the secondary side beneath a layer of deposits such as those shown in Figure 47. Unfortunately, no ATEM work was ever conducted on these SCCs.

2.10 Distributed Data, Variability, First Failures, Bad Heats

1. Introduction

Degradation in nuclear plants has occurred in different types of materials, different components, different configurations, and different bulk and local environments. Such degradation has occurred in not only several different locations of SGs, but also in piping, pressurizers, pumps, core structurals, instrument nozzles, turbines, generators, and fuels. Many of these data have been analyzed using statistical methods with great success in finding consistent patterns. As a result of 40 years of experience with operating PWR plants, the following general trends, relative to statistical patterns, seem clear:

- Rarely has there been a single failure that was not actually the first of many. However, these first failures are usually labeled as "bad heats" and "poor fabrication," until the inevitable occurrences of continuous failures indicated that the first failure was not a bad heat but rather the first of many.
- The fact that there is often some time between failures simply is an expression of the lower statistical shape factor that is characteristic of a particular mode of degradation.
- Almost none of the early failures and their subsequent statistical set have been surprises when they occurred. Precedents for such failures have always been available but were often ignored or inconsistent with the convenience of designers or operators.

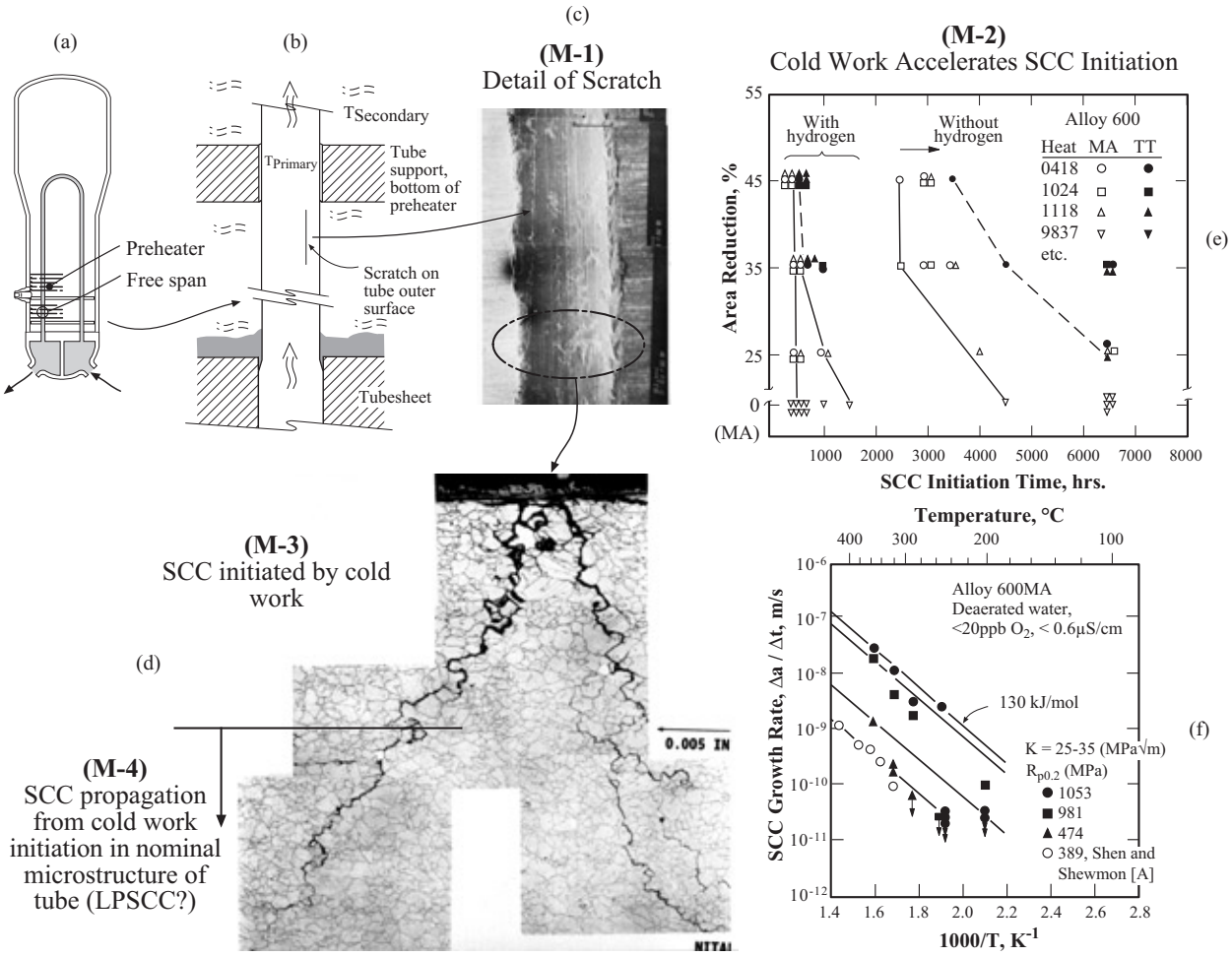

Figure 63 SCC at free-span cold leg at McGuire-2 in an Alloy 600MA tube. (a) General location of scratch and SCC. (b) Schematic view of location of SCC. (c) Detail of scratch with SEM. (d) Cross section of SCC. Courtesy of R. Eaker.[147] (e) Area reduction vs. SCC initiation time for Alloy 600 for several heats in environments with and without hydrogen. From Airey.[148] (f) SCC growth rate vs. 1000/T for Alloy 600MA with various yield strengths achieved by cold work. From Speidel and Magdowski[144] with data from [A] Shen and Shewmon.[145]

- Designers and operators often ignore data from the laboratory. No failures have occurred for which there was not a credible precedent from laboratory testing (from nuclear or non-nuclear industries) or from reasonable expert assessment of precedent engineering or scientific data. Unfortunately, such early signals are not pursued to assess, not whether they will occur—since that would have been established, but rather how rapid and serious could be the degradation.
- Some degradation is much more rapid in material from one vendor than another as with housings for control rod drives as discussed in Section 2.10-4c in connection with Figure 74. Conclusions based on such limited sets is often wrong.
- Engineers allow themselves to be influenced by such terms as "non-sensitized," as with both stainless steels and high nickel alloys. In general, experience has shown that both sensitized and non-sensitized materials may be both prone to SCC, non-prone, or opposite in one environment than another. In using these terms, it is necessary to be more precise as to what metallurgical condition sustains degradation in what environment.
- While the example is from BWR technology, it is instructive to recall the experience in SCC of sensitized stainless steel piping. The first failures, starting in late 1960s, occurred in small diameter, 2-4" piping. It was presumed by the "experts" that this mode of failure would not occur in larger diameters owing to the presumed lack of congruence of high stresses and sensitization. However, over time, this argument was successively applied to larger diameters of pipes when, at last, the largest piping failed by the same mode. The same example can be applied to the early LPSCC in thin walled tubes compared with later, and inevitable, failures of thick walled components. Eventually, the latter also are failing.

With this background, the purpose of this section is to consider elements of probabilistic occurrence of degradation mainly in SGs and ancillary equipment according to the scope of this discussion.

2. Statistical background

In this Section 2.10, it is useful to describe some statistical nomenclature. The Weibull distribution has been widely used to characterize degradation data and is used here for illustrative purposes although there are other statistical distributions that can be used. The main expressions that are used are the following:

$$f(t)=\left[\frac{\beta}{(\theta-t_o)^{\beta}}\right](t-t_o)^{\beta-1}\exp\left[-\left(\frac{t-t_o}{\theta-t_o}\right)^{\beta}\right],\ t>t_o \qquad (1)$$

$$F(t)=P\{t'\le t\}=\int_0^t f(t)dt \qquad (2)$$

$$F(t)=1-\exp\left[-\left(\frac{t-t_o}{\theta-t_o}\right)^{\beta}\right] \qquad (3)$$

$$\ln\left[\ln\left(\frac{1}{1-F(t)}\right)\right]=\beta\left[\ln(t-t_o)-\ln(\theta-t_o)\right] \qquad (4)$$

$$R(t) = P\{t > t\} = \int_t^{\infty} f(t)dt = 1 - F(t) = \exp\left[-\left(\frac{t - t_o}{\theta - t_o}\right)^{\beta}\right] \quad (5)$$

$$h(t) = \frac{f(t)}{1 - F(t)} \quad (6)$$

$$h(t) = \left(\frac{\beta}{\theta - t_o}\right)\left(\frac{t - t_o}{\theta - t_o}\right)^{\beta - 1} = \frac{\beta}{(\theta - t_o)^{\beta}}(t - t_o)^{\beta - 1} \quad (7)$$

$$F_T(t) = 1 - [1 - F_1(t)][1 - F_2(t)] \bullet\bullet\bullet [1 - F_n(t)] \quad (8)$$

where:

- t = Time
- t_o = Location parameter, sometimes called, erroneously, the "initiation time"
- θ = Scale parameter or the Weibull characteristic which is evaluated at $t = \theta$ where the probability is 0.632
- β = Shape parameter or often called the "Weibull slope" as is evident from the linearized version in Eqn. (4). β is also called the "dispersion"
- $f(t)$ = Probability density function, pdf
- $F(t)$ = Cumulative distribution function, cdf, also the probability of failure in time
- $F_T(t)$ = Total probability including the i^{th} element
- $F_i(t)$ = Probability for the i^{th} element
- $R(t)$ = Reliability
- $R_T(t)$ = Total reliability
- $R_i(t)$ = Reliability of i^{th} element
- $h(t)$ = Hazard function

Figure 64 shows the probability density function, the cumulative distribution function and the hazard function in (a), (b), and (c) respectively.

Since the cumulative distribution function, cdf, is so widely used, as for example in Figure 72, Figure 65 shows some important details as they are used in prediction and interpretation. Figure 65 shows the probability vs. time for two values, 1.0 and 4.0, of the shape parameter, β. These two values generally bound values that are typical of ones that are observed in the degradation discussed here. Shape factors up to about 20 and as low as about 0.5 are also observed but are less frequent. These shape factors are shown in Figure 69.

Using Figure 65, the concept of the first failure can be understood. For example, if the shape parameter is 4.0, the time of the first failure is about 0.1 of the mean value. However, if the shape parameter is 1.0, the first failure occurs at 0.0001 of the mean. In the later case, the first failure may seem more like a "bad heat" than a part of a coherent statistical distribution. The Weibull plots for the failure of stainless steel pipes in Figure 72 exhibit shape factors of about 1.0; whereas, for the failures of SG tubing the slope factor is generally in the range of 3.0-4.0 as shown in Figure 69.

(a)

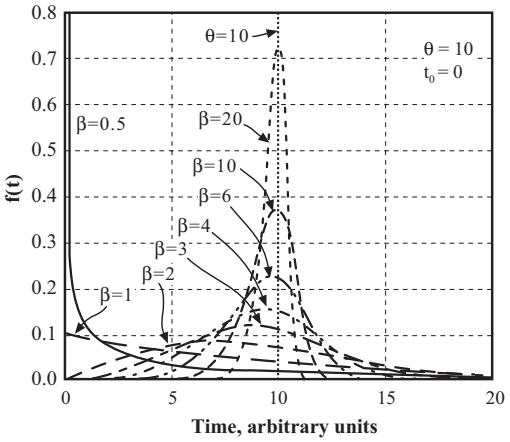

$$f(t)=\left[\frac{\beta}{(\theta-t_o)^{\beta}}\right](t-t_o)^{\beta-1}\exp\left[-\left(\frac{t-t_o}{\theta-t_o}\right)^{\beta}\right],\ t>t_o \quad (1)$$

(b)

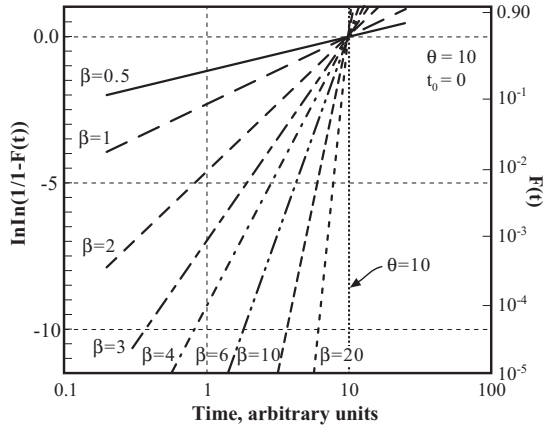

$$F(t)=P\{t\le t\}=\int_0^t f(t)dt \quad (2)$$

$$F(t)=1-\exp\left[-\left(\frac{t-t_o}{\theta-t_o}\right)^{\beta}\right] \quad (3)$$

(c)

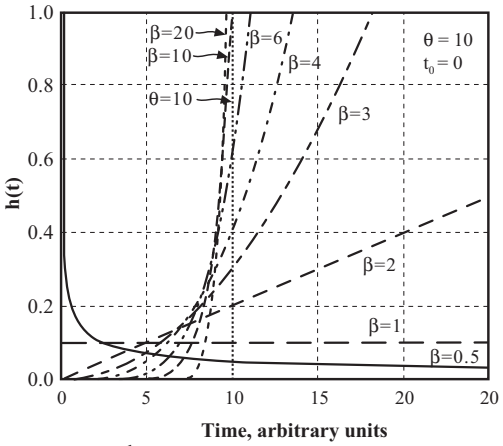

$$h(t)=\frac{f(t)}{1-F(t)} \quad (6)$$

$$h(t)=\left(\frac{\beta}{\theta-t_o}\right)\left(\frac{t-t_o}{\theta-t_o}\right)^{\beta-1}=\frac{\beta}{(\theta-t_o)^{\beta}}(t-t_o)^{\beta-1} \quad (7)$$

where:

t = Time

t_o = Location parameter, sometimes called, erronously, the "initiation time."

θ = Scale parameter or the Weibull characteristic which is evaluated at $t=\theta$ where the probability is 0.632.

β = Shape parameter or often called the "Weibull slope" as evident when the linearized version in Eqn. (4). β is also called the "dispersion."

Figure 64 Weibull based expressions: (a) Probability density function (pdf) vs. time. (b) Cumulative distribution function (cdf) or probability vs. time. (c) Hazard function (hf) vs. time. Equations under each plot apply respectively and are taken from the eight previous expressions. From Staehle.[149]

These shape parameters can be shown to have some physical significance, as in Figure 66, that compares the cumulative distribution function (Figure 66(a)) with the hazard function (Figure 66(b)). The hazard function is understood to be the probability of failure of the as yet non-failed elements, e.g. tubes. With a β of 1.0, the hf is a horizontal line indicating that the probability of failure does not change with time. Such a condition can be understood as a random process over time and space as with pitting or some other IGC process as shown in Figure 66(e). On the other hand, for a β of 4.0, the probability of failure rises slowly with time initially, and then rises more rapidly after the value of θ is reached. This pattern suggests that there is some initial physical resistance such as a diffusion or migration process as illustrated in Figures 66(c,d).

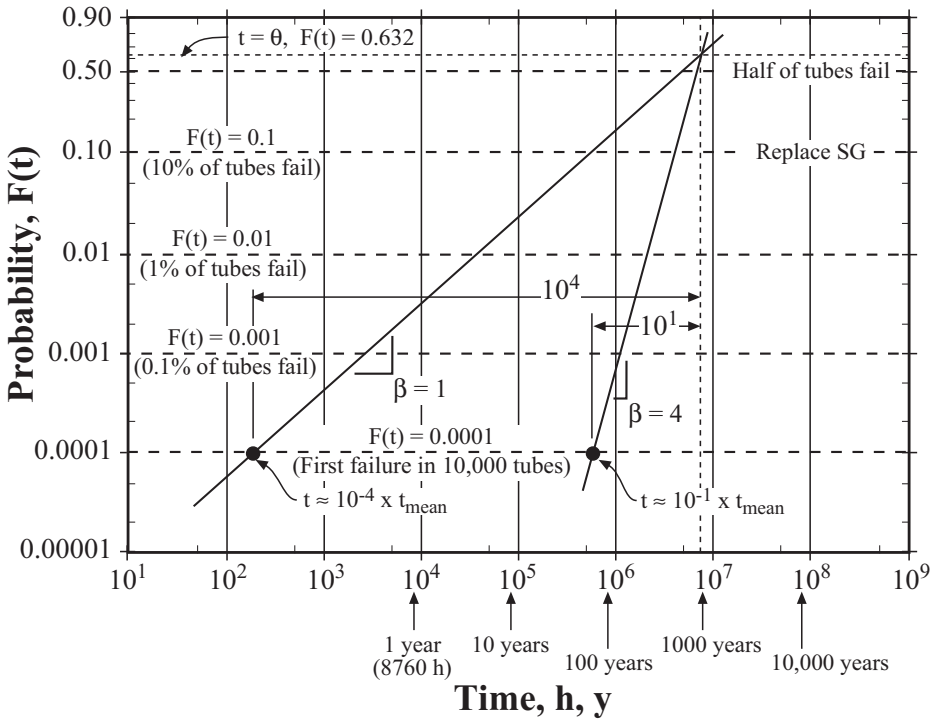

Figure 65 Cumulative distribution function with two values of β shown together with relationship between the failure time at F(t)=0.0001 and the mean failure time. From Staehle.[149]

3. Background from past experience

This section considers mainly the degradation of RSG SGs with Alloy 600MA tubing and drilled hole tube supports. The experience with other SGs using Alloy 800NG tubes with line contact TSPs have performed well with no significant failures. Also the VVWR SGs, which use Type 321SS tubes, have exhibited good performance with few failed tubes.

However, the past experience of failures with RSG-600MA-drilled-supports provides what is an upper limit of failures and should be examined in this perspective, since, in the future, the other SGs may eventually sustain an array of failures that are related to longer times, increased requirements of performance, and less inspection.

In the past, RSG steam generators with Alloy 600MA and drilled hole tube supports sustained 25 different mode-location cases of degradation. These are summarized in Figure 67. The

cumulative failure times for the steam generators in which these different mode-location cases of degradation were occurring are shown in Figure 68. In general, an SG is removed from service after about 10% of the tubes have been plugged.

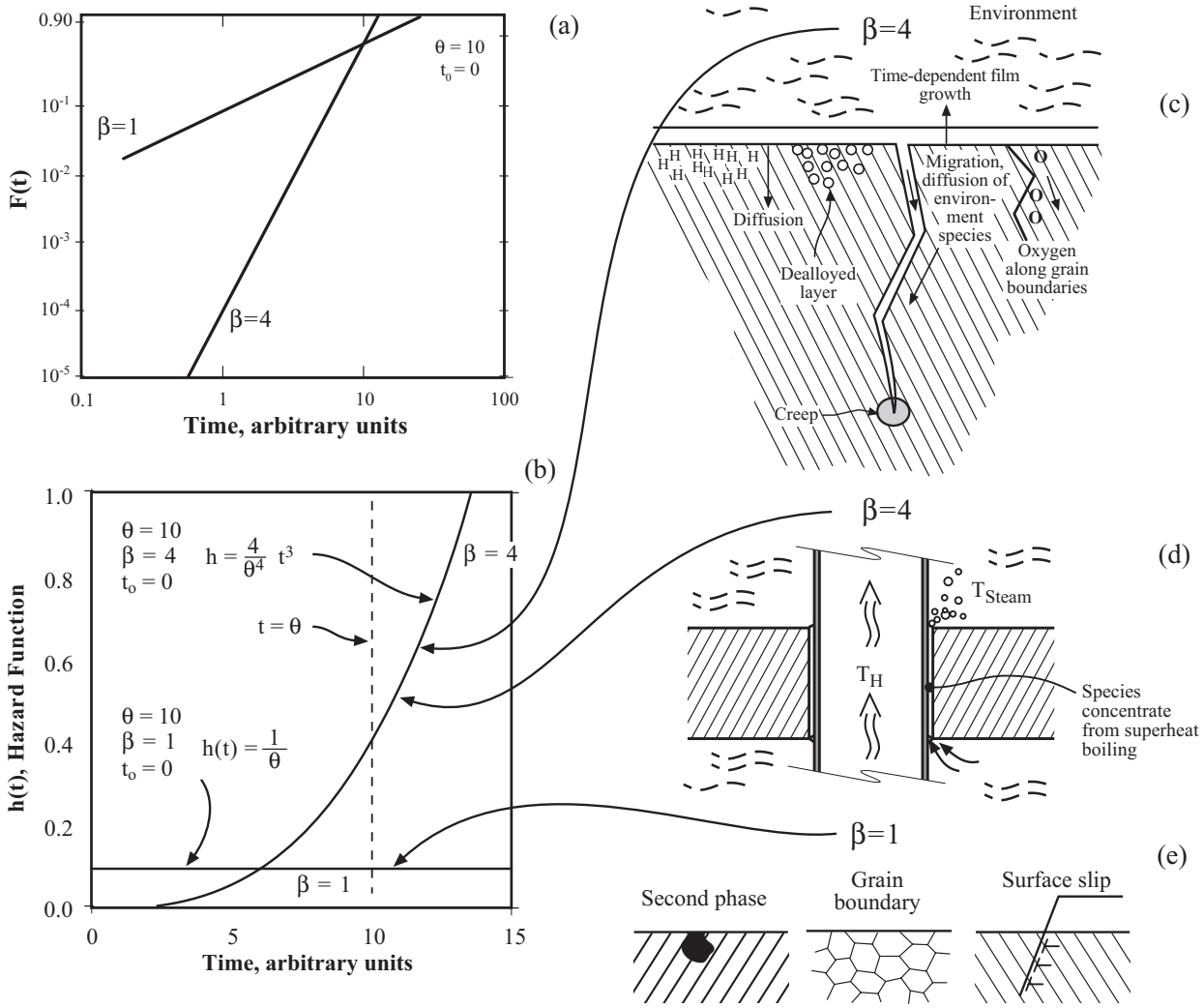

Figure 66 (a) cdf for β=1 and β=4 vs. time. (b) hf vs. time for β=1 and β=4 cases at θ=10 and t_o=0. (c) Possible contributions in the metal substrate, for a growing SCC, to the accumulation case for β=4. (d) Possible contributions to the accumulation case β=4 from a superheated tube support geometry. (e) Possible contributions to the β=1 case from surface processes. From Staehle.[149]

Examples of statistical distributions of failures of the various mode-location cases in the "RSG-600MA-drilled–supports" are shown in Figure 69. Figure 66(a) shows the failures, in terms of cumulative fraction or probability, from various submodes and the aggregate of all mechanisms. The latter is then used to determine when to replace the steam generator—more or less when 10% of the tubes have failed. The plot in Figure 66(a) shows that about 10% of the tubes will have failed after about 20 EFPY while the data show that the SG has operated about 10 years. These data can then be used by the utility to decide on a course of action.

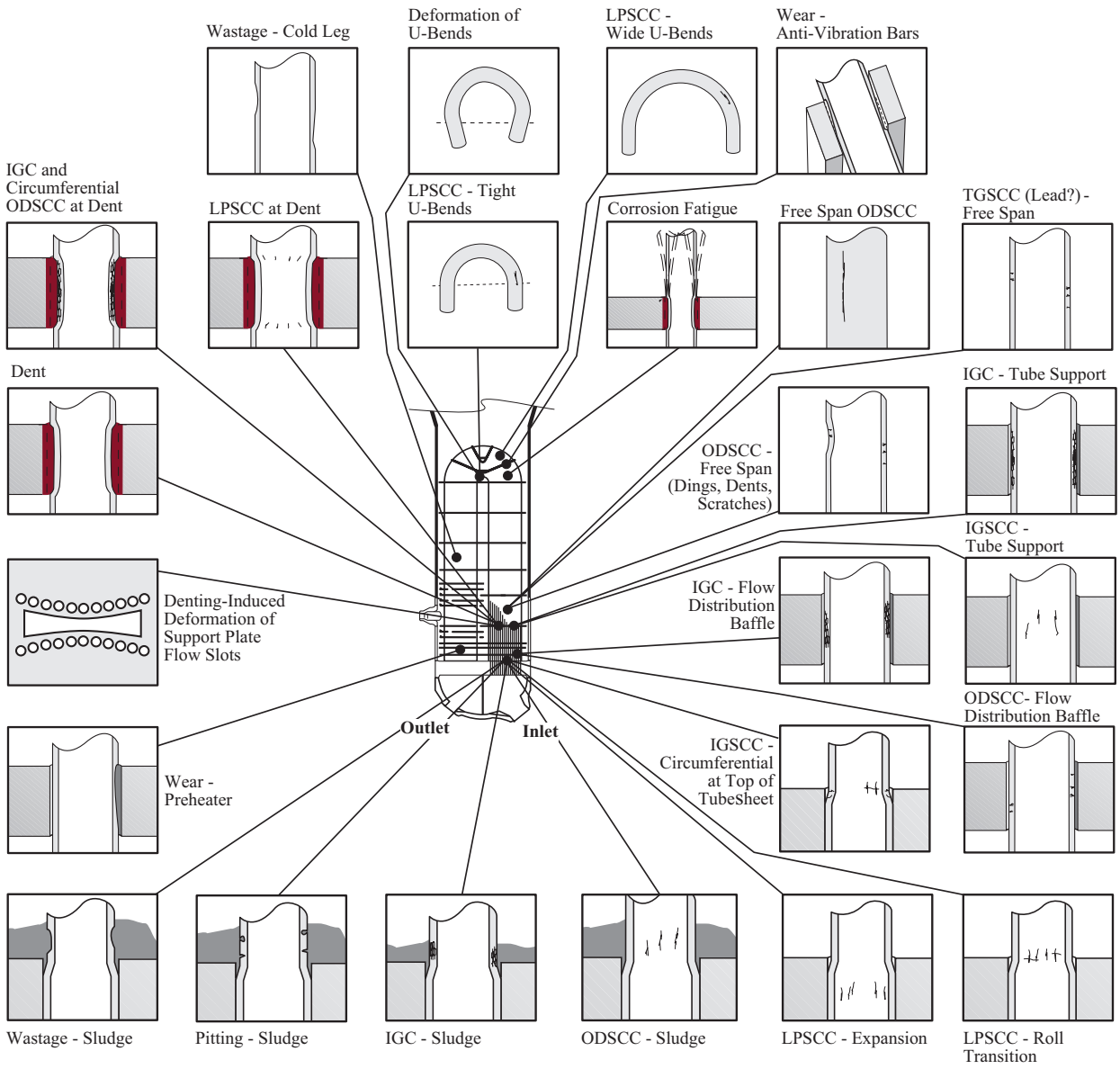

Figure 67 Array of modes of failure at various locations (mode-location cases) that have occurred in recirculating steam generators. From Staehle and Gorman.[5]

A plot similar to Figure 66(a) is shown in Figure 66(b) for data from several different plants. Here, the data for probability vs. service time are consistent with high values of the square of the correlation coefficient, r^2. The statistical parameters (Weibull)[152,153] of θ and β are consistent with other well-known data from SG performance.

Scott[154] analyzed data for "affected tubes" from both primary side and secondary side defects from two different SGs in Figure 70. He selected consecutive heats from one manufacturer where the tubes were then processed by a single tube mill. He compared these heats with the percent of the tubes from that heat that had been "affected." In Figure 70, the number at the top of the bars is the number of tubes in the SG from the heat indicated on the abscissa. The height of the bars is

the percent "affected." What is notable here is the great differences among the heights of the bars as well as the fact that many of the heats including those with many tubes, produced no "affected" designations. The data are all the more important for the long times shown in Figures 67(a, b) with 40,000 and 75,000 EFPY for primary and secondary sides, respectively.

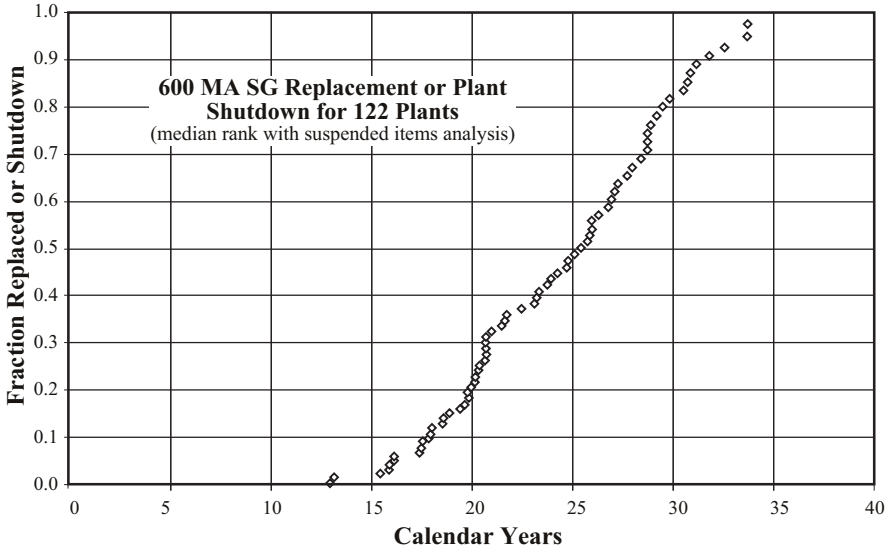

Figure 68 Fraction of replaced or shutdown steam generators vs. calendar years for Alloy 600MA plants in the world. Data from Steam Generator Progress Report.[150]

4. Perspectives on the future

From the point of view of "what is past is prologue," Section 2.0 is the past and the prologue to the future of modern SGs that are supposed to last longer than any preceding units with many new features and challenged by more intense stressors and less inspection. Further, there are already laboratory data, which suggest that failures in the future are inevitable, and these are discussed in detail in Sections 3.0 and 4.0.

Before addressing the future problems in Sections 3.0 and 4.0 certain additional patterns are discussed:

a. Variability

Aside from the variability discussed in Figures 69 and 70, another perspective on variability is shown in Figure 71 from Jiang and Staehle.[155,156] Here, they studied the SCC behavior of stainless steels in boiling $MgCl_2$, as was also used by Copson in Figure 17(a) where extensive work has been conducted by many investigators. Figure 71(a) shows data from 23 separate studies of effects of temperature and Figure 71(b) shows data from 40 separate studies of effects of stress. From each of these studies activation energies and stress exponents were determined in Figures 71(c,d) and Figures 71(e,f), respectively. It is apparent that the variabilities in the activation energies and stress exponents are large.

The experimenters associated with the work in Figures 71(a,b) were all known to us. These experiments were conducted using a narrow range of stainless steel alloys (essentially the 18-8

type), temperatures, and environments. However, it is clear that the variability is large. These data should be taken as examples of responses that would come from using many nominally similar heats for a single application. The data in Figures 71(a,b) suggest a range of data of about four orders of magnitude. This is not unlike the pattern of data that were analyzed by Scott[154] as shown in Figure 70, and the effects of different manufacturers shown in Figure 74.

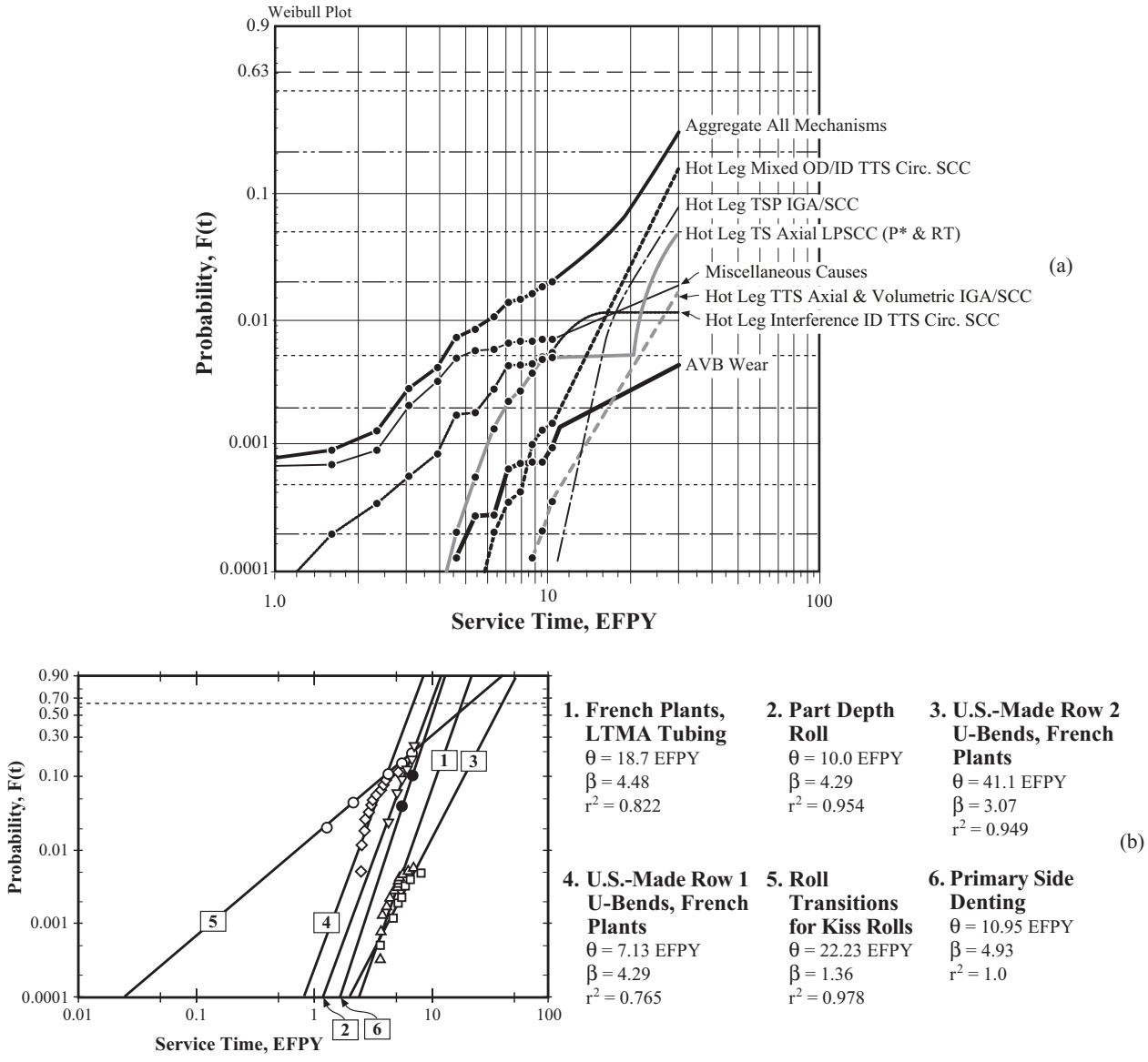

Figure 69 (a) Probability of failure vs. EFPY for Ringhals-4 PWR for various mode-location cases and the aggregate probability. Alloy 600MA tubing. From L. Björnkvist and J. Gorman.[151] (b) Probability vs. service time (EFPY) for the LPSCC occurring on the primary side of tubes from operating SGs in PWRs. Temperatures in the range of 315°C to 320º C. From Staehle, et al.[7]

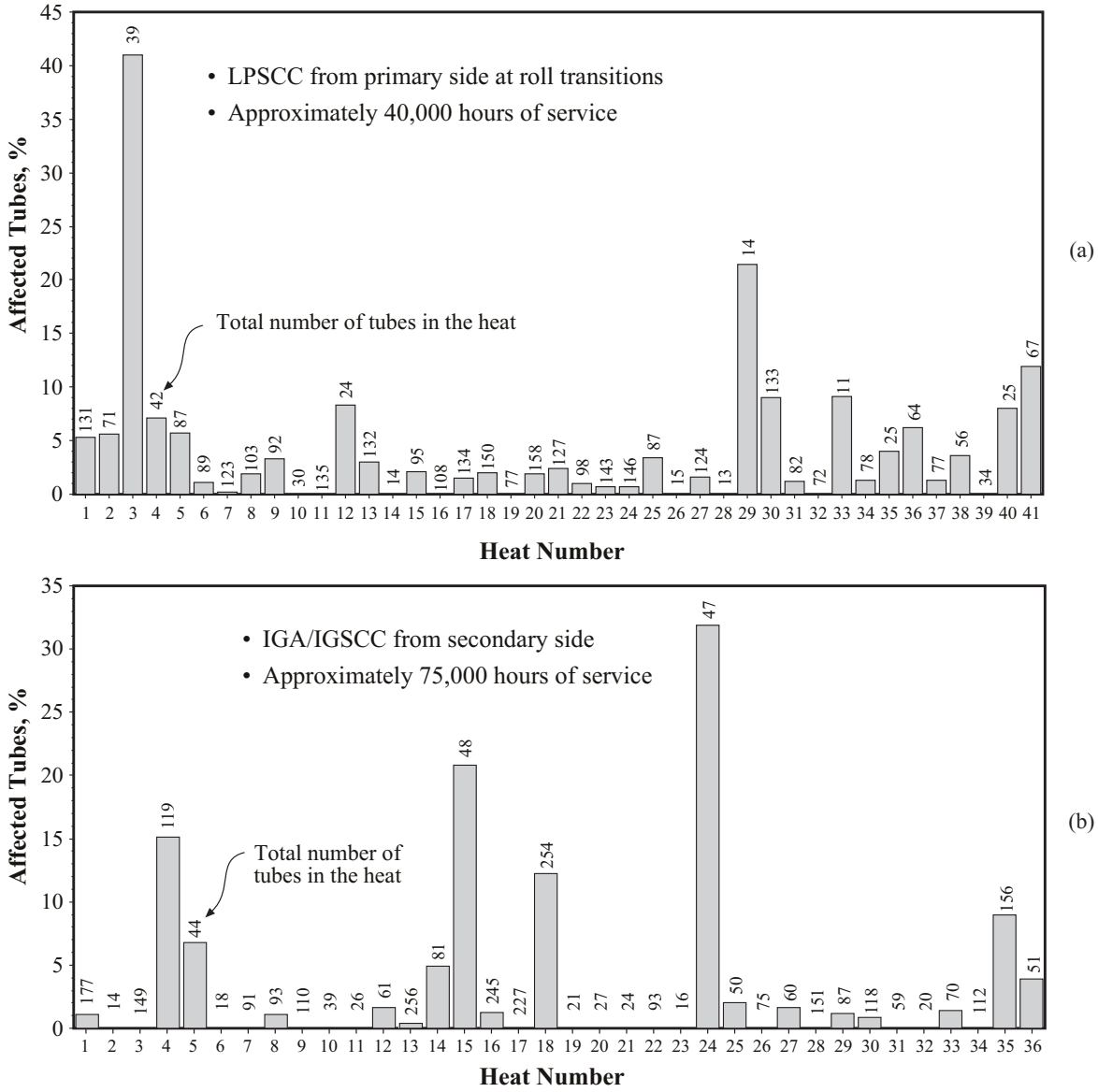

Figure 70 Percent of Alloy 600MA tubes affected by LPSCC from the primary side of a PWR steam generator vs. heat number determined at roll transitions after approximately 40,000 hours of service. Primary surface temperature at this location about 310°C. All heats from the same manufacturer and produced in sequence shown. Environment primary water. (b) Percent of tubes affected by IGA and IGSCC vs. heat number from secondary side of a PWR steam generator in heat-transfer crevices after approximately 75,000 hours of service. From Scott.[154]

Together, Figures 70 and 71 show that single heats used for testing will not produce a balanced view of the trends. In fact, they could produce quite the wrong answers. Such a lesson should be applied to future testing as well as to assessing the meaning of data from the field.

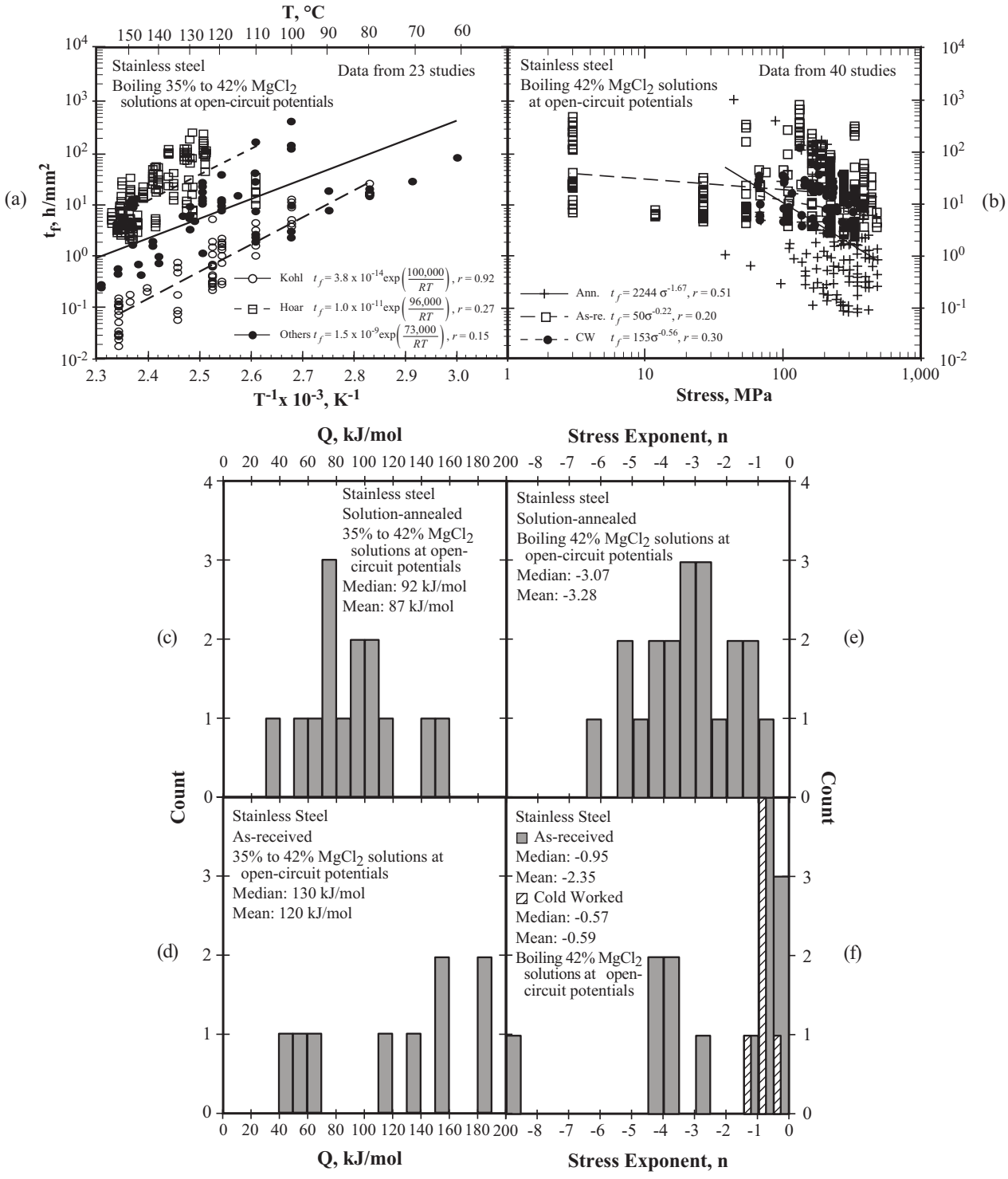

Figure 71 Time-to-failure vs. temperature (a) and vs. stress (b) for stainless steel in concentrated $MgCl_2$ solutions. The units of time-to-failure have been normalized by a cross-sectional area of specimens used by different investigators. (c), (d), (e), and (f) show the array of activation energies and stress exponents from the various studies which were analyzed. Adapted from Jiang and Staehle.[155,156]

While the data from Figure 69 have been correlated using a Weibull distribution (cdf) for the failures of thin walled SG tubes, the same Weibull distribution (cdf) has been applied to stainless steel piping of 2 and 4 inch diameter as shown in Figure 72. This piping was used in BWR plants. Here, the data follow the Weibull distribution well, as can be seen from the coefficients of correlation; and the shape parameters, β, are approximately the same. Only the space parameter, θ, differs. This shape parameter is about unity and is consistent with the data coming from many different sources as well its corrosion depending on surface processes as rationalized by Staehle[152] as shown in Figure 66.

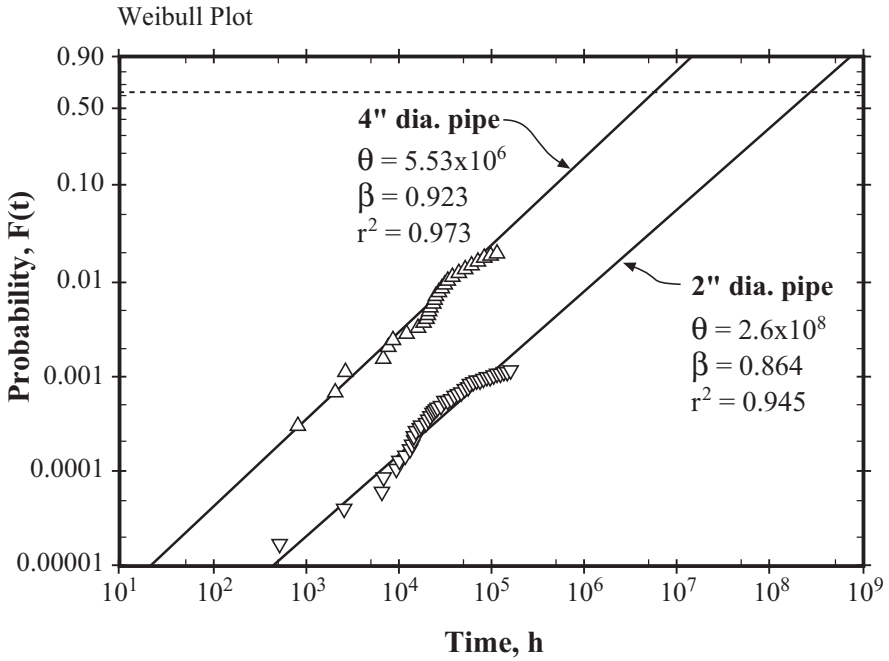

Figure 72 Probability vs. time since startup for SCC failure of welded stainless steel pipes from piping used in boiling water nuclear reactors (BWR). "Large pipe" refers to 4-inch diameter. "Small pipe" refers to 2-inch diameter. Adapted from Eason and Shusto.[157]

The comparison of Figures 69 and 72 suggests that it is legitimate to compare patterns of SCC damage of thin wall tubing and piping. A similar comparison is suggested in Figure 73. Here, the locations where Alloy 600 or 182/82 are used are identified. In general, the tubes have the thinnest cross sections. However, over time, many of the thick sections of Alloy 600 are failing or have failed. The point here is that the thicker sections of SCC-prone materials just take longer—like the comparison of SCC in small diameter and progressively thicker diameters of sensitized stainless steel pipes in BWRs, as discussed in Section 2.10-1.

From Figure 73 and its implications, whatever is observed in the thin wall tubes will inevitably occur in thicker wall components of the same materials after longer times.

b. Manufacturers

It is often the case that degradation is more intense for the same piece of equipment made to the same drawings and manufacturing specifications, but which has been fabricated by different

manufacturers. Such differences are produced by different methods of machining, grinding, deformation schedules, and heat treatments. Figure 74 is an excerpt from a presentation by Bamford and Hall[158] showing effects of different manufacturers on the degradation of control rod drive housings. Here, the differences among manufacturers are substantial. The pattern shown in Figure 74 is similar to the patterns in Figures 70 and 71 as shown by Scott[154] and Jiang and Staehle.[155,156]

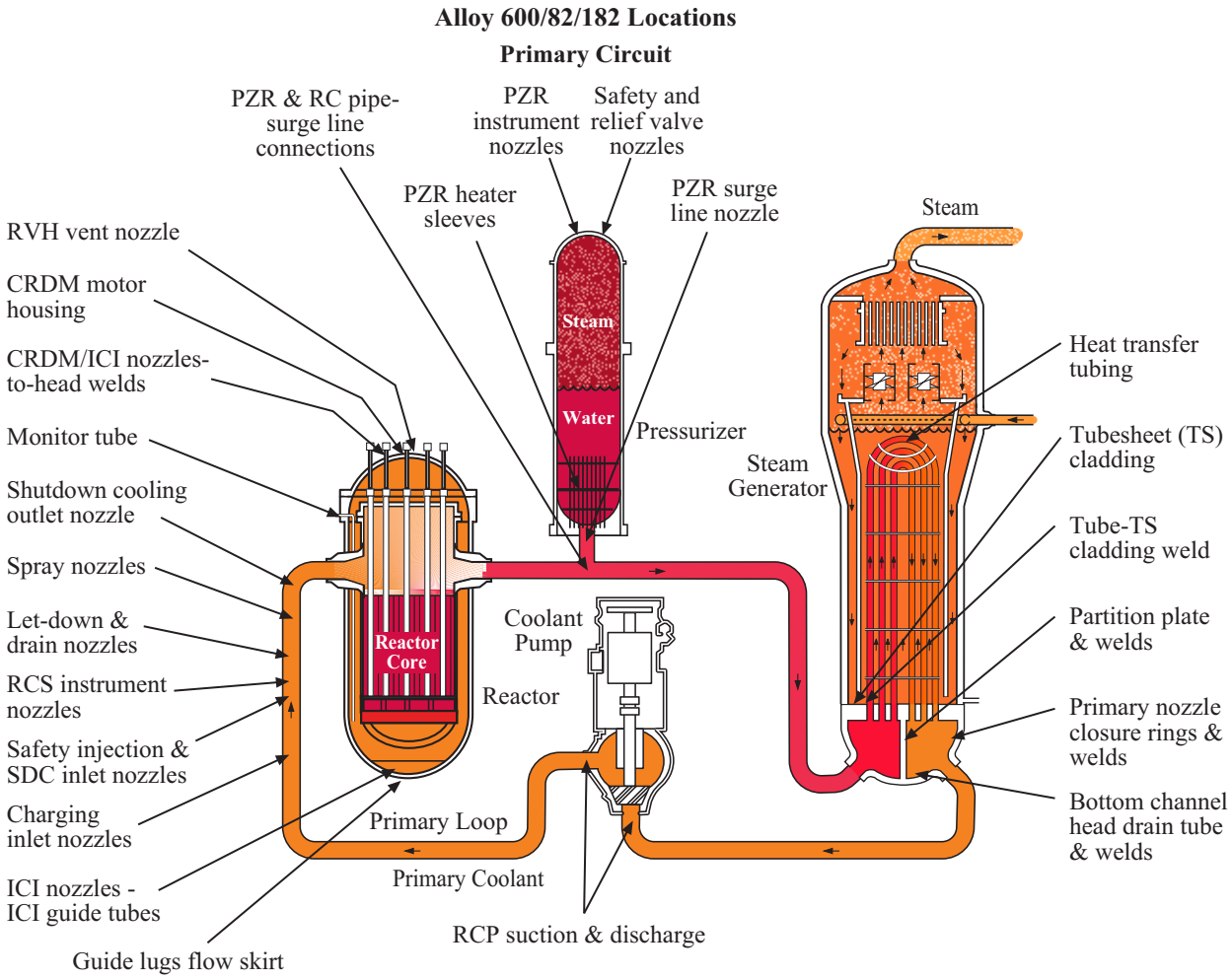

Figure 73 Locations of Alloy 600 and 182/82 in primary PWR system including the steam generator. Courtesy of EPRI.

Thus, in addition to what is nominally an intrinsic statistical distribution as in Figure 64, there are strong biases from individual manufacturers that need to be accounted for. For such reasons, the trend toward fewer inspections as the stressors and life are increased, should be reconsidered. Further, while Alloy 690TT appears to be an improved material, it should be noted that it is also a reactive material especially above about pH 7 according to the trends in solubility shown in Figures 21 and 22.

c. Comments on data

To some extent, predicting the future depends on how data are taken aside from the conceptual

framework of precursors. In general, testing should be responsive to the needs for prediction. It is not usually the mean value of data that is needed but rather the time of the earliest failures. When such an objective is examined in the framework of Figures 69 and 72, the accelerated or predictive testing that is needed is that which gives an indication of these earliest failures. Using Figure 75, an assumed distribution of many failures over time is shown as line N-1 with a β=1. The unity value of β is common for larger numbers of failures of materials fabricated by different sources such as the welds in Figure 72. The bases for such a trend is discussed by Staehle.[152]

Head Penetration J-Groove Attachment Welds

- In 1992, Ringhals 2 found extensive lack of fusion in their J-groove weld regions - repairs implemented
- To date (spring 2003), inspections are complete on about 350 J-groove welds, with the following result:
  - Rotterdam dockyard: ~85% cracked (70 inspected)
  - Combustion Engineering: 0% cracked (242 inspected)
  - Chicago Bridge and Iron: 0% cracked (10 inspected)
  - Babcock and Wilcox: ~70% cracked (31 inspected)
- EdF reported that 11 reactor-vessel heads were inspected after replacement, about 754 welds, with no cracking found

Figure 74 Summary of inspections of J-groove attachment welds for control rod drive penetrations according to manufacturer, utility, or site. From Bamford and Hall.[158]

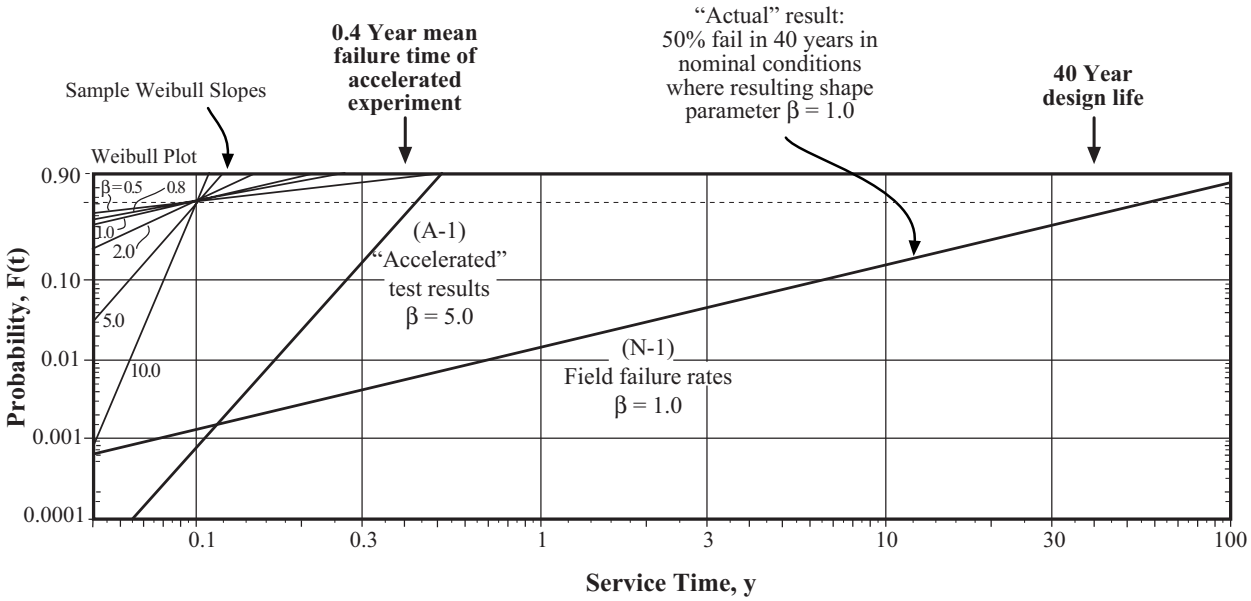

Figure 75 Schematic plot of probability of failure vs. time for field data and accelerated tests based on Weibull coordinates. N-1 corresponds to assumed field results as from Figure 72; A-1 corresponds to assumed accelerated testing. From Staehle. [149]

Nominally, in Figure 75 the target for accelerated testing is the mean value that might be around 40 years. Thus, under normal approaches to accelerated testing, the acceleration should be in the range of 10-100 times, and here it is shown as about 100 based on mean times. Thus, if the accelerated testing produces data with such a factor of acceleration as 100, the test is viewed as a good test. However, such a result gives the wrong answer if the objective is to predict the earliest failures. Usually, an accelerated test exhibits a much higher value of β than the field data. The reasons for this higher value of β are related to the effect of stressors on β as explained by Staehle.[152] The value of β tends to be somewhat proportional to the magnitude of stressors.

If the value of β is 5.0, which would be a good assumed value, for the accelerated testing, then the acceleration of the mean might be a factor of 100; but at a probability of 0.001, there is no acceleration. A probability of 0.001 would be 10 tubes failed out of 10,000.

Aside from the methods of testing, the issue of manufacturer and testing site, as discussed in connection with Figure 74, needs to be considered. Of the methods of manufacture, which of the manufacturers is "typical?" The answer is that they are all typical, just as each of the heats from Scott's analysis in Figure 70 is typical, as are each of the tests in the Jiang and Staehle[155,156] data in Figure 71. Consequently, for serious engineering data to be obtained, it is necessary to obtain test materials from a variety of sources, or at least from the sources to be used in the particular application.

From a practical point of view, there are two kinds of variability:

- Inherent variability can be viewed as the data of Scott[154] in Figure 70. Here, all the conditions are as similar as they can possibly be—same melter, same fabricator, same exposure, and same specification. Such data can be analyzed to determine some space parameter, shape parameter, and location parameter. Intrinsic variability tends to have higher values of β, although lower values may be also found since it is the nature of the physical process. These values of 4 may be in the range around 4 but might be as high as 20 and as low as 1.
- Extrinsic variability can be viewed as the data in Figures 71 and 72 for many elements, each prepared by a different welder or different laboratory for a different location, and for many different runs of piping in different reactors. Data, which are aggregated from extrinsic sources, tend to have low values of β in the range of 1.0.

For some years, there has also been an interest in "deterministic" data, which is understood as not stochastic. Without engaging in a debate here, there is no deterministic aspect of degradation data. Degradation can only be treated on a statistical basis.

3.0 Possible Modes of Degradation-Precursors and Actions

3.1 Introduction

The purpose of this section is to identify possible future degradations, which could be expected after long times, in the framework of the precursor concept, which is described in Section 2.3, particularly for modern steam generators.

The topics in this section are organized essentially as important issues rather than as specific scenarios of precursors and subsequent degradations, because synthesizing scenarios depends upon understanding first, as is emphasized here, the detailed sequence of the degradations and precursors.

The approach to developing practical scenarios would initially be simple and practical. However, developing the detailed scenarios themselves, according to the approach developed by Staehle[45,46] would involve specific analyses. The issues in this section and Section 4.0 would become parts of such "scenario analyses."

In this Section 3.0, SG tubes are considered and in Section 4.0, non-tubing aspects of SGs are considered. Degradation of tubing mostly involves initiation processes; whereas, degradation of non-tubing subjects mostly involves propagation, following the pattern of Figure 3.

Section 3.2 on effects of Pb and PbSCC is extensive owing to its potential seriousness.

In Section 5.0, approaches to investigating the validity of the issues in this Section 3.0 as well as Section 4.0 are recommended as specific tasks.

3.2 Lead: PbSCC

1. Introduction

PbSCC is of great concern because Pb seems irrepressibly present in the feedwater and has the capacity to be concentrated on heat transfer surfaces to the extent that it can produce SCC. It can be concentrated in TSPs (including line contact), TTS, OTSG surfaces, and on fouled surfaces.

PbSCC is a concern to the long term satisfactory performance of modern steam generators since it has already been shown to be inimical to Alloys 690TT and 800NG as well as Alloy 600 in laboratory testing. Few data are available for Type 321 stainless steel with respect to PbSCC. While laboratory testing has shown that PbSCC is aggressive to these alloys, such degradation has not occurred in operating plants in either Alloy 690TT or 800NG to the present, although it has occurred in Alloy 600TT in a line contact geometry at the Seabrook plant (with a possible defective heat treatment) as described in Section 2.8-1a. The questions that have to be considered are the following:

1. Why has PbSCC not occurred in the field for either Alloy 690TT or 800NG?
2. Is it feasible that PbSCC will occur in the future and under what conditions?
3. What are the critical conditions for placing Pb in a condition that will produce PbSCC in modern plants?
4. How can possible PbSCC be mitigated?

Three reviews of PbSCC have been prepared by Staehle and provide most of the important data for the background of this section.[16,17,159]

The first mention of PbSCC was published in the Copson and Dean paper in 1965[160] where they demonstrated that PbSCC could occur in pure high temperature water to which Pb had been added in various forms such as PbO, Pb, and Pb in grease. While the paper was useful in identifying this submode in conditions of secondary environments, it was misleading in suggesting that the SCC was transgranular. The correct morphology for Alloy 600MA is intergranular as shown in Section 3.2-5d and are shown in Figure 83.

A more comprehensive study, as shown in Figure 76, of a wide range of alloys was published by Sarver,[161] Copson et al.,[65] and Flint and Weldon[162] and is shown as a function of Fe, Cr, Ni composition for testing in pure water at 316°C. The original plots have been expanded by Staehle[17] to include compositions of SG alloys. This figure shows both SCC and a scaling reaction as discussed in Section 3.3. These data are important to modern interests since the experiments were carried out in approximately secondary conditions.

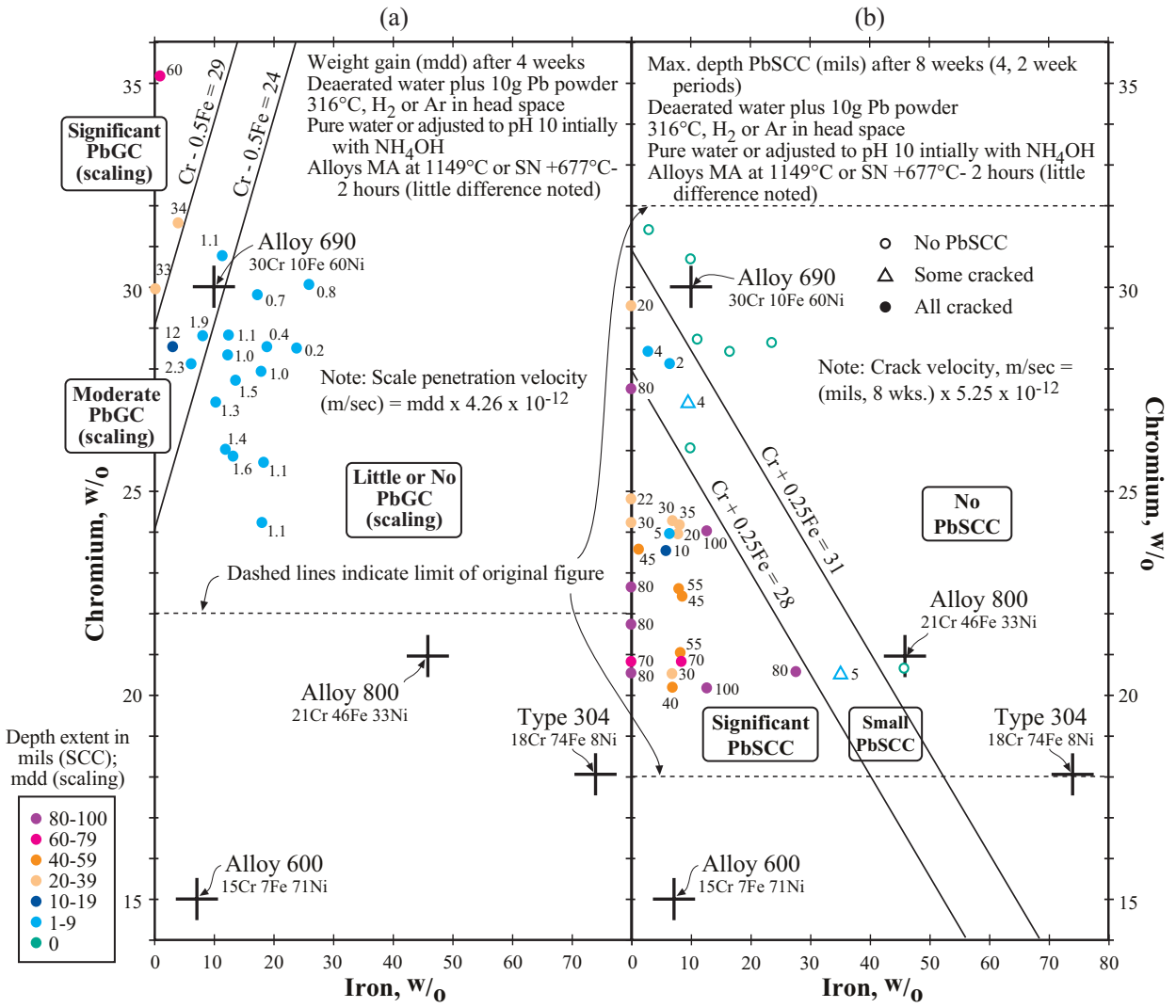

Figure 76 Cr vs. Fe for Ni-Cr-Fe alloys with locations of alloys tested in pure water at 316°C with either argon or H_2 added to headspace and with 10g of Pb powder added to the autoclaves. Numbers in parentheses show weight gain rate in mdd or mils penetration of SCC in test time. (a) Scaling, PbGC, after four weeks. (b) PbSCC with specimens stressed as single U-bends and tested for eight weeks. Original boundaries of figures are noted with dotted lines. Figures expanded to include other important alloys. Note in the figure that increasing aggressiveness is indicated by a transition from blue to orange to red. Reported by Sarver[161] based on work of Copson et al.[65] and Flint and Weldon.[162] Extent of original figures noted and compositions of commercial SG alloys have been added by Staehle.[17]

2. Availability of Pb

The first observations of the very low concentrations of Pb in secondary water was published by Takamatsu[104] and shown in Figure 48. Similar results were published in the PbS workshop by

U.S. utilities.[105] While it was initially common to consider the sources of Pb, as from accidents such as leaving lead blankets or lead hammers in the secondary system, it is now realized that even the 1-100 ppt of Pb in the feedwater can concentrate sufficiently in heat transfer crevices to produce PbSCC.

The overall cycle of Pb in the secondary system from feedwater to TSPs is shown in Figure 77 from work by Millett and Fruzzetti.[163] Assuming a low value for the concentration of Pb in the feedwater of 10 ppt, a significant amount of Pb can accumulate in the TSP crevices as noted by the calculation of number of monolayers (taken as the full peripheral area of a typical drilled hole) accumulated per year.

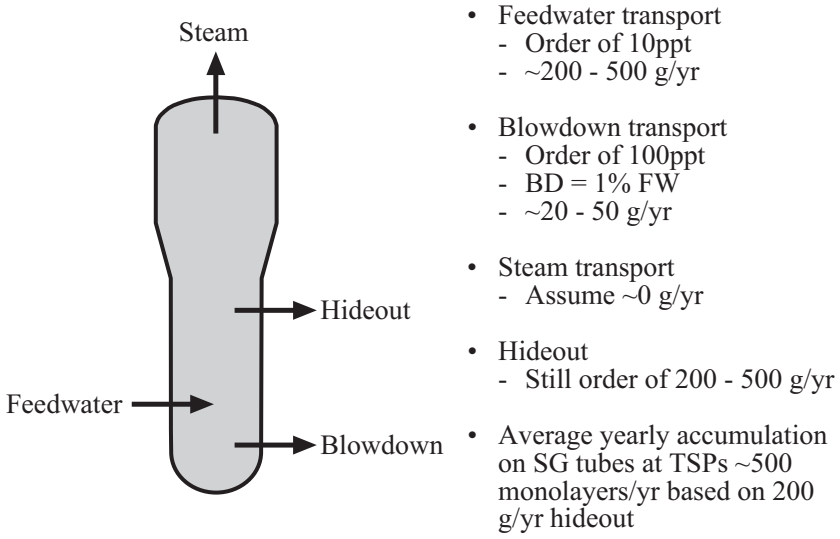

Figure 77 Schematic overview of accumulation of Pb including sources and sinks. Average growth rate of Pb layers shown for 0.75 inch OD of tubes with 1.0 inch thickness of tube supports. Schematic view from Millett and Fruzzetti.[163]

3. ODSCC in the past most probably PbSCC

Historically, it is now clear that most of the ODSCC (secondary side) that has occurred in the past, as shown in Figures 67 and 68, (except where the failures are due to LPSCC on the primary side) is due to Pb for the following reasons:

a. Water chemistry from blowdown and shutdown analyses shows that heat transfer crevices are generally neutral.

b. No other submodes except LPSCC produce SCC in the neutral range. LPSCC tends to require higher temperatures.

c. Laboratory studies show that PbSCC occurs at ppm concentrations in AVT chemistry.

d. ATEM examination of secondary side tube pulls by Thomas et al.[164] show 14 of 17 SCC sites examined exhibited Pb at the crack tip at concentrations of 1-10%. The remainder of the tips contained S (although the valence was not determined) as discussed in Section 3.4.

e. These cracks in 3.1-3d in general, exhibited no Na^{+}, Ca^{++}, Mg^{++} nor any Cl^{-}, regardless of the large concentration of Pb.

f. PbSCC of Alloy 600MA is intergranular and not transgranular as originally suggested erroneously by Copson and Dean in 1965.[160] PbSCC of Alloy 600 was shown in Copson's own lab to be IGSCC.[161]

g. PbSCC has now been shown by Thomas and Bruemmer[99] to occur in line contact crevices at the Seabrook plant as described in Section 2.8-1a and Figure 40.

h. The data of Stevens et al.,[165] as analyzed by Staehle,[17] confirms that very dilute Pb from the feedwater accumulates on the TTS OD and that this Pb enters the SCC as well as most likely producing the PbSCC.

In view of the ubiquity and aggressiveness of Pb and the reasons a-h, the fact that Pb produces PbSCC in Alloys 690TT and 800NG, and the fact that Pb has been observed in line contact crevices as shown in Figures 40, it must be assumed that PbSCC will be the most likely cause of SCC in modern plants. Further, there is not support for any other submode that could characterize past SCC data, e.g. AcSCC or AkSCC.

4. Steps in lead arriving at the tip of PbSCC

Staehle has demonstrated[16,17,159] that the steps toward PbSCC from such low input of Pb are essentially the following:

a. Pb arrives in the SG through the feedwater in the range of 1-100 ppt as shown in Figure 77. This low initial concentration in the feedwater has now been measured by four investigators.[105,163] Note that, while there have been "lead accidents," these have not been the dominant source of Pb.[5]

b. Pb concentrates on the superheated surfaces as do many other species.

c. Pb migrates preferentially to the metal-deposit surface and concentrates in the range of 1-5% at the surface, based on the work of Bickel et al.[166]

d. Pb, to some extent, combines as a phase compound and/or an adsorbed species so the activity of the Pb is reduced.

e. Some Pb is available to migrate or diffuse along the SCC.

f. Pb at the tip of advancing SCC is in the range of 1-10%.

A view of important steps from feedwater to PbSCC is shown schematically in Figure 78.

Stevens[165,167] has followed the path of Pb from feedwater to the inside of PbSCC as shown in Figure 79. He shows the presence of Pb on the TTS surfaces as shown in Figures 79(a,b). In Figure 79(c), he shows the presence of Pb on the three important locations: free span OD, OD in TTS crevice, and TTS crack face. Figure 79(d) from his work shows the correlation between Pb on the outside surface and on corresponding SCC faces.

The Stevens work corresponds with that of Laire et al.[168] in Figure 80, which shows results from the chemical examination of both the TSP crevice in a drilled hole configuration and the freespan.

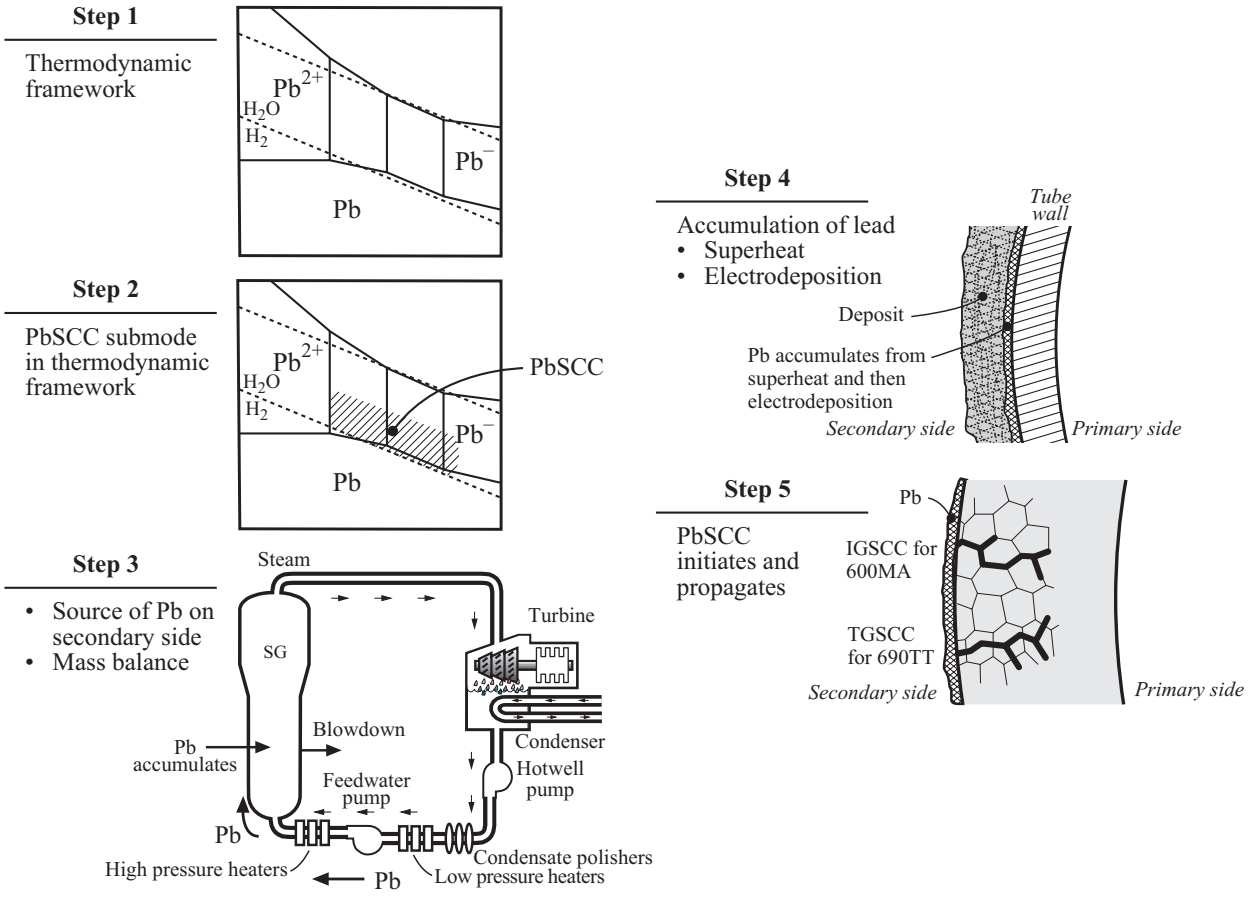

Figure 78 Important steps toward PbSCC in SGs: Step 1—Pb is soluble in the same range as Ni in high temperature water. Step 2—PbSCC occurs over the same range of potentials and pH as occurs in SGs. Step 3—Pb enters the SG through the feedwater. Step 4—Pb accumulates on superheated surfaces and migrates to the metal surface. Step 5—PbSCC commences and propagates.

5. Important dependencies

Important patterns and dependencies in PbSCC are the following:

a. PbSCC occurs over the range of pH of interest to the secondary side as shown schematically in Figure 81 as well as in the mode diagram of Figure 26(b). The most rapid PbSCC occurs in the alkaline range with Alloy 690TT being the most prone to PbSCC. The rate of PbSCC in the neutral region, i.e. AVT region, is generally the lowest and is moderate in the acidic region. However, there is a tendency in acidic environments for the Pb to produce little effect in sulfate environments relative to finite effects in chloride environments.[16,17] In the neutral region the rate of PbSCC in Alloy 690TT is low relative to the other alloys. However, there is non-published evidence for the PbSCC occurring in neutral solutions.

b. PbSCC occurs over a broad range of electrochemical potential as shown in Figure 82. Figure 82 shows that the range of PbSCC includes about 500mV starting with the deaerated open circuit potential. Such data have been obtained at three values of pH that include nominal

operating conditions. This is a broad range of occurrence and broader than AkSCC and AcSCC. Figure 82 also shows that PbSCC occurs in both Alloy 800 and 600MA although at different values of pH. The range of PbSCC for the Alloy 800 in concentrated alkaline solutions is about the same as for Alloy 600 in lower pHs.

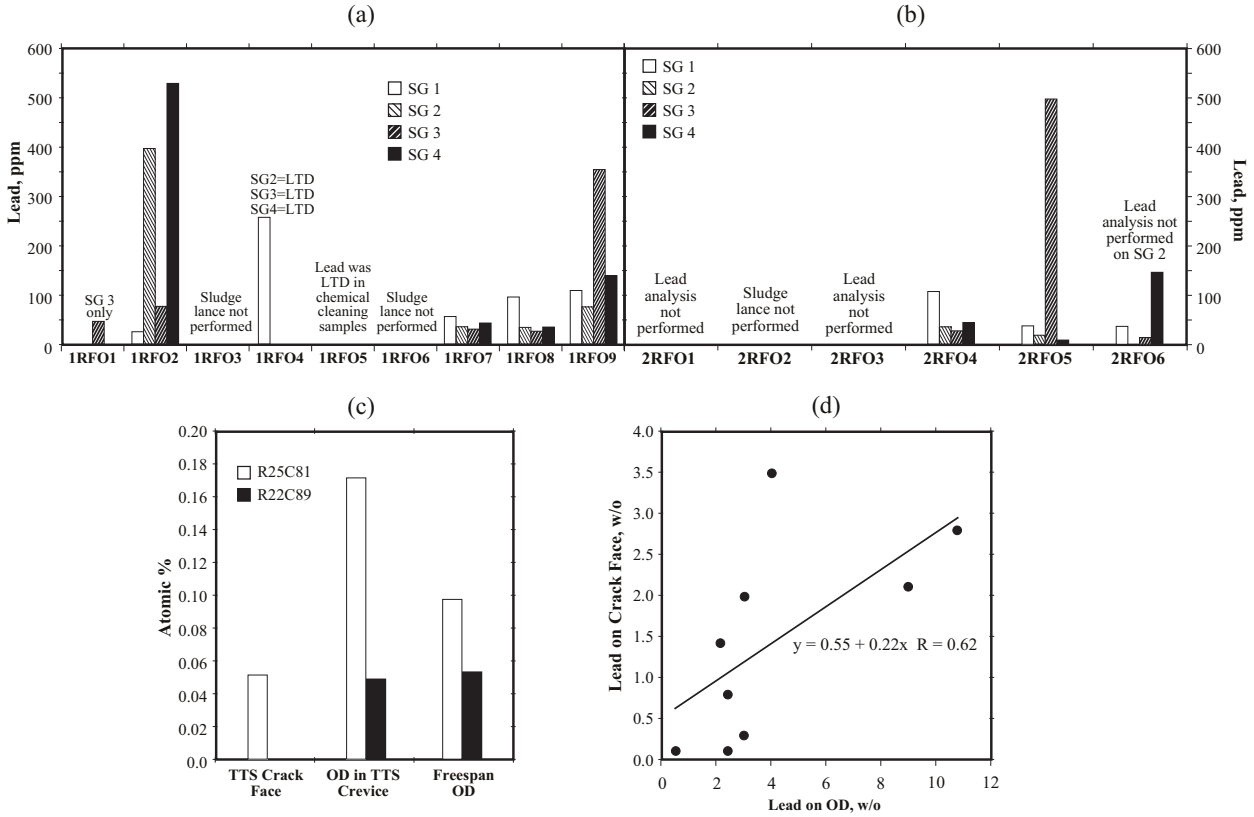

Figure 79 (a) (b) Concentrations of Pb in sludge measured at successive refueling outages for two units and for up to four SGs. (c) Atomic concentration of Pb from SCC in tube at TTS, OD adjacent to SCC, and free span for two tubes. (d) Concentration of Pb on face of SCC taken by XPS vs. Pb on OD for several plants. From Stevens et al.[165,167]

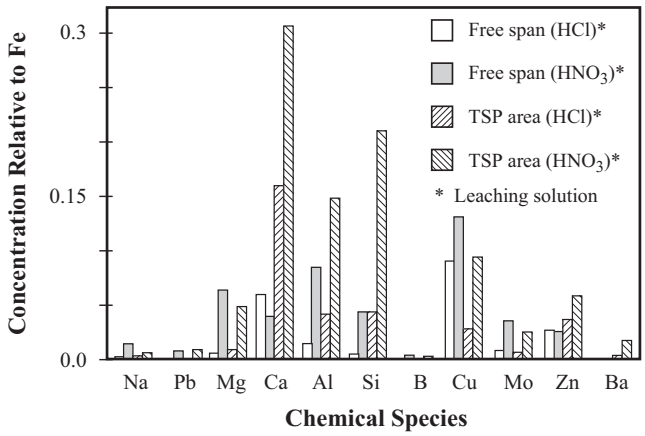

Figure 80 Concentration of species relative to Fe vs. species for measurements from free-span and occluded region of heated crevice. Two different acidic extraction environments used. From Laire et al.[168]

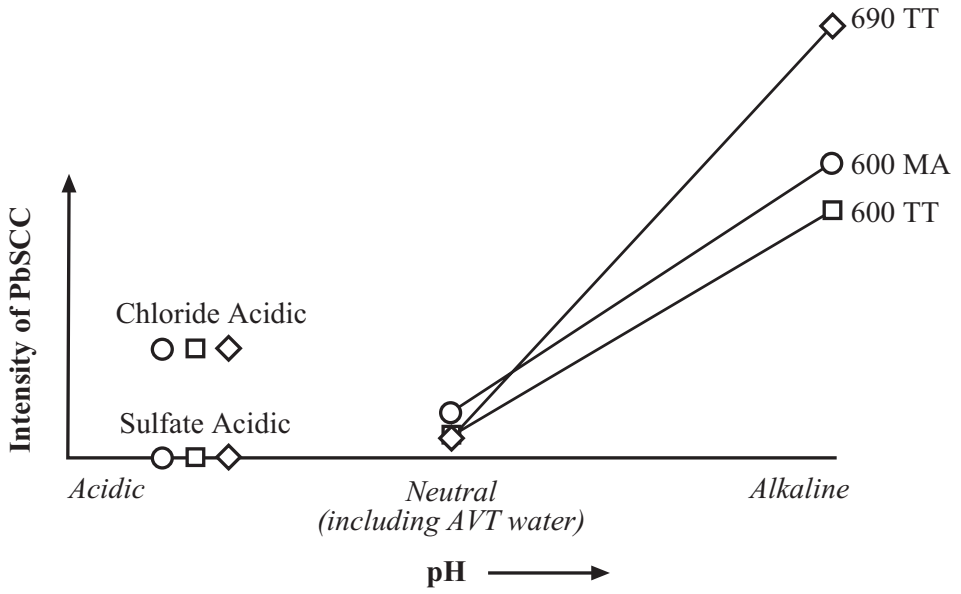

Figure 81 Schematic illustration of dependence of SCC intensity on pH for Alloys 600MA, 600TT and 690TT in the range of 300˚C.

c. Thomas et al.[164] have shown that Pb accumulates at crack tips of SG specimens in ranges of 1-10% of the atoms. Figure 40 shows such concentrations from examination of SCC of Alloy 600TT at a line contact crevices from the Seabrook plant. They have identified similar concentrations in other specimens.

d. Contrary to the 1965 suggestion of Copson and Dean,[160] the crack path in Alloy 600MA is intergranular and that in TT, stress relieved, and sensitized Alloy 600 in generally transgranular although the 600TT is somewhat intermediate as shown in Figure 83 from the work of Lumsden et al.[169] Further, Figure 84 shows that the PbSCC of Alloy 690TT is severe in both the immersed and saturated steam cases, which are associated with concentrated alkaline solutions. In general, as shown in the schematic illustration of Figure 85, Alloy 600MA exhibits a generally IGSCC in PbSCC at nominal stresses; Alloys 600 and 690 in SN/SR/TT conditions exhibit TGSCC; and all materials tend to exhibit TGSCC at very high stresses and slow strain rate tests (not always). While Figures 83-85 describe the microstructure well for the Alloys 600-690 in their various heat treatments, Alloy 800 does not follow the same patterns. These differences and possible speculations are not discussed here.

e. It appears that the lack of a PbSCC epidemic with first generation SGs is the immobilization of the Pb either by forming adsorption bonds or by forming phase compounds. Both have been described by Staehle.[16,17,159] This effect is illustrated in Figure 86. Here, if there is a stoichimetic excess of the compound formers or adsorption bonds, Pb will be immobilized. If not, ionic Pb will be available and will produce PbSCC. Some indication of the relative magnitudes of species is shown in Figure 80 from the work of Laire et al.;[168] here, species on the freespan and in the adjacent crevice are shown. It seems reasonable that, from this array of chemistry, some immobilizing compounds can form.

The pattern of Figure 86 suggests that some species or conditions are the source of the immobilization of Pb. This suggestion implies also that an absence of such an immobilizing condition would release the Pb, and extensive PbSCC could occur. Such conditions for release are not known and need to be thoroughly investigated.

The possibility that Pb is not present in line contact crevices is not a viable option as shown by the Seabrook data in Figure 40 in Section 2.8-1a.

A possible reason for PbSCC not being epidemic in the present line contact geometries is a possibly lower surface temperature owing to the more efficient cooling. However, the Seabrook data suggest that any such minor change in temperature of the metal surface is not important.

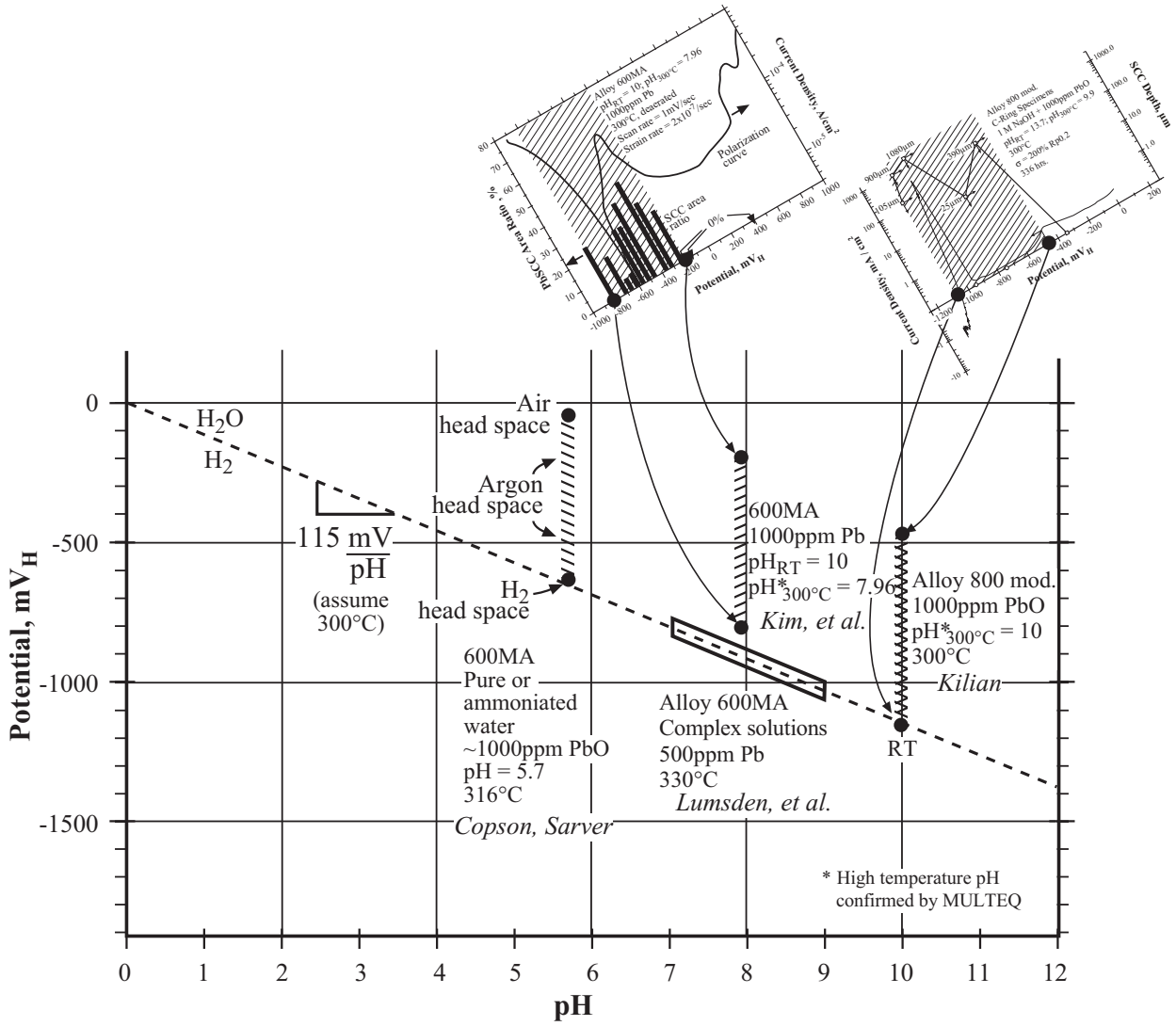

Figure 82 Combined plot of data for the dependence of PbSCC on potentials. Data from Lumsden et al.[169] Kim et al.,[170] Kilian,[171] and Copson and Economy[172] via Sarver.[161]

f. The overall progression of Pb concentrations is shown in Figure 87. The Pb arrives in feedwater at 1-100 ppt, which is also noted by Takamatsu[104] in Figure 48. This low concentration is concentrated in the superheated crevices and then on surfaces to a range of about 1-10% following the sequence described in Figure 78. Some of this Pb is then available to produce PbSCC, and the Pb concentration at the SCC tip is in the range of 1-10%. If the conditions or species that immobilize the Pb are reduced, i.e. bulk solution is more pure, then PbSCC might occur.

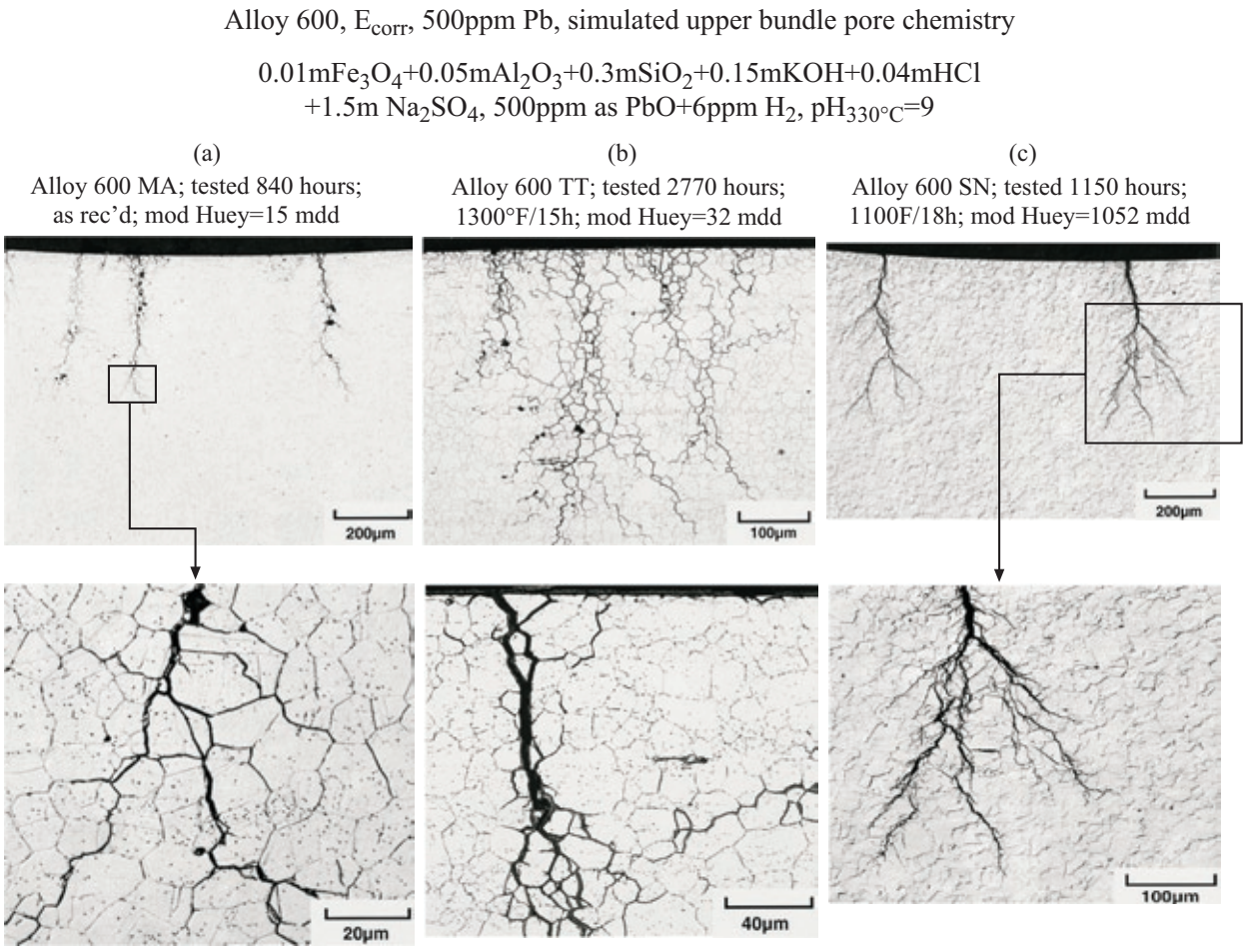

Figure 83 Alloy 600 exposed to 500 ppm Pb plus 0.01m Fe_3O_4+0.05mAl_2O_3+0.3 mSiO_2+0.15mKOH+0.04HCl+1.5mNa_2SO_4+6ppmH_2 $pH_{330°C}$9. Open circuit potential. Times-to-failure shown. Modified Huey test results shown (>200mdd indicates "sensitization"). (a) MA. (b) TT. (c) SN. From Lumsden et al.[169]

6. Future occurrences

There appears to be no reason that PbSCC should not occur in modern SGs. Essential reasons that support such a probability are the following:

a. Pb accumulates in line contact crevices following the Seabrook data shown in Figure 40. This accumulation may be less rapid for lattice bar supports, and accumulation may be slower.

b. Alloys 690TT and 800NG sustain PbSCC over a broad range of pH and potential as well as at low concentrations.

c. It is doubtful that the already low Pb in the feedwater will decrease, although greatly reducing the feedwater Pb would be a useful project.

d. Formation of the deposits in line contact geometries may be slower, and the resulting deposit might be more porous with the result that accumulation might be less rapid—but inevitable.

e. There is a trend in operating SGs to increase the pH using advanced amines. While this trend has already been shown to decrease iron in the water, raising of the pH may also accelerate PbSCC by releasing Pb from whatever chemical combination that immobilizes the Pb, i.e. the intensity of PbSCC is generally proportionate to the pH_6 as shown quantitatively in Figure 81.

f. There is also a trend to add dispersants to secondary water in order to facilitate removing iron in the blowdown. However, such dispersants may also break the bonds of Pb with its immobilizers and thereby increase the activity of Pb.

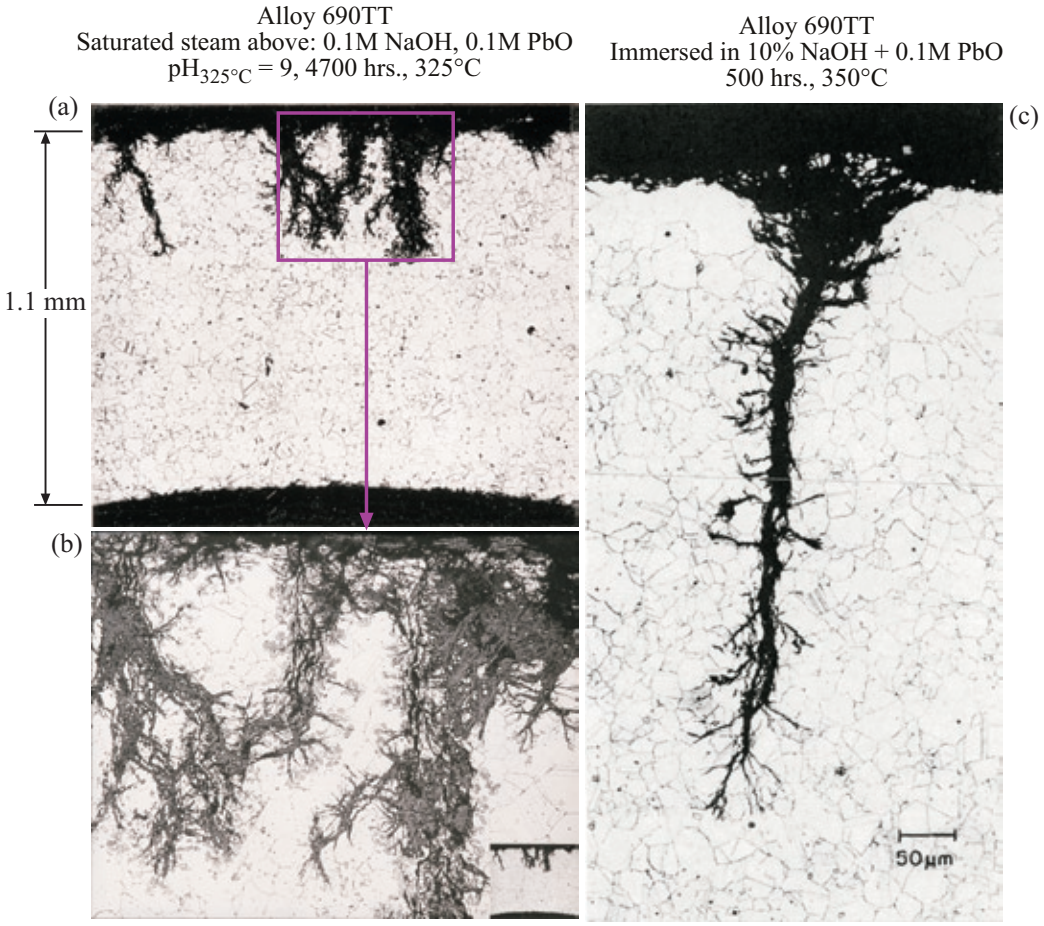

Figure 84 (a) Metallographic cross section of PbSCC of Alloy 690TT exposed to saturated steam above a solution of 1M NaOH + 0.1M PbO at 325°C. (b) Detail of (a) from work of Miglin and Sarver.[173] (c) Metallographic cross-section of PbSCC from Alloy 690TT exposed in a solution of 10%NaOH + 0.1MPbO at 350°C. From work by Castano-Marin et al.[91]

g. With the application of some inhibitors to the secondary side, they may accelerate PbSCC while they reduce other types of corrosion. Such species as Zn, B, and TiO_2 should be considered in this regard.

h. Finally, there appears to be a general trend toward increasing operating temperatures. This trend would accelerate PbSCC according to the presently scant data on the dependence of PbSCC on temperature as shown by Staehle and Gorman.[5]

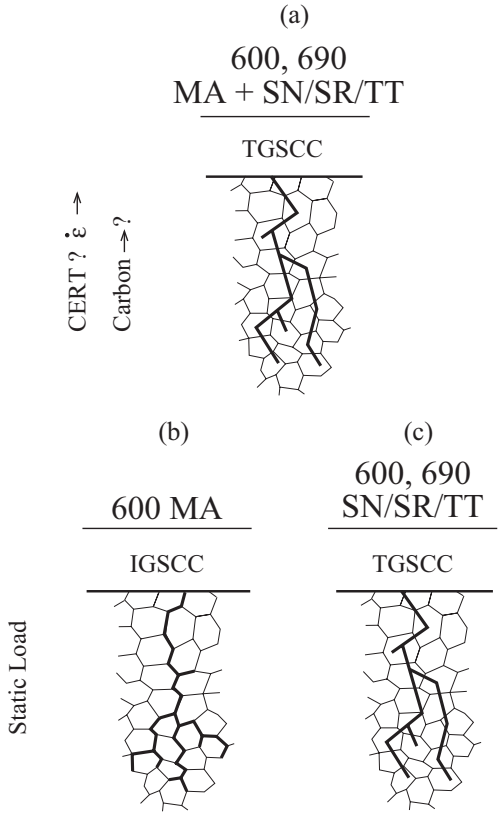

Figure 85 Schematic views of crack morphology associated with PbSCC for various alloys and heat treatments. From Staehle.[17]

3.3 Lead: Scaling

1. Introduction

Figure 76 shows that the higher Cr alloys, e.g. Alloys 690TT and 800NG are prone to producing relatively thick scales in high temperature water. While these observations were published in 1972, little work has been conducted to assess the quantitative aspects of this scaling.

2. Dependencies

The scaling shown in Figure 76 has two important implications:

- The scaling leads to relatively large amounts of corrosion product inside advancing SCC as shown in Figure 88 and is likely to produce the same wedging effect as shown in Figure 61 from

Pickering et al.[143] Once a small SCC begins, as shown in Figure 88 from Lumsden et al.,[169] this wedging reaction produced by Pb, as shown in Figure 89, in the higher chromium alloys would most likely assure its continuation.

- Also shown in Figure 88 is a relatively thick scale on the outer surface. This amount of scale is much greater than ever observed on Alloy 600. This amount of scale has implications for a type of "denting."
- A limited amount of metallographic evidence of scaling over a range of pH is summarized in Figure 90 and includes a range of pH and the 690TT and 800NG alloys. The data in the last column show slow but significant rates of growth of scale related to the presence of Pb in the environment.
- The growth of scale, as shown in Figures 88 and 90, is likely to produce a kind of denting especially in lattice bar tube supports as suggested schematically in Figure 91.

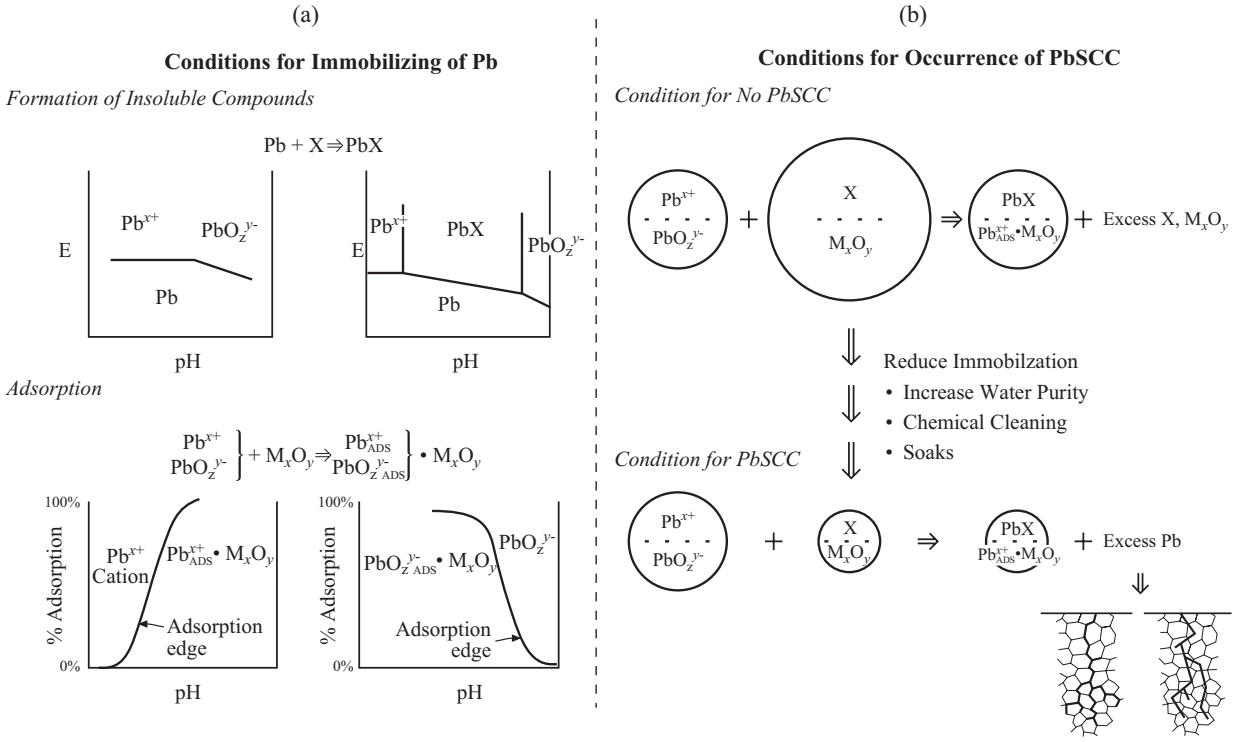

Figure 86 Steps associated with immobilization of Pb and the consequent occurrence of PbSCC. (a) Immobilization by forming phase compounds or adsorbed bonding. (b) Consequences of excess and deficient immobilizing species.

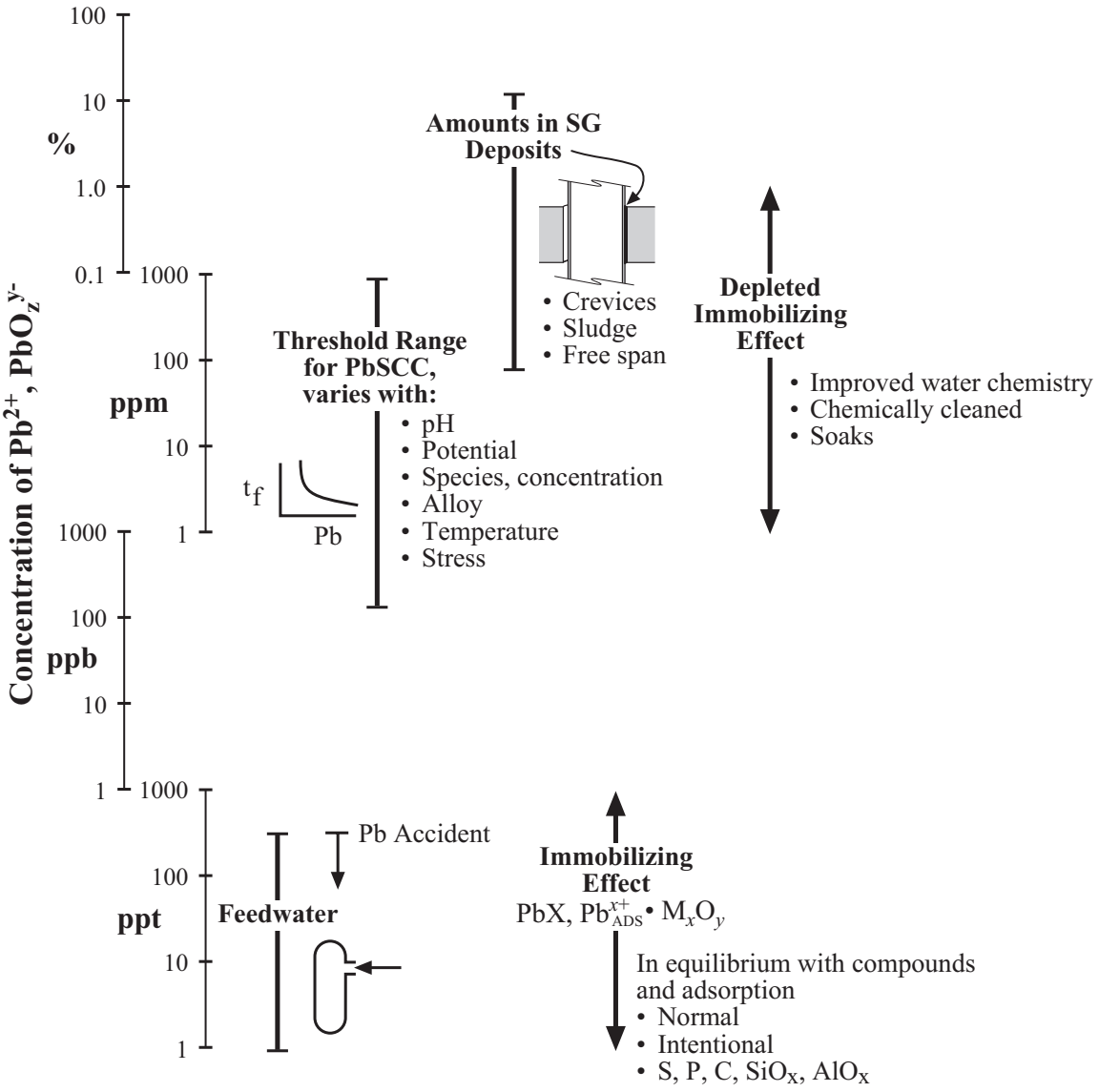

Figure 87 Sequence of concentrations of Pb: Pb in feedwater is 1-100 ppt; thresholds for PbSCC in range of 0.1 to 1000 ppm; amount of Pb in deposits 0.01 to 10%; lowered Pb by immobilizing to 1-1000 ppt; depleting immobilizing to 1-10,000 ppm.

3. Future occurrences

a. Figure 89 and 91 show schematically probably reasonable future conditions for the damaging effects due to large oxide growth or scaling. Figure 89 illustrates the wedging effects following the initiation of PbSCC. Such SCC would require only small initiations.

b. Figure 91 shows the consequence of Pb-accelerated scaling on OD surfaces noting that the growth rate of scales seems to increase with increased chromium, e.g. the Alloys 690TT and 800NG.

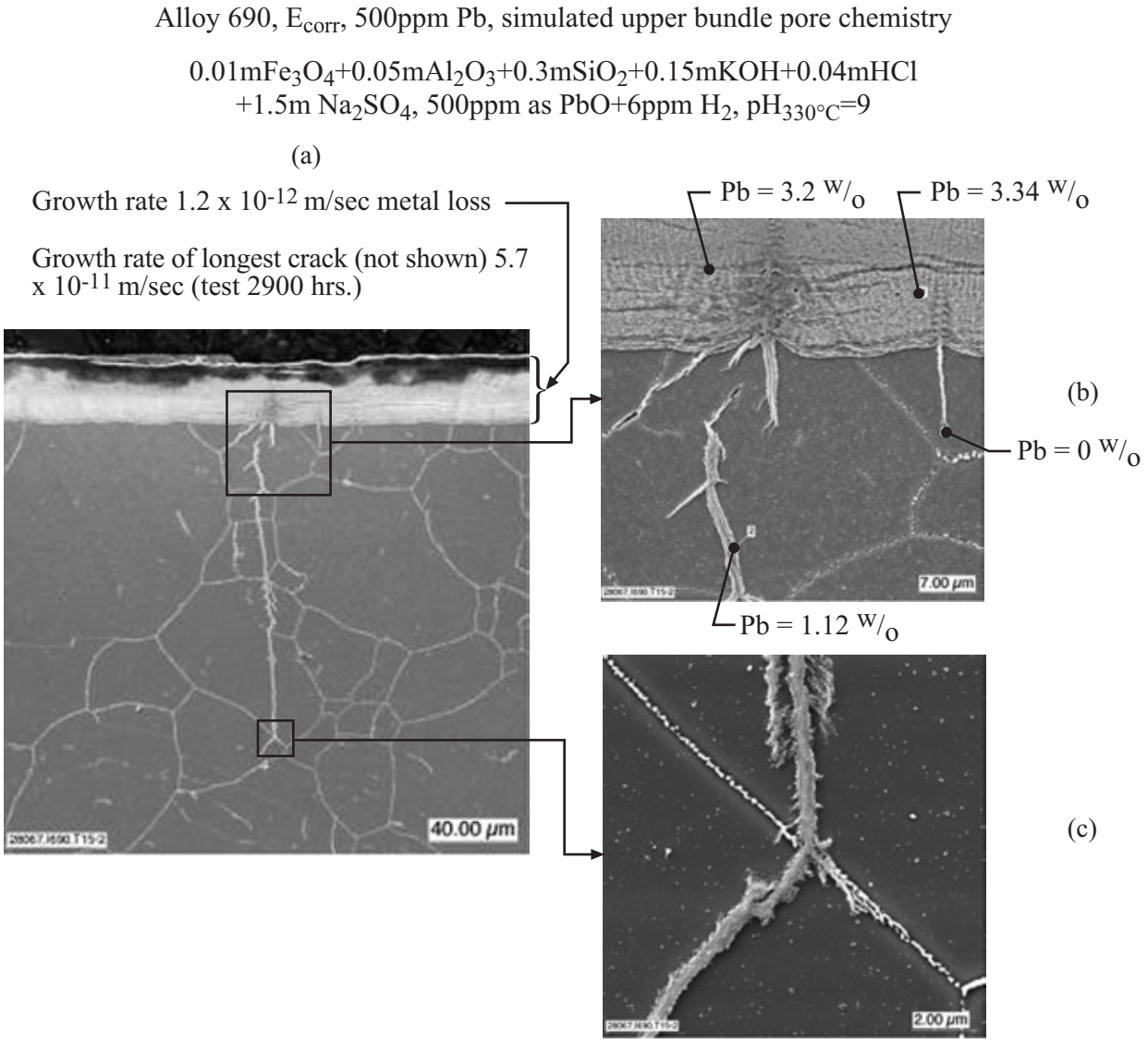

Figure 88 Metallography of Alloy 690TT exposed in $pH_{330°C}$9 for 2900 hours at open circuit potential at 330°C. (a)-(c) are successive micrographs. Composition of solution: 0.01m Fe_3O_4 (m=molal) + 0.05m + Al_2O_3 + $0.3mSiO_2$ + 0.15KOH + 0.04mHCl + $1.5mNa_2SO_4$ + 6ppmH_2 + 500ppm Pb (Pb as PbO). Locations of AES analyses shown. Rates of PbSCC and PbGC growth shown. From Lumsden et al.[169]

3.4 S^{y-}SCC on SG Tubes

1. Introduction

The purpose of this section is to identify SCC due to the presence of low valence sulfur, S^{y-}SCC, as credible and important to the future degradation of modern SGs. S^{y-}SCC results from the reduction of impurity sulfates by hydrazine. This sulfate is present in the secondary system generally at concentrations <5 ppb, as shown in Figure 32. Sulfur can enter the secondary system by the release of sulfur-containing resins, as well as by other undefined sources.

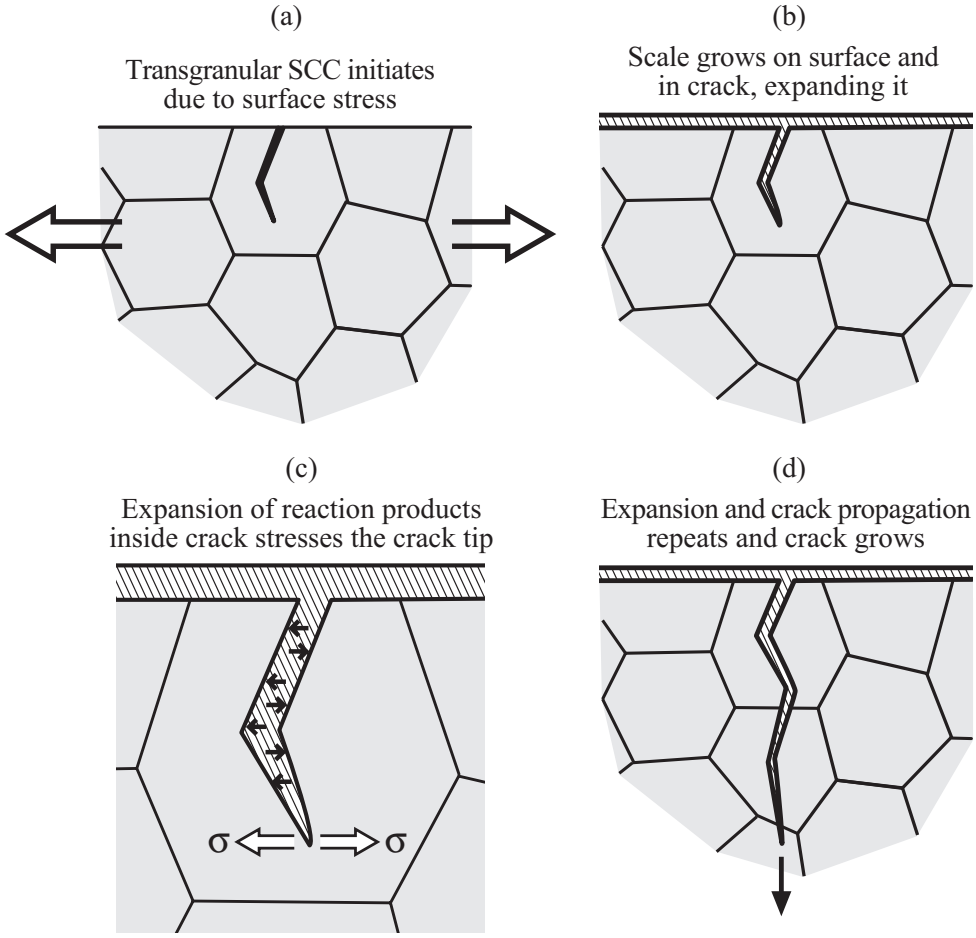

Figure 89 Schematic illustration of the advance of PbSCC under the influence of PbGC inside SCC. (a) Early micro-crack due to surface stresses. (b) Scaling on outside surface and inside PbSCC. (c) Scaling expands and applies force to tip. (d) Tip propagates only due to scaling forces. From Staehle.[17]

Reference	Alloy	Environment	pH_T	Temp, °C	Average Velocity, Metal Penetration, m/s
Kilian	690TT	1M NaOH, 1000ppm PbO	9.9	300	1.9×10^{-10}
Lumsden, *et al.*	690TT	Mixed, 500ppm	9	330	1.2×10^{-12}
Sarver	690TT	Pure water, deaerated with Pb powder	~7.0	316	6×10^{-12}
Sakai, *et al.*	690TT	$PbCl_2$, 300ppm Pb	4.5	340	1.4×10^{-12}
Lu	800	Neutral crevice chem, OCP+100mv, 500ppm Pb	-	300	1.3×10^{-6}

(0.001 in/year = 0.8×10^{-12}m/sec)

Figure 90 Comparison of scaling rates (calculated as rates of metal recession). From work by Kilian,[171] Lumsden et al.,[169] Sarver,[161] Sakai et al.,[174] and Lu.[175]

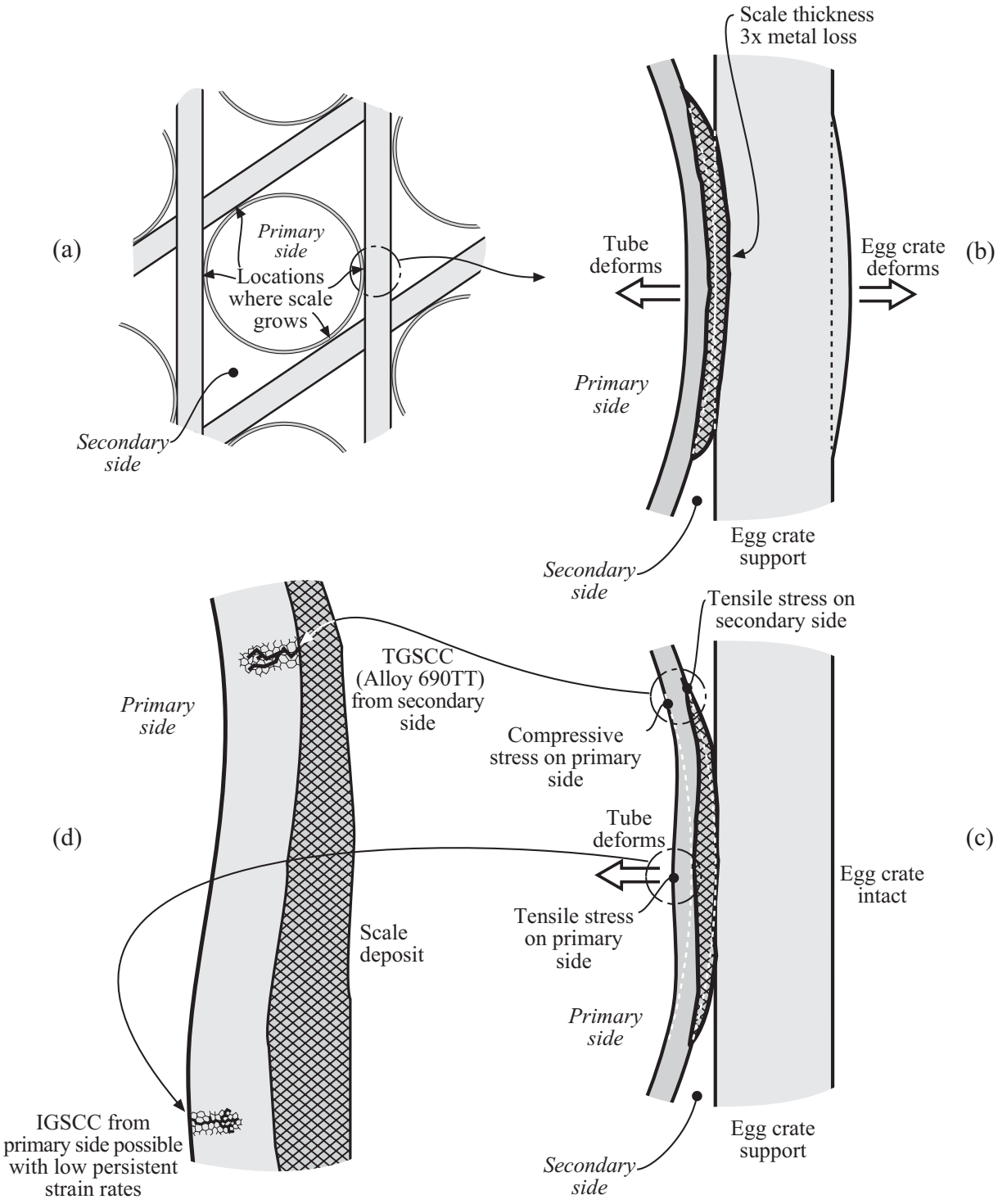

Figure 91 Schematic illustration of denting of SG tubes due to the expansion of corrosion products through PbGC and resulting SCC of the SG tubes. (a) Location of tube in egg crate design. (b) Scale forms and exerts forces on egg crate and tube wall. (c) Location and direction of stresses in tube. (d) SCC results from slow straining due to expansion of scale. From Staehle.[17]

The general range of S^{y-}SCC should respond to pH, and is described in the mode diagram of Figure 26(b).

The concept of "low valence sulfur," which is abbreviated here by S^{y-}, starts with a +6 valence of sulfur in sulfate, a +4 valence of sulfur in sulfite, a +2.5 valence in tetrathionate, a +2 valence in thiosulfate, and a -2 valence in the set of sulfide, bisulfide and hydrogen sulfide, S^{2-}, HS^-, and H_2S, respectively. The +2.5, +2, and -2 valences are in this category of low valence sulfur species that generally accelerate SCC of Fe-Ni-Cr alloys. These deleterious effects have been known for many years in the petroleum industry and account for certain limitations on the choices of materials and their strength.

S^{y-}SCC is especially important because it, like PbSCC, produces SCC in both Alloys 690TT and 800NG.

The maximum amount of SO_4^{2-}, which is permitted by most guidelines, is about 5.0 ppb. This relatively small amount of sulfate reacts with hydrazine which, in modern SGs, may be present in amounts of 100-200 ppb. This reduction reaction produces the S^{y-} of interest here, but the distribution of species and rates of their production, as well as the dependence of this production on the primary variables, are not understood. It has been well known for many years, mainly due to work in connection with the petroleum industry, where H_2S and other low valence species are present in the petroleum without the reaction due to hydrazine, that the low valence sulfur accelerates pitting, general corrosion and SCC.

The fact that S^{y-} species are produced in secondary systems has been known for some time and some details of the reduction reactions have been studied by Sala et al.,[107] Daret et al.,[106] and de Bouvier et al.[108,109] have established that the reduction of sulfates actually occurs and Daret et al.[106] have established that the S^{y-}SCC occurs in AVT type water using model boiler testing. S^{y-}SCC has been studied in alkaline solutions by Gomez-Briceno and Castano[176] as well as by King.[177]

In general, the pattern of intensity of S^{y-}SCC is similar to that of PbSCC being high in the concentrated alkaline solutions and lower in the AVT operating regions.

With PbSCC, the S^{y-}SCC is one of the virulent species with respect to the SCC of Alloys 690TT and 800NG, as well as probably stainless steel. AcSCC, as described in Section 3.5, is also aggressive.

2. Dependencies

a. S^{y-}SCC has been studied in concentrated alkaline solutions by Gomez-Briceno and Castano[176] and by King.[177] Their data are shown in Figures 92 and 93. They have observed the following:

- Both -2 and +2 valence sulfur species, produce S^{y-}SCC.
- Alloys 690 and 800 are particularly prone to S^{y-}SCC.
- In the alkaline solutions neither the CO_3^{2-} nor SO_4^{2-} anions produce SCC; whereas, the -2 and +2 sulfur ions produce intense S^{y-}SCC.

b. S^{y-}SCC has been studied in an AVT environment of a model boiler by Daret et al.[106] Properties of their water chemistry are discussed in Section 2.8-4. Results from their S^{y-}SCC work are shown in the data of Figure 94, and the following important results were obtained:

- The rate of growth of these S^{y-}SCC is 25-100 times less, at least, than those in Figure 92 based on simple depth of SCC divided by time comparison.

- The Alloy 690TT was substantially superior to Alloy 800SP and 600MA, which were about the same as each other.

Material	10% NaOH	10% NaOH + 0.1M CuO	10% NaOH + 0.1 M PbO	50% NaOH + 5% $Na_2S_2O_3$	0.75% M Na_2SO_4 + 0.25% M $FeSO_4$	0.75% M Na_2SO_4 + 0.25% M $FeSO_4$
Alloy 800 7-73243	3/3	3/3	4/4	4/4	4/4	0/4 (3/4)**
Alloy 800SP 81373	15/15	15/15	15/15	15/15	15/15	11/15 (15/15)**
Alloy 690TT WF816T	0/15	0/15	15/15	14/14	0/15	1/15
Alloy 690TT 764408	0/15	0/15	15/15	15/15	0/15	0/15
Alloy 600MA 1450	8/9	0/9 (2/9)**	0/9 (3/9)**	2/9	6/9 (8/9)**	9/9

* 500 hours exposure; C-ring specimens; 2% strain.

** Visual examination after bending the samples.

Figure 92 Results from visual examination of specimens exposed to alkaline solutions at 350°C with added species (cracked samples/tested samples). From Gomez-Briceno and Castano.[176]

5% Addition	Alloy 600		Alloy 690	
	Worst Case	Observations	Worst Case	Observations
Na_2CO_3	No difference*	General attack	No difference*	Slight g.b. intrusions
Na_2S	TT ring	Heavy general attack	MA C-ring	TGSCC
NaHS	No difference	Heavy general attack	MA C-ring	TGSCC
$Na_2S_2O_3$	No difference	Heavy general attack	MA C-ring	TGSCC
Na_2SO_4	No difference	Slight general attack	MA C-ring	Slight g.b. intrusions

* No difference indicates no substantial difference between ring or C-ring specimens for mill-annealed and thermally-treated condition.

MA - Heat treatment not defined

TT - Mill annealed plus 704°C /16 hrs

TGSCC - Transgranular stress corrosion cracks

Figure 93 Results of cathodic polarization scans in 50% NaOH with 5% additions at 316°C. From King.[177]

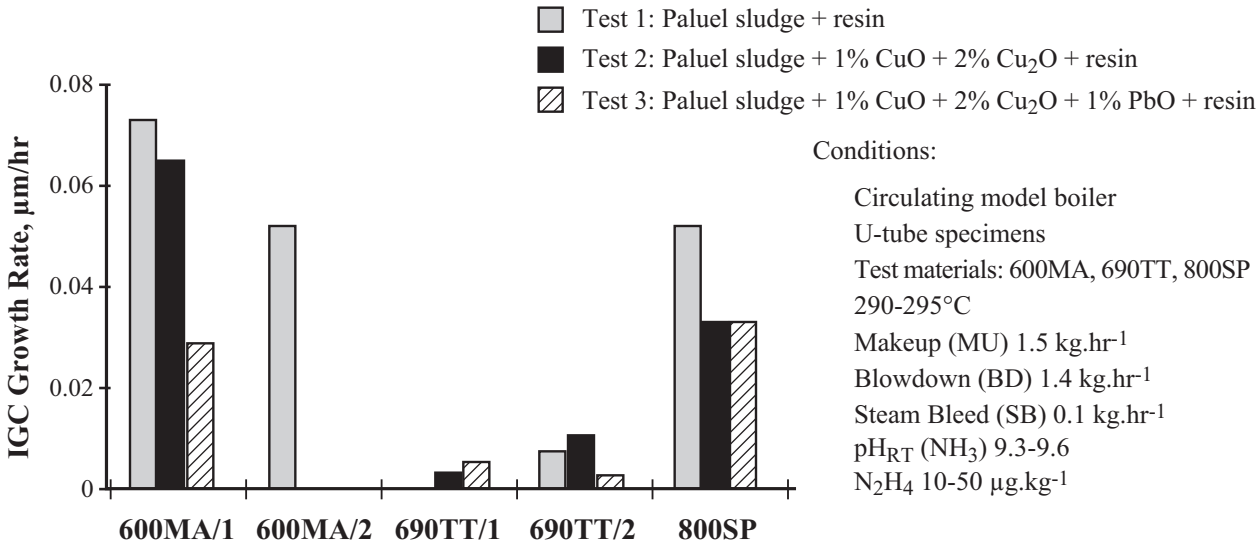

Figure 94 Approximate rates of corrosion penetration (depth/time) vs. alloy for Tests 1, 2, 3 at the noted conditions. Tests conducted for about 6000-8000 hours. Total penetration included intergranular penetration or IGSCC. From Daret et al.[106]

c. The effects of hydrazine and potential on the SCC of Alloy 600MA were studied by de Bouvier et al.[108] and their results are shown in Figure 95. It is not clear as to the identity of the local chemistry, since the specific species were not explicitly identified. However, the data and concentrations for the tests are similar to those that would support S^{y-} species.

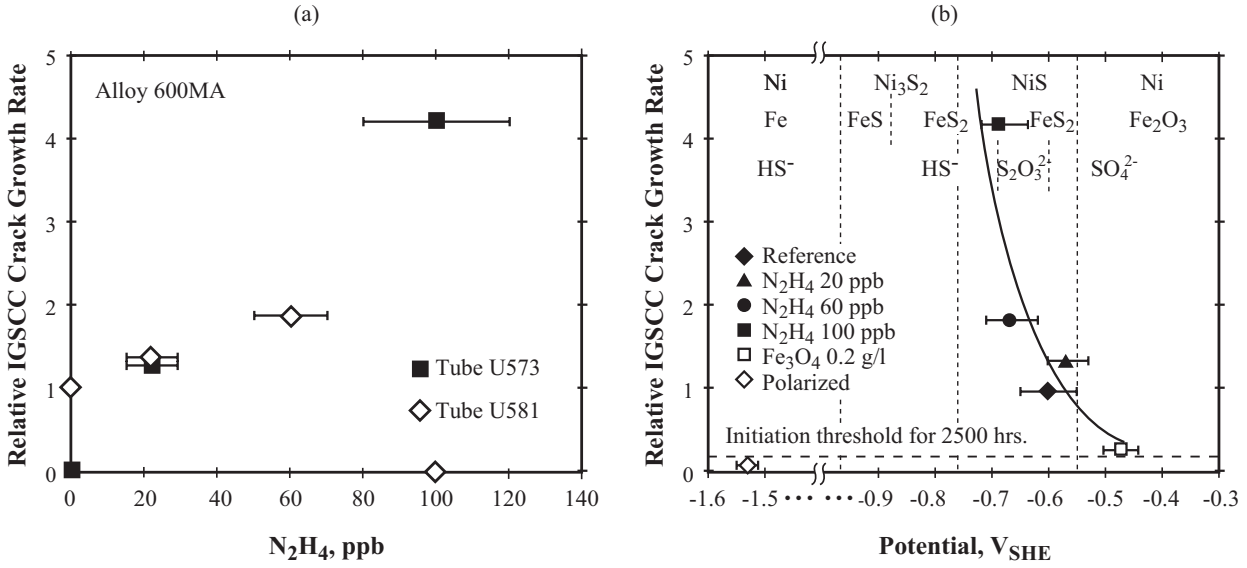

Figure 95 (a) Relative IGSCC crack growth rate vs. concentration of N_2H_4 for Alloy 600MA tested at 320°C for two specimens with SO_4^{2-} of 0.005M and pH_T of 6.5. (b) Relative IGSCC crack growth rate vs. potential for different chemistries. Alloy 600MA at 320°C for SO_4^{2-} of 0.005M and pH_T of 6.5. From de Bouvier et al.[108]

The data in Figure 95 agree with those in Figure 94 taken by Daret et al.[106] in that they are both in the same range of pH and both show relatively rapid SCC for Alloy 600MA. de Bouvier et al.[108] also showed that Alloy 690TT did not sustain S^{y-}SCC in the range of approximately neutral environments studied.

d. Daret et al.[106] identified the presence of a high concentration of sulfide at the location of SCC on the surface as shown in Figure 96. The Test 2 notation refers to the same Test 2 on Figure 94. Such evidence may be similar to that showing sulfur inside SCC. There was no sulfide prior to exposing the sulfate to the hydrazine. Here, the concentration of sulfide is maximum next to the SCC. These experiments were from those shown in Figure 94.

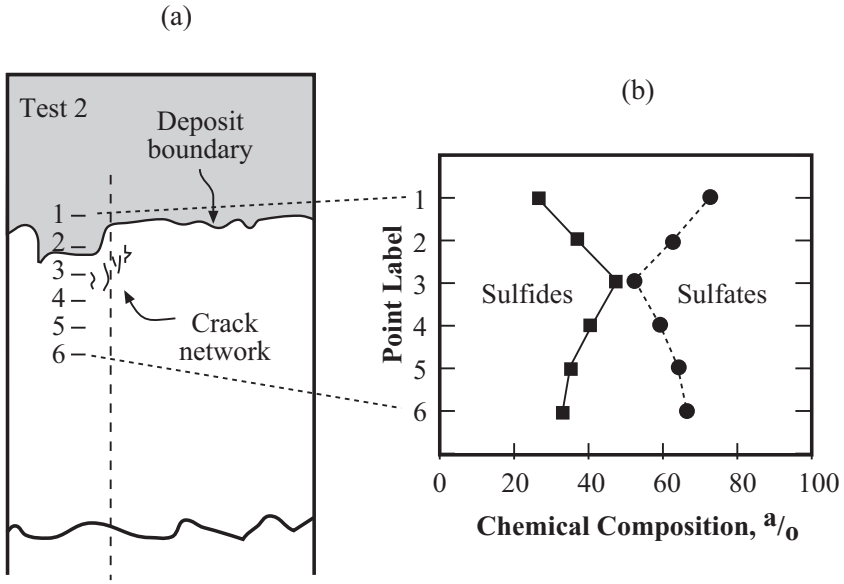

Sulfide is reduced to S^{2-} by hydrazine

$$2(SO_4)^{2-} + 18H^+ + 12e^- \rightarrow 2(HS^-) + 8H_2O$$

Hydrazine is oxidized

$$3(N_2H_4) + 12OH^- \rightarrow 3N_2 + 12H_2O + 12e^-$$

Figure 96 (a) Network of SCC from Test 2 in Figure 94. (b) Location of chemical analysis vs. atomic percent of sulfide and sulfate as measured by the XPS. From Daret et al.[106]

3. Future occurrences

a. So long as hydrazine is used on the secondary side, S^{y-} will continue to be produced together with its potential for accelerated degradation.

b. If the hydrazine were to be eliminated, the concentration of low valence sulfur would be reduced. Such decreased low valence sulfur might be further reduced with the higher potential on the secondary side with negligible hydrogen. Such a somewhat higher potential would improve resistance also to FAC.

c. Considering the juxtaposition of the E-pH diagrams for Pb and S in Figure 25, the relative properties suggest that there should be a minimum in PbSCC owing to the tendency for decreased solubility in the mid-range of pH. However, Figure 25(b) suggests that S^{y-} should be progressively

more soluble with decreased pH starting from alkaline and therefore the neutral range should favor more rapid S^{y-}SCC. However, the data from Figure 94, as well as for PbSCC from Figure 81, show a minimum of SCC in the neutral AVT region for both Pb and S^{y-} environments. Since these two do not follow patterns of solubility, it is possible that the metallurgical composition is more influential; perhaps, the pattern of solubility of the Cr as shown in Figure 22 is the most influential pattern.

d. If a pH dependence can be derived from linking the high pH environments containing S^{y-} of Figures 92 and 93, with the relatively neutral pH of the AVT environment of Figure 94 as well as Figure 95, a dependence of S^{y-}SCC on pH is suggested. This means that whatever steps are taken to raise the pH may accelerate the S^{y-}SCC, especially with reference to Alloys 690TT and 800NG.

e. It should also be noted in Figure 94 that, whereas the overall S^{y-}SCC is reduced in Figure 94, the Alloys 600MA and 800SP still sustain S^{y-}SCC about equally, whereas S^{y-}SCC for Alloy 690TT is minimal. A similar pattern obtains for PbSCC.

f. In addition to increasing the pH and accelerating SCC degradation (Figure 92) by PbSCC, as suggested from Figure 50 for future SG operation, the addition of dispersants may also be damaging in that they may release these aggressive species from being immobilized by various compounds that prevent even greater damage.

3.5 Acidic Sulfate, AcSCC (SO_4^{2-})

1. Introduction

Acidic SCC, AcSCC, is important because sulfates are permitted if <5 ppb. This concentration is low but, for reference, it should be noted that Pb concentrates in superheat crevices when it enters with the feedwater at 0.001 to 0.1 ppb. Also, sulfates are important because of the infrequent but important release of sulfur-containing resins.

While Section 3.4 considered only S^{y-}SCC owing to its chemical difference from SO_4^{2-}, the latter is important in its own +6 identity and exerts different dependencies for alloys and in different pHs. Thus, whether or not hydrazine is present to reduce SO_4^{2-} to lower valences, or whether there is significant SO_4^{2-} that is not reduced by hydrazine, the sulfate remains an important consideration in predicting future degradation, mainly as AcSCC, as shown in the mode diagram of Figure 26a.

In this section, AcSCC related to SO_4^{2-}, is emphasized and AcSCC related to chloride is not. Of course, the acidic chloride solutions are important, but they have not been so extensively studied although should be, in view of their presence in molar ratio control.

In general, the data in the discussion of dependencies here, Section 3.5-2, shows that Alloy 800 is substantially more prone to AcSCC than Alloy 690TT in acidic solutions. Alloy 690TT seems to become prone to AcSCC only when the potential is raised.

2. Dependencies

a. Figure 97 shows the dependencies of AcSCC(SO_4^{2-}) on pH, concentration of SO_4^{2-}, electrochemical potential, and alloy composition. These data exhibit the following patterns:

- The rate of the AcSCC(SO_4^{2-}) depends generally on the -½ power of hydrogen ion concentration as shown in Figures 97(a,b) but seems to have a steeper dependence in Figure 97(e) of -0.84, perhaps because of the lower temperature.

- For Alloy 600MA, the crack growth rate increases with increasing potential and then decreases as shown in Figure 97(f). This general pattern is similar to that observed in AkSCC although it is not discussed here.
- The rate of AcSCC(SO_4^{2-}) seems to be proportional approximately to the first power of the SO_4^{2-} concentration as shown in Figures 97(a,b).
- Increasing the stress to >Y.S. increases the rate of the AcSCC(SO_4^{2-}).
- There is little difference among Alloys 600MA, 600TT, and 800 as shown in Figures 97(a,b,c,d).
- At open circuit potential, Alloy 690TT does not seem prone to AcSCC(SO_4^{2-}).

b. Figure 98 shows results for Alloy 690TT compared with Alloy 600MA in the presence of solutions much like those in Figure 97 although Pb is present in two of these solutions. Note that, in the presence of sulfate, as shown in Figure 81, Pb exerts little effect in acidic SO_4^{2-} solutions owing to the interaction of Pb and SO_4^{2-} to decrease the activity of Pb.

Results similar to those in Figure 98 are also shown in Figure 92 for acidic sulfate solutions. Taken together, Figures 92 and 98 show the following:

- Alloy 800 sustains significant AkSCC, whereas the AkSCC of Alloy 690TT is finite but minimal.
- AkSCC occurs in Alloy 690TT when the potential is increased. Note in Figure 98a that Alloy 600MA sustains AkSCC in the absence of increased potentials whereas Alloy 690TT does not.
- In the presence of increased potentials, as shown in Figure 98(b), Alloy 690TT sustains AcSCC(SO_4^{2-}) only when the $NaSiO_3$ is absent, as well as the cationic resins being absent (although the former influence is most likely the dominating one).
- The term "increased potentials," used in connection with Figure 98, is derived from the oxidizing capacity of the copper oxides. Such an effect of copper oxides is illustrated in Figures 21 and 23 where the relatively high equilibrium potentials are shown.
- Figure 98 also indicates that potential is raised as hydrogen is withdrawn. This effect is similar to that in Figure 99 from Nagano et al.[182] While these data are taken in concentrated alkaline solutions where AkSCC is studied, they serve to illustrate the general quantitative effects of adding copper oxides and hydrogen in acidic solutions. Figure 99 shows that adding copper oxide raises the potential by 500-600 mV, which is similar to the effect in Figure 23 for the equilibrium potential. Figure 99 shows that adding hydrogen lowers the potential as also shown in Figure 98. Thus, the effect of removing hydrogen on Alloy 600MA in Figure 98 is the same as that in Figure 97(f) for raising the potential. Figure 98(b) also shows that the additional potential achieved by omitting the hydrogen is necessary for Alloy 690TT to sustain significant AcSCC noting particularly solution #3 in Figure 98(b). Such a skewed dependence on potential for Alloy 690TT is similar to that for Alloy 600MA shown in Figure 97(f).
- While Alloy 690TT is shown in Figure 98 to sustain AcSCC at relatively high potentials, such potentials are not practically realized in PWR environments and particularly in superheated crevices.

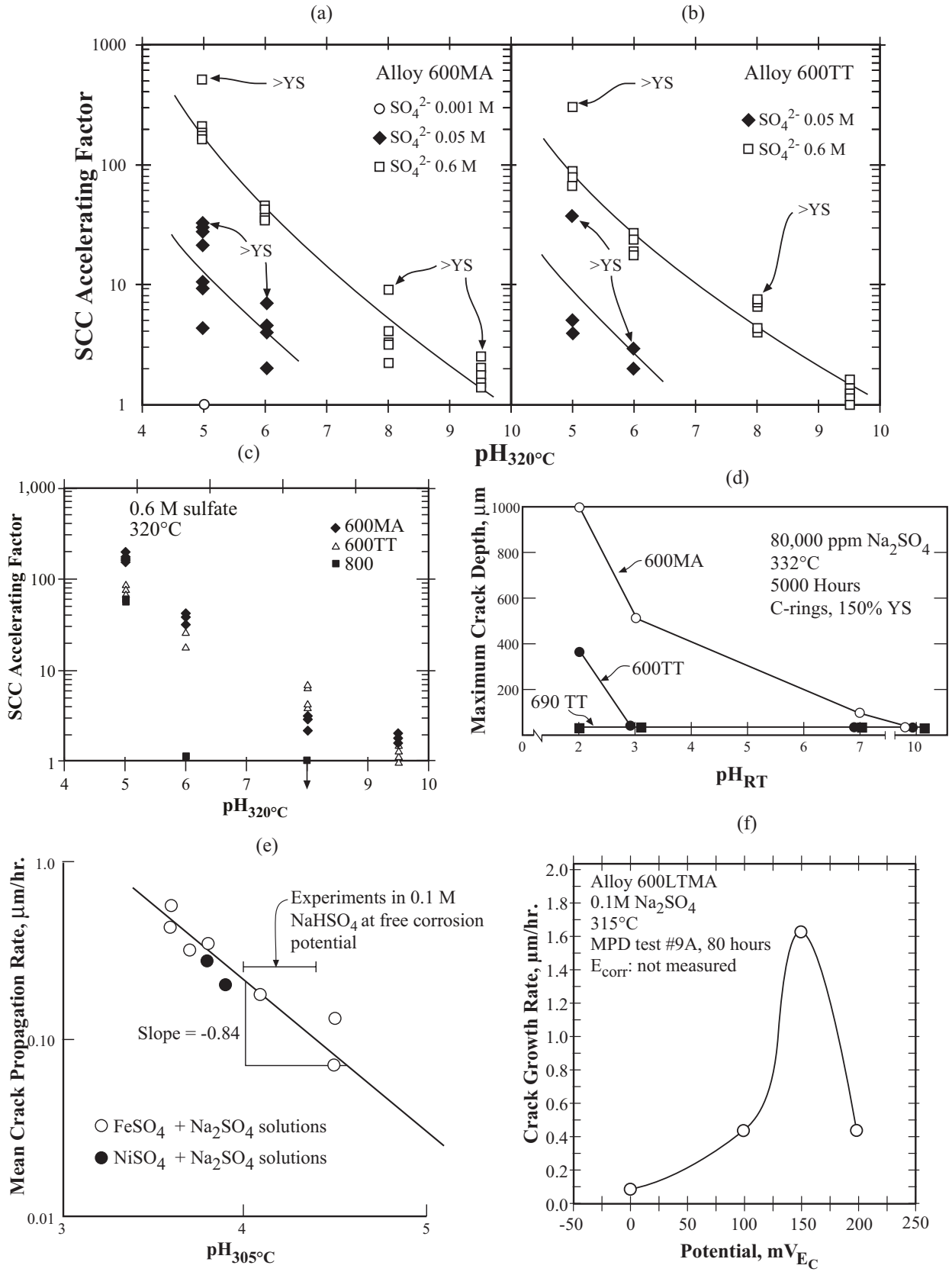

Figure 97 SCC accelerating factor vs. pH with different concentrations of SO_4^{2-}

and with different stresses for (a) Alloy 600MA and (b) Alloy 600TT. (c) SCC accelerating factor vs. pH for three alloys in 0.6M sulfate environments at 320°C. Accelerating factor taken from rate of crack initiation at 0.001M ($pH_{320°C}$ = 6) being the reference. >YS refers to "two legs touching" condition of the branches of the C-ring; below this stress, specimens were stressed at 0.8 YS and 1.0 YS. From de Bouvier, et al.[87] (d) Maximum crack depth vs. room temperature pH for Alloy 600MA, Alloy 600TT, and Alloy 690TT exposed in acidic sulfate solutions at 332°C for 5000 hours as C-rings stressed to 150% of the yield strength. From Smith et al.[178] (e) Mean crack propagation rate vs. pH for nonsensitized Alloy 600MA in sulfate at 305ºC. From Newman.[179] (f) Crack growth rate vs. applied potential for Alloy 600LTMA exposed in 0.1M Na_2SO_4 at 315°C. From Cullen.[180]

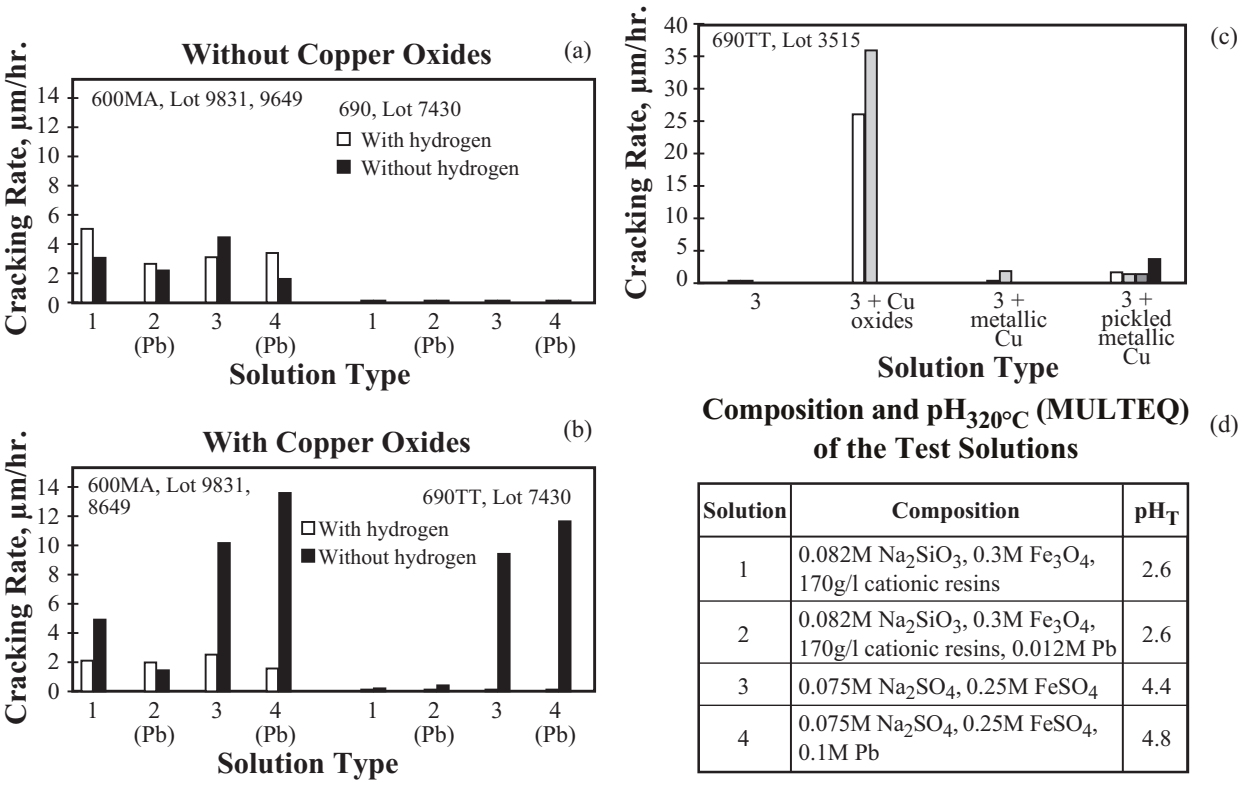

Solution	Composition	pH_T
1	0.082M Na_2SiO_3, 0.3M Fe_3O_4, 170g/l cationic resins	2.6
2	0.082M Na_2SiO_3, 0.3M Fe_3O_4, 170g/l cationic resins, 0.012M Pb	2.6
3	0.075M Na_2SO_4, 0.25M $FeSO_4$	4.4
4	0.075M Na_2SO_4, 0.25M $FeSO_4$, 0.1M Pb	4.8

Figure 98 Effects of Pb and no Pb compared in acidic solutions in Figures (a) and (b). (a) Maximum cracking rates for Alloys 600MA and 690TT in acidic solutions without copper oxides with and without 5% H_2 added to argon cover gas in capsules for 320°C. (b) Maximum cracking rates for Alloys 600MA and 690TT in acidic solutions with copper oxides with and without 5% H_2 added to argon cover gas in capsules for 320°C. (c) Maximum cracking rates obtained for Alloy 690 with solution 3 and with the same solution containing copper oxides or metallic copper (pickled or not). (d) Composition of solutions. From Pierson and Laire.[181]

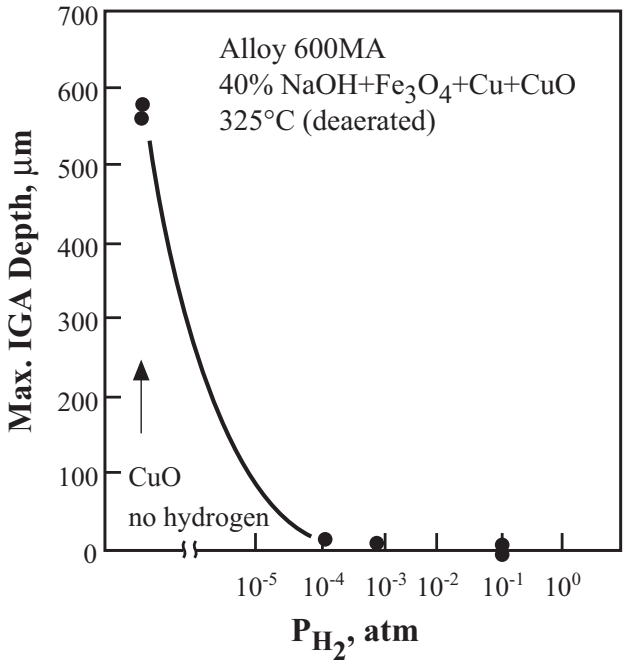

Figure 99 Maximum IGA depth vs. hydrogen pressure for Alloy 600MA in a solution of 40% NaOH + Fe_3O_4 + Cu + CuO at 325°C tested for 200 hours using pre-cracked C-ring specimens stressed at 30 kgf/mm^2. From Nagano et al.[182]

3. Future occurrences

a. The AcSCC(SO_4^{2-}) would be most intense for Alloy 800 in the future and where the sulfate could reach the highest concentrations in mild acidity. Such locations would be in the superheat crevices and perhaps most aggressive later as the "burrowing" crevices that might develop at the TTS as shown in Figure 46.

b. It is not likely that Alloy 690TT would sustain AcSCC(SO_4^{2-}) since the potentials under which it does occur are not present either in superheat crevices or in PWRs in general. However, the data here are meager and need more confirmation. Further, possible effects of Cl^- have not been investigated but should be.

3.6 TSP Line Contact Crevice

1. Introduction

In contrast to older designs, modern SGs using either broached holes or lattice bars (egg crates), as shown in Figures 36 and 37, have line contact crevices at the intersection of tubes and tube supports (TSPs) as shown in Figure 39. The line contact crevices were chosen, in contrast to the drilled hole, to minimize the accumulation of deposits adjacent to the tube surface. Also, in contrast to the drilled hole design with flow holes, the line contact designs involve the flow passing adjacent to a nominally large fraction of the periphery of the tube, although the accumulation of deposits interferes with this objection.

It is necessary that these line contact TSPs be understood in order to assess the possible effects

of Pb, S^{y-}, and SO_4^{2-} on SCC since their relative effects depend on concentrating. Unfortunately, there is little quantitative information for developing such judgments.

2. Dependencies

a. Deposits are not confined to the very narrow contacts between the tube support and tube. Present observations show that deposits tend to spread as shown in Figure 39. In fact, such deposits begin to approach the deposit geometries of the drilled hole geometry.

b. Figure 39 shows the gradients of flow, temperature, concentration, and reactivity. For the present, such gradients are schematic since they have not been considered quantitatively, either experimentally or analytically. Regardless, the flow gradient would certainly produce net migration of charged particles owing to streaming potential effects.

c. The sharp gradients in temperature shown in Figure 39(d) can be expected to produce thermal stresses.

d. From the PbSCC in Seabrook, Section 2.8-a.1 and Figure 40, with line contact broached hole TSPs, it is clear that Pb can accumulate in these line contact geometries.

e. From Figure 41 it is clear that the same essential chemistries that accumulate in drilled hole crevices also accumulate in line of contact crevices, although neither the drilled hole nor the broached hole chemistries indicated the presence of Pb. Regardless, if the overall chemistries are the same, it is reasonable to assume that the lead was the same.

3. Future occurrence

a. There seems to be no evidence that the same chemicals, which accumulate in drilled hole crevices, will not also accumulate in line contact deposits; but perhaps a longer time will be required.

b. Perhaps the higher purity of water and the improved alloys reduce the early onset of degradation, which is associated with these line contact crevices.

c. It is also possible that the surface temperatures of the tubes, even in contact with deposits, may be lower owing to the propinquity of the rapidly flowing coolant. Such a lower gradient may also reduce the superheating capacity of the deposits in line contact geometries. Of course, this trend is contrary to the ease with which Pb was observed in the SCC at Seabrook, as shown in Figure 42.

d. Owing to the capacity of S^{y-} to segregate significantly to the vapor phase, as discussed in Section 2.8-4 and shown in Figure 49, such high relative concentrations in vapor phases of superheated crevices could become extraordinarily aggressive.

e. Segregation of Pb and SO_4^{2-} will also become significant in the line contact crevices at long times.

3.7 Top of the Tubesheet ODSCC (Pb, S^{y-}, SO_4^{2-})

1. Introduction

At the top of the tubesheet, there is a small but important superheated crevice that has changed

little from those used in the previous generation of SGs and is shown in Figures 42, 43, and 44. This crevice is important for the following reasons:

a. The crevice is circumferential in contrast to the axial line of contact crevices discussed in Section 3.6. This circumferential facilitates full tube breaking.

b. At the same location, the tubes have been expanded and sustain increased cold work and high residual stresses, both of which exacerbate the degradation effects of whatever environments accumulate.

c. Being at the bottom of a vertical SG, the surface inevitably accumulates deposits that increase the length of crevices as shown in Figure 43.

2. Dependencies

a. The likelihood for superheating increases with time as the crevice fills with reaction products from the corroding tubesheet.

b. The potential for superheating also increases as deposits accumulate owing to the vertical geometries.

c. With time and with the accumulation of deposits and corrosion products, the steel of the tubesheet will corrode more rapidly.

d. The presence of the cold work and higher residual stresses compared with the line contact crevices at the TSPs will accelerate corrosion reactions in the tubing.

e. This location is the hottest superheat crevice in the SG.

f. In addition to the local stresses due to expansion of the tubes, there are longer range bending stresses from bowing of the tubesheet that are produced by the primary pressure being greater than the secondary pressure.

3. Future occurrence

a. Owing to the simultaneous presence of cold work, slow stress cycling, bending, growth of iron oxide, concentrating chemistry (Pb, S^{y-}, SO_4^{2-} as well as other species), maximum temperature, and increasing deposits on the TTS, degradation of the tubes should be expected. This multiple stimulation is shown schematically in Figure 46.

b. Possible increases in pH in the future, as suggested in Figure 50, produce possibly opposite effects: On the one hand, raising the pH decreases the amount of deposits; on the other hand, raising the pH increases the rate of PbSCC and S^{y-}SCC while decreasing the rate of AcSCC(SO_4^{2-}). Which of these countervailing influences becomes important in the future is not clear.

c. The use of dispersants, as shown in Figure 55, may disperse the Pb and S^{y-} with the result that PbSCC and S^{y-}SCC could become more active.

3.8 Denting at the TTS

1. Introduction

The term, “denting” is discussed in connection with Figures 13 and 61. This section is

concerned with the geometry shown in Figure 44. Here, the crevice sequesters chemicals owing to the superheat and corrodes the carbon steel. The corrosion products expand and deform the adjacent tube. Such a deformation further increases local stresses already high owing to prior tube expansion. Further, this expansion produces a slow straining effect as discussed in connection with Figure 58 in Section 2.9-1. The corrosion products expand according to the prediction of Pilling and Bedworth[55] as discussed in Section 2.9-4.

2. Dependencies

a. There are no data for the rate of growth of the corrosion shown in Figure 44 nor is there any knowledge of the effects of the sequestered chemistry and local pH. Some insight could be gained from the data on denting that occurred in the middle 1970s at drilled hole tube supports.

b. It is known that the volume of the reaction products would be about 3 times the original volume of the metal that produced the corrosion projects based on the 1923 work of Pilling and Bedworth.[55]

c. It is also known that the exterior potential is on the order of 200mV above that on the primary side owing to the very low hydrogen concentration on the secondary side. This might produce a more insoluble and possibly harder oxide.

d. This location on the hot side is the hottest of all the locally superheated crevices. Reactions here should be more rapid that ones higher in the bundle.

e. Expansion of the corrosion products at a slow rate can be expected to produce SCC over some longer time.

f. The fact that the region where stresses are exerted is also cold worked with high residual stresses and should act to accelerate both initiation and propagation of SCC.

g. If Pb and S^{y-1} are present, the Alloys 690TT and 800NG should be expected to sustain SCC. If only SO_4^{2-} is present, the Alloy 800NG should be expected to sustain SCC.

3. Future occurrence

The rate of growth and stressing can be bounded using existing information on the corrosion of carbon steel in concentrated chemical environments and the mechanics of uniformly applied load. Such corrosion rates might be obtained from the work on denting in drilled hole crevices but would have to be modified since it is known that denting in TTS crevices has been minor to the present time.

3.9 Growing Crevice Below TTS ("Burrowing Crevice")

1. Introduction

The process identified in Figure 44 can be extended to producing longer crevices as shown in Figure 45 over long times. The corrosion products would essentially burrow downward to cause the tube to become detached from the wall. Ultimately, this would produce a result not unlike that of the long crevices, such as shown in Figure 42(a), that could be considered a bounding case.

While the possibility of a slowly continuing corrosion process has been thought to be

unreasonable, the fact that the TTS joint is not welded makes it accessible, especially with a crevice already present and the ever-present corrosion processes of the steel tubesheets that can produce great forces in tight geometries as shown in Figure 61. There is no question that the greater force of expanding corrosion products can produce burrowing over time.

2. Dependencies

a. The dependencies at the initiation are those described in Section 3.7 and 3.8. As the burrowed crevice depends together with the presence of porous, but tight, rust and the local chemistry, the local chemistry will change but the nature of this change is not clear.

b. This crevice might be driven somewhat by the oxidizing capacity of the low hydrogen and the secondary side.

c. In the absence of hydrazine, sulfate might be a preferred electrolyte. According to the data in Figures 97 and 98, such an environment would be inimical to Alloy 800 but not to Alloy 690TT.

d. The surface temperature at the tip of the burrow would be the highest in the SG; therefore the reaction rate due only to temperature would be relatively high.

e. The slow but persistent straining would accelerate SCC degradation in the tube wall.

3. Future occurrence

The burrowing crevice would take time to propagate but would be aggressive once it reaches some depth where the environments concentrate to aggressive concentrations and species. These conditions are not yet established and would rely on experiments. Some of the past history with partially rolled crevices, as shown in Figure 43(a), could be useful.

3.10 Fouling

1. Introduction

Fouling, as understood in the Figure 47, is not well defined in terms of superheat and accumulated chemistry. Certainly, the extent of chemical accumulation depends on the surface temperature and the local flow. The extent of fouling is also affected by any chemical cleaning. Nonetheless, some SCC degradation on free spans has occurred as discussed by the Staehle and Gorman review,[5] with time and thicker deposits.

2. Dependencies

a. To some extent, the chemistry on the metal surface depends on the chemistry of the bulk secondary coolant with respect to intentional and impurity compositions. The intentional additions include inhibitors (B, TiO_2, Zn), pH control agents as well as the resulting pH, and dispersants. The impurities include those well known in water chemistry impurities such as S, Cl, Al, Si, Pb, Ca, Na, and others.

b. To the extent that the fouling depends on temperature of the substrate, this is reasonably well known unless the fouling changes the heat transfer resistance.

c. To the extent that electrochemical potential is important, one can expect a higher potential

on the secondary side owing to the low hydrogen concentration, in the range of 1 ppb. This potential can be approximately calculated.

d. How flow enters into the growth of fouling deposits is not clear.

e. The free surfaces are no more stressed than the TSP locations although stresses in the latter may be higher owing to sharp local thermal gradients shown in Figure 39(d). Free surfaces can be scratched to the point of initiating SCC as shown in Figures 14 and 63.

3. Future occurrence

The length of time between successive chemical cleanings may be the most important time period with respect to corrosion related to fouling on free surfaces.

While the bounding conditions for corrosion on the fouled free spans can be determined, predicting degradation may be more problematic. However, this large area cannot be neglected for the long term, especially with respect to changes in surface chemistry of protective films and metal substrates, as described in Section 2.8-1d.

3.11 pH Change

1. Introduction

There is a continuing effort in secondary water chemistry to reduce the amount of iron deposits in modern SGs mainly to minimize plugging and fouling on the secondary side and activation and subsequent transport of species on the primary side. This is approached in two ways. One, on the secondary side, is to introduce advanced amines or to increase the concentration of ammonia, in order to minimize the solubility of iron, as shown in Figures 21 and 22, and as discussed in Section 2.5. Here, the iron is immobilized by minimizing its solubility, and this is accomplished by adjusting the pH as close to the minimum solubility, shown specifically in Figure 22, as possible. The other means for reducing the iron is to use dispersants, which is discussed in Section 3.12.

2. Dependencies

a. Any discussion of pH must start with Figure 22 or a similar set of data, assuming that this is exactly applicable for modern SGs. Figure 22 shows that at 300˚C, for Cr_2O_3, NiO, and Fe_3O_4, the pHs of the respective minima are about 3.8, 6.0 and 6.7.

b. These experimental data in Figure 22 show that the slope of the alkaline side as well as the acidic side of each of these sets of data is about +1 or -1 meaning that an increase of one unit of pH gives an order of magnitude change of solubility.

c. Based on Figure 22, the target for secondary water treatment relative to minimizing iron solubility is about pH_T 6.7.

d. Figure 22 means that being at pH 6.7 produces a solubility for Cr about three orders of magnitude greater than that for iron.

e. Figure 50 indicates that the pH could be raised on the order of 0.5 pH units from the present in order to minimize iron deposits, and this means that the solubility of Cr would be increased about half an order of magnitude from a present reference.

f. The rate of S^y-SCC in Figure 92 (pH 12-13) is about two orders of magnitude greater than that

at AVT conditions, as shown in Figure 94, based on comparing crack growth rates although this comparison is approximate. This means that the coefficient on pH is about ½ in the correlation of log of crack growth rate vs. pH. An increase of pH from 7 to 7.5 would increase the rate of S^{y-}SCC 2-4 times.

g. Figure 81, while qualitative, shows that the intensity of PbSCC increases with increasing pH toward the alkaline direction. It would be reasonable to assume that the pH dependence of PbSCC is the same as that of the S^{y-}SCC, since the comparisons of each mode from the alkaline environments to the AVT environment is somewhat similar.

h. Relative to items f and g, the coefficient on pH for AcSCC(SO_4^{2-}) is as low as about ½ although negative following the data in Figures 97(a,b,c) and as high as about 0.8 following the data of Figure 97(e). It seems that using a ½ coefficient, up to the value of about 1.0, would be a reasonable correlation with pH in both acidic and alkaline directions. These, incidentally, follow qualitatively the patterns of the solubility plots.

3. Future occurrence

Raising the pH may well reduce the concentration of iron in the system as shown in Figure 50. However, there are at least two potential disadvantages of raising the pH:

a. Raising the pH by ½ a pH unit will increase the rates of PbSCC and S^{y-}SCC significantly.

b. Raising the pH will also increase the rate of dissolution of Cr from the metal surface and the passive film, as described in Section 3.14. Thus, the altered surface chemistry will change the nature of the degradation, e.g. this would convert a high chromium material like Alloy 690TT to Alloy 600.

c. The basis for the loss of Cr is shown in Figure 100, and it is related to the relatively high solubility of Cr in alkaline solutions. Here, the E-pH diagram of Figure 21(c) is compared with the solubility data of Figure 22. Figure 21(c) shows the clear basis for the solubility of Cr_2O_3 in even mild alkalinity. Under these conditions, it is reasonable that Cr would be preferentially dissolved from Fe-Cr-Ni alloys. The situation in Figure 100 leads to the preferential dissolution and possible SCC degradation as shown in Figure 101. M-1 in Figure 101(a) shows the condition of Figure 100. Figure 101(b), M-2, shows direct data from Lumsden and Stocker[183] at high pH using AES (Auger electron spectroscopy) profiling, which shows a substantial loss of Cr after 240 hours at 320°C, i.e. the Cr dissolves preferentially at high pH. Figures 101(c,d) show the dependence of LPSCC and AkSCC on Cr. Figure 101(e) shows schematically the effect of dissolving Cr preferentially on the degradation of the surface by first depletion of Cr and then SCC.

3.12 Dispersants

1. Introduction

Figure 55, as discussed in Section 2.8-9 shows that dispersants reduce iron by solubilizing iron deposits. Of course this work is still in progress, but it was sufficiently attractive to merit testing in an operating reactor as shown in Figure 55. The dispersed iron can then be removed in blowdown.

2. Dependencies

While removing iron by solubilizing is attractive, the action of dispersants may also affect degradation processes.

3. Future occurrence

The use of dispersants could accelerate the following processes of degradation:

a. PbSCC could be accelerated by breaking the bonds that immobilize Pb such as either the adsorbed condition or the Pb-containing phases.

b. S^{y-} could be similarly accelerated.

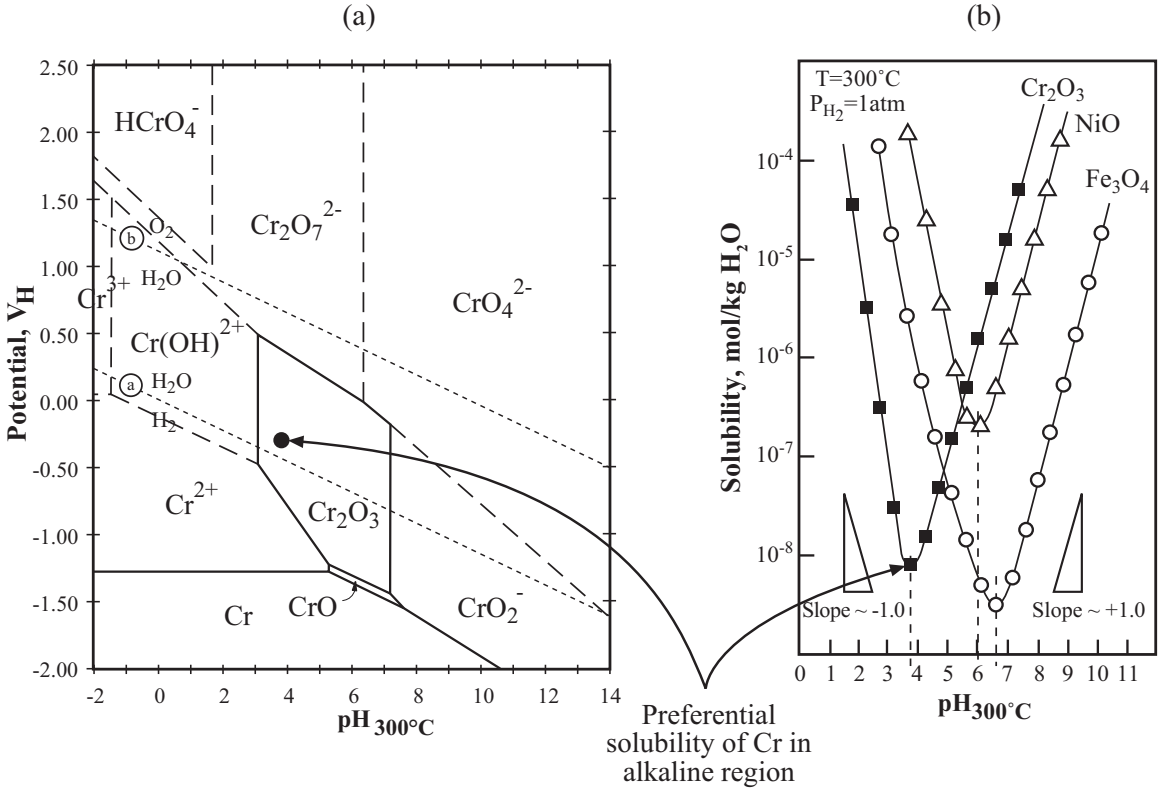

Figure 100 (a) E-pH diagram for Cr in water at 300°C. From Staehle and Gorman[5] and from Chen et al.[71] and Miglin.[72] (b) Solubility of Fe, Ni, and Cr oxides in water vs. pH at 300°C. From Arioka et al.[73]

3.13 OTSG Region

1. Introduction

Figure 14 shows the occurrence of SCC on the OD surfaces of the upper bundle in OTSGs. These free surfaces behave like superheated crevices.

2. Dependencies

These surfaces accumulate impurities, and with them Pb and S^{y-} as shown in Figure 102. This

upper bundle is the same as those shown in Figure 14. In Figure 102, both Pb and S^{y-} are shown to have been accumulated in SCC of the upper bundle. Regardless of the tube materials chosen, including Alloys 690TT and 800NG, PbSCC and S^{y-}SCC can occur.

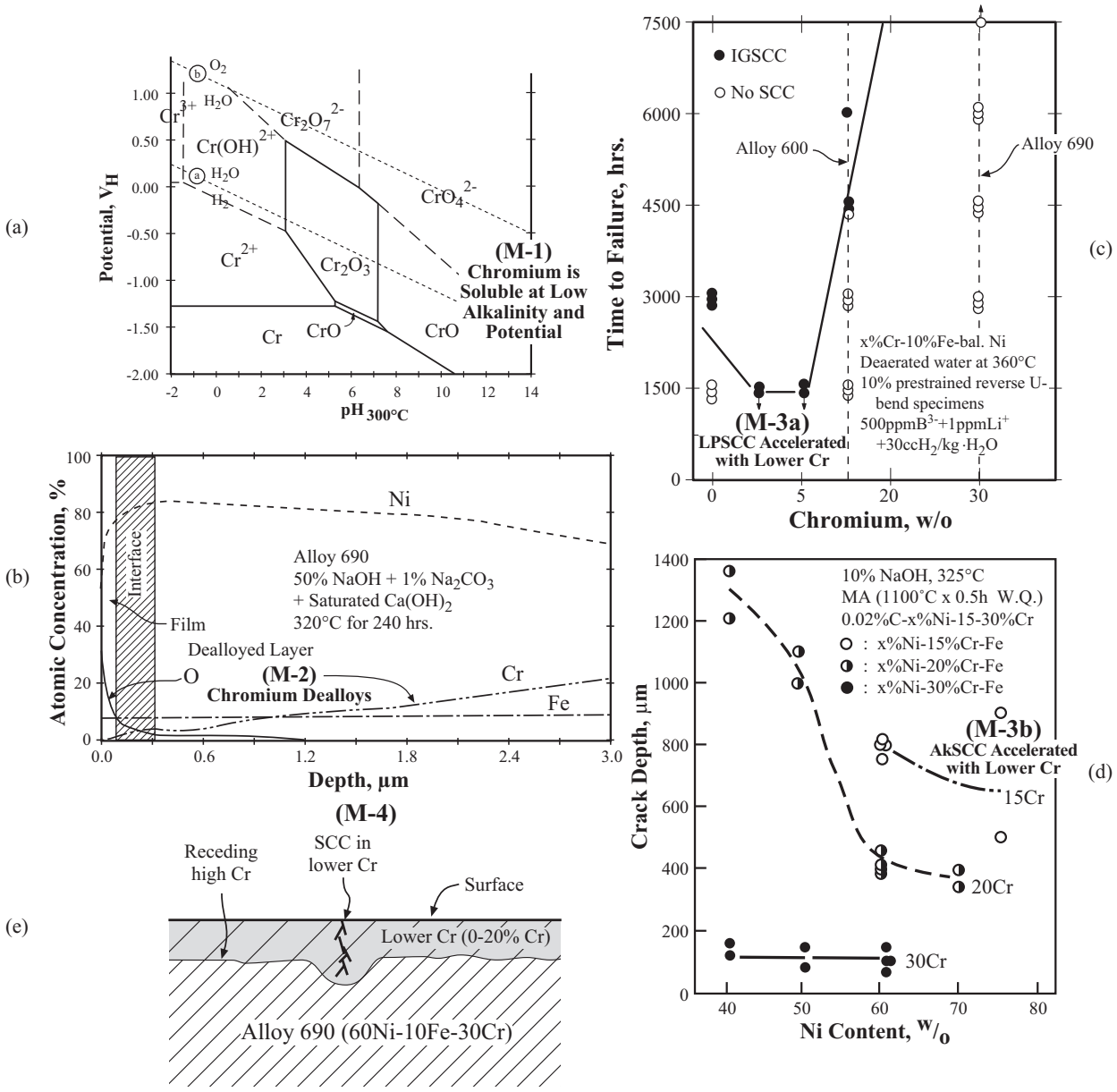

Figure 101 (a) [M-1] E-pH diagram for Cr in water at 300°C. From Staehle and Gorman[5] and from Chen et al.[71] and Miglin.[72] (b) [M-2] Atomic concentration vs. depth for Fe, Cr, Ni, O species for Alloy 690 exposed in concentrated alkaline solution for 240hr at 320°C. From Lumsden and Stocker.[183] (c) [M-3a] Time-to-failure vs. Cr for LPSCC. From Staehle.[43] (d) [M3-b] Crack depth vs. Ni for various Cr concentrations in high alkalinity at 325°C. From Staehle and Gorman.[5] (e) [M-4] Schematic illustration of depletion of Cr and subsequent SCC degradation.

Elevation, m	Composition, a/o														
	Ni	Cr	Fe	O	C	N	Si	Al	Mg	Ca	Sulfate	Sulfide	Zn	Na	Ni/Cr
8.8	16.93	1.62	-	34.43	40.91	2.61	1.77	-	-	-	0.14	-	-	0.88	10.45
10.1	15.15	1.60	0.07	35.99	41.38	0.58	3.39	-	-	-	0.18	-	Trace	-	9.47
10.4	6.41	0.64	-	37.04	39.07	-	6.25	10.12	0.48	-	-	-	-	-	10.02
11.2	6.19	2.90	0.89	29.47	46.22	1.23	3.31	8.79	-	0.76	-	-	-	-	2.13
11.8	9.21	1.52	0.76	34.98	49.20	-	2.78	-	-	-	-	0.83	-	0.57	6.06
12.6	13.30	0.94	0.80	45.62	35.11	1.17	1.56	-	-	-	0.45	-	-	-	14.15
13.8	18.51	2.38	0.90	31.91	41.08	-	4.67	-	-	-	0.55	-	-	-	7.78
14.2	9.78	2.48	0.58	39.12	43.13	1.21	2.01	-	0.38	0.37	0.42	0.22	-	0.33	3.98
15.0	11.58	0.93	-	41.06	45.12	0.89	-	-	-	-	-	0.42	-	-	12.45
16.7	6.02	2.72	1.53	37.27	41.48	0.09	3.33	3.82	1.42	1.09	0.79	-	0.09	-	2.21
Ductile Fracture	16-21	2-3	0.5-1.6	27-34	41-48	-	1-3	-	-	-	-	-	-	-	6.3-7.9

(a)

Location Designation #	a/o O	a/o Si	a/o S	a/o Ca	a/o Cr	a/o Fe	a/o Ni	a/o Pb	Ni/Cr	Impurities
49	26.5	0.3	0.3	0.0	33.7	4.5	32.8	2.0	0.97	Cr-Ni-O with Pb
50	2.3	0.5	0.2	0.0	11.4	7.7	80.8	0.2	7.1	Metal matrix
51	0.7	0.0	0.1	0.0	3.8	2.1	91.5	2.6	24.1	Fe-Cr-depleted boundary - with Pb
52	1.5	0.0	0.0	0.0	2.6	2.3	94.2	0.4	32.4	Fe-Cr-depleted boundary - with minor Pb
53	30.2	0.6	0.2	0.1	30.3	12.4	25.3	1.2	0.8	Cr-Ni-O with Pb
45	21.1	0.4	3.7	0.1	23.8	6.3	37.2	7.5	1.6	High Pb, S in degraded GB particle
48	28.8	0.7	2.7	0.0	30.1	5.8	29.2	4.6	0.97	High Pb, S in degraded GB particle
31	25.3	0.2	0.4	0.0	38.2	3.6	28.8	7.7	0.7	High Pb in degraded GB particle

(b)

Figure 102 (a) Chemistry inside cracks at increasing elevations inside OTSG. From Rochester and Eaker.[59] (b) Chemical analyses by nano-EDS (0.7 nm spot) of local regions. Near tip of SCC as identified by ATEM from OTSG. From Rochester.[58]

3. Future occurrence

Since Pb, SO_4^{2-}, and S^{y-} will accumulate on the upper bundle surface, it should be assumed that SCC can occur, regardless of prior scratches which accelerate the degradation, which are shown in Figure 14. It should be noted that Figure 14 shows significant SCC only after 12 years with Alloy 600SR. With tubing like Alloys 690TT or 800NG this SCC should not occur until longer times.

3.14 Loss of Cr from Metal Surface and Passive Film

1. Introduction

Modern SGs are tending to use materials with higher Cr, i.e. Alloys 690TT and 800NG, than Alloy 600 owing to their good performance, including good resistance to general corrosion, and

laboratory testing. However, alloys with higher Cr at the values of pH in AVT type of secondary environments, as well as primary environments, are expected to lose Cr by selective dissolution, as shown in Figures 100 and 101, over long times. The bases for such losses are discussed in Section 3.11. This long term loss of Cr before significant degradation can occur is an important category of precursors according to Figure 5.

This process of preferential depletion of more active alloy species is well known and has been studied actively since the middle 1960s by Pickering and Swann,[184] Pickering,[185,186] Newman et al.,[187,188,189] Sieradzki et al.,[190,191] and Staehle.[192]

The discussion on Figures 100 and 101 has emphasized preferential dissolution from the point of view of the pH vector. However, Cr is also unstable with respect to the vector of electrochemical potential in contrast to most important engineering materials including Fe and Ni as shown in Figure 21. Here, Ni exhibits broad insolubility with increasing potential; Fe indicates a soluble species at higher potentials but the breadth of stability larger than for Cr.

At higher potentials, Cr is unstable relative to forming the chromate ion, CrO_4^{2-} in the alkaline region. Potentials for the formation of the CrO_4^{2-} are within reach of the pH of PWR secondary chemistries if the potentials are slightly higher than what deaeration permits. However, oxidizing conditions as produced during layup and startup would place the PWR secondary environment in this domain. Thus, Cr in the mildly alkaline range is unstable both respect to pH and electrochemical potential. Both of these influences will tend to produce preferential depletion over long times

2. Dependencies

a. Some of the essential dependencies of preferential dissolution of active species are discussed in Section 3.11.

b. Figure 103 from the work of Sakai et al.[193] shows that Alloy 600MA sustains preferential depletion of Cr from surfaces at pH as low as 4.5 and 7 in HCl solutions. The pH at which the Cr is preferentially dissolving, in Sakai's work, is lower than that suggested as a minimum for such preferential dissolution by Figures 100 and 101. The mechanism for preferential dissolution at these lower values of pH is not clear but the result cannot be ignored over the long time. Figure 103 also shows data from the presence of Pb, which can be ignored in this discussion but are important in considering the fundamental mechanism of PbSCC.

c. Figure 104 from the work of Staehle[192] and Rockel and Staehle[194] shows the preferential dissolution of Ni and Cr from Type 304 stainless steel as a function of potential when exposed to boiling $MgCl_2$. Figure 104 also shows the polarization curve for this alloy as determined by calculating the average currents using Faraday's Law from the amount of material dissolved. This approach of measuring the amount of dissolved species was necessary in order to find the full polarization curve below the open circuit potential. While these results are not entirely consistent with predictions from the E-pH plots of Figure 21, they show that the active material may dissolve preferentially according to mechanisms that are not readily rationalized but are nonetheless important.

3. Future occurrence

As the Cr is removed from the alloy as noted in Figures 100 and 101, the surface changes its composition from that of Alloy 690 to that of Alloy 600 and to even lower Cr. This implies that corrosion processes that might have been resisted by Alloy 690 would be available at longer times

and the alloy would behave more like Alloy 600 and with less Cr as well. These implications are discussed in Section 3.11.

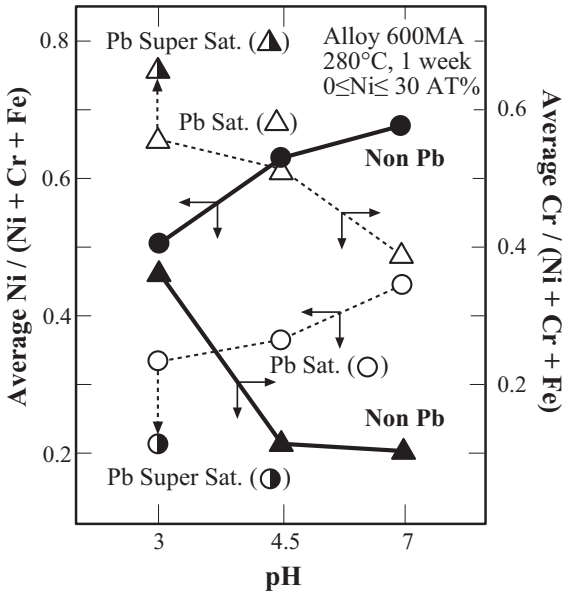

Figure 103 Average relative concentrations of Ni and Cr after exposure to solutions with and without $PbCl_2$ at 280°C for one week. pH adjusted with HCl. From Sakai, et al.[193]

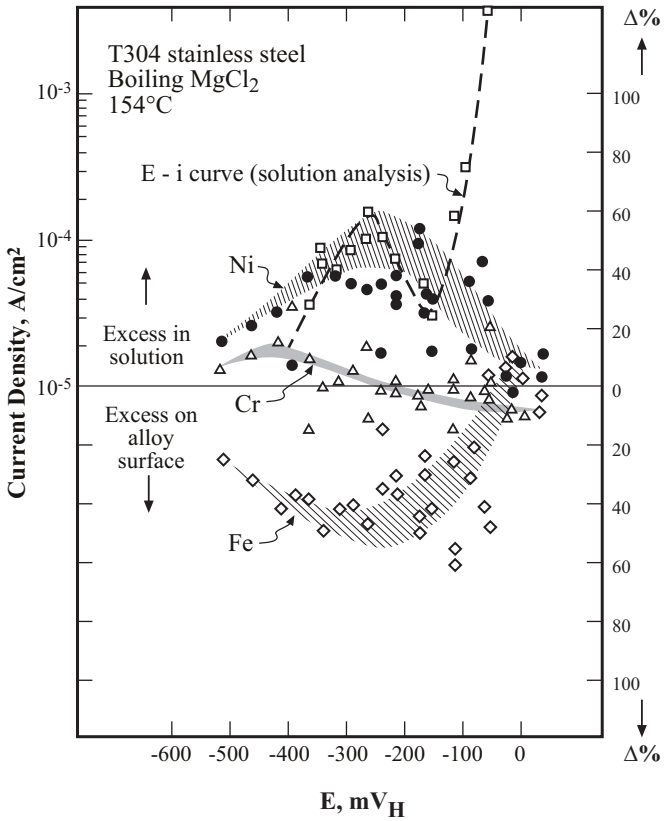

Figure 104 Current density and relative depletion of Fe, Cr, and Ni vs. potential for Type 304 stainless steel exposed to boiling $MgCl_2$ at 154°C. From Staehle[192] and Rockel and Staehle.[194]

3.15 Multiple Chemistries, "Pure" May Not Be Desirable

1. Introduction

With the nominal improvements in SGs through improved tubing materials, improved TSP designs, more pure water chemistry, and special changes in additives, it seems that the rates of degradation and fouling have decreased. However, few, if any, of these improvements have been actually evaluated by removing tubes and evaluating TSP, nor TTS joints using advanced surface technology, nor has the time dependence of these improvements been evaluated by careful examinations of surfaces over time.

The present direction for water chemistry control is "pure is better." This has seemed beneficial. However, such a pursuit of greater purity may abet degradation if the impurities are beneficial with respect to minimizing the release of Pb or affecting similarly other degradation processes.

However, regardless of purity, e.g. the concentration of Pb from 1-100 ppt, impurities can concentrate on superheated surfaces.

Intentionally added species for primary and secondary sides are:

- Advanced amines
- Boron
- TiO_2
- Zinc
- Hydrazine
- Dispersants
- Hydrogen
- LiOH

These intentional additives interact with low concentrations of feedwater impurities such as Pb and SO_4^{2-} as well as those shown in Figures 38, 41, and 80 that seem to come from nowhere. The fact that there are important interactions among impurities is shown by the lack of extensive PbSCC in the Alloy 600 plants due most likely to the immobilization of Pb. The possibility of forming phase compounds between lead and other species can be seen from the relatively high concentrations of other species in superheated crevices as shown in Figures 11, 14, 38, 41, and 80.

It seems prudent to evaluate these additions and their interactions on modes of degradation, both on fouled free surfaces as well as on superheated surfaces, that are both occluded and not (e.g. OTSG).

2. Dependencies

Important dependencies, one at a time in secondary chemistry, seem to be the following:

- Advanced amines reduce iron as shown in Figure 50.
- Boron additions reduce the rate of SCC of Alloy 600 as shown in Figure 51.
- TiO_2 seems to be beneficial but results are mixed as shown in Table 1.
- Zinc seems to stabilize spinel type protective films as shown in Figure 53.
- Hydrazine lowers oxygen concentration.

- Dispersants solubilize iron oxides and facilitate ready blowdown as shown in Figure 55.
- Impurity Pb concentrates on metal surfaces to produce PbSCC as shown in Figure 78.
- Impurity sulfate reacts with hydrazine to produce low valence sulfur species and S^{y-}SCC as shown in Figure 49.
- Impurity sulfate concentrates to produce AcSCC as shown in Figure 97.
- Substantial absence of dissolved hydrogen on the secondary side raises the electrochemical potential as shown schematically in Figure 24.
- Other impurities, e.g. Al, Si, participate in forming deposits in superheated crevices as shown in Figures 38, 41, and 80.

How this range of intentional and impurity chemicals interacts is not clear, nor have such interactions been evaluated by pulled tubes or removed tube supports.

3. Future occurrence

Possible adverse interactions from the interactions of the many intentional and adventitious species are not clear. However, the precedent for excessively pure systems leading to degradation in corrosion is not good and there are many examples.

3.16 Cold Work

1. Introduction

Cold work is well known to accelerate both initiation and propagation of SCC following Figures 19(b) and 62. Cold work is accelerative in cases were only the surface is cold worked, as with scratches shown in Figures 14 and 63, and where the full cross section is cold worked as with expanded tubes or with heat affected zones in welds. Available data now show that cold work accelerates the SCC of Alloy 690TT even in pure and primary water.

2. Dependencies

Cold work accelerates the growth rate of SCC and lowers the stress for initiation. However, these dependencies are not so quantitative. Cold work should be evaluated in testing.

3. Future occurrence

All of the locations where surface in bulk cold work occurs should be carefully evaluated together with local chemistry. SCC type degradation should be expected over time as stimulated by cold work. Investigation of such cold work in operating plants should consider both bulk and surface cold work. Special attention should be given to such locations since they are not routinely inspected except at welds and TTS expansions of tubes.

3.17 Wear

1. Introduction

Some wear has traditionally occurred in the anti-vibration bar locations. These seem to reach self-limiting conditions. More recently, excessive wear has been occurring at the TSPs in OTSGs.

This wear seems more aggressive than that in the AVBs. This problem is still being evaluated.

2. Dependencies

In addition to the loss of material, it seems that the continued impingement that produces wear should also be producing local cold work that could initiate SCC. While such SCC has not been observed, it should not be neglected.

It could also be argued that the impingements, which produce wear, could be producing a kind of shot peening that would inhibit the initiation of SCC.

While the penetration rate of the AVB wear seems to have abated, that in the OTSGs is not yet clarified.

3. Future occurrence

Wear, in general, depends on design including flow rates, tube geometries, and TSPs. The wear rate may depend some on the environment but seems mostly to depend on these design aspects.

4.0 Non-Tubing Aspects of SGs

4.1 Introduction

Figure 2 identifies locations where degradation can occur in SGs including tubing and non-tubing locations. Also, this figure identifies potential degradation of immediately ancillary equipment including steam lines, feedwater lines, turbines, and attachment welds to primary and secondary piping. Figure 73 also identifies locations where Alloy 600 and Alloy 182/82 are present mainly in the primary system, including the SG. This figure indicates all of those locations, following Alloy 600 tubes, where LPSCC should occur.

Most of the attention in the past for SGs has been given to the performance of tubes. Since the tubes have a relatively thin wall and must endure the concentrated environments that accumulate at tube supports, this attention is reasonable. However, there are certain aspects of SGs where other degradation can occur and where this can be serious; such aspects are included in this section.

4.2 SCC of Vessel

1. Introduction

Stress corrosion cracking has been observed near the upper girth welds of SGs, and a report and technical paper on these incidents has been prepared by Fleming et al.[102,103] Essential features of these SCCs are the following:

- By the time of publication of the references in 1993-94, such SCC had occurred in six plants.
- The alloys affected were SA 302Gr.B (normalized) or SA 533Gr.A Class 2 (quench and tempered Mn-Mo low alloy steel).
- SCC was oriented circumferentially with some branching.
- SCC varied from shallow to through wall and from a few mm to 3 m in length.
- SCC was found in the weld, HAZ, and matrix.

- Post weld heat treatments (PWHT) in affected SGs were in the range of 537°C and in the non-affected plants in the range of 593°C.
- SCC seems to have initiated at pits, which seem to have formed in association with oxygen contamination.
- It is not clear to what extent the SCC grew at operating or shut down conditions.
- It is not clear to what extent cyclic loading was important.
- There was no information on the magnitudes of residual stresses relative to applied stresses.

2. Dependencies

There are few data on the dependencies of initiation and propagation on temperature, stress, PWHT, welding, electrochemical potential, and water treatment, that provide any bases for prediction. No significant experimental work was undertaken to assess the primary dependencies of this SCC.

3. Future occurrence

There are no bases for assuring that future girth weld SCC could not continue to occur especially at longer times as load cycles increase and as secondary environments change.

SCC at girth welds should be expected in the future.

4.3 Welds on Primary Piping Attached to SGs

1. Introduction

While primary piping is outside the SG proper, the SG is connected to the primary systemwith such piping, and its integrity is important to the reliable operation of the SG. Some SCC has been occurring at welds in this piping as described by Bamford and Hall.[158] Figure 10 shows an example of SCC in a weld at the outlet of the reactor from the Summer plant.

Welds in the primary system are inspected routinely, but the Summer weld went undetected until the wall was perforated. Welds are often difficult to inspect.

2. Dependencies

SCC at welds in the primary system has been associated with Alloy 182/82 weld metal as noted in Figure 10. Figure 73 shows the locations of Alloy 600 or 182/82 welds that may be prone to further SCC.

3. Future occurrence

Structural materials, thick sections of Alloy 600, as well as Alloy 182/82 compositions will continue to sustain SCC. Replacement materials, such as Alloys 690 and 152/52 have shown significant resistance to LPSCC, although the effects of cold work, microstructure, and residual stresses have not been fully investigated, and reliable future performance of these advanced materials cannot be assumed.

4.4 Divider Plates

1. Introduction

The divider plate is located at the bottom of the SG and separates the hot incoming water from the cooler outgoing water. This divider plate has been fabricated from Alloy 600 and is welded by welding materials Alloys 82 and 182. These divider plates have sustained SCC; and as this degradation occurs, they are being replaced with improved materials.

2. Dependencies

Divider plates are much thicker than tube walls although both mainly have been fabricated in the past from Alloy 600MA. LPSCC in divider plates seems to follow the same dependencies on temperature and stress as the tubes. Thus, other conditions being equal, the time for LPSCC to occur in divider plates would follow the ratio of thicknesses of divider plates to tube walls.

3. Future occurrence

Divider plates fabricated from Alloy 600MA can be expected to sustain continued degradation.

It should be noted that Alloy 690TT sustains LPSCC when cold worked although the detailed dependencies do not seem to be well established.

4.5 Low Temperature Crack Propagation (LTCP)

1. Introduction

Certain high nickel alloys sustain a kind of low temperature crack propagation, LTCP; in particular, Alloys 600 and 690 do not sustain this phenomenon significantly but Alloys X-750, 182/82 and 152/52 do so in decreasing order of intensity. This phenomenon occurs at nominally less than 150°C and seems to be a type of hydrogen embrittlement. LTCP was first recognized in 1999 in a series of papers by Mills and colleagues,[195,196,197,198,199] and has been reviewed by A.G. Demma and R. Jones.[200] While LTCP represents a serious form of degradation, it appears to be restricted by temperature and alloy composition.

2. Dependencies

LTCP occurs mainly in Alloys X-750, 182/82 and 152/52 when the following conditions are met:

- Temperatures are less than about 150°C.
- Dissolved hydrogen is less than 150 cc/kg of water but above 0 (for X-750) and 10 cc/kg for the other materials. Note that primary water contains about 25cc/kg.
- Sharp initiating cracks are available from the environment side.
- The applied stress intensity exceeds the critical stress intensity factor for LTCP as determined from experiments.
- The loading rate is slow.

3. Future occurrence

Since the critical temperature for LTCP is below normal plant operating conditions, these lower temperatures, as well as loading rates required for degradation, can occur only at conditions of startup and shutdown. Analyses of operating conditions, as identified by Demma and Jones[200] show that the conditions necessary for LTCP can occur only on shutdown for some plants.

4.6 Cold Work

1. Introduction

Cold work is of concern for most thick sections as well as for surfaces where the surface has been abused or otherwise treated or machined with a resulting increase in surface hardness. Figure 62 illustrates the general effects of cold work on properties of Alloy 600. This example is typical of most effects of cold work. Alloy 690TT also sustains LPSCC when cold worked.

Cold work also includes surface scratches as noted in Figures 14 and 63.

2. Dependencies

In general, the crack velocity increases with increasing cold work, and the K_{Iscc} decreases. Abundant data on these dependencies are in the literature.

3. Future occurrence

Cold work, especially in piping, is often not inspected. Therefore, cold work where inspections are not usually carried out should be carefully reviewed.

4.7 Flow Assisted Corrosion, FAC

1. Introduction

FAC is important to steam generators since it occurs in both the steam exit and the feedwater entry piping as well as occurring sometimes at tube supports. Figure 7 shows an example of an explosion resulting from thinned walls in the feed train of a nuclear plant. Tapping has reviewed significant issues associated with FAC.[67,201]

2. Dependencies

FAC is an electrochemical process that depends on velocity. FAC is generally maximum in the region of 130 to 180°C for streamlined and two phase flow, respectively. FAC is maximum for iron base alloys in the lowest potential range, since the protective film in this range is the relatively non-protective magnetite and since this is also the natural range of potential in PWR secondary systems. This means that the presence of hydrazine tends to accelerate FAC, although there is some controversy about the details and dependencies. FAC of iron base alloys is also maximum for low alloy or carbon steel. Adding about 1% Cr produces a major improvement as shown in Figure 18.

During FAC, hydrogen is produced and enters the steel. There is no evidence that such hydrogen has actually produced any special damage but it should not be neglected in design or in future experiments.

3. Future occurrence

With time it is expected that many of the locations, which are prone to FAC owing to their being low carbon steel, will be replaced with alloys containing higher Cr, following the well-established effect of Cr as shown in Figure 18. The Cr concentration in these replacements would be in the range of 0.5 to 2.0%.

However, it is known that SCC should be occurring in the present carbon steel used in feedwater trains, but, generally, no such SCC occurs. This lack of SCC can most likely be explained by the fact that the FAC penetration rate exceeds the rate of initiating SCC so that the SCC never reaches the propagation condition. If a higher Cr material is used, the FAC penetration rate will be much less and the penetration rate of the initiation stage of FAC will be exceed the penetration rate of FAC. Such a sequence of events is described in Figure 105.

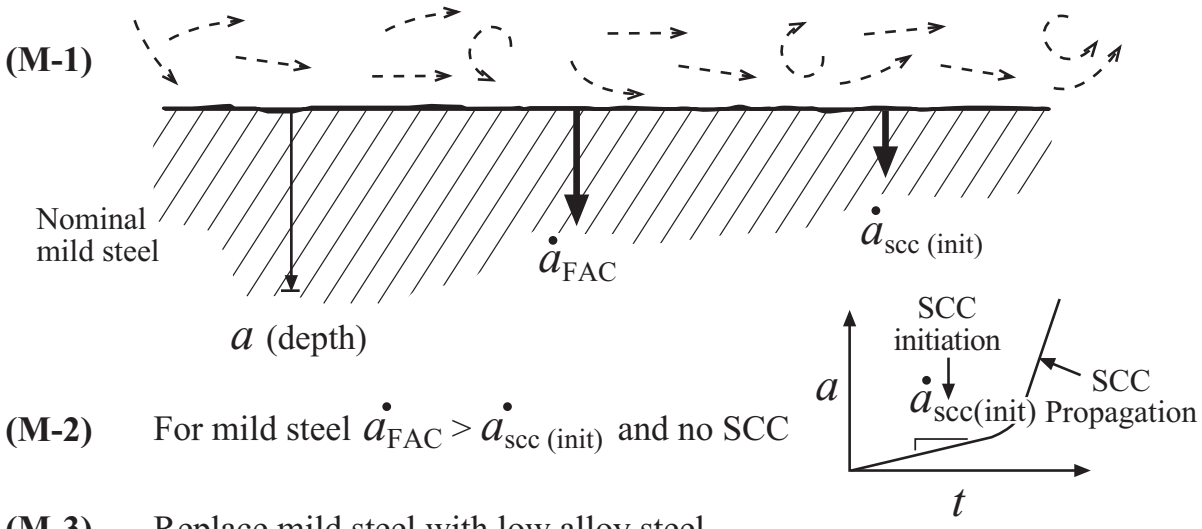

Figure 105 Schematic illustration of the relative rates of FAC penetration rates compared with the rates of initiation penetration for the cases of carbon steel and a higher alloy steel. Conditions for SCC damage defined.

4.8 S^{y-} Carryover and SCC in Turbines

1. Introduction

Volatile reduced sulfides, which are described in Section 2.8-4, Figure 49, and which are produced in the secondary side of a SG, will inevitably be carried to the turbine as suggested in Figure 106. In the turbine, the blades, attachments, and rotor are all fabricated from relatively

high strength steels, and the environment is deoxygenated and wet. It is likely that the high strength turbine steels are prone to intense SCC in the simultaneous presence of these sulfides and deoxygenation.

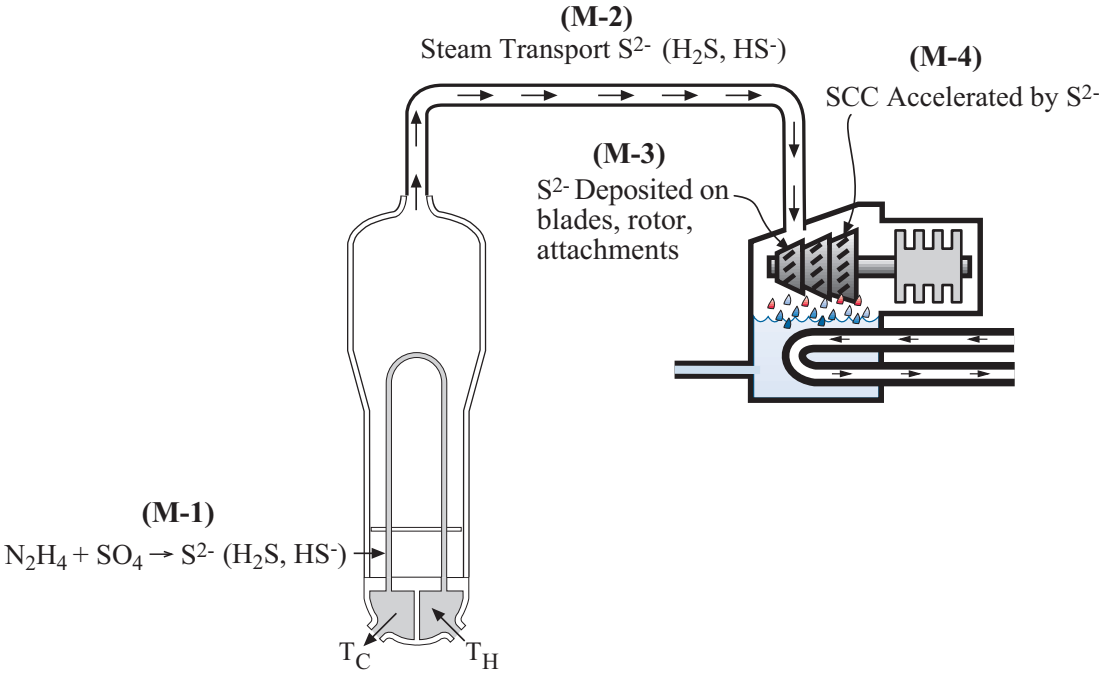

Figure 106 Schematic illustration of the carryover of S^{y-} from the SG to turbine together with the chemical reactions associated with the reduction of sulfate impurities by hydrazine.

The likelihood for SCC degradation by S^{y-}SCC is high depending on where the sulfide accumulates and the proneness of the steels to SCC in the conditions of the turbine and the reduced sulfur.

There are no reported incidents of such S^{y-}SCC occurring in turbines, but it is also not clear that such an option has been considered or the carryover of sulfide has been quantitatively evaluated. However, there are reported incidents of SCC in turbine components.

2. Dependencies

The occurrence of S^{y-}SCC depends on the presence of reduced sulfur, and the sensitivity increases with increased strength of the steel. Such reduced sulfur results from the reduction of impurity sulfate by hydrazine as described in Section 2.8-4. Since the presence of such reduced sulfur, aside from sulfur at all, has not been investigated in nuclear turbines it is not possible to assess the likelihood of such S^{y-} related failures.

The work of Daret et al.[106] shows that the low valence sulfur is substantially disproportionated to the steam phase by a factor in the range of about 100 as shown in Figure 49. While the species that is actually volatilized is not clear, the disproportionation of the sulfur has been measured.

This disproportionation to the steam phase would be important both to the local steam phases in two-phase superheated crevices, as shown in Figure 38, and to carryover to the turbine.

3. Future occurrence

The first step in assessing the possible occurrence of S^{y-}SCC is to simply take an inventory of turbine surfaces to determine what species accumulate on the surfaces. Further, provisions should be made to identify the valence of any sulfur.

If such preliminary inspections show the presence of sulfur, and if, especially, this sulfur is shown to be lower valence, then some preliminary SCC studies should be carried out for materials of the blades, attachments and rotors. Studies of initiation as well as propagation should be considered.

Further, when inspections find cracks in turbines, the surfaces should be chemically analyzed and especially for sulfur in its low valences.

4.9 Shutdowns, Layups, Startups

1. Introduction

During the evolution of shutdowns, layups, and startups, adventitious impurities have entered the reactor environments in the past, and certain corrosion processes can be linked to such contamination, e.g. mainly by oxygen but sometimes including chloride or sulfates. For example, pitting has been observed in the welded upper transition as discussed in Section 4.2, and this pitting is considered to have initiated much if not all of the SCC in the upper girth welds. Other such pitting related to contamination has been observed in steam generators. Also, lead impurities are sometimes introduced by lead blankets or lead hammers.

2. Dependencies

The primary influences producing degradation are oxygen and species, such as chloride, that promote pitting.

3. Future occurrence

The occurrence of accidents due to pitting and/or subsequent SCC seem to have been reduced, if not prevented, by minimizing oxygen and other water impurities during shutdown, layup, and startup times.

5.0 Work Needs Doing

5.1 Introduction

The purpose of this section is to identify what tasks are relative to predicting future degradation in SGs.

5.2 Tasks

Task 1: Line Contact Tube Supports, TSP

The purpose of this task is to characterize line contact crevices, as in Figure 39, in order to assess how PbSCC, S^{y-}SCC, and possibly other modes of degradation can occur. This is important

because there are so many of these crevices and since such modes of degradation can readily degrade Alloys 690TT and 800NG. Specific subtasks are:

Task 1-1: Assess the properties of line contact crevices in service.

Remove a set of line contact crevices from the hot side at the first support having a long exposure. Evaluate the deposits with respect to distribution, porosity, chemicals and their distribution together with chemical bonding information, and thermal conductivity. Evaluate the interaction of secondary chemical additives in these crevices.

Task 1-2: Assess the properties of the tube segment associated with the TSP segment (taken to give sections within and outside the TSP).

Evaluate the tube geometries with respect to locations of contact and between contacts: corrosion damage; properties of passive film and substrate chemistry distribution with AES and XPS profiling; ATEM assessment of degradation. The same tubing should be used to evaluate the primary surface with respect to degradation and chemistry of passive films and the alloy substrate. Note changes of surface composition as discussed in Figures 100 and 101.

Task 1-3: Compare water chemistry evidence (blowdown, shutdown) taken before sample removal with chemistry of sample.

Determine the relationship between chemical description of crevices taken from exterior chemistry with direct measurements taken from removed specimens.

Task 1-4: Modeling line contact crevice and tube.

Figure 39(d) shows that the line contact crevice includes: large flow gradients, large thermal gradients, and large chemical gradients. These gradients should be modeled in such a way as to support 5.2-2.

Task 1-5: Develop a line contact tube support test facility.

A realistic experimental facility to study line contact crevices and tube(s) should be built and operated so that it can be used to develop a model for prediction with inputs from the other subtasks. This facility should contain monitoring capability for electrochemical properties, thermal properties, streaming potentials, and flows in the same ranges as on operating surfaces.

Task 2: TTS Crevices

The purpose of this task to characterize TTS crevices, as in Figures 42-46, in order to assess how PbSCC, S^{y-}SCC, AcSCC(SO_4^{2-}) and possibly other modes of degradation, can occur in this context in addition to and beyond the TSP geometry. This is important since the conditions seem more severe, and the SCC is likely to be circumferential in contrast to axially dominated SCC at the TSPs. This increased severity, relative to the TSP crevice, results from the expansion stresses and cold work of the tubes, possible bending stresses due to the tubesheet bending, higher temperatures, and ready availability of Fe_3O_4 from corroding the tubesheet. Finally, there is the possibility of the "burrowing" crevice that is described in Figure 45 of Section 2.8-1c. These chemical evaluations are important because the expected occurrence of PbSCC, S^{y-}SCC, and AcSCC are so aggressive

to Alloys 800 and 690TT. Specific subtasks are:

Task 2-1: Assess the properties of TTS crevices in service.

Remove a set of TTS crevices, where the severity of bending stresses is greatest. Evaluate the deposits with respect to distribution, porosity, chemicals and their distribution together with bonding information and thermal conductivity. Evaluate the oxide formed by the oxidation of the tubesheet material; also evaluate deposits that form on the TTS. Determine the presence of secondary additives and their distribution. Determine the nature of forces being exerted by the expanding corrosion products. Finally, determine whether the "burrowing" phenomenon occurs as suggested in Figure 45.

Task 2-2: Assess the properties of the tube segment associated with the TTS segment (taken to give sections within and outside the TTS as well as deep inside the TS crevice).

Evaluate the tube with respect to locations along the length outside and inside the TTS: corrosion damage and distribution; chemical properties of passive film and substrate chemistry using depth profiling with AES and XPS; ATEM assessment of degradation; extent of burrowing; properties of the tubing including microhardness distribution and microstructure over the length of the expanded region. Also, review the fabrication scheme of the tube and especially the mode of expansion. The same tubing should be used to evaluate the primary surface with respect to degradation and chemistry of passive films and the alloy substrate.

Task 2-3: Compare water chemistry evidence (blowdown, shutdown) taken before sample removal with chemistry of sample.

Determine the relationship between the chemical description of crevices taken from exterior chemistry with direct measurements taken from removed specimens. Also, compare chemistry of deposits and surfaces between the TSP and TTS surface deposits and metal surface reactions.

Task 2-4: Modeling TTS crevice and tube.

Figure 46 shows the complexity of conditions at the TTS with respect to the TTS crevice: tube above the TTS, tube below, expanded tube, small crevice, thin surface deposits, expanding corrosion products, burrowing, cold work, and residual stresses in the tube. A model for this system should be developed to help understand the experimental data and develop insights for minimizing degradation.

Task 2-5: Develop a TTS test facility.

A realistic experimental facility a TTS crevice and tube(s) should be built and operated to facilitate modeling the course of PbSCC, S^{y-}SCC, AcSCC(SO_4^{2-}), and others with inputs from the other subtasks. This facility should contain monitoring capability for electrochemical processes, thermal properties, measuring expansion forces from growing oxides, and a capacity to assess the burrowing phenomenon.

Task 3: Fouling and Associated Degradation on Free Surfaces

The purpose of this task to characterize fouled free surfaces, as in Figure 47, in order to assess

how PbSCC, S^{y-}SCC, AcSCC(SO_4^{2-}) and possibly other modes of degradation could occur on a free surface and degrade Alloys 690TT and 800NG. Specific subtasks are:

Task 3-1: Assess the properties of fouled surfaces in service.

Remove fouled surfaces from the hot side over the length of the tube. Evaluate the deposits with respect to their distribution, porosity, structure, chemicals (including inhibitors) and their distribution together with chemical bonding information, thermal conductivity.

Task 3-2: Assess the properties of the tube segment associated with the fouling segment.

Evaluate the tube with respect to: corrosion damage; properties of passive film and substrate chemistry distribution with depth profiling AES and XPS; ATEM assessment of degradation.

Task 3-3: Compare water chemistry evidence (blowdown, shutdown) taken before sample removal with chemistry of sample.

Determine the relationship between chemical evidence from water chemistry with direct measurements taken from removed specimens.

Task 3-4: Modeling fouling deposition.

Figure 47 shows that fouling deposits are complex and change over time. Modeling should account for the distribution of deposits along the length of tubes and the structure and chemistry of deposits including secondary additives and impurities. Modeling should also account for measurements from blowdown compared with direct measurements.

Task 3-5: Develop a fouling test facility.

A realistic experimental facility for fouling should be built so that it can help develop a model for prediction of fouling over long times with inputs from the other subtasks. This facility should contain monitoring capability for electrochemical properties, thermal properties, and flows.

Task 4: OTSG Upper Bundle Surfaces

The purpose of this task is to assess only the upper bundle of OTSG SGs and particularly the superheated surfaces where SCC has occurred in the past. The new tubing for the OTSGs is Alloy 690TT.

Task 4-1: Assess the properties of fouled surfaces in service.

Remove tubes particularly over the length of the upper bundle region. Evaluate the deposits with respect to their distribution, porosity, structure, chemicals, and their distribution together with chemical bonding information, thermal conductivity.

Task 4-2: Assess the properties of the tube segment associated with the superheated segment.

Evaluate the tube with respect to: corrosion damage; properties of passive film and substrate chemistry distribution with AES and XPS depth profiling; ATEM assessment of degradation.

Task 4-3: Compare water chemistry evidence (blowdown, shutdown) taken before sample removal with chemistry of samples.

Determine the relationship between chemical evidence from water chemistry with direct measurements taken from removed specimens.

Task 4-4: Modeling deposition.

Figure 14 shows that deposits on OTSG upper bundle in the superheated region are complex. Modeling should account for the distribution of deposits along the length and the structure and chemistry of deposits including secondary additives and impurities. Modeling should also account for measurements from blowdown compared with direct measurements.

Task 4-5: Develop a upper bundle test facility.

A realistic experimental facility for monitoring the deposition of chemistry on upper bundles should be built. This facility should contain monitoring capability for flow, chemistry of steam, and deposition rate of impurities. Specimens should be removable for study of surface chemistry and the evolution of degradation.

Task 5: Quantify PbSCC

The purpose of this task is to quantify the evolution and mitigation of PbSCC on tubing of Alloys 690TT, 800NG, and possibly Type 321SS in realistic operating conditions. In order to predict such processes, understanding the following under realistic conditions are important:

- Mechanism of PbSCC initiation and propagation.
- Immobilization and release of Pb.
- Occurrence of PbSCC in a relevant range of potentials and pH.
- Effects of water treatments including additives that change the pH and solubility of Pb, e.g. advanced amines and dispersants.

Task 5-1: Develop a dedicated facility for well controlled testing of PbSCC

A dedicated facility for studying PbSCC is required since the existing data are not usefully quantitative for developing predictions of occurrence and mitigation. At least three dedicated units would be required. These facilities should be capable of testing at conditions similar to those expected in both TSP and TTS conditions, where the relevant environments are in the occluded regions. Some of these facilities should be capable of modeling conditions where the concentration of lead starts with the typical feed water concentration and evolves to those in superheated crevices.

Dedicated facilities are required since Pb contamination would alter results from studies should they involve other environments.

Task 5-2: Mechanistic studies, initiation and propagation

These mechanistic studies are directed toward predicting initiation and propagation of PbSCC in realistic environmental, metallurgical, and stress conditions. These studies would also consider the effects of thick reaction products produced inside advancing SCC according to Figures 88 and 89.

Task 5-3: Mitigation and release

These studies depend on results from Task 5-2. Once the occurrence of PbSCC can be predicted, it is necessary to know how it can be mitigated. Mitigation might also involve reducing the amount in the feedwater.

Task 5-4: pH and potential dependence, including advanced amines and dispersants

The solubility of Pb is generally minimum in the neutral region although, nominally, Pb is fully soluble over the range of pH. The suggestion of a minimum solubility effect comes from the pattern of PbSCC in Figures 21(b) and 81. The dependence of PbSCC on pH is important relative to the use of higher ammonia or advanced amines to reduce the amount of soluble iron. Thus, the range of pH studied should include a range somewhat greater than those expected both in alkaline and acidic directions owing also to effects of local concentrations due to superheat.

In addition to considering the effects of pH on PbSCC, effects of other additives, e.g. Zn, B, and TiO_2, should be investigated. Possibly the most important to consider are dispersants as discussed in Section 2.8-9 and Figure 55. These dispersants are important because they might cause the immobilizers to release lead and accelerate PbSCC.

Dependencies on steam and liquid phases should be included since it has been established that PbSCC in the steam phase is aggressive and since some steam phase probably exists even in the line contact but certainly in the TTS crevices.

Task 6: Quantify S^{y-}SCC

The purpose of this task is to provide bases for predicting and mitigating S^{y-}SCC. The background of S^{y-}SCC is not so well established, as for PbSCC; the essence of this background for S^{y-}SCC is described in Sections 2.8-4 and 3.4. While the background is not extensive, the S^{y-}SCC is aggressive to both Alloys 690TT and 800NG based both on testing in alkaline and neutral solutions as well as observations from failed tubes.

Predicting and mitigating S^{y-}SCC also needs to be considered relative to the fact that low valence sulfur is produced by the reduction of impurity sulfates by hydrazine. This sequence is important to the occurrence of S^{y-}SCC, and its quantitative aspects need to be considered.

Task 6-1: Develop a dedicated facility for well controlled testing of S^{y-}SCC

A dedicated facility for testing S^{y-}SCC is required since the existing data are not usefully quantitative for developing predictions of degradation and mitigation. The data are meager, especially relative to the possible damage that can result as shown in Figures 49 of Section 2.8-4 and Figures 92-96 of Section 3.4. At least three dedicated units would be required. These facilities should be capable of testing at conditions similar to those expected in both TSP and TTS conditions where the relevant environment are in the occluded regions. Some of these facilities should be capable of modeling conditions where sulfate is reduced by hydrazine.

Task 6-2: pH and potential dependence

S^{y-}SCC has been studied in high alkalinity, as shown in Figures 92 and 93 and as discussed in Section 3.4, and in AVT conditions as in Figure 94. Unlike the data for PbSCC, the data for S^{y-}SCC are much less extensive. The data of Figure 94 compared with Figures 92 and 93 suggest

that the rate of S^{y-}SCC is about 100 times less in the AVT environment than in the highly alkaline environments. This is surprising since, as shown in Figure 25, the low valence sulfur should be more soluble with decreasing pH and therefore should become more aggressive in the region of pH where the secondary side operates both in bulk and occluded environments. However, the comparison of Figures 94 with 92 and 93 suggest that the S^{y-}SCC is a minimum in the AVT environment just as with PbSCC. Thus, there are some important fundamental matters, which need to be clarified, in order to provide a good basis for prediction.

This task would investigate the dependence of S^{y-}SCC on pH, potential, and concentration. Also, at a lower level of effort, the effects of dispersants and presently used inhibitors would be investigated. The dispersants might be important, as they could cause any sulfide compound to dissolve or de-couple, thereby releasing active reduced sulfur species that would accelerate S^{y-}SCC. Also, the trend toward raising the pH, in order to reduce the secondary Fe, would increase the rate of S^{y-}SCC.

Dependencies in steam and liquid phases should be included since S^{y-} disproportionates by about 100x to the steam phase.

Task 6-3: Mechanistic studies, initiation and propagation

Mechanistic studies are necessary in order to predict future degradation due to S^{y-}SCC. These mechanistic studies would consider aspects relative to the occluded and superheated environments. Nothing is known about the most aggressive of the reduced sulfur species (e.g. S^{2-}, HS^-, H_2S), the concentration dependence, stress dependence, nor the segments of initiation and propagation.

Further, while the S^{y-}SCC is little understood, the rate of reduction of SO_4^{2-} impurities by hydrazine, the pH dependence of this reaction, its competitive effects on potential with low hydrogen as occurs on the secondary side of SGs, and the presence of intentional secondary additives are not understood nor quantified.

S^{y-} is known from the work of Daret in Sections 2.8-4 and 3.4 to disproportionate substantially to the steam phase. However, the identity of the species that disproportionate are not known nor is the relative aggressiveness in the steam and water phases, which contain the S^{y-1} species known.

Task 6-4: Mitigation

These studies depend on results from Task 6-3. However, there is evidence from the work by Thomas et al.[164] that some SG tubes appear to have been degraded by S^{y-}SCC. Thus, mitigating S^{y-}SCC is an important task.

Another approach to mitigating S^{y-}SCC would involve minimizing the use of hydrazine. Such an option that would retain the benefits of hydrazine, but reduce the reduction of SO_4^{2-}, should be considered.

Task 7: Quantify AcSCC

AcSCC is important, as it is likely that SO_4^{2-} and Cl^- would be key species that enter the TTS crevices. In general, the dependence of AcSCC on pH is opposite to those of PbSCC and S^{y-}SCC being a negative slope rather than positive as shown in Figure 97. The absolute magnitude of its negative dependence on pH is about the same as the absolute magnitude of the positive slopes of the PbSCC and S^{y-}SCC. The emphasis here would be on both SO_4^{2-} and Cl^- simultaneously. The sulfate and Cl^- would be important in activating the denting and the burrowing crevice shown in

Figures 44, 45, and 46.

Task 7-1: Develop a dedicated facility for well controlled testing of AcSCC

Separate facilities should be developed for this testing so that quantitative information can be developed. Three units should be built, and means for measuring such variables as temperature, pH, potential, flow, and impurity concentrations should be included. Provisions for flow should be developed so that testing conditions are controlled.

Task 7-2: pH and potential dependence

Dependencies on temperature, pH, potential, and concentration should be determined as they are relevant to bulk and crevice geometries. Dependencies on liquid and steam phases should be included. Effects of dispersants on any compound formation should be determined.

Task 7-3: Mechanistic studies, initiation and propagation

The negative slope of the AcSCC(SO_4^{2-}) needs to be assessed, as well as similar dependencies for Cl^-. Also, the reason for the ranges of the negative slopes between 0.5 and 0.8 should be considered as the pH dependence especially in crevices is important.

The interaction of sulfates and chloride with forming TTS crevices, TTS denting and TTS burrowing should be determined.

Task 7-4: Mitigation

There has been no significant consideration of the details of either the mechanism or the mitigation of AcSCC(SO_4^{2-} or Cl^-). Since this submode is so important, its mitigation should be considered.

Task 8: Pb Scaling

The Pb-induced scaling as described in Section 3.3 and Figures 76, 88 and 89 is different from the PbSCC process. The growth rate of scaling, as shown in Figure 90, is on the order of the rate of slow SCC propagation and is therefore important. This scaling, of course, occurs only in the presence of Pb. The scaling reaction is also more intense as the chromium concentration of the alloy increases, i.e. the scaling rate of Alloy 600 due to Pb is negligible; whereas, that for Alloys 690TT and 800 are significant as shown in Figures 88 and 90. The existing data show, from Section 3.3, that scaling occurs at least over the pH range from about 10 to 4 (high temperature pH).

The scaling reaction is important since it produces wedging stresses inside SCC as with Figures 88 and 89 and because it can produce denting type effects as illustrated in Figure 91.

Task 8-1 Rate of scaling reaction

The scaling rate due to Pb should be measured for Alloys 690TT and 800NG under SG relevant conditions in the presence of Pb to determine effects of major variables: Pb concentration, pH, potential, temperature, and presence of significant inhibitors normally added to secondary environments. This initial task should be a survey since there is so little information available except for the various metallographic data in the literature.

It is clear, however, that this is a potential problem and should be given attention.

Task 9: Primary Side of Tubes

Corrosion processes on the primary side seem less complex than those on the secondary side owing to lack mainly of superheated crevices and the much larger amount of iron in the water as well as access to the carbon steel in the tube sheet and the steam/feedwater lines. The primary concerns are the release and deposition of activated species and the occurrence of LPSCC on the tubes. From the point of view of LPSCC, the Alloys 690TT and 800NG have exhibited good resistance following the prediction of Coriou and his colleagues shown in Figure 17(c). The Alloy 800NG, in fact, has exhibited excellent resistance to LPSCC for over 30 years in operating plants and Alloy 690TT has exhibited similar resistance for up to 17 years.

Task 9-1 Mechanistic study of LPSCC

Following the observation of Coriou and his colleagues,[64] as shown in Figure 17(c) as well in Figure 17(d)[66] alloys, with Ni concentrations greater than about 45% and Cr concentrations below 20% sustain LPSCC at least at deaerated open circuit potentials. Extensive work has shown that the peak in LPSCC for Alloy 600 initiation and propagation, as in Figure 56, occurs around the NiO/Ni equilibrium. However, this correlation does not explain the resistance of either Alloy 690TT nor Alloy 800NG. Thus, there are still some unexplained patterns of LPSCC. Reaching some more satisfying understanding of LPSCC as it integrates Alloys 600MA, 600TT, 690TT, 800, and Type 321SS is important for long term predictions. Such mechanistic studies should consider at least:

- Change of surface composition of the passive film and metal substrate with time.
- Effect of cold work on initiation and propagation.
- Effect of surface condition on slip in the matrix and grain boundaries.
- Properties of grain boundaries including adsorption and diffusivity.

Task 10: Sulfur transport to turbine

In Task 6, work that should be undertaken for predicting the occurrence of S^{y-}SCC was identified. Another aspect of the low valence sulfur, which is produced by the reduction of sulfate impurity by hydrazine, is the fact that the HS^- and H_2S species could be readily transported to the turbine as shown schematically in Figure 106. In the turbine, the steel alloys are all relatively high strength, and such materials are well known to sustain SCC in environments that contain reduced sulfur. Any SCC of a critical turbine component could result in extensive damage.

Task 10-1 Carryover to turbine of low valence sulfur

The first step in considering possible S^{y-}SCC in turbine components is establishing the extent to which the sulfur is carried to the turbine. Important aspect to such an investigation should include:

- Obtain swipe samples over the turbine surfaces of blades, attachments, and rotor.
- Determine whether the sulfur is low valence. The environment in the turbine does not contain oxygen, and a rapid effort to collect specimens should find the reduced valence.
- Determine the distribution of the sulfur.

- Such an investigation should be carried out on a turbine that has a long exposure.

Task 10-2 S^{y-}SCC of turbine materials

While the turbine alloys have been subjected to limited studies of propagation using conventional pre-cracked specimens, there is little if any work on either the initiation or propagation of SCC of these alloys in the presence of S^{y-}. A survey of such SCC should be carried out for typical turbine conditions. Such a program should wait until the results from Task 10-1.

Task 11: Vessel SCC

In the middle 1990s, SCC was observed in the upper girth welds of SG vessels from several utilities[102,103] It seems that this SCC was related to initiation by pitting that presumably resulted from the presence of oxygen during shutdown, layup, or startup. Also, residual stresses and heat treatment were implicated. However, there were never any following studies of the factors that affect the SCC of these alloys. The initiation and SCC of these alloys has yet to be satisfactorily understood with respect to the initiation and propagation of SCC in SG secondary environments.

Task 11-1 SCC of SG turbine vessel materials, weld and non-weld

Conduct initiation and propagation studies of SCC in secondary SG water for materials typical of matrix, heat affected zone, and weld. Particular attention should be given to low hydrogen and to relevant heat treatments.

Task 12: FAC on Improved Alloy

FAC continues to be an important damage process. In some cases serious explosions occur and in others there are leaks first. The rate of FAC has been extensively studied. The main issues seem to be the following:

- What are the consequences, e.g. stimulate SCC in view of the consequences shown in Figure 105, of replacing piping in the secondary system with a higher Cr alloy?
- What is the effect of the hydrogen produced in FAC on the integrity of alloys?

Task 12-1 SCC of Cr additions on SCC of feedwater piping

It is not obvious that a simple replacement of the present carbon steel by an alloy of higher Cr would not involve a change in the SCC behavior. Therefore, some exploratory SCC studies on initiation and propagation of SCC in such new alloys should be undertaken.

Task 12-2 Hydrogen absorption and effects on mechanical and SCC properties

It is not clear than anyone has investigated adequately the implications of absorbed hydrogen, which is produced in the FAC reaction, on the mechanical properties of the piping especially at welds, heat affected zones or possibly with local cold work at welds.

Some exploratory work should be undertaken to determine whether such hydrogen is important both in initiation and propagation of SCC.

6.0 Summary and Conclusions

1. This paper discusses possible degradation that could occur after long times in modern steam generators. Such degradations are discussed in Sections 3.0 and 4.0. Quantitative data are included.
2. A method for predicting long time degradation is presented in Section 2.3 where the longest time for degradation is shown to be the precursors that must develop before corrosion damage can start.
3. The backgrounds for the degradations, which are discussed in Sections 3.0 and 4.0, are discussed in Section 2.0.
4. Possible modes of long term damage or precursors relative to tubing only for modern steam generators are likely to be the following as discussed in Section 3.0:

   Precursors

   a. Tube support line contact crevice (Section 3.6)
   b. Denting at the TTS (Section 3.8)
   c. Deep crevice formed in tubesheet by corrosion burrowing (Section 3.9)
   d. Fouling of free surfaces (Section 3.10)
   e. pH change on the secondary side (Section 3.11)
   f. Dispersants (Section 3.12)
   g. OTSG region (Section 3.13)
   h. Loss of Cr from passive film and metal surface (Section 3.14)
   i. Multiple chemistries (Section 3.15)
   j. Cold work (Sections 3.16)

   Degradation damage

   a. Lead SCC (Section 3.2)
   b. Lead scaling (Section 3.3)
   c. Reduced sulfur SCC (Section 3.4)
   d. Acidic SCC mainly with sulfates (Section 3.5)
   e. Top of the tubesheet ODSCC, including Pb, S^{y-}, SO_4^{2-} (Section 3.7)
   f. Wear (Section 3.17)

5. Possible modes of long term damage or precursors relative to non-tubing aspects for modern steam generators are most likely to be the following as discussed in Section 4.0:

   Precursors

   a. Cold work on pipes and components (Section 4.6)
   b. Carryover of reduced sulfur to turbine (Section 4.8)
   c. Shutdowns, layups, startups (Section 4.9)

Degradation damage

a. SCC of SG vessel (Section 4.2)
b. SCC at divider plates (Section 4.4)
c. Welds on primary piping (Section 4.3)
d. Low temperature crack propagation (Section 4.5)
e. Flow assisted corrosion with associated hydrogen (Section 4.7)

6. Important new scenarios of sequential precursors and degradation damage are identified as the following:
   a. Top of the tubesheet denting (Section 3.8) and corrosion burrowing (Section 3.9) produce extended locations for superheating and concentrating chemicals that produce SCC.
   b. Preferential dissolution of more active Cr in Alloy 690TT reduces resistance to SCC. (Section 3.11)
   c. Sulfide carryover from SG to turbine can produce SCC in turbine components. (Section 4.8)
   d. Raising the pH on the secondary side increase likelihood of PbSCC and S^{y-}SCC. (Section 3.11)
   e. Adding dispersants may cause release of Pb and reduced sulfur for accelerating SCC. (Section 3.12)
   f. Changing to higher Cr alloy to minimize FAC may accelerate SCC. (Section 4.7)
   g. Long time required for initiation of SCC at SG vessel welds but eventual development into propagating SCC. (Section 4.3)
   h. Long time required for cold worked stainless steel piping to initiate SCC for reasons not well explained and then propagation ensues. (Section 3.16)

7. Twelve tasks for work aimed at minimizing the long term occurrence of degradation are identified in Section 5.0 and are:
   Task 1: Line contact tube supports
   Task 2: TTS crevices
   Task 3: Fouling and associated degradation on free surfaces
   Task 4: OTSG upper bundle surfaces
   Task 5: Quantify PbSCC
   Task 6: Quantify S^{y-}SCC
   Task 7: Quantify AcSCC(SO_4^{2-})
   Task 8: Pb scaling
   Task 9: Primary side of tubes
   Task 10: Sulfur transport to turbine
   Task 11: Vessel SCC
   Task 12: FAC on improved alloy

7.0 Acknowledgements

I appreciate very much being invited to present this plenary paper. The opportunity to present this lecture greatly stimulated me to prepare this assessment of possible degradation in future steam generators. Especially, I appreciate the encouragement by the organizers, Graham Macdonald, Revi Kizhatil, and Bill Schneider. I appreciate also the continuing encouragement by Jovica Riznic.

I appreciate the continuing support and encouragement by the United States NRC and in particular Joe Muscara of the NRC as well as Bill Shack of ANL for my continuing work to analyze and predict corrosion in steam generators.

I appreciate the many conversations as well as assistance with locating information from many friends including the following: Peter Andresen of GE, Koji Arioka of INSS, Chi Bum Bahn of ANL, Anna Brozova of Nuclear Research Institute Rez, Stephen Bruemmer of PNL, Bruce Bussert of Lockheed Martin, Thierry Cassagne of TOTAL, Francois Cattant of EDF, Steve Chambers of DOE, Pierre Combrade of Areva, Jacques Daret of Corrodys, Odile de Bouvier of EDF, Dan Duncan of Lockheed Martin, David Enos of Sandia, Damien Feron of CEA, Keith Fruzzetti of the Electric Power Research Institute, Rick Gangloff of University of Virginia, Jeffrey Gorman of DEI, Mac Hall of Bechtel Bettis, Dennis Hussey of the Electric Power Research Institute, Robin Jones of EPRI, Karen of Swedish Nuclear Power Inspectorate, Ken Kasza of ANL, Rob Kelly of The University of Virginia, Renate Kilian of Areva, Uh Chul Kim of KAERI, Peter King of Babcock & Wilcox, Nathan Lewis of Lockheed Martin, Yucheng Lu of AECL, Jesse Lumsden of Rockwell Scientific, Graham Macdonald of Areva, Chuck Marks of Dominion Engineering, Al McIlree of EPRI, Todd Mintz of NRC, Joe Muscara of NRC, Roger Newman of The University of Toronto, Suat Odar of Areva, Ellen Mary Pavageau of EDF, Howard Pickering of The Pennsylvania State University, Robert Rapp of The Ohio State University, Jovica Risznic of Canadian Nuclear Safety Commission, Dewey Rochester of Duke Energy, Jeff Sarver of Babcock & Wilcox, Bill Schneider of Babcock & Wilcox, Peter Scott of Areva, John Scully of The University of Virginia, Greg Selby of EPRI, Bill Shack of ANL, Tetsuo Shoji of Tohoku University, John Slade of New Brunswick Power, Vladimir Sorokin of Podolsk Russia, J.P. Sursock of EPRI, Robert Tapping of AECL, Larry Thomas of PNL, Takao Tsuruta of MHI, Carl Turner of AECL, Francois Vaillant of EDF, Glenn White of Dominion Engineering, Mike Wright of AECL, Rosa Yang of EPRI, and Toshio Yonezawa of Tohoku University.

Finally, I appreciate the enormous efforts by members of my office staff in preparing this article. Julie Daugherty in particular prepared the manuscript in finished form with references and editorial criticisms. Erin Kate Rediger assisted with locating reference sources and preparing parts of the manuscript. John Ilg prepared the graphics and integrated graphics and text. Finally, I appreciate the support of Mary Elizabeth Ilg, my office manager, who assures that my office is running smoothly.

8.0 References

[1] R.W. Staehle, "Understanding 'Situation-Dependent Strength': A Fundamental Objective in Assessing the History of Stress Corrosion Cracking," Proceedings of NACE-10, Environment-Induced Cracking of Metals, R.P. Gangloff and M.B. Ives, Eds., co-sponsored by ASM and TMS, Kohler, WI, October 2-7, 1988, p. 561.

[2] R.W. Staehle, J.A. Gorman, A.R. McIlree, and R.L. Tapping, "Status and Future of Corrosion in PWR Steam Generators," Proceedings of Fontevraud VI; Contribution of Materials Investigations to Improve the Safety and Performance of LWRs, SFEN, Paris, September 18-22, 2006.

[3] A. McIlree, K. Fruzetti, J. Gorman, W. Shack, R.W. Staehle, and J. Stevens, "A Case for the Major Influence of Lead and Sulfur in the Secondary Side Degradation of PWR Steam Generators Tubing," Proceedings of Fontevraud VI; Contribution of Materials Investigations to Improve the Safety and Performance of LWRs, SFEN, Paris, September 18-22, 2006.

[4] R.W. Staehle, "Approach to Predicting Corrosion of SG Tubes Based on Quantifying Submodes of SCC in Statistical Framework," presented at the Joint EPRI-ANL Heated Crevice Seminar, Argonne National Laboratory, October 7-11, 2002.

[5] R.W. Staehle and J.A. Gorman, "Quantitative Assessment of Submodes of Stress Corrosion Cracking on the Secondary Side of Steam Generator Tubing in Pressurized Water Reactors," *Corrosion*, Part 1 Vol. 59 No. 11 November 2003, Part 2 Vol. 60 No. 1 January 2004, Part 3 Vol. 60 No. 2 February 2004, NACE, Houston, TX.

[6] R.W. Staehle, "Bases for Predicting the Earliest Penetrations Due to SCC for Alloy 600 on the Secondary Side of PWR Steam Generators," NUREG-CR-6737, U.S. Nuclear Regulatory Commission, Washington, D.C., 2001.

[7] R.W. Staehle, J.A. Gorman, K.D. Stavropoulos, C.S. Welty, Jr., "Application of Statistical Distributions to Characterizing and Predicting Corrosion of Tubing in Steam Generators of Pressurized Water Reactors," Life Prediction of Corrodible Structures, Proceedings of the 3rd International Relations Committee Symposium, September 23-26, 1991, Cambridge, England. NACE, Houston, TX, 1994, p. 1374-1399.

[8] R.W. Staehle and J.A. Gorman, "Status and Issues in Corrosion on the Secondary Side of Steam Generators," Paper No. 122, Corrosion '96, NACE, Houston, TX, 1996, pp. 122/1-122/38.

[9] R.W. Staehle and J.A. Gorman, "Predicting the Occurrence of Corrosion Failures in Nuclear Power Components with Emphasis on Applications of Alloy 690," Proceedings of the 2003 Nuclear Safety Research Conference, Marriott Hotel at Metro Center, Washington, D.C., October 20-22, 2003, NUREG/CP-0185, U.S. Nuclear Regulatory Commission, Washington, D.C.

[10] J.A. Gorman, J.E. Harris, R.W. Staehle, and K. Fruzzetti, "Secondary Side Corrosion of 600MA Tubing in PWR Steam Generators – Causes, Implications for Alloys 600TT and 690TT, and Needed Research," Proceedings of the 11th International Conference on Environmental Degradation of Materials in Nuclear Power Systems – Water Reactors, Chair, L. Nelson, August 10-14, 2003. Stevenson, Washington, ANS, La Grange Park, IL.

[11] J.A. Gorman and A.P.L. Turner, "Corrosion Experience with the Secondary Side of Steam Generators in the United States," Proceedings of Improving the Understanding and Control of Corrosion on the Secondary Side of Steam Generators, Airlie House Conference in October 1995, R.W. Staehle, J.A. Gorman and A.R. McIlree, Eds., Warrenton, VA, NACE, Houston, TX, 1996.

[12] J. Gorman, "Inferences Regarding PWR SG Crevices from Plant Operating Experience," presented at the Joint EPRI-ANL Heated Crevice Seminar, Argonne National Laboratory, October 7-11, 2002.
[13] J.A. Gorman, J.E. Harris, and D.B. Lowenstein, "Steam Generator Tube Fitness-for-Service Guidelines," Report prepared for the Atomic Energy Control Board, AECB Project No. 2.228.2, July, 1995.
[14] J.A. Gorman, Guidelines for PWR Steam Generator Tubing Specifications and Repair, Volume 2, Revision 1: Guidelines for Procurement of Alloy 690 Steam Generator Tubing; EPRI TR-016743-V2R1, EPRI, Palo Alto, CA, 1999.
[15] Proceedings of Improving the Understanding and Control of Corrosion on the Secondary Side of Steam Generators, Airlie House Conference in October 1995, R.W. Staehle, J.A. Gorman and A.R. McIlree, Eds., Warrenton, VA, NACE, Houston, TX, 1996.
[16] R.W. Staehle, "Assessment of and Proposal for a Mechanistic Interpretation of the SCC of High Nickel Alloys in Lead-Containing Environments," Proceedings of the 11th International Conference on Environmental Degradation of Materials in Nuclear Power Systems – Water Reactors, Chair, L. Nelson, August 10-14, 2003. Stevenson, Washington, ANS, La Grange Park, IL.
[17] R.W. Staehle, "Clues and Issues in the SCC of High Nickel Alloys Associated with Dissolved Lead," Proceedings of the 12th International Conference on Environmental Degradation of Materials in Nuclear Power Systems – Water Reactors, T.R. Allen, P.J. King, and L. Nelson, Eds., TMS, Warrendale, PA, 2005.
[18] Proceedings: 1983 Workshop on Secondary Side Stress Corrosion Cracking and Intergranular Corrosion of PWR Steam Generator Tubing; EPRI NP-4458, M.J. Partridge, ed., EPRI, Palo Alto, CA, 1983.
[19] Proceedings: 1984 Workshop on Secondary-Side Stress Corrosion Cracking and Intergranular Corrosion of PWR Steam Generator Tubing; EPRI NP-4478, M.J. Partridge, ed., EPRI, Palo Alto, CA, 1984.
[20] Proceedings: 1985 Workshop on Remedial Actions for Secondary-Side Intergranular Corrosion; EPRI NP-4929, M.J. Partridge, ed., EPRI, Palo Alto, CA, 1985.
[21] Proceedings: 1985 Workshop on Primary Side Stress Corrosion Cracking of PWR Steam Generator Tubing; EPRI NP-5158, A.R. McIlree, ed., EPRI, Palo Alto, CA, 1987.
[22] 1987 EPRI Workshop on Secondary Side Intergranular Corrosion Mechanisms; EPRI NP 5971, M.J. Partridge, ed., EPRI, Palo Alto, CA, 1987.
[23] Proceedings: 1983 Workshop on Primary Side Stress Corrosion Cracking of PWR Steam Generator Tubing; EPRI NP-5498, A.A. Stein and A.R. McIlree, eds., EPRI, Palo Alto, CA, 1987.
[24] Proceedings: 1987 Workshop on Mechanisms of Primary Water Intergranular Stress Corrosion Cracking; EPRI NP-5987M, J.A. Gorman and M.J. Partridge, eds., EPRI, Palo Alto, CA, 1988.
[25] PWSCC Remedial Measures Workshop; EPRI NP-6719, J.A. Gorman, ed., EPRI, Palo Alto, CA, 1989.
[26] Proceedings: 1990 Workshop on Circumferential Cracking of Steam Generator Tubes; EPRI NP-7198M, D.B. Lowenstein and J.A. Gorman, eds., EPRI, Palo Alto, CA, 1990.
[27] Proceedings: 1991 Workshop on Secondary Side Intergranular Corrosion Mechanisms; EPRI TR-101103, M.J. Partridge and W.S. Zemitis, eds., EPRI, Palo Alto, CA, 1991.

[28] Proceedings: 1991 Workshop on PWSCC of Alloy 600 in PWRs; EPRI TR-100852, E.S. Hunt and J.A. Gorman eds., EPRI, Palo Alto, CA, 1992.
[29] Proceedings: 1992 Workshop on Secondary Side IGA/SCC, San Antonio, Texas, December 8-10, 1992; EPRI TR-106546, M.J. Partridge, ed., EPRI, Palo Alto, CA, 1992.
[30] Proceedings of EPRI Workshop on Directions for Research on Corrosion Assisted Cracking Initiation, held in Arlington Heights, Illinois, September 23-25, 1992, J. Gilman, ed., EPRI, Palo Alto, CA, 1992.
[31] Proceedings: 1992 Workshop on PWSCC of Alloy 600 in PWRs; EPRI TR-103345, J.A. Gorman and E.S. Hunt, eds., EPRI, Palo Alto, CA, 1993.
[32] Proceedings: Specialist Meeting on Environmental Degradation of Alloy 600; EPRI TR-104898, R.G. Ballinger, A.R. McIlree and J.P.N. Paine, eds., EPRI, Palo Alto, CA, 1994.
[33] Proceedings: 1994 Workshop on Primary Water Stress Corrosion Cracking of Alloy 600 in PWRs; EPRI TR-105406, J.A. Gorman, ed., EPRI, Palo Alto, CA, 1995.
[34] Proceedings: 1997 Workshop on PWSCC of Alloy 600 in PWRs; EPRI TR-109138, S. Hunt, ed., EPRI, Palo Alto, CA, 1997.
[35] Inhibition of IGA/SCC on Alloy 600 Surfaces Exposed to PWR Secondary Water, Volume 1-3; EPRI TR-106212, J. Daret, ed., EPRI, Palo Alto, CA, 1997.
[36] Proceedings: 1993 Workshop of Secondary Side IGA/SCC; EPRI TR-107883, M.J. Partridge and J.E. Broussard, eds., EPRI, Palo Alto, CA, 1998.
[37] 2000 Workshop on PWSCC of Alloy 600 in PWRs; EPRI TR-1000873, R.S. Pathania and A.R. McIlree, eds., EPRI, Palo Alto, CA, 2000.
[38] Steam Generator Reference Book, Steam Generator Owners Group, EPRI, Palo Alto, 1985.
[39] Steam Generator Reference Book, Steam Generator Owners Group, EPRI, Palo Alto, 1994.
[40] M.R. Fleming, A.P.L. Turner, J.A. Gorman, and R.W. Staehle, "Review of Steam Generator Girth Weld Cracking," EPRI TR-103498, Research Project S407-52, EPRI, Palo Alto, CA, January, 1994.
[41] EPRI Materials Degradation Matrix, August 2004, from Materials Reliability Program: Pressurized Water Reactor Issue Management Tables (MRP-205), EPRI, Palo Alto, CA.
[42] Proactive Materials Degradation Assessment, PMDA-PIRT Report, Joseph Muscara, NRC Project Manager, NUREG/CR-XXXX, to be published by the U.S. Nuclear Regulatory Commission, Washington, D.C., 2006.
[43] R.W. Staehle, "Corrosion of Steam Generator Tubes," Appendix B.7 in Proactive Materials Degradation Assessment, PMDA-PIRT Report, Joseph Muscara, NRC Project Manager, NUREG/CR-XXXX, to be published by the U.S. Nuclear Regulatory Commission, Washington, D.C., 2006.
[44] P.M. Scott, "SCC of Alloys 600, 690, 182, 82, 152, and 52 in PWR Primary Water," Appendix B.6 in Proactive Materials Degradation Assessment, PMDA-PIRT Report, Joseph Muscara, NRC Project Manager, NUREG/CR-XXXX, to be published by the U.S. Nuclear Regulatory Commission, Washington, D.C., 2006.
[45] R.W. Staehle, "Predicting Failures in Light Water Nuclear Reactors Which Have Not Yet Been Observed – Microprocess Sequence Approach (MPSA)," Proceedings of EICM-2, Environment-Induced Cracking of Metals, Second International Conference, Banff, Alberta, September 19-23, 2004.

[46] R.W. Staehle, "Predicting Failures Which Have Not Yet Been Observed – Microprocess Sequence Approach (MPSA)," Appendix B.15 in Proactive Materials Degradation Assessment, PMDA-PIRT Report, Joseph Muscara, NRC Project Manager, NUREG/CR-XXXX, to be published by the U.S. Nuclear Regulatory Commission, Washington, D.C., 2006.

[47] S. Le Hong, C. Amzallag, and A. Gelpi, "Modelling of Stress Corrosion Crack Initiation on Alloy 600 in Primary Water of PWRs," F.P. Ford, S.M. Bruemmer, and G.S. Was, Eds., Proceedings of the Ninth International Conference on Environmental Degradation of Materials in Nuclear Power Systems - Water Reactors, S.M. Bruemmer, F.P. Ford, and G.S. Was, Eds., TMS, Warrendale, PA, 1999, p. 115.

[48] R. Bandy and D. van Rooyen, Tests with Inconel 600 to Obtain Quantitative Stress Corrosion Cracking Data for Evaluating Service Performance; BNL-NUREG-31814, U.S. Nuclear Regulatory Commission, Washington, D.C., 1983.

[49] P.M. Scott, "Prediction of Alloy 600 Component Failures in PWR Systems," Proceedings of Corrosion '96: Part 1: Life Prediction of Structures Subject to Environmental Degradation, P.L. Andresen and R.N. Parkins, chair., NACE, Houston, TX, 1996, p. 135.

[50] W.L. Clarke and G.M. Gordon, "Investigation of Stress Corrosion Cracking Susceptibility of Fe-Ni-Cr Alloys in Nuclear Reactor Waste Environments," *Corrosion Vol. 29*, NACE, Houston, TX, 1973, p. 1.

[51] T.M. Angeliu, P.L. Andresen, E. Hall, J.A. Sutliff, S. Sitzman, and R.M. Horn, "Intergranular Stress Corrosion Cracking of Unsensitized Stainless Steels in BWR Environments," Proceedings of the Ninth International Conference on Environmental Degradation of Materials in Nuclear Power Systems – Water Reactors, S.M. Bruemmer, F.P. Ford, G.S. Was, Eds., TMS, Warrendale, PA, 1999, p. 567.

[52] D. Alter, Y. Robin, M. Pichon, A. Teissier, and B. Thomeret, "Stress Corrosion Cracking of Pressurizer Instrumentation Nozzles in the French 1300 Mwe Units," Proceedings of the Fifth International Symposium on Environmental Degradation of Materials in Nuclear Power Systems - Water Reactors, D. Cubicciotti, chair, ANS, La Grange Park, IL, 1992, p. 661.

[53] Courtesy of EPRI, Palo Alto, CA. Private communication.

[54] E. Hillner, "Corrosion of Zirconium-Base Alloys – An Overview," Zirconium in the Nuclear Industry, ASTM STP 633, A.L. Lowe, Jr. and G.W. Parry, Eds., ASTM, 1977, pp. 211-235.

[55] N.B. Pilling and R.E. Bedworth, "The Oxidation of Metals at High Temperatures," presented at the Annual General Meeting, American Institute of Metals, London, March 8, 1923, Vol. XXIX, p. 529.

[56] M. Pourbaix, Atlas of Electrochemical Equilibria in Aqueous Solutions, NACE, Houston, TX, and CEBELCOR, Brussels, 1974.

[57] Courtesy of D. Rochester of Duke Energy, presented at Experts Panel on IGA/IGSCC in Oconee OTSG, July 28-29, 1998.

[58] D.P. Rochester, "Laboratory Investigation of Free-Span Axial Corrosion in Oconee Nuclear Station's Once Through Steam Generators," Water Chemistry of Nuclear Reactor Systems 8, British Nuclear Energy Society, London, U.K., 2000, p. 1.

[59] D.P. Rochester and R. W. Eaker, "Laboratory Examination Results from Oconee Nuclear Station Once Through Steam Generator Tubes," Proceedings of the Ninth International Conference on Environmental Degradation of Materials in Nuclear Power Systems - Water Reactors, S.M. Bruemmer, F.P. Ford, and G.S. Was, Eds., TMS, Warrendale, PA, 1999, p 639.

[60] J.W. Pugh and J.D. Nisbet, "A Study of the Iron Chromium Nickel Ternary System," *Journal of Metals Vol. 188,* 1950, p. 269.

[61] H.R. Copson and C.F. Cheng, "Some Case Histories of Stress Corrosion Cracking of Austenitic Stainless Steels Associated with Chlorides," *Corrosion Vol. 13,* NACE, Houston, TX, 1957, p. 397.

[62] H.R. Copson, "Effect of Stress Corrosion Cracking of Some Alloys Containing Nickel," Physical Metallurgy of Stress Corrosion Fracture, T.N. Rhodin, Ed., Interscience, New York, NY, 1959, p. 247.

[63] Ph. Berge and J.R. Donati, "Materials Requirements for Pressurized Water Reactor Steam Generator Tubing," *Nuclear Technology Vol. 55*, 1981, p. 88.

[64] H. Coriou, L. Grall, P. Olivier, and H. Willermoz, "Influence of Carbon and Nickel Content on Stress Corrosion Cracking of Austenitic Stainless Alloys in Pure or Chlorinated Water at 350°C," Fundamental Aspects of Stress Corrosion Cracking; NACE-1, R.W. Staehle, A.J. Forty, and D. van Rooyen, Eds., NACE, Houston, TX, 1969, p. 352.

[65] H.R. Copson, D. van Rooyen, and A.R. McIlree, "Stress Corrosion Behavior of Ni-Cr-Fe Alloys in High Temperature Aqueous Solutions," 5th International Congress on Metallic Corrosion, Tokyo, NACE, Houston, TX, 1972.

[66] H. Nagano and H. Kajimura, "Clarification of Stress Corrosion Cracking Mechanism on Nickel Base Alloys in Steam Generators for their Long Lifetime Assurance," Proceedings of the Seventh International Symposium on Environmental Degradation of Materials in Nuclear Power Systems – Water Reactors, R.E. Gold, A.R. McIlree, and S.M. Bruemmer, Eds., TMS, Warrendale, PA, 1995.

[67] R.L. Tapping, "Flow-Accelerated Corrosion," Proceedings of Materials Problems in Light Water Nuclear Power Plants: Status, Mitigation, Future Problems, Suzhou, China, February 20-23, 2005.

[68] F. Cattant, D. Garriga-Majo, F. de Keroulas, P. Todeschini, and J.C. van Duysen, "Effectiveness of 700°C Thermal Treatment on Primary Water Stress Corrosion Sensitivity of Alloy 600 Steam Generator Tubes: Laboratory Tests and In Field Experience," Proceedings of the Fifth International Symposium on Environmental Degradation of Materials in Nuclear Power Systems - Water Reactors, D. Cubicciotti, E.P. Simonen, and R.E. Gold, Eds., ANS, La Grange Park, IL, 1992.

[69] H. Nagano, K. Yamanaka, K. Kobayashi, and M. Inoue, "Development and Manufacturing System of Alloy 690 Tubing for PWR Steam Generators," *The Sumitomo Search*, No. 40, 1989.

[70] Courtesy of A. McIlree, Electric Power Research Institute. Private communication.

[71] C.M. Chen, K. Aral, and G.J. Theus, Computer Calculated Potential pH Diagrams to 300°C; Volumes 1-3; NP-3137, EPRI, Palo Alto, CA, 1983.

[72] B.P. Miglin, Investigation of Lead as a Cause of Stress Corrosion Cracking at Support Plate Intersections; NP-7367, EPRI, Palo Alto, CA, 1991.

[73] K. Arioka, T. Yamada, T. Terachi, and G. Chiba, "Cold Work and Temperature Dependence on Crack Growth Behaviors of Austenitic Stainless Steels in Hydrogenated and Oxygenated High Temperature Water," Proceedings of Fontevraud VI; Contribution of Materials Investigations to Improve the Safety and Performance of LWRs, SFEN, Paris, September 18-22, 2006, pp. 51-57.

[74] R.W. Staehle and J.A. Gorman, "Development and Application of Intensity and Operating Diagrams for Predicting the Occurrence and Extent of Stress Corrosion Cracking," Corrosion Science and Engineering: Proceedings of an International Symposium in Honour of Marcel Pourbaix's 85th Birthday, R.A. Rapp, N.A. Gokchen, and A. Pourbaix, Eds., Rapports Techniques CEBELCOR, Brussels, Vol. 157-158, 1989, p. 199.

[75] P. Combrade, O. Cayla, M. Foucault, D. Vancon, A. Gelpi, and G. Slama, "About the Role of Surface Films on Alloy 600 Corrosion in High Temperature Deaerated Environments," Proceedings of the Third International Symposium on Environmental Degradation of Materials in Nuclear Power Systems – Water Reactors, G.J. Theus and J.R. Weeks, Eds., TMS, Warrendale, PA, 1988, p. 525.

[76] R.N. Parkins, "Stress Corrosion Cracking of Low Carbon Steels," Proceedings of Fundamental Aspects of Stress Corrosion Cracking, R.W. Staehle, A.J. Forty, and D. van Rooyen, Eds., NACE, Houston, TX, 1969, p. 361.

[77] I. Ohsaki, K. Onishi, Y. Ohkubo, T. Hattori, and S. Tokunaga, "Study of the Improvement of Steam Generator Tubing and Tube Support Plate Materials," 2nd International Steam Generator and Heat Exchange Conference, D.E. Anderson, Ed., Canadian Nuclear Society, Toronto, 1994, p. 8.93.

[78] S. Tsujikawa and S. Yashima, "Results of Steam Generator Tubing Reliability Test," 2nd International Steam Generator and Heat Exchange Conference, D.E. Anderson, Ed., Canadian Nuclear Society, Toronto, 1994, p. 6.73.

[79] P.L. Andresen, "Perspective and Direction of Stress Corrosion Cracking in Hot Water," Proceedings of the Tenth International Symposium on Environmental Degradation of Materials in Nuclear Power Systems - Water Reactors, P. Ford, G. Was, and L. Nelson, Eds., NACE, Houston, TX, 2002.

[80] P.L. Andresen, "Stress Corrosion Cracking Prediction in Light Water Reactors," Proceedings of Corrosion 2003 Research Topical Symposium: Modeling and Prediction of Lifetimes for Corrodible Structures, J.R. Scully and D.W. Shoesmith, Eds., NACE, Houston, TX, 2003, pp. 1-34.

[81] P.L. Andresen, "Critical Processes to Model in Predicting SCC Response in Hot Water," Corrosion 2005, Paper No. 05470, NACE, Houston, TX, 2005.

[82] P.L. Andresen, P.W. Emigh, and M.M. Morra, "Effects of Primary Water Chemistry and Deaerated Water on SCC," Corrosion 2005, Paper No. 05592, NACE, Houston, TX, 2005.

[83] S. Wang, Y. Takeda, K. Sakaguchi, and T. Shoji, "The Initiation of Environmentally Assisted Cracking in BWR High Temperature Water," Proceedings of the 12th International Conference on Environmental Degradation of Materials in Nuclear Power Systems – Water Reactors, T.R. Allen, P.J. King, and L. Nelson, Eds., TMS, Warrendale, PA, 2005, pp. 49-55.

[84] Y. Lee, T. Shoji, and K.S. Raja, "Evaluation of Crack Tip Solution Chemistry of Low Alloy Steel in Oxygenated High Temperature Water," Proceedings of the Ninth International Conference on Environmental Degradation of Materials in Nuclear Power Systems – Water Reactors, S.M. Bruemmer, F.P. Ford, and G.S. Was, Eds., TMS, Warrendale, PA, 1999, pp. 893-899.

[85] T. Shoji, Y. Lee, and S. Ishikawa, "Crack Tip Solution Chemistry and Crack Growth Behavior of Low Alloy Steels in High Temperature Water," Proceedings of the ICG-EAC Meeting, Helsinki, Finland, May 17-21, 1999.

[86] S. Rangarajan, Y. Takeda, and T. Shoji, "High Temperature pH Probes for Crevice / Crack Tip Solution Chemistry Applications – A Preliminary Study," presented at the Joint EPRI-ANL Heated Crevice Seminar, Argonne National Laboratory, October 7-11, 2002.

[87] O. de Bouvier, B. Priex, and F. Vaillant, "Nickel Alloy Stress Corrosion Cracking in Neutral and Lightly Alkaline Sulfate Environments," Proceedings of the Ninth International Conference on Environmental Degradation of Materials in Nuclear Power Systems – Water Reactors, S.M. Bruemmer, F.P. Ford, and G.S. Was, Eds., TMS, Warrendale, PA, 1999.

[88] N. Pessall, "Prediction of Stress Corrosion Cracking in 10% Caustic Soda Solutions at 315°C (600°F)," *Corrosion Science Vol. 20,* Pergamon Press, 1980, p. 225.

[89] M.D. Wright and M. Mirzai, "Lead-Induced SCC Propagation Rates in Alloy 600," Proceedings of the Ninth International Conference on Environmental Degradation of Materials in Nuclear Power Systems - Water Reactors, S.M. Bruemmer, F.P. Ford, and G.S. Was, Eds., TMS, Warrendale, PA, 1999, p. 657.

[90] M.D. Wright, "Establishing Thresholds for Lead Induced Cracking of Steam Generator Tube Alloys," Water Chemistry of Nuclear Reactor Systems 7, T. Swan, chair, British Nuclear Energy Society, London, 1996, p. 435.

[91] M.L. Castano-Marin, D. Gomez-Briceno, and F. Hernandez-Arroyo, "Influence of Lead Contamination on the Stress Corrosion Resistance of Nickel Alloys," Proceedings of the Sixth International Symposium on Environmental Degradation of Materials in Nuclear Power Systems-Water Reactors, R.E. Gold and E.P. Simonen, Eds., TMS, Warrendale, PA, 1993, p. 189.

[92] H. Takamatsu, B.P. Miglin, P.A. Sherburne, and K. Aoki, "Study on Lead-induced Stress Corrosion Cracking of Steam Generator Tubing under AVT Water Chemistry Conditions," Proceedings of the Eighth International Symposium on Environmental Degradation of Materials in Nuclear Power Systems - Water Reactors, A.R. McIlree, chair, ANS, La Grange Park, IL, 1997, p. 216.

[93] R.W. Staehle, "Assessment of and Proposal for a Mechanistic Interpretation of the SCC of High Nickel Alloys in Lead Containing Environments," Proceedings of the Eleventh International Conference on Environmental Degradation of Materials in Nuclear Power Systems - Water Reactors, G.S. Was, chair, ANS, La Grange Park, IL, 2003, p. 381.

[94] J.F. Eckel, "Stress Corrosion Crack Nucleation and Growth in Austenitic Stainless Steels," *Corrosion Vol. 18*, NACE, Houston, TX, 1962.

[95] Ph. Berge and J.R. Donati, "Materials Requirements for Pressurized Water Reactor Steam Generator Tubing," *Nuclear Technology Vol. 55*, 1981, p. 88.

[96] K. Fruzzetti and C.J. Wood, "Developments in Nuclear Power Plant Water Chemistry," Proceedings of the International Conference on Water Chemistry of Nuclear Reactor Systems, Paper 1.1, Jeju Island, Korea, October 23-26, 2006, pp. 1-6.

[97] F. Cattant, M. Dupin, B. Sala, and A. Gelpi, "Analyses of Deposits and Underlying Surfaces on the Secondary Side of Pulled Out Tubes From a French Plant," Contribution of Materials Investigation to the Resolution of Problems Encountered in Pressurized Water Reactors; Proceedings of the International Symposium: Fontevraud III, F. de Keroulas, chair., French Nuclear Energy Society, Paris, 1994, p. 469.

[98] Courtesy of A. McIlree, Electric Power Research Institute. Private communication.

[99] L.E. Thomas and S.M. Bruemmer, "Summary of Analytical Electron Microscopy Observation of Intergranular Attack and Stress Corrosion Cracks in Alloy 600 Steam Generator Tubing, EPRI Report No. 1011683, Palo Alto, CA, 2005.

[100] P. Ollar and L. Viricel-Honorez, "Better Understanding Flow Restricted Environments from Hideout Return Analyses," Contribution of Materials Investigation to the Resolution of Problems Encountered in Pressurized Water Reactors; Proceedings of the International Symposium: Fontevraud IV, F. de Keroulas, chair., French Nuclear Energy Society, Paris, 1998, p. 465.

[101] R. Varrin Jr., Characterization of PWR Steam Generator Deposits; EPRI Report TR-106048, Palo Alto, CA, 1996.
[102] M.R. Fleming, A.P.L. Turner, J.A. Gorman, and R.W. Staehle, Review of Steam Generator Girth Weld Cracking; EPRI Report TR-103498, Palo Alto, CA, 1993.
[103] M.R. Fleming, A.P.L. Turner, J.A. Gorman, R.W. Staehle, and A.R. McIlree, "Review of Steam Generator Girth Weld Cracking," Contribution of Materials Investigation to the Resolution of Problems Encountered in Pressurized Water Reactors; Proceedings of the International Symposium: Fontevraud III, F. de Keroulas, chair., French Nuclear Energy Society, Paris, 1994, pp. 394-401.
[104] H. Takamatsu, "Japanese SG Related R&D Program," presented at the June 1994 EPRI Technical Advisory Group Meeting, Denver, Colorado, EPRI, Palo Alto, CA, 1994.
[105] Proceedings: 2005 EPRI/ANL/NRC Workshop of Effects of Lead (Pb) and Sulfur (S) on the Performance of Secondary Side Tubing of Steam Generators in PWRs, EPRI Report No. 1012780, Palo Alto, CA, 2005.
[106] J. Daret, T. Cassagne, Y. Lefevre, T.Q. Tran, R. Benoit, and R. Erre, "Evidence for the Reduction of Sulfates under Representative SG Secondary Side Conditions, and for the Role of Reduced Sulfates on Alloy 600 Tubing Degradation," Proceedings of the Ninth International Conference on Environmental Degradation of Materials in Nuclear Power Systems – Water Reactors, S.M. Bruemmer, F.P. Ford, and G.S. Was, Eds., TMS, Warrendale, PA, 1999, p. 567.
[107] B. Sala, P. Combrade, R. Erre, R. Benoit, and M. Le Calvar, "Chemistry of Sulfur in High Temperature Water Reduction of Sulfates," Proceedings of the Fifth International Symposium on Environmental Degradation of Materials in Nuclear Power Systems - Water Reactors, D. Cubicciotti, chair., American Nuclear Society, Chicago, 1992, p. 39.
[108] O. de Bouvier, E-M. Pavageau, F. Vaillant, and D. Vermeeren, "Influence of High Reducing Conditions on IGA/SCC of Alloy 600 in Neutral Sulfate Environments," Proceedings of the 11th International Conference on Environmental Degradation of Materials in Nuclear Power Systems – Water Reactors, Chair, L. Nelson, August 10-14, 2003. Stevenson, Washington, ANS, La Grange Park, IL.
[109] O. de Bouvier, B. Prieux, F. Vaillant, M. Bouchacourt, and P. Lemaire, "Nickel Alloy Stress Corrosion Cracking in Neutral and Lightly Alkaline Sulfate Environments," Proceedings of the Ninth International Conference on Environmental Degradation of Materials in Nuclear Power Systems – Water Reactors, S.M. Bruemmer, F.P. Ford, and G.S. Was, Eds., TMS, Warrendale, PA, 1999, p. 695
[110] H. Neder, M. Jurgensen, D. Wolter, U. Staudt, S. Odar, and V. Schneider, Proceedings of the International Conference on Water Chemistry of Nuclear Reactor Systems, Paper 1.3, Jeju Island, Korea, October 23-26, 2006, pp. 1-6.
[111] S.S. Choi and C. Libby, "PWR Chemistry Performance Monitoring and Assessment," Proceedings of the International Conference on Water Chemistry of Nuclear Reactor Systems, Paper 5.12, Jeju Island, Korea, October 23-26, 2006, pp. 1-4.
[112] M. Seo, M. Sato, J.B. Lumsden, and R.W. Staehle, "Auger Analysis of the Anodic Oxide Film on Iron in Neutral Solution," *Corrosion Science Vol. 17*, Pergamon Press, 1977, pp. 209-217.
[113] W.A. Byers, J. Deshon, G.P. Gary, J.F. Small, and J.B. Mcinvale, "Crud Metamorphosis at the Callaway Plant," Proceedings of the International Conference on Water Chemistry of Nuclear Reactor Systems, Paper 7.3, Jeju Island, Korea, October 23-26, 2006, pp. 1-6.

[114] A. Tigeras, G. Debec, B. Jeannin, and A. Rocher, "EDF Zinc Injection: Analysis of Power Reduction Impact on the Chemistry and Radiochemistry Parameters," Proceedings of the International Conference on Water Chemistry of Nuclear Reactor Systems, Paper 2.1, Jeju Island, Korea, October 23-26, 2006, pp. 1-10.

[115] D. Wolter, M. Baschnagel, J. Haag, V. Schneider, and B. Stellwag, "Ten Years Zinc Injection for Radiation Field Reduction at the Biblis Power Station," Proceedings of the International Conference on Water Chemistry of Nuclear Reactor Systems, Paper 2.2, Jeju Island, Korea, October 23-26, 2006, pp. 1-7.

[116] J.A. Wilson, D. Morey, R.P. Walton, W.E. Allmon, B.G. Lockamon, and J.M. Riddle, "Application of Zinc Addition and Elevated, Constant pH Control to a 24-Month Fuel Cycle at Three Mile Island Unit 1," Proceedings of the International Conference on Water Chemistry of Nuclear Reactor Systems, Paper 2.3, Jeju Island, Korea, October 23-26, 2006, pp. 1-10.

[117] W.Y. Maeng, Y.S. Cho, and U.C. Kim, "Effect of Zn Injection on the SCC Crack Growth of Alloy 600 in Water at 360˚C," Proceedings of the International Conference on Water Chemistry of Nuclear Reactor Systems, Paper 2.4, Jeju Island, Korea, October 23-26, 2006, pp. 1-5.

[118] C.C. Lin, "A Review of Corrosion Product Transport on Fuel Cladding Surfaces," Proceedings of the International Conference on Water Chemistry of Nuclear Reactor Systems, Paper 1.6, Jeju Island, Korea, October 23-26, 2006, pp. 1-8.

[119] J. Korb and B. Stellwag, "Thermodynamics of Zinc Chemistry in PWRs: Effects and Alternatives to Zinc," Proceedings of Water Chemistry of Nuclear Reactor Systems 7, Vol. 2, Paper No. 90, BNES, London, 1996.

[120] V.F. Baston, M.F. Garbauskas, and J. Bozeman, *Nuclear Technology Vol. 114*, 337, 1996.

[121] H.W. Rich, M. Lips, and G. Meier, "27 Cycles of Primary Water Chemistry at Gösgen Nuclear Power Plant," Proceedings of the International Conference on Water Chemistry of Nuclear Reactor Systems, Paper 2.10, Jeju Island, Korea, October 23-26, 2006, pp. 1-6.

[122] J.B. Lumsden, S.L. Jeanjaquet, J.P.N. Paine, and A. McIlree, "Mechanism and Effectiveness of Inhibitors for SCC in a Caustic Environment," Proceedings of the Seventh International Symposium on Environmental Degradation of Materials in Nuclear Power Systems – Water Reactors, G. Airey, et al., Eds., NACE, Houston, TX, 1995, p. 317.

[123] D. Rochester, P. Hull, J. Nolin, T. Henrickson, L. Wilson, K. Fruzzetti, M. Kreider, A. Miller, P. King, and J. Jevec, "Dispersant Trial at McGuire Unit 2 for Mitigation of Steam Generator Deposit Fouling," Proceedings of the International Conference on Water Chemistry of Nuclear Reactor Systems, Paper 5.9, Jeju Island, Korea, October 23-26, 2006, pp. 1-6.

[124] Proceedings of the 1987 Workshop on the Mechanism of Primary H_2O IGSCC; NP-5987-SP, G. Economy, R.J. Jacko, J.A. Begley, and F.W. Pement, Eds., EPRI, Palo Alto, CA, 1987.

[125] P.M. Scott and P. Combrade, "On the Mechanisms of Secondary Side PWR Steam Generator Tube Cracking," Proceedings of the Eighth International Symposium on Environmental Degradation of Materials in Nuclear Power Systems - Water Reactors, A.R. McIlree, chair., ANS, La Grange Park, IL, 1997, p. 65.

[126] D.S. Morton, S.A. Attanasio, and G. A. Young, "Primary Water SCC Understanding and Characterization Through Fundamental Testing in the Vicinity of the Nickel/Nickel Oxide Phase Transition," Proceedings of the Tenth International Symposium on Environmental Degradation of Materials in Nuclear Power Systems - Water Reactors, P. Ford, G. Was, and L. Nelson, Eds., NACE, Houston, TX, 2002.

[127] S. Odar, V. Schneider, T. Schwarz, and R. Bouecke, "Cleanliness Criteria to Improve Steam Generator Performance," Proceedings of the International Conference on Water Chemistry of Nuclear Reactor Systems, Paper 5.5, Jeju Island, Korea, October 23-26, 2006, pp. 1-6.
[128] Stress Corrosion Cracking: The Slow Strain Rate Technique; STP 668, G.M. Ugiansky and J.H. Payer, Eds., ASTM, Philadelphia, PA, 1979.
[129] R.N. Parkins, "Development of Strain-Rate Testing and Its Implications," Stress Corrosion Cracking: The Slow Strain Rate Technique; STP 668, G.M. Ugiansky and J.H. Payer, Eds., ASTM, Philadelphia, PA, 1979, p. 5.
[130] M. Henthorne, Ph.D. Thesis, University of Newcastle upon Tyne, England, 1965.
[131] M. Henthorne and R.N. Parkins, *Corrosion Science Vol. 6*, Pergamon Press, 1966, p. 357.
[132] M. Henthorne and R.N. Parkins, *British Corrosion Journal Vol. 5*, 1967, p. 186.
[133] M.J. Humphries and R.N. Parkins, Proceedings of the Conference on Fundamental Aspects of Stress Corrosion Cracking, The Ohio State University, NACE, Houston, TX, 1969, p. 384.
[134] M.J. Humphries and R.N. Parkins, *Corrosion Science Vol. 7*, Pergamon Press, 1967, p. 747.
[135] E.G. Coleman, D. Weinstein, and W. Rostoker, *Acta Metallurgica Vol. 9*, Elsevier, 1961, p. 491.
[136] R.N. Parkins, "A Critical Evaluation of Current Environment-Sensitive Fracture Test Methods," Environment-Sensitive Fracture: Evaluation and Comparison of Test Methods; STP 821, S.W. Dean, E. N. Pugh, and G.M. Ugiansky, Eds., ASTM, Philadelphia, PA, 1984, p. 5.
[137] J.H. Payer, W.E. Berry, and R.N. Parkins, "Application of Slow Strain-Rate Technique to Stress Corrosion Cracking of Pipeline Steel," Stress Corrosion Cracking: The Slow Strain Rate Technique; STP 668, G.M. Ugiansky and J.H. Payer, Eds., ASTM, Philadelphia, PA, 1979, p. 222.
[138] C.D. Kim and B.E. Wilde, "A Review of the Constant Strain-Rate Stress Corrosion Cracking Tests," Stress Corrosion Cracking: The Slow Strain Rate Technique; STP 668, G.M. Ugiansky and J.H. Payer, Eds., ASTM, Philadelphia, PA, 1979, pp. 97-112.
[139] F.P. Ford and P.L. Andresen, "Corrosion in Nuclear Systems: Environmentally Assisted Cracking in Light Water Reactors," Corrosion Mechanisms in Theory and Practice, P. Marcus and J. Oudar, Eds., Marcel Dekker, New York, NY, 1995, p. 501.
[140] S. Ritter and H.P. Seifert, "Strain-Induced Corrosion Cracking of Low-Alloy Reactor Pressure Vessel Steels Under BWR Conditions," Paper No. 02516, Corrosion 2002, NACE, Houston, TX, 2002, p. 02516/1.
[141] R.N. Parkins, "Environment Sensitive Fracture and its Prevention," *British Corrosion Journal Vol. 14*, 1979, p. 5.
[142] R.N. Parkins and B.S. Greenwell, "The Interface Between Corrosion Fatigue and Stress Corrosion Cracking," *Metal Science Vol. 8*, 1977, p. 405.
[143] H.W. Pickering, F.H. Beck, and M.G. Fontana, "Wedging Action of Solid Corrosion Product During Stress Corrosion of Austenitic Stainless Steels," *Corrosion Vol. 18*, NACE, Houston, TX, 1962.
[144] M.O. Speidel and R. Magdowski, "Stress Corrosion Crack Growth of Cold Worked Nickel Base Alloy 600," International Conference on Corrosion-Deformation Interactions; CDI'92, Electricite de France, Paris, 1992, p. 107.
[145] C.H. Shen and P.G. Shewmon, "A Mechanism for Hydrogen-Induced Intergranular Stress Corrosion Cracking in Alloy 600," *Metallurgical Transactions Vol. 21A*, 1990, p. 1261.

[146] L.E. Thomas and S.M. Bruemmer, "Observations and Insights into Pb-Assisted Stress Corrosion Cracking of Alloy 600 Steam Generator Tubes," Proceedings of the 12th International Conference on Environmental Degradation of Materials in Nuclear Power Systems – Water Reactors, T.R. Allen, P.J. King, and L. Nelson, Eds., TMS, Warrendale, PA, 2005.

[147] Courtesy of R. Eaker of Duke Power, Charlotte, NC. Private communication.

[148] G. P. Airey, "Optimization of Metallurgical Variables to Improve Corrosion Resistance on Inconel Alloy 600," EPRI NP-3051, EPRI, Palo Alto, CA, 1983.

[149] R.W. Staehle, "Predicting the First Failure," presented at Corrosion 2003, San Diego, NACE, Houston, TX, March 16-20, 2003.

[150] B.L. Dow, Jr., Steam Generator Progress Report, Revision 14; TE-106365-R14, EPRI, Palo Alto, CA, 1999.

[151] Courtesy of L. Björnkvist of Vattenfall and J. Gorman of Dominion Engineering, April, 1999. Private communication.

[152] R.W. Staehle, "Bases for Predicting the Earliest Penetrations Due to SCC for Alloy 600 on the Secondary Side of PWR Steam Generators," RWS-151, NUREG-CR-6737," U.S. Nuclear Regulatory Commission, Washington, D.C., 2001.

[153] R.W. Staehle, "Bases for Predicting the Earliest Failures Due to Stress Corrosion Cracking," Chemistry and Electrochemistry of Stress Corrosion Cracking: A Symposium Honoring the Contributions of R.W. Staehle, New Orleans, TMS, Warrendale, PA, 2001.

[154] P.M. Scott, "2000 F.N. Speller Award Lecture: Stress Corrosion Cracking in Pressurized Water Reactors – Interpretation, Modeling, and Remedies," *Corrosion Vol. 56,* NACE, Houston, TX, 2000, p. 771.

[155] X.C. Jiang and R.W. Staehle, "Effects of Stress and Temperature on Stress Corrosion Cracking of Austenitic Stainless Steels in Concentrated Magnesium Chloride Solutions," *Corrosion Vol. 53*, No. 6, NACE, Houston, TX, 1997, pp. 448-466.

[156] R.W. Staehle, "Variability in the Corrosion of Materials in LWR Environments," Appendix B.19 in Proactive Materials Degradation Assessment, PMDA-PIRT Report, Joseph Muscara, NRC Project Manager, NUREG/CR-XXXX, to be published by the U.S. Nuclear Regulatory Commission, Washington, D.C., 2006.

[157] E.D. Eason and L.M. Shusto, Analysis of Cracking in Small Diameter BWR Piping, EPRI NP-4394, Electric Power Research Institute, Palo Alto, CA, 1986.

[158] W.H. Bamford and J.F. Hall, "A Review of Alloy 600 Cracking in Operating Nuclear Plants: Historical Experience and Future Trends," Proceedings of the Conference on Vessel Head Penetration Inspection, Cracking and Repairs, Sponsored by USNRC and ANL, Gaithersburg, MD, September 29 - October 2, 2003.

[159] R.W. Staehle, "Lead SCC in Two Perspectives: Chronological and Phenomenological Mechanistic," Proceedings: 2005 EPRI/ANL/NRC Workshop of Effects of Lead (Pb) and Sulfur (S) on the Performance of Secondary Side Tubing of Steam Generators in PWRs, EPRI Report No. 1012780, Palo Alto, CA, 2005.

[160] H.R. Copson and S.W. Dean, "Effect of Contaminants on Resistance to Stress Corrosion Cracking of Ni-Cr Alloy 600 in Pressurized Water," *Corrosion Vol. 21,* NACE, Houston, TX, 1965, p. 1.

[161] J.M. Sarver, "IGSCC of Nickel Alloys in Lead Contaminated High Purity Water," EPRI Workshop on Intergranular Corrosion and Primary Water Stress Corrosion Cracking Mechanisms; NP-5971, EPRI, Palo Alto, CA, 1987, p. C11/1.

[162] G.N. Flint and B.A. Weldon, "Some Investigations into the Stress Corrosion Behaviour of Fe-Ni-Cr Alloys in High Temperature Water," P-N2 56, Direction des Etudes et Recherches, EDF, Ermenonville, France, March 13-17, 1972.

[163] P. Millett and K. Fruzzetti, "Considerations for Lead Transport in PWR Crevices," Proceedings: 2005 EPRI/ANL/NRC Workshop of Effects of Lead (Pb) and Sulfur (S) on the Performance of Secondary Side Tubing of Steam Generators in PWRs, EPRI Report No. 1012780, Palo Alto, CA, 2005.

[164] L. Thomas, S. Bruemmer, and A. McIlree, "Lead Observations at Crack Tips in Alloy 600 Steam Generator Tubing," Proceedings: 2005 EPRI/ANL/NRC Workshop of Effects of Lead (Pb) and Sulfur (S) on the Performance of Secondary Side Tubing of Steam Generators in PWRs, EPRI Report No. 1012780, Palo Alto, CA, 2005.

[165] J. Stevens, B. Fellers, R. Theimer, S. Nasrazadani, and H. Namduri, "Secondary System Oxide Characterization Study at Comanche Peak (Interim Report), Proceedings of the Steam Generator Secondary Side Management Conference, Savannah, GA, February 10-12, 2003.

[166] G.A. Bickel, D. Guzonas, W. Hocking, K. Irving, A. Lockley, I. Muir, F. Szostak and M. Wright, "Examination of Steam Generator Tube Samples from the Upper Bundle Free Span Regions of Oconee Units 1, 2 and 3 Once Through Steam Generators," Atomic Energy of Canada Limited, Chalk River, Ontario, 2000.

[167] J. Stevens, R. Theimer, S. Nasrazadani, and H. Namduri, "Secondary System Oxide and Lead Study at Comanche Peak," Proceedings of the International Conference on Water Chemistry of Nuclear Reactor Systems, Paper 5.2, Jeju Island, Korea, October 23-26, 2006, pp. 1-7.

[168] C. Laire, G. Platbrood, and J. Stubbe, "Characterization of the Secondary Side Deposits of Pulled Steam Generator Tubes," Proceedings of the Seventh International Symposium on Environmental Degradation of Materials in Nuclear Power Systems - Water Reactors, G. Airey, et al., Eds., NACE, Houston, TX, 1995, p. 387.

[169] J.B. Lumsden, G. Pollock, and A. McIlree, "Effects of pH, ECP and Pb Concentration on PbSCC of High Ni Alloys," Proceedings: 2005 EPRI/ANL/NRC Workshop of Effects of Lead (Pb) and Sulfur (S) on the Performance of Secondary Side Tubing of Steam Generators in PWRs, EPRI Report No. 1012780, Palo Alto, CA, 2005.

[170] K.M. Kim, U.C. Kim and E.H. Lee, "Lead Induced Stress Corrosion Cracking of SG Tubing Materials in Caustic Environments," Proceedings: 2005 EPRI/ANL/NRC Workshop of Effects of Lead (Pb) and Sulfur (S) on the Performance of Secondary Side Tubing of Steam Generators in PWRs, EPRI Report No. 1012780, Palo Alto, CA, 2005.

[171] R. Kilian, "Influence of Lead on the SCC Behavior of SG Tubing Materials," IAEA Specialists Meeting on Steam Generator Problems and Replacement, International Atomic Energy Agency, Madrid, 1993, p. 137.

[172] H.R. Copson and G. Economy, "Effect of Some Environmental Conditions on Stress Corrosion Behavior of Ni-Cr-Fe Alloys in Pressurized Water," *Corrosion Vol. 24*, NACE, Houston, TX, 1968, p. 55.

[173] B.P. Miglin and J.M. Sarver, Investigation of Lead as a Cause of Stress Corrosion Cracking at Support Plate Intersections; NP-7367-S, EPRI, Palo Alto, CA, 1991.

[174] T. Sakai, T. Senjuh, K. Aoki, T. Shigemitsu, and Y. Kishi, "Study on Corrosion Resistance of Alloy 600 and 690 in High Temperature Water Containing Lead," *Corrosion Vol. 48*, NACE, Houston, TX, 1992.

[175] Y. Lu, "Effect of Pb on the Electrochemical Behavior of SG tube Alloys under SG Crevice Conditions," Proceedings: 2005 EPRI/ANL/NRC Workshop of Effects of Lead (Pb) and Sulfur (S) on the Performance of Secondary Side Tubing of Steam Generators in PWRs, EPRI Report No. 1012780, Palo Alto, CA, 2005.

[176] D. Gomez-Briceno and M.L. Castano, "Inconel 690TT and Incoloy 800 in S, Cu and Pb Environments," Proceedings: 1991 Workshop on Secondary Side Intergranular Corrosion Mechanisms; TR-101103, M.J. Partridge and W.S. Zemitis, Eds., EPRI, Palo Alto, CA, 1991.

[177] Courtesy of P. King, Babcock and Wilcox, Alliance, OH, September 2001. Private communication.

[178] K. Smith, A. Klein, P. Saint-Paul, and J. Blanchet, "Inconel 690; A Material with Improved Corrosion Resistance for PWR Steam Generator Tubes," Proceedings of the Second International Symposium on Environmental Degradation of Materials in Nuclear Power Systems – Water Reactors, J.T.A. Roberts, J.R. Weeks, and G.J. Theus, Eds., ANS, La Grange Park, IL, 1986, p. 319.

[179] J. F. Newman, Stress Corrosion of Alloys 600 and 690 in Acidic Sulfate Solutions at Elevated Temperatures; NP-3043, EPRI, Palo Alto, CA, 1983.

[180] W.H. Cullen, "Review of IGA, IGSCC and Wastage of Alloys 600 and 690 in High Temperature Acidified Solutions," Control of Corrosion on the Secondary Side of Steam Generators, R.W. Staehle, J.A. Gorman, and A.R. McIlree, Eds., NACE, Houston, TX, 1996, p. 273.

[181] E. Pierson and C. Laire, "The Influence of Copper on the SCC of Alloy 600 and Alloy 690 Steam Generator Tubes," Contribution of Materials Investigation to the Resolution of Problems Encountered in Pressurized Water Reactors; Proceedings of the International Symposium: Fontevraud IV, F. de Keroulas, chair., French Nuclear Energy Society, Paris, 1998, p. 381.

[182] H. Nagano, K. Yamanaka, K. Tokimasa, and H. Miyuki, "Intergranular Attack Behavior and Mechanisms for Nickel-Base Alloys in Caustic Solutions at Elevated Temperatures," Environment Induced Cracking of Metals: NACE-10, R.P. Gangloff and M.B. Ives, Eds., NACE, Houston, TX, 1990, p. 407.

[183] J.B. Lumsden and P.J. Stocker, "Inhibition of IGA in Nickel Base Alloys in Caustic Solutions, Paper No. 252, Corrosion '88, NACE, Houston, TX, 1988.

[184] H.W. Pickering and P.R. Swann, "Electron Metallography of Chemical Attack Upon Some Alloys Susceptible to Stress Corrosion Cracking," *Corrosion Vol. 19*, NACE, Houston, TX, 1963, pp. 373-389.

[185] H.W. Pickering and Y.S. Kim, "De Alloying at Elevated Temperatures and at 298 K Similarities and Differences," *Corrosion Science Vol. 22*, No. 7, Pergamon Press, 1982.

[186] H.W. Pickering, "Characteristic Features of Alloy Polarization Curves," *Corrosion Science Vol. 23,* No. 10, Pergamon Press, 1983.

[187] R.C. Newman, R.R. Corderman, and K. Sieradzki, "Evidence for Dealloying of Austenitic Stainless Steels in Simulated Stress Corrosion Crack Environments," *British Corrosion Journal Vol. 24*, No. 2, 1989, pp. 143-48.

[188] R.C. Newman, S. G. Corcoran, J. Erlebacher, M.J. Aziz and K. Sieradzki, "Alloy Corrosion," *MRS Bulletin*, 1999.

[189] K. Sieradzki, R.C. Newman, T. Shahrabi, "Dealloying," Advances in Localized Corrosion, Proceedings of the Second International Conference on Localized Corrosion: NACE-9, H.S. Isaacs, U. Bertocci, J. Kruger, and S. Smialowka, Eds., NACE, Houston, TX, 1987.

[190] F. Friedersdorf and K. Sieradzki, "Film Induced Intergranular Cracking of Binary Noble Alloys," Paper No. 166, Corrosion '95, NACE, Houston, TX, 1995.
[191] K. Sieradzki, N. Dimitrov, D. Movrin, C. McCall, N. Vasiljevic, and J. Erlebacher, "The Dealloying Critical Potential," *Journal of the Electrochemical Society Vol. 149*, No. 8, 2002, pp. B370-B377.
[192] R.W. Staehle, "Stress Corrosion Cracking of Fe-Cr-Ni Alloy Systems," Theory of Stress Corrosion Cracking, J.C. Scully, Ed., NATO Scientific Affairs Division, Brussels, 1971, p. 222.
[193] T. Sakai, S. Okabayashi, K. Aoki, K. Matsumoto, and Y. Kishi, "A Study of Oxide Thin Film of Alloy 600 in High Temperature Water Containing Lead," Paper No. 520, Corrosion '90, NACE, Houston, TX, 1990, p. 520/1.
[194] M. Rockel and R.W. Staehle, unpublished results.
[195] W.J. Mills, M.R. Lebo, and J.J. Kearns, "Hydrogen Embrittlement, Grain Boundary Segregation, and Stress Corrosion Cracking of Alloy X-750 in Low and High Temperature Water," *Metallurgical & Materials Transactions A Vol. 30A*, June, 1999.
[196] W.J. Mills and C.M. Brown, "Fracture Behavior of Nickel-Based Alloys in Water" Proceedings of the Ninth International Symposium on Environmental Degradation of Materials in Nuclear Power Systems - Water Reactors, S.M. Bruemmer, F.P. Ford, and G.S. Was, Eds., TMS, Warrendale, PA, 1999.
[197] W.J. Mills and C.M. Brown, "Fracture Toughness of Alloy 600 and EN82H Weld in Air and Water," Bettis Atomic Power Lab. for US Dept. of Energy, BT 3264, 1999.
[198] W.J. Mills and C.M. Brown and M.G. Burke, "Fracture Behavior of Alloy 600, Alloy 690 EN82H Welds and EN52 Welds in Water," Bettis Atomic Power Lab. for US Dept. of Energy, BT 3303, 1999.
[199] C.M. Brown and W.J. Mills, "Effect of Water on Mechanical Properties and Stress Corrosion Behavior of Alloy 600, Alloy 690, EN82H Welds, and EN52 Welds," *Corrosion Vol. 55*, No. 2, NACE, Houston, TX, 1999, pp. 173-186.
[200] A.G. Demma and R. Jones, "Degradation of Fracture Resistance: Low Temperature Crack Propagation (LTCP) in Nickel-Base Alloys," Appendix B.13 in Proactive Materials Degradation Assessment, PMDA-PIRT Report, Joseph Muscara, NRC Project Manager, NUREG/CR-XXXX, to be published by the U.S. Nuclear Regulatory Commission, Washington, D.C., 2006.
[201] R. Tapping, "Stress Corrosion Cracking and Pitting: Contaminating External Environments," Appendix B.3 in Proactive Materials Degradation Assessment, PMDA-PIRT Report, Joseph Muscara, NRC Project Manager, NUREG/CR-XXXX, to be published by the U.S. Nuclear Regulatory Commission, Washington, D.C., 2006.